

The Pennsylvania State University
The Graduate School

**DYNAMICS OF ELECTROCATALYTIC NANOMOTORS AND
POWERED RANDOM WALKERS**

A Dissertation in
Chemical Engineering
by
Amir Nourhani

© 2012 Amir Nourhani

Submitted in Partial Fulfillment
of the Requirements
for the Degree of

Doctor of Philosophy

August 2012

The dissertation of Amir Nourhani was reviewed and approved* by the following:

Ali Borhan
Professor of Chemical Engineering
Graduate Program Chair
Co-Chair of Committee
Dissertation Co-Advisor

Vincent H. Crespi
Distinguished Professor of Physics
Professor of Material Science and Engineering
Professor of Chemistry
Co-Chair of Committee
Dissertation Co-Advisor

James S. Vrentas
Dow Professor of Chemical Engineering

Kristen A. Fichthorn
Merrell Fenske Professor of Chemical Engineering
Professor of Physics

Thomas E. Mallouk
Evan Pugh Professor of Materials Chemistry
Professor of Physics

*Signatures are on file in the Graduate School.

Abstract

A variety of synthetic catalytic nanomotors have been fabricated in recent years, one aim being to mimic microscopic biological motors. We propose and analyze a model for deterministic dynamics of hydrogen peroxide powered bimetallic motors, which have been shown to operate by electrokinetic self-propulsion. Using perturbation analysis and the method of matched asymptotic expansions, we find the particle velocity to leading order in Debye length and first order in reaction-induced ion flux for spherical and spheroidal particles. The results are consistent with experiments and numerical calculations. The velocity depends linearly on interfacial potential at the particle surface and hydrogen ion production intensity, as well as inversely on the fluid viscosity, background ion concentration in the electrolyte and hydronium diffusion coefficient. In the regime of low Reynolds flow, both the deterministic and the stochastic dynamics of the nanomotor contribute to the dynamics of the particle. The coupling between these two types of dynamics results in quasi-circular trajectories. We analyzed the proposed mechanisms of motion for some nanomotors and proposed some design principles for making faster rotors. We also showed that the coupling of deterministic dynamics and stochastic orientational dynamics of nanomotors leads to an effective translational diffusion which can be as significant as the translational diffusion of unpowered nanorod.

Table of Contents

| | |
|--|------------|
| List of Figures | vii |
| Acknowledgments | xii |
| Chapter 1 | |
| Nanomotors and Nanorotors | 1 |
| 1 Introduction and Background | 1 |
| 2 The scope of the thesis | 5 |
| Chapter 2 | |
| Electrokinetic Self-Propulsion; Concepts and Modeling | 7 |
| 1 Introduction | 7 |
| 2 Electrokinetic self-propulsion | 9 |
| 3 Formulation of the Model | 11 |
| 4 Perturbation Analysis | 14 |
| Chapter 3 | |
| Spherical Nanomotor | 16 |
| 1 Introduction | 16 |
| 2 The Governing Equation | 16 |
| 3 Perturbation Analysis | 18 |
| 3.1 Singular Perturbation | 18 |
| 3.1.1 Inner Region Near The Particle Surface | 19 |
| 3.1.2 Outer region | 21 |
| 3.2 Slip Velocity | 22 |
| 3.3 Regular Perturbation | 26 |
| 3.4 Particle Velocity | 28 |

| | | |
|------------------|--|-----------|
| 3.5 | The Effect of Source-Sink Geometry | 32 |
| Chapter 4 | | |
| | Spheroidal Nanomotor | 35 |
| 1 | Prolate Spheroidal Coordinates | 35 |
| 2 | Spheroid | 38 |
| 3 | Velocity and Pressure Field for Flow Over a Prolate Spheroid . . . | 39 |
| 4 | The Model of Electrokinetic Self-Propulsion | 40 |
| 5 | Perturbation Analysis | 42 |
| 5.1 | Singular Perturbation Analysis | 43 |
| 5.2 | Regular Perturbation Analysis | 56 |
| Chapter 5 | | |
| | Design Principles | 64 |
| 1 | Introduction | 64 |
| 2 | Scaling Analysis | 65 |
| 3 | The limits | 67 |
| 4 | Discussion | 71 |
| Chapter 6 | | |
| | Dynamics of Nanorotors | 72 |
| 1 | Introdcution | 72 |
| 2 | Stochastic Brownian Contribution | 80 |
| 3 | Discussion | 85 |
| Chapter 7 | | |
| | Coupling of Deterministic and Stochastic Dynamics in Powered Random Walkers | 86 |
| 1 | Introduction | 86 |
| 2 | Modeling | 88 |
| 3 | Mathematical Derivations | 92 |
| 3.1 | Velocity Correlation Function | 93 |
| 3.2 | Diffusion on the C-Frame Circle | 94 |
| 3.3 | Displacement of the Center of Mass | 100 |
| 3.4 | Displacement of the Guiding Center | 102 |
| 3.5 | Displacement Correlation Function on the C-Frame Circle . | 104 |
| 3.6 | Displacement Correlation Function for the Center of Mass . | 105 |
| 3.7 | Displacement Correlation Function for the Guiding Center . | 106 |
| 4 | Results and Discussion | 107 |

| | |
|---|------------|
| Chapter 8 | |
| Future Research | 117 |
| Appendix A | |
| Stokes' Flow Past a Sphere | 119 |
| Appendix B | |
| Stokes' Flow Past a Spheroid | 126 |
| 1 Spheroid | 126 |
| 2 Velocity and Pressure Field | 126 |
| 2.1 Simplified Velocity Field | 130 |
| 3 The Distribution of Traction on the Surface of the Spheroid | 132 |
| 3.1 Introduction to Strain Tensor E_{ji} | 132 |
| 3.2 Term $n'_j E_{ji}^{(1)}$ | 133 |
| 3.3 Term $n'_j E_{ji}^{(2)}$ | 135 |
| 3.4 Term $n'_j E_{ji}^{(3)}$ | 139 |
| 3.5 Strain Tensor | 147 |
| 3.6 Stress Tensor and Distribution of Traction | 149 |
| Bibliography | 152 |

List of Figures

| | | |
|-----|---|---|
| 1.1 | (a) The millimeter size boat with a platinum covered plate attached on underside. [17] The boat decomposes the hydrogen peroxide catalytically and the formation and releasing of bubbles results in impulses that push the boat in the direction opposite the platinum end. (b) The bimetallic nanorod [18] decomposes the hydrogen peroxide electrocatalytically through oxidation of hydrogen peroxide on the platinum side and reduction of oxygen molecules and hydrogen peroxide on the gold side. The asymmetric cloud of hydrogen ions pulls the negatively charged particle toward the platinum end. | 2 |
| 1.2 | Different modes of nanorod motion (a) linear (b) rotary with one end anchored to the substrate (c) rotating parallel to a substrate on a quasi- circular path. (d) fast rotors. (with modification from Ref [6]) | 3 |
| 2.1 | (a) The distribution of positive and negative ions of a binary symmetric electrolyte in contact with an infinite flat plate at thermal equilibrium. The ions in the stern layer $0 < x < s$ are immobile. The ions are mobile in the diffuse layer $s < x < \lambda_D$ (b) Most of the electric potential is screened out over the diffuse layer. (c) The charge density in the double layer is non-zero. (with modification from [35]) | 8 |
| 2.2 | Due to asymmetric electrocatalytic decomposition of hydrogen peroxide, hydrogen ions are produced on the anode surface (source) and consumed on the cathode surface (sink). The phenomena can be modeled as source and sink of hydrogen using a position dependent flux of hydrogen ions. | 9 |

| | | |
|-----|---|----|
| 3.1 | The fluid around the particle is divided to an inner region, where the high variation in the electric potential compensates for the smallness of λ^2 , and an outer region. By changing the variable from r to ρ , we expand the inner region. Matching of the inner and the outer solutions happens at the boundary of inner and outer regions. . . . | 19 |
| 3.2 | The relative areas of the source and sink can be described by θ_0 . . . | 32 |
| 4.1 | The ellipse and hyperbola in the xy -plane; in (a) r_A+r_B is constant, while in (b) $ r_A - r_B $ is constant. (with modification from [37]) . . | 36 |
| 4.2 | Constant coordinate curves for prolate spheroidal coordinate in a half- plane of constant ϕ | 37 |
| 4.3 | The fluid around the spheroid is divided into an inner region, where the high variation in the electric potential compensates for the smallness of λ^2 , and an outer region. By change of variable from ξ to ρ , we can expand the inner region. The surface of the spheroid is represented by $\xi = \xi_s$. We calculate the unknown coefficients of the inner and outer solutions by matching these solutions at the boundary of the two regions. | 42 |
| 5.1 | (a) Maximum velocity versus interfacial potential at different pH's. (b) maximum hydrogen ion flux versus interfacial potential at different pH's. (c) maximum velocity versus maximum interfacial potential at different pH's. | 70 |
| 6.1 | Nanorotors must break axial symmetry in some manner. Experimental implementations include (a) Au rods with asymmetric Pt patches [30] , (b) Rh/Au rods with SiO ₂ /Au/Pt layers applied to one side [31], and (c) [41] and (d) [42] tadpole-like SiO ₂ /Pt/TiO ₂ structures. | 73 |
| 6.2 | The deterministic motion of a nanorotor along a circular path with nanorotor head pointing (a) outside and (b) outside of the circle. (c) The angle ϕ is between the axis of the nanorod of direction $\hat{\mathbf{n}}$ and the direction of velocity. (d) If there is no force acting along the axis of the nanorod, its axis is perpendicular to its trajectory. . | 74 |
| 6.3 | With an increase in the aspect ratio of the spheroid or an increase in the angle ϕ the ratio of the force perpendicular to the symmetry axis and the force parallel to symmetry axis increases. | 77 |

| | | |
|------|--|----|
| 6.4 | For a given particle geometry and magnitude of driving force, the particle whose angle ϕ is smaller will achieve a higher velocity. The highest velocity occurs at $\phi = 0$ when the the symmetric axis of spheroid is tangent to the trajectory. | 78 |
| 6.5 | The final structure has a minimized net force and a maximized net torque. The angle between the arm and the substrate during the fabrication can adjust the force and torque. The lower the angle, the lower the net force in the direction of the axis of the arm. . . . | 79 |
| 6.6 | Trajectory of one counter-clockwise rotation of the slow nanorotor in Ref [30] . (Green) Actual path of the center of mass of the nanorod; which shows stochastic fluctuations of the center of mass position. (Blue) The fitted equivalent circle to the actual trajectory. The rod is almost pointing toward the inside of the circle or tangent to the circle. (The frames are not equidistance in time) | 79 |
| 6.7 | Angular fluctuation $\Delta\theta(t)$ for nanorotors in (red) Ref [30] and (blue) Ref [31]. The deviation of the orientation of the nanomotor from the deterministic orientation can be significant (up to 90°). | 80 |
| 6.8 | The fit distributions of the temporal angular deviation $\delta\theta$ for the nanorotor of Ref [31] to normal distribution for different time intervals Δt | 83 |
| 6.9 | The fit distributions of the temporal angular deviation $\delta\theta$ for nanorotor of Ref [30] to normal distribution for different time intervals Δt | 84 |
| 6.10 | Orientational Diffusion Coefficient $D_{ort} = \frac{\sigma^2}{2\Delta t}$ for (a) Ref [30]: $D_o = 0.102 \text{ rad}^2 \text{ s}^{-1}$ and (b) Ref [31]: $D_o = 0.462 \text{ rad}^2 \text{ s}^{-1}$ | 85 |
| 7.1 | The particle rotates due to the net torque and its velocity has an angle with respect to the axis of the rod due to the asymmetric distribution of force on the particle. The Brownian orientational diffusion deviates the particle's path from a circular (solid) to a quasi-circular (dashed). This process results in change in the direction of velocity $\mathbf{v}_1 \neq \mathbf{v}_2$, the displacement in the position of center of mass $\Delta\mathbf{x}$, and the displacement $\Delta\mathbf{c}$ in position of the guiding center after one rotation. \mathbf{o}_1 and \mathbf{o}_2 are the guiding centers in the beginning and end of one rotation, respectively. | 87 |

| | | |
|-----|--|-----|
| 7.2 | Dynamics of nanorotor in the time span $[t, t + dt]$ (a) At time t the particle exhibits a stochastic orientational change of size $d\theta_{RND}$. A displacement of $d\mathbf{c} = \mathbf{r}_1 - \mathbf{r}_2$ is resulted in the instantaneous center of rotation. (b) During the time period $(t, t + dt)$, the particle does deterministic translational motion, leading to displacement of the center of mass by $d\mathbf{x} = \mathbf{r}_3 - \mathbf{r}_2$. (c) In the frame of reference of the guiding center, the nanorotor performs a deterministic displacement $d\mathbf{x}$ superimposed by stochastic displacement $d\mathbf{c}$ leading to a displacement $d\mathbf{p} = d\mathbf{x} - d\mathbf{c}$ on a circular path. | 89 |
| 7.3 | One dimensional powered random walkers (a) on an unbounded line, since the deterministic displacement scales with t while the stochastic part scales with $t^{\frac{1}{2}}$, on long run as $t \rightarrow \infty$, the deterministic dynamics dominates the total dynamic of the random walker. (b) Constraining the dynamics from unbounded line to the motion on a line segment with periodic boundary condition changes physics of the problem and introduce a natural time scale $2\pi\omega^{-1}$ depending on the length of the segment and velocity of the particle. This dynamic can be well represented by a powered random walker on a circular path with translational velocity v and angular velocity ω | 90 |
| 7.4 | Stochastic rotational dynamics of the nanorotor deviates its path from circular to quasi-circular. Simultaneously, after one rotation, the direction of velocity v_2 of the particle changes with respect to its initial direction v_1 | 108 |
| 7.5 | The diffusion $\frac{\langle \mathbf{p}(T_n) ^2 \rangle}{T_n}$ of powered random walker on a circle whose center is the guiding center. Increase in the time span, $T_n = 2\pi n$, over which the random walker moves, the diffusion on the circle reduces, approaching zero. | 109 |
| 7.6 | The functions, f_x (solid blue curve), and f_c (dashed red curve), multiplied by $\frac{\langle \mathbf{p}(T_n) ^2 \rangle}{T_n}$ show the deviation of $\frac{\langle \mathbf{x}(T_n) ^2 \rangle}{T_n}$ and $\frac{\langle \mathbf{c}(T_n) ^2 \rangle}{T_n}$ from the limiting value $4D_\infty$ | 110 |
| 7.7 | (a) The curves of $\langle \mathbf{x}(T_1) \rangle / T_1$ (dashed green), $\langle \mathbf{c}(T_1) \rangle / T_1$ (dotted blue), and $4D_\infty$ (red). (b) the same curve in more details near the peak. The maximum of $4D_\infty$ occurs at $\sigma^2 = 2$ | 110 |

- 7.8 The curves of $\frac{\langle |\mathbf{x}(T_1)|^2 \rangle}{T_1}$ (dashed red) and $4D_\infty$ (solid green) vs σ^2 . In the linear-linear plot (a) it seems as both curves almost fall over each other even for small values of σ^2 , however the log-linear plot (b) shows that for small values of σ^2 the two curves are distinct and after the peak for large values of σ^2 they coincide. (c) is the peak in more details and (d) is the region where the curves begin to coincide. (Inset: the linear-linear plot of the main log-linear plot.) 111
- 7.9 The curves of $\frac{\langle |\mathbf{c}(T_1)|^2 \rangle}{T_1}$ (dashed red) and $4D_\infty$ (solid green) vs σ^2 . The linear-linear (a) and log-linear (b) plots show that for small values the two curves coincide and near the peak dissociate. (c) is the peak in more details and (d) is the region where the curves take parts. (Inset: the linear-linear plot of the main log-linear plot.) . . 112
- 7.10 (Dotted blue) $C_{\Delta\mathbf{p}}(2)$ (Dashed red) $C_{\Delta\mathbf{x}}(2)$ (Solid Green) $C_{\Delta\mathbf{c}}(2)$. Both $C_{\Delta\mathbf{p}}(2)$ and $C_{\Delta\mathbf{c}}(2)$ go to -1 at large values of σ 114
- 7.11 $\Delta\mathbf{p}(1)$ can be written as the sum of two vectors $\Delta\mathbf{p}(1) = \mathbf{a} + \mathbf{b}$ where \mathbf{a} is a constant vector, and \mathbf{b} varies depending on the amount of the stochastic component of dynamics over one period. For large values of $\sigma \gg 1$ \mathbf{b} can achieve all the possible orientations. The average of $\Delta\mathbf{p}(2)$ given $\Delta\mathbf{p}(1)$ fixed, in this domain of σ is a vector that begins at the end of $\Delta\mathbf{p}(1)$ and ends at the center of the circle. Therefore, we have $\langle \Delta\mathbf{p}(2) \rangle_{\Delta\mathbf{p}(1)} = -\mathbf{b}$ 115

Acknowledgments

It gives me great pleasure to acknowledge those whose guidance contributed invaluable to the preparation and completion of this study. First and foremost, I offer my sincerest gratitude to my advisers, Professor Ali Borhan and Professor Vincent H. Crespi, whose patience, motivation, and immense knowledge, made this research a fascinating and fun scientific work to do. In addition, their dignity and integrity in approaching professional and academic conduct demonstrated for me the principles that should be the aim of the academic world.

It is with immense gratitude that I acknowledge the support and help of Dr. Paul E. Lammert, who mentored me on all aspects of my research and made this dissertation possible. Chapter 7 of this thesis is the result of our collaboration. It was my lifetime opportunity to be supervised by an extraordinarily knowledgeable, yet, extremely humble theoretical physicist. His courtesy and ethical principles proved me that such a combination is possible and I consider it an honor to have him as a role model to follow in my future academic career.

Besides my advisors and mentor, I would like to thank the rest of my dissertation committee: Professor James S. Vrentas, Professor Kristen A. Fichthorn, and Professor Thomas E. Mallouk, for reading this dissertation, their insightful comments and valuable questions. I would like to thank Young-Moo Byun for image analysis data, Jason M. Binz for his meticulous feedback, and all the others who have contributed in some small way, even without my notice, to this dissertation.

I am indebted to Professor Manouchehr Khorassani for advising me throughout my undergraduate studies and later, encouraging and supporting me to pursue my graduate studies. His help has been a life changer in my professional career. I am extremely thankful to Professor Nader Taheri Qazvini, whose advice and insightful comments have been always a valuable source of guidance in my academic life.

Last, but not least, I would like to thank my parents and brothers for cherishing me and their unconditional support. My parents receive my deepest gratitude and love for inculcating in me the dedication and discipline to be fair and act honorably in life challenges. It is my honor to carry their name as their son.

Dedication

To my beloved parents

Nanomotors and Nanorotors

1 Introduction and Background

The past decade has witnessed remarkable progress in powering at the nanoscale. Before that, biological systems at low Reynolds number were the focus of dynamics at micro- and nanoscales [1, 2, 3, 4, 5]. With rapid developments in nanotechnology and the need to power at these scales, researchers started to focus on ways to develop artificial systems that can convert different types of energy into mechanical energy at the nanoscale [6, 7, 8, 9, 10, 11, 12, 13, 14, 15, 16].

Ismagilov *et al* [17] pioneered the development of small scale artificial autonomous motors that could interact with each other. They fabricated millimeter-scale boats consisting of a hemicylindrical plate attached to a small platinum-covered glass. The motors floated on the air-liquid interface of an aqueous solution of hydrogen peroxide (see Fig. 1.1a). The platinum decomposed hydrogen peroxide catalytically according to $2\text{H}_2\text{O}_2 (\text{liquid}) \rightarrow \text{O}_2 (\text{gas}) + 2\text{H}_2\text{O} (\text{liquid})$, resulting in impulses of generated oxygen bubbles. This process led to motion of the boat away from the platinum-coated glass tail.

Subsequently, in an attempt to move from the millimeter scale to the nanoscale, Paxton *et al.* [18] fabricated half-gold/half-platinum bimetallic rods of about $2\ \mu\text{m}$ in length and $350\ \text{nm}$ in diameter and placed them in aqueous solution of hydrogen peroxide. The nanorods moved autonomously with speeds of $10 - 20\ \mu\text{m/s}$. Surprisingly, not only was there no bubble formation, but also the rods moved toward the platinum head. This scale-down and change in the composition of motors from

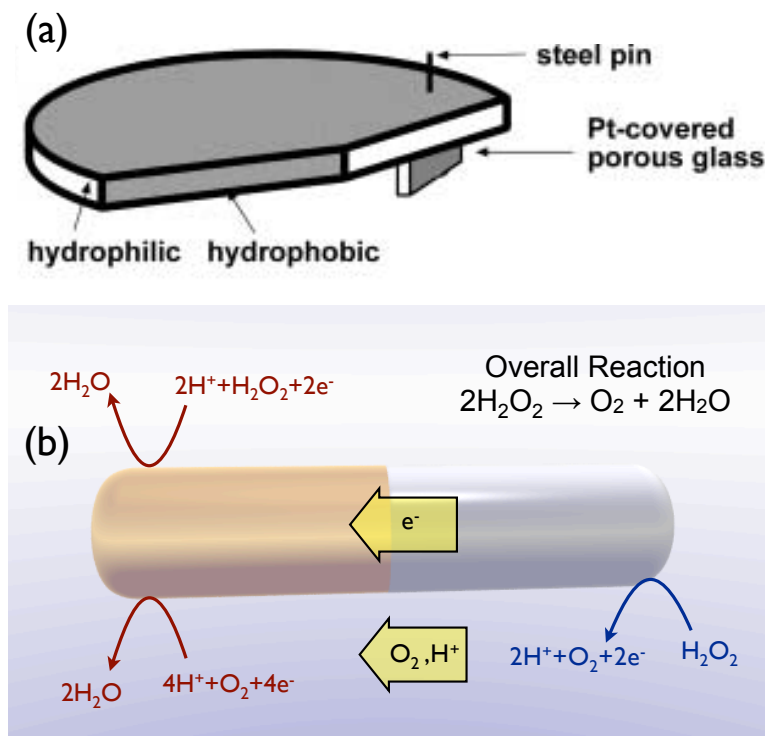


Figure 1.1. (a) The millimeter size boat with a platinum covered plate attached on underside. [17] The boat decomposes the hydrogen peroxide catalytically and the formation and releasing of bubbles results in impulses that push the boat in the direction opposite the platinum end. (b) The bimetallic nanorod [18] decomposes the hydrogen peroxide electrocatalytically through oxidation of hydrogen peroxide on the platinum side and reduction of oxygen molecules and hydrogen peroxide on the gold side. The asymmetric cloud of hydrogen ions pulls the negatively charged particle toward the platinum end.

single metallic to bimetallic structures had changed the direction of motion, revealing a change in the mechanism of motion. The development of these self-propelling colloidal particles gave birth to a fascinating new field in colloid science.

Among the many mechanisms proposed to explain the motion of the nanomotors [19, 20, 21, 22, 23], electrokinetic self-propulsion has proved to be an accurate/dominant mechanism [23, 24, 25, 26] for explaining the dynamics of the bimetallic nanomotors. A bimetallic nanorod and hydrogen peroxide solution comprise an electrochemical cell. As depicted in Fig. 1.1b, hydrogen ions are produced on the platinum side through anodic reaction, and are consumed on the gold side through cathodic reactions. An asymmetric cloud of ions forms around the nanomotor, which pulls the negatively charged particle toward the side with a

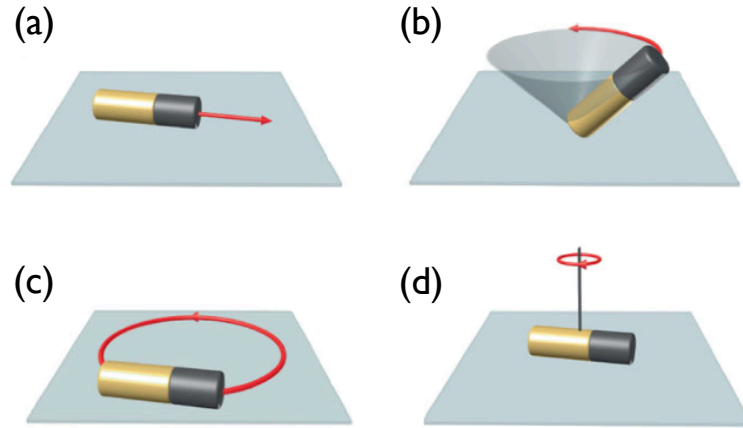


Figure 1.2. Different modes of nanorod motion (a) linear (b) rotary with one one end anchored to the substrate (c) rotating parallel to a substrate on a quasi- circular path. (d) fast rotors. (with modification from Ref [6])

higher concentration of hydrogen ions, i.e., the platinum end. The non-equilibrium state of the asymmetric cloud of ions is sustained by the continuous chemical reaction on the surface of the nanorod, and keeps the particle moving.

Up until recently, colloid scientists dealt with particles whose non-equilibrium state was imposed externally by imposed flow, gravity, electric field, concentration gradient of solutes, etc [27]. In this new motor system, however, the particles are active and transduce the chemical energy of their environment to mechanical energy, which has opened up fascinating possibilities, including the tantalizing possibility of mimicking the behavior of biological motors and microorganisms, or of programming artificial motors to perform specific tasks, such as carrying chemical cargo or engaging in complex collective behavior.

More recently, many research groups have focused on design, fabrication and enhancement of the performance of autonomous nanomotors. Spherical bimetallic Janus particles have been fabricated [28], expanding on the diversity of geometries of such systems. Different modes of motion for nanorods have been observed. Ozin et al [29] fabricated Au/Ni nanowires, anchored from the gold side to the substrate, that could perform rotary motion (Fig. 1.2b). Qin et al [30] fabricated Au/Pt nanorods that could rotate parallel to the substrate (Fig. 1.2c) with an angular velocity of about 23.7 rpm. Wang et al [31] reported ultrafast nanorotors (Fig. 1.2d) with one order of magnitude enhancement in the average angular

velocity to about 180 rpm.

Paxton *et al.* [18], in their aforementioned pioneering work, reported Au/Pt nanorods having linear deterministic motion coupled to Brownian stochastic dynamics on a glass substrate. This early generation of nanorods could move as fast as $10 - 20\mu\text{m/s}$ ($5 - 10$ body lengths per second). Incorporation of carbon nanotubes into the platinum side increased nanomotor speeds up to $50\mu\text{m/s}$ [32]. Further enhancement of dynamics was achieved by replacing the gold segment with cathodic silver/gold alloys leading to speeds of over $150\mu\text{m/s}$ [33] due to the higher rates of electron transfer reactions of hydrogen peroxide on these alloys. It was also observed that increasing the surface area of catalysts by roughening can increase the speed of bimetallic nanomotors [34]. Wang et al [24] observed that the direction of motion of the nanorod was toward the metal with the lower mixed potential (the potential at which anodic and cathodic reactions happen at the same rate for a specific metal). As the difference in the mixed potentials of the two metals in a nanomotor increased, the particle moved with higher speed. The order of mixed potentials of metals in their study was $\text{Rh} < \text{Pt} < \text{Ni} < \text{Pd} < \text{Au} < \text{Ru}$.

In order to control the dynamics of nanomotors or develop more efficient systems, it is essential to understand the principles underlying the dynamics of these species. This motivated us to develop mathematical models that could give more insight into the relationship between the performance of nanomotors and the parameters of the system. Such models not only give us the power of prediction, but also give more insight into the physics of the problem and can be used as a basis for further research in the field.

Moran *et al.* [26] examined electrokinetic self-propulsion by numerical calculation of a model system in which the surface reaction was modeled by the flux of hydrogen ions based on experimental data. The calculated range of velocities for the nanomotors was consistent with the experimental observations. They observed a linear relationship between the velocity of nanorods and both the flux of hydrogen ions and the interfacial electric potential on the surface of the particle.

Although experiments and computations illustrate the physics of the problem, they do not provide a complete understanding of the interplay between the physical parameters of the system. A standard approach for attaining such a knowledge is to use perturbation analysis in the limit of small values for the driving force in the

system. Yariv [23] used perturbation theory to relate the velocity of a spherical nanomotor (and slender body) to physical parameters of the system and kinetic parameters of a Butler-Volmer type reaction of hydrogen peroxide on the surface of the nanomotor. In our study, we use a more general approach by solving the problem for spherical and spheroidal nanomotors based on a general form of the distribution of hydrogen ion flux of the surface on the nanomotor.

In addition to linear nanomotors, we will study the dynamics of nanorotors. Nanorotors are a specific class of nanomotors that perform deterministic circular motion coupled to stochastic Brownian motion, leading to motion on quasi-circular orbits. To date, most modeling efforts have focussed on clarifying the mechanisms of linear motion in axisymmetric nanomotors. However, the large class of recently developed colloidal *rotary* motors remains largely unexplored. Here, we provide a fundamental theory for driven nano/micro-scale rotary motion in fluids at low Reynolds number and explain how to infer important aspects of motor function – i.e. force and torque distributions – directly from an analysis of the rotor trajectory.

2 The scope of the thesis

In chapter 2 we explain the physics of electrokinetic self-propulsion and formulate a mathematical model for the problem. In chapter 3, we apply the method of matched asymptotic expansions to solve the model for the velocity of a spherical nanomotor in the limit of small Debye length and small intensity of hydrogen ion flux. The resulting expression explains the relationship between the nanomotor velocity and background concentration, interfacial potential, hydrogen ion flux, diffusivity of hydrogen ion, etc. We further study the effect of geometry and distribution of hydrogen ion flux on the performance of the nanomotor.

In chapter 4, we solve the electrokinetic model for a spheroidal particle. The more general analysis presented in this chapter has the advantage that by changing eccentricity from zero to one we can model a range of geometries from a sphere to a rod. The result is similar to the case of a spherical particle up to a geometrical coefficient which in the limit of zero eccentricity reduces to the geometrical factor of a sphere.

In chapter 5, we examine the application of scaling analysis to derive an equa-

tion for the nanomotor velocity. We observe that this result is misleading in representing the relationship between the nanomotor velocity and some parameters of the system. Based on the results of previous chapters, we discuss the motion of the particle in more detail, stating the the range of validity of the perturbation analysis, and bring up issues that need to be considered in designing nanomotors.

Motion at the micro- and nanoscale is characterized by two main features: (1) irreversibility of deterministic dynamics at low Reynolds number and (2) stochastic Brownian dynamics. In chapter 6, we study the deterministic and stochastic dynamics of nanorotors. We show that the deterministic motion of a nanorotor is along a circular path. The contribution of the stochastic component to the dynamics of the nanorotor results in deviation of the trajectory from a circular to a quasi-circular path.

In chapter 7, we study the coupling between deterministic and stochastic dynamics of nanorotors within the context of powered random walkers. We show the long time behavior of nanorotors resulting from a combination of their deterministic and stochastic dynamics manifests itself in the form of an effective translational diffusion. We examine the importance of this effective diffusion compared to the natural translational diffusion of unpowered nanorotors to identify the contribution of powered motion to the translational dynamics of the nanorotors.

In chapter 8, we suggest future research ideas that have not been studied in this thesis.

Electrokinetic Self-Propulsion; Concepts and Modeling

1 Introduction

Any molecule in the bulk of a simple liquid experiences the same interaction forces that other molecules in that liquid experience. This results in a homogeneous isotropic structure in the liquid. However, the liquid molecules near the wall of the liquid's container experience a different form of force field than the molecules in the bulk, because the type of interaction between the liquid molecules is different from liquid and solid molecules. Therefore, the structure of the liquid and the orientation of molecules near the wall are different from those in the bulk. Liquid electrolytes form more complicated molecular structures when the liquid is brought in contact with a particle surface or wall.

An electrolyte consists of positive and negative ions i with charge z_i and a background concentration \mathcal{C}_∞ . The ions organize so that the chemical potential

$$\mu_i = k_B T \ln \frac{\mathcal{C}_i}{\mathcal{C}_\infty} + z_i e \phi \quad (2.1)$$

of each species i is constant everywhere in the fluid (k_B is the Boltzmann constant, e is the charge of a proton, and T is the absolute temperature). This leads to a uniform concentration \mathcal{C}_i of ionic species and constant electric potential ϕ in

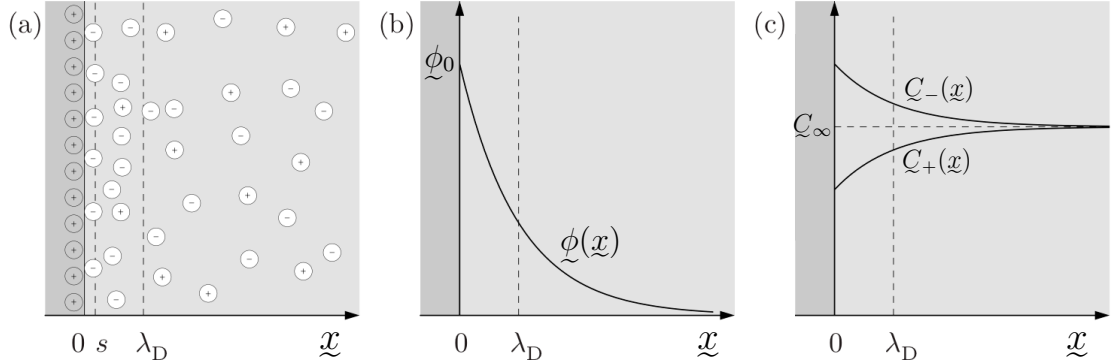


Figure 2.1. (a) The distribution of positive and negative ions of a binary symmetric electrolyte in contact with an infinite flat plate at thermal equilibrium. The ions in the stern layer $0 < x < s$ are immobile. The ions are mobile in the diffuse layer $s < x < \lambda_D$ (b) Most of the electric potential is screened out over the diffuse layer. (c) The charge density in the double layer is non-zero. (with modification from [35])

the bulk of the liquid. When the ionic solution is brought into contact with a charged surface, the ions reorganize to reach equilibrium such that $\nabla \mu_i = 0$. For an infinite flat plate in contact with a binary symmetric electrolyte $z = z_+ = -z_-$, this condition leads to

$$\mathcal{Q}_\pm = \mathcal{Q}_\infty \exp\left(\mp \frac{zF}{RT} \phi\right) \quad (2.2)$$

where F is the Faraday constant and R is the universal gas constant. The ions form a double layer near the wall, which screens out the electric potential over a length scale λ_D , called the Debye length. There is a layer of counter-ions that stick to the wall and neutralize the charge on the plate. This immobilized layer is called Stern layer. The ions outside this layer are mobilized in a layer whose thickness is of the order of the Debye length, called the diffuse layer.

The Poisson-Boltzmann equation relates the charge density to the electric potential,

$$\nabla^2 \phi = 2 \frac{zR\mathcal{Q}_\infty}{\epsilon} \sinh\left(\mp \frac{zF}{RT} \phi\right). \quad (2.3)$$

Integrating this equation with boundary conditions $\phi(x=0) = \phi_0$ and $\phi(x \rightarrow \infty) = 0$ gives the Gouy-Chapmann equation

$$\phi(x) = \frac{4RT}{zF} \tanh^{-1} \left[\tanh\left(\frac{zF\phi_0}{4RT}\right) \exp\left(-\frac{x}{\lambda_D}\right) \right] \quad (2.4)$$

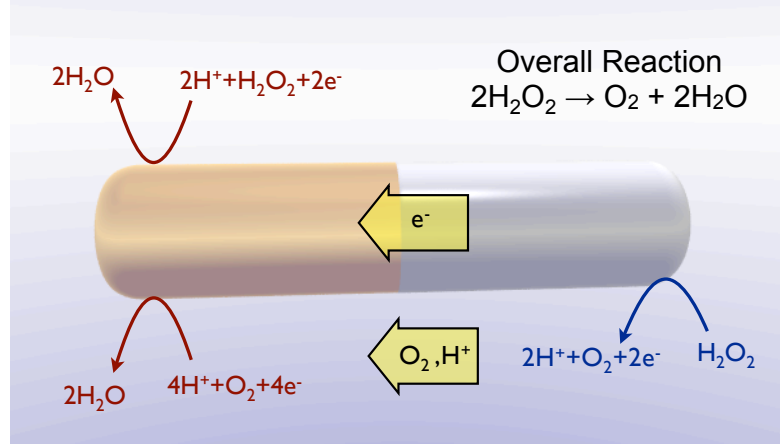


Figure 2.2. Due to asymmetric electrocatalytic decomposition of hydrogen peroxide, hydrogen ions are produced on the anode surface (source) and consumed on the cathode surface (sink). The phenomena can be modeled as source and sink of hydrogen using a position dependent flux of hydrogen ions.

where

$$\lambda_D = \sqrt{\frac{\epsilon RT}{2C_\infty z^2 F^2}} \quad (2.5)$$

is the Debye length based on the physical parameters of the system.

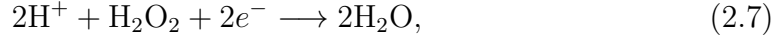
A bimetallic nanomotor and a solution of hydrogen peroxide constitute an electrochemical cell. In the next section, we discuss the physics of electrokinetic self-propulsion and the importance of the double layer and Debye length in the formulated mathematical model.

2 Electrokinetic self-propulsion

Electrocatalytic bimetallic nanomotors are made out of two different metals that can decompose hydrogen peroxide through an electrochemical mechanism. The connected metals in hydrogen peroxide solution act like an electric pile where H_2O_2 is used as a fuel. There are three main electrokinetic reactions (see Fig (2.2)); oxidation of hydrogen peroxide



happens at anode, and reduction of hydrogen peroxide



and reduction of oxygen



occur at the cathode. The overall reaction



can take part non-electrocatalytically (catalytically) on the surface of both metals with different rates. The overall reaction doesn't contribute the the concentration of hydrogen ions in the solution and we are mainly concerned with the electrocatalytic reactions.

The asymmetric electrocatalytic decomposition of hydrogen peroxide results in the production (source) of hydrogen ions at the anode and the consumption (sink) on the cathode. This source-sink process can be represented by a position dependent flux of hydrogen ions on the surface of the nanomotor. At steady state, there will be an excess of hydrogen ions compared to the background concentration. The same amount, but with negative charge, of electrons will be accumulated in the nanorod following the principle of charge neutrality.

After placing the nanomotor in water, it absorbs some ions from the aqueous media and acquires a negative interfacial potential. Addition of hydrogen peroxide to the system results in a further negative charge on the particle at steady state. The asymmetric flux of hydrogen ions results in an asymmetric distribution of ions around the particle, and consequently, an electric field pointing from the anode to the cathode. The negatively charged particle moves towards the anode side under the electric field.

This propulsion mechanism works through the non-equilibrium state of the ionic cloud around the nanomotor. At each instance, the negatively charged particle and the positive cloud of ions move toward each other in order to reach mechanical equilibrium in which the net force acting on charged entities is zero. However, the

asymmetric electrochemical reactions preserve the shape of the asymmetric cloud of ions as nanomotors moves toward the anode side and consequently keeps the system out of mechanical equilibrium.

Hydrogen ions can electrodiffuse toward the sink from the source or background. They can also move as a part of bulk flow due to an electrostatic body force acting on a charged fluid and pulls it toward the sink. Momentum is conserved in these processes.

3 Formulation of the Model

Our model consists of a conductive axisymmetric particle in a symmetric binary electrolyte of positive (+) and negative ions (-) with charges z_+ and z_- ($z = z_+ = -z_-$) and diffusion coefficients D_+ and D_- , respectively. The particle, consisting of two different catalytic metals, decomposes hydrogen peroxide electrochemically through surface reactions. Part of the nanomotor acts as the source and the other acts as the sink of hydrogen ions. The normal component of the flux of hydrogen ions on the surface is represented by $\hat{\mathbf{n}} \cdot \mathbf{J}_+ = j_p f(\mathbf{x})$ where j_p is a measure of hydrogen peroxide that decomposes electrochemically and $f(\mathbf{x})$ represents the distribution of flux over the surface. The particle is impermeable to negative ions: $\hat{\mathbf{n}} \cdot \mathbf{J}_- = 0$. An asymmetric distribution of positive ions is produced around the particle. At the steady state, the production and consumption of positive ions will be equal. This imposes the constraint

$$\int_{\underline{S}} d\underline{s} f(\mathbf{x}) = 0 \quad (2.10)$$

on the surface distribution of hydrogen ion flux.

The metallic particle in aqueous solution attracts ions and acquires a negative surface potential. Adding hydrogen peroxide to the system initiates the electrochemical reactions, which in part, adds to the negative surface potential on the particle's surface. The electric potential Φ is ϕ on the surface of the particle and vanishes at infinity. The Poisson equation relates the distribution of ions in solution

to the local electric potential Φ ,

$$\nabla^2 \Phi = -F(z_+ \mathcal{C}_+ + z_- \mathcal{C}_-) / \epsilon \quad (2.11)$$

where F is the Faraday constant, \mathcal{C}_+ is the molar concentration of hydrogen ions, \mathcal{C}_- is the molar concentration of negative ions and ϵ is the permittivity of the solution. For the symmetric binary electrolyte in our model, $z = z_+ = -z_-$ is the absolute value of charge on each ion. The asymmetric distribution of ions is the result of asymmetric production and consumption of hydrogen ions on the surface while negative ions do not participate in any reaction. The ionic flux is related to ion concentration and electric potential via

$$\underline{\mathbf{J}}_{\pm} = -D_{\pm}(\nabla \mathcal{C}_{\pm} + \frac{Fz_{\pm}}{RT} \mathcal{C}_{\pm} \nabla \Phi) \quad (2.12)$$

in which D_+ is the diffusion coefficient of hydrogen ions, D_- is the diffusion coefficient of negative ions, R is the universal gas constant and T is the absolute temperature. The conservation of species leads to the steady state Nernst-Planck equation

$$\nabla \cdot \underline{\mathbf{J}}_{\pm} + \underline{\mathbf{U}} \cdot \nabla \mathcal{C}_{\pm} = 0 \quad (2.13)$$

where $\underline{\mathbf{U}}$ is the velocity field of the fluid.

The local electric field acts on ions and consequently applies forces to the fluid element containing the ions. This leads to the flow of fluid around the nanomotor. As we are in the regime of low Reynolds number, this flow is represented by the Stokes equation,

$$-\nabla \underline{\mathcal{P}} + \mu \nabla^2 \underline{\mathbf{U}} + \epsilon \nabla^2 \Phi \nabla \Phi = 0 \quad (2.14)$$

where $\underline{\mathcal{P}}$ is the pressure and μ is the viscosity of the fluid. Finally, assuming an incompressible fluid, the continuity equation gives

$$\nabla \cdot \underline{\mathbf{U}} = 0 \quad (2.15)$$

Let's define $D_s = \min(D_+, D_-)$, and $\delta_{\pm} = D_s / D_{\pm}$. To proceed further, we work in units of length

$$\underline{\mathbf{x}}^* = a, \quad (2.16)$$

concentration

$$\underline{C}^* = \underline{C}^\infty, \quad (2.17)$$

flux

$$\underline{J}^* = D_s \underline{C}^\infty / a, \quad (2.18)$$

electric potential

$$\underline{\Phi}^* = RT/zF, \quad (2.19)$$

pressure

$$\underline{P}^* = \underline{\Phi}^{*2}/a^2, \quad (2.20)$$

and velocity

$$\underline{U}^* = \epsilon \underline{\Phi}^{*2}/\mu a. \quad (2.21)$$

We also define the Peclet number

$$Pe = \underline{U}^* a / D_s \quad (2.22)$$

as the ratio of characteristic time of diffusion over the characteristic time of convection. In the regime of low Peclet number, where the diffusion transport dominates the convective transport, the convective term in the Nernst-Planck equation becomes negligible. We also define the Debye length

$$\lambda_D = \sqrt{\frac{\Phi^* \epsilon}{2zF C^\infty}} \quad (2.23)$$

as the length scale over which the electric potential is significantly screened out.

Using the dimensionless Debye length $\lambda = \lambda_D/a$ and the dimensionless strength of hydrogen ions flux $j_p = j_p/J^*$ the above mentioned equations take the dimensionless forms

$$2\lambda^2 \nabla^2 \Phi = -(C_+ - C_-) \quad (2.24)$$

$$\mathbf{J}_\pm = -\delta_\pm^{-1} (\nabla C_\pm \pm C_\pm \nabla \Phi) \quad (2.25)$$

$$\nabla \cdot \mathbf{J}_\pm + Pe \mathbf{U} \cdot \nabla C_\pm = 0 \quad (2.26)$$

$$-\nabla P + \nabla^2 \mathbf{U} + \nabla^2 \Phi \nabla \Phi = 0 \quad (2.27)$$

$$\nabla \cdot \mathbf{U} = 0 \quad (2.28)$$

with boundary conditions on the surface of the particle

$$\hat{\mathbf{n}} \cdot \mathbf{J}_+ = j_p f(\mathbf{x}) \quad (2.29)$$

$$\hat{\mathbf{n}} \cdot \mathbf{J}_- = 0 \quad (2.30)$$

$$\Phi = \phi \quad (2.31)$$

$$\mathbf{U} = 0 \quad (2.32)$$

and boundary conditions at infinity ($r = \infty$)

$$C_{\pm} = 1 \quad (2.33)$$

$$\Phi = 0 \quad (2.34)$$

$$\mathbf{U} = -\mathcal{U} \quad (2.35)$$

In the next section, we solve these nonlinear equations through perturbation analysis [36] to the leading order in dimensionless Debye length and first order in the dimensionless strength of hydrogen ions flux.

4 Perturbation Analysis

Perturbation analysis provides a controlled approximation to solve nonlinear equations in the regime of small parameters [36]. Regular perturbation analysis is applied in systems where the leading order behavior of the equation does not change the nature of the equation. In situations where the small parameter is multiplied by the highest order of derivative in the equation, the equation to the leading order in the small parameter loses its highest order. In such systems in the domain of study may be a small region(s) wherein the highest derivative is large such that it compensates for the small parameter. The domain of study is then divided into an inner region (boundary layer), where we have fast change in the field, and an outer region where the small parameter dominates the higher derivative.

In the set of governing equations, the dimensionless Debye length is multiplied by the laplacian of electric potential, which is the highest order of the derivative in

that equation. The dimensionless flux of hydrogen ions appears in the boundary condition and the equations, to the leading order in j_p , doesn't lose its nature. In what follows, we first use singular perturbation for small dimensionless Debye length $\lambda \ll 1$ to calculate for slip velocity around the particle. We further apply regular perturbation to the first order in small dimensionless flux of hydrogen ions $j_p \ll 1$ to linearize the equations further and solve for the velocity of the particle.

In equation (2.24) λ^2 is multiplied by $\nabla^2\Phi$. While $\lambda^2\nabla^2\Phi$ can be zero to the leading order in λ in the majority of the domain of study, near the surface of the particle, this term can be of order one due to rapid change in Φ . We divide the domain into an inner domain near the surface where the radial change in electric potential is fast enough for $\lambda^2\nabla^2\Phi$ to be of order one, and an outer domain where this term vanishes to the leading order in λ^2 . All the fields match at some transition region between the inner and outer region. We identify the fields in the inner and the outer regions by superscripts i and o , respectively.

Spherical Nanomotor

1 Introduction

The sphere is the simplest geometry in colloid science. It is both isotropic and symmetric. Classically, problems involving the motion of particles in a fluid are first solved for a spherical particle. In this chapter, we solve the equations governing electorokinetic self-propulsion for a spherical nanomotor in spherical coordinates, where each point is characterized by (r, θ, φ) . For an axisymmetric spherical nanomotor, the physics is independent of the azimuth angle φ .

2 The Governing Equation

In chapter 2 we discussed the physics of electorokinetic self-propulsion and formulated a mathematical model with some governing equations and their boundary conditions that explain the interactions between a nanomotor and its surrounding fluid and ions. In this chapter, we would like to solve the model for the velocity of the nanomotor in the domain of thin Debye layer and to the first order in the intensity of hydrogen ion flux. The radius of the sphere is used as the characteristic length scale in this problem. In order to use the method of matched asymptotic expansion, we work with dimensionless equations in the frame of reference of the particle. The flow field is explained by the Stoke's equation,

$$-\nabla P + \nabla^2 \mathbf{U} + \nabla^2 \Phi \nabla \Phi = 0. \quad (2.27)$$

and the continuity equation

$$\nabla \cdot \mathbf{U} = 0 \quad (2.28)$$

where on the surface of the particle we have no slip boundary condition

$$\mathbf{U}(r = 1) = 0 \quad (2.32)$$

and far field unperturbed velocity field is

$$\mathbf{U}(r \rightarrow \infty) = -\mathcal{U} \quad (2.35)$$

in which \mathcal{U} is the nanomotor velocity in the laboratory frame of reference. The body force $\nabla^2\Phi\nabla\Phi$ in the Stokes equation depends on the electric potential Φ . The Poisson equation relates the the electric potential to the concentration of positive C_+ and negative C_- ions in the electrolyte,

$$2\lambda^2\nabla^2\Phi = -(C_+ - C_-). \quad (2.24)$$

where λ is the dimensionless Debye length. The electric potential on the equipotential surface of the conductive nanomotor is

$$\Phi(r = 1) = \phi, \quad (2.31)$$

and at far distances,

$$\Phi(r \rightarrow \infty) = 0. \quad (2.34)$$

The motion of the ions in the electrolyte is governed by the equations of continuity of species

$$\nabla \cdot \mathbf{J}_{\pm} + Pe \mathbf{U} \cdot \nabla C_{\pm} = 0 \quad (2.26)$$

in which

$$\mathbf{J}_{\pm} = -\delta_{\pm}^{-1}(\nabla C_{\pm} \pm C_{\pm}\nabla\Phi) \quad (2.25)$$

are the molar fluxes of the positive and the negative ions and the Peclet number Pe is the ratio of characteristic time of diffusion over the characteristic time of

convection. The nanomotor surface is impermeable to negative ions

$$\hat{\mathbf{n}} \cdot \mathbf{J}_- \Big|_{r=1} = 0 \quad (2.30)$$

and the flux of positive ions is asymmetrically distributed over the surface in the form of

$$\hat{\mathbf{n}} \cdot \mathbf{J}_+ \Big|_{r=1} = j_p f(\mathbf{x}) \quad (2.29)$$

where $f(\mathbf{x})$ is a general function whose definition depends on the physics of the problem and the prefactor j_p is the dimensionless strength of positive ion flux on the surface of the sphere. For the axisymmetric spherical nanomotor, we represent the position dependence of distribution function $f(\mathbf{x})$ by $f(\cos\theta)$. We will work in the domain of $j_p \ll 1$ and since this second small parameter appears in the boundary condition, we will apply regular perturbation analysis for j_p . At far distances, the electro-neutrality condition for the electrolyte holds and we have

$$C_{\pm}(r \rightarrow \infty) = 1. \quad (2.33)$$

3 Perturbation Analysis

We would like to solve the governing equation in the limit of small dimensionless Debye length λ and small dimensionless strength of hydrogen ions flux j_p .

3.1 Singular Perturbation

In the Poisson equation (2.24), the small parameter λ is multiplied by the highest derivative $\nabla^2\Phi$ in the equation. Therefore, near the surface of the particle there is a region where the change in the electric potential is high enough to compensate for the smallness of λ and their product is of order one. We call this region the boundary layer or inner region (see Fig. 3.1). The remainder is called the outer region where to the leading order in λ the term $\lambda^2\nabla^2\Phi$ vanishes. There is a region at the end of inner region and the beginning of the outer region where the solution of these two region matches.

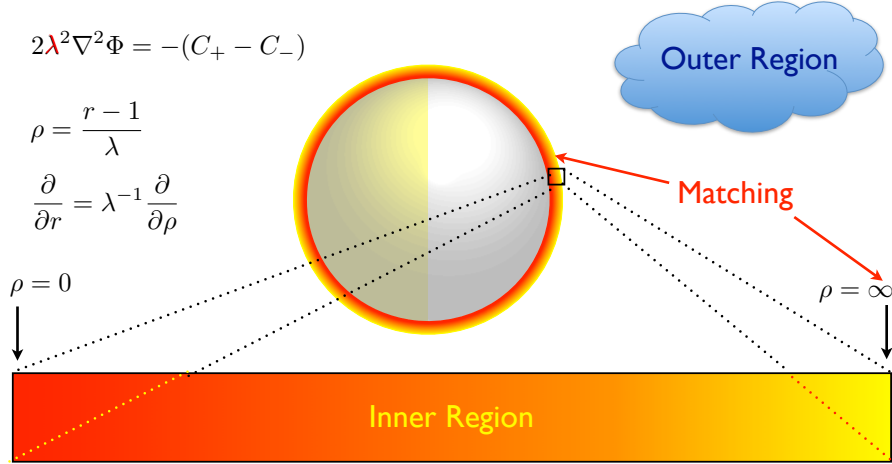


Figure 3.1. The fluid around the particle is divided to an inner region, where the high variation in the electric potential compensates for the smallness of λ^2 , and an outer region. By changing the variable from r to ρ , we expand the inner region. Matching of the inner and the outer solutions happens at the boundary of inner and outer regions.

3.1.1 Inner Region Near The Particle Surface

To capture the rapid radial variation of electric potential in the thin boundary layer of thickness $\mathcal{O}(\lambda)$ at the surface of the particle, we stretch the domain using the transformation

$$\rho = \frac{r-1}{\lambda}, \quad (3.1)$$

$$r = 1 + \lambda\rho, \quad (3.2)$$

$$\partial_r = \lambda^{-1} \partial_\rho. \quad (3.3)$$

For the fields in this inner region, we can write asymptotic expansions of the form

$$G^i = \sum_{n=n_0}^{\infty} \lambda^n G^{i(n)} \quad (3.4)$$

where $n_0 = -2$ for P^i , $n_0 = -1$ for $J_{\pm\rho}$, $n_0 = 0$ for C_{\pm} , Φ , $J_{\pm\theta}$, ϕ , \mathcal{U} and U_θ , and $n_0 = 1$ for U_ρ .

Our main goal in this section is to calculate the slip velocity $U_{slip}^{(0)}$ to the leading order in λ . To do this, we need to calculate the angular component of velocity $U_\theta^{i(0)}$ to the leading order in λ in the inner region, and evaluate it at the end of the inner layer, that is, $U_{slip}^{(0)} = \lim_{\rho \rightarrow \infty} U_\theta^{i(0)}$. To calculate $U_\theta^{i(0)}$ we use the angular

component of the Stokes' flow to the order $\mathcal{O}(\lambda^{-2})$,

$$-\partial_\theta P^{i(-2)} + \partial_\rho^2 U_\theta^{i(0)} + \partial_\theta \Phi^{i(0)} \partial_\rho^2 \Phi^{i(0)} = 0. \quad (3.5)$$

To solve this equation, we need to have a relation for the pressure $P^{i(-2)}$ and the electric potential $\Phi^{i(0)}$. We use the radial component of the Stokes' equation to the order $\mathcal{O}(\lambda^{-3})$,

$$-\partial_\rho P^{i(-2)} + \frac{1}{2} \partial_\rho (\partial_\rho \Phi^{i(0)} \partial_\rho \Phi^{i(0)}) = 0 \quad (3.6)$$

which relates the pressure to the electric potential. To find $\Phi^{i(0)}$, we use the Poisson equation to the order $\mathcal{O}(\lambda^0)$,

$$\partial_\rho^2 \Phi^{i(0)} = - \left(C_+^{i(0)} - C_-^{i(0)} \right) / 2. \quad (3.7)$$

For solving this equation, we need the concentration of the position and the negative ions. The order $\mathcal{O}(\lambda^{-2})$ of the continuity of the species equation gives us

$$\partial_\rho J_{\pm\rho}^{i(-1)} = 0 \quad (3.8)$$

in which the ion fluxes are

$$J_{\pm\rho}^{i(-1)} = -\delta_\pm^{-1} \left[\partial_\rho C_\pm^{i(0)} \pm C_\pm^{i(0)} \partial_\rho \Phi^{i(0)} \right]. \quad (3.9)$$

Also, we would like to know how the leading order fluxes $J_{\pm\rho}^{i(0)}$ of the positive and the negative ions behave in the inner region and match to the outer region at the matching region. We use the continuity of species to the order $\mathcal{O}(\lambda^{-1})$,

$$\partial_\rho J_{\pm\rho}^{i(0)} + 2J_{\pm\rho}^{i(-1)} = 0. \quad (3.10)$$

For the boundary condition at the surface of the sphere ($\rho = 0$), we have

$$U_\theta^{i(0)} = 0, \quad (3.11)$$

$$\Phi^{i(0)} = \phi^{(0)}, \quad (3.12)$$

$$J_{+\rho}^{i(-1)} = J_{-\rho}^{i(-1)} = J_{-\rho}^{i(0)} = 0, \quad (3.13)$$

and

$$J_{+\rho}^{i(0)} = j_p f(\cos \theta). \quad (3.14)$$

3.1.2 Outer region

In the outer region, we can write asymptotic expansions of the form

$$G^o = \sum_{n=0}^{\infty} \lambda^{2n} G^{o(2n)}. \quad (3.15)$$

for the independent variables and boundary conditions since λ^2 is the small parameter appearing in the governing equations. We would like to calculate the nanomotor velocity $\mathcal{U}^{(0)}$ to the leading order in λ . To do this, we need to solve the Stokes' equation to the order $\mathcal{O}(\lambda^0)$ in the frame of reference of particle,

$$-\nabla P^{o(0)} + \nabla^2 \mathbf{U}^{o(0)} + \nabla \Phi^{o(0)} \nabla^2 \Phi^{o(0)} = 0 \quad (3.16)$$

with the far field, $r \rightarrow \infty$, boundary condition

$$\mathbf{U}^{o(0)} = -\mathcal{U}^{(0)} \hat{\mathbf{z}} \quad (3.17)$$

The Poisson equation to the leading order in λ^2 leads to electroneutrality condition in the outer region

$$C_+^{o(0)} - C_-^{o(0)} = 0 \quad (3.18)$$

subjected to far field boundary condition

$$C_{\pm}^{o(0)} = 1. \quad (3.19)$$

Finally, the motion of ions is governed by the continuity of species

$$\nabla \cdot \mathbf{J}_{\pm}^{o(0)} + Pe \mathbf{U}^{o(0)} \cdot \nabla C_{\pm}^{o(0)} = 0 \quad (3.20)$$

where

$$J_{\pm r}^{o(0)} = -\delta_{\pm}^{-1} \left[\partial_r C_{\pm}^{o(0)} \pm C_{\pm}^{o(0)} \partial_r \Phi^{o(0)} \right] \quad (3.21)$$

is the flux of ions to the leading order in λ^2 . The far field ($r \rightarrow \infty$) boundary conditions are

$$\nabla\Phi^{o(0)} = 0 \quad (3.22)$$

$$\mathbf{J}_{\pm}^{o(0)} = 0 \quad (3.23)$$

3.2 Slip Velocity

In the previous two sections, we presented the appropriate governing equation and their boundary conditions for calculating the nanomotor velocity to the leading order in λ . By solving the equations in the inner and the outer region, and matching the the solutions, we can calculate the nanomotor velocity. In this section, however, we lump all the flow properties of the inner layer into the slip velocity, and in the next section, we will use it as a boundary condition on the surface of the particle for flow field in the outer region.

Equation (3.18) states the electro-neutrality condition to the leading order in λ in the outer region.

$$C_+^{o(0)} = C_-^{o(0)} \equiv C^{o(0)} \quad (3.24)$$

Since we have an electro-neutrality condition at the beginning of the outer region, the same condition holds at the end of the inner region, due to the matching criteria. We represent the concentration of ions at the end of the inner region and beginning of the outer region by

$$C^{o(0)}(1, \theta) \equiv \lim_{r \rightarrow 1} C^{o(0)}(r, \theta) = \lim_{\rho \rightarrow \infty} C_{\pm}^{i(0)}(\rho, \theta), \quad (3.25)$$

that is, to the leading order in λ , as we approach the end of the inner region, the concentration of the positive ions and negative ions become equal to $C^{o(0)}(1, \theta)$.

We also represent

$$\Phi^{o(0)}(1, \theta) \equiv \lim_{r \rightarrow 1} \Phi^{o(0)}(r, \theta) = \lim_{\rho \rightarrow \infty} \Phi^{i(0)}(\rho, \theta) \quad (3.26)$$

as the matching value of the inner $\Phi^{i(0)}$ and outer $\Phi^{o(0)}$ electric potentials to the leading order in λ . The equations for the continuity of species in the inner region (3.8) to the order $\mathcal{O}(\lambda^2)$ can be integrated, along with the zero boundary condition

for ion flux of order $\mathcal{O}(\lambda^{-1})$ at the surface of the particle, $j_{\rho\pm}^{i(-1)}(0) = 0$, to yield

$$\partial_\rho C_\pm^{i(0)} \pm C_\pm^{i(0)} \partial_\rho \Phi^{i(0)} = 0. \quad (3.27)$$

Integrating this equation, considering the matching conditions (3.25) for $C_\pm^{(0)}$ and (3.26) for $\Phi^{(0)}$, we obtain

$$C_\pm^{i(0)}(\rho, \theta) = C^{o(0)}(1, \theta) \exp [\mp (\Phi^{i(0)}(\rho, \theta) - \Phi^{o(0)}(1, \theta))] \quad (3.28)$$

The Poisson equation (3.7) then takes the form

$$\begin{aligned} \partial_\rho^2 \Phi^{i(0)} &= - \left(C_+^{i(0)} - C_-^{i(0)} \right) / 2 \\ &\equiv C^{o(0)}(1, \theta) \sinh [\Phi^{i(0)}(\rho, \theta) - \Phi^{o(0)}(1, \theta)]. \end{aligned} \quad (3.29)$$

Defining

$$\psi(\rho, \theta) = \Phi^{i(0)}(\rho, \theta) - \Phi^{o(0)}(1, \theta), \quad (3.30)$$

the nonlinear Poisson-Boltzmann equation (3.29) takes the form

$$\partial_\rho^2 \psi = C^{o(0)}(1, \theta) \sinh \psi. \quad (3.31)$$

Keeping in mind that in the inner region ψ is negative and $\partial_\rho \psi$ is positive, using the identity $\partial_\rho (\partial_\rho \psi)^2 = 2 \partial_\rho \psi \partial_\rho^2 \psi$, we integrate the above equation to obtain

$$\partial_\rho \psi = -2 \sqrt{C^{o(0)}(1, \theta) \sinh(\psi/2)}. \quad (3.32)$$

where we have used the matching condition for the radial component of the electric field E_r of order $\mathcal{O}(\lambda^{-1})$,

$$\lim_{r \rightarrow 1} E_r^{o(-1)} = 0 = \lim_{\rho \rightarrow \infty} E_\rho^{i(-1)} = \lim_{\rho \rightarrow \infty} \partial_\rho \Phi^{i(0)} \equiv \lim_{\rho \rightarrow \infty} \partial_\rho \psi. \quad (3.33)$$

Further integration gives us

$$\tanh \frac{\psi}{4} = \tanh \frac{\psi_0}{4} e^{-\rho \sqrt{C^{o(0)}(1, \theta)}} \quad (3.34)$$

where

$$\psi_0(\theta) = \Phi^{i(0)}(0, \theta) - \Phi^{o(0)}(1, \theta) \equiv \phi^{(0)} - \Phi^{o(0)}(1, \theta). \quad (3.35)$$

is the potential drop across the inner layer. Recasting (3.34) yields the familiar Gouy-Chapman equation

$$\Phi^{i(0)}(\rho, \theta) = \Phi^{o(0)}(1, \theta) + 4 \tanh^{-1} \left[\tanh \left(\frac{\psi_0(\theta)}{4} \right) e^{-\rho \sqrt{C^{o(0)}(1, \theta)}} \right]. \quad (3.36)$$

The non-zero pressure in the outer region starts from the leading order in λ . Therefore, using the matching condition for the order $\mathcal{O}(\lambda^{-2})$ of pressure,

$$\lim_{r \rightarrow 1} P^{o(-2)}(r, \theta) = 0 = \lim_{\rho \rightarrow \infty} P^{i(-2)}(\rho, \theta) \quad (3.37)$$

and the matching condition (3.33) for $\mathcal{O}(\lambda^{-1})$ of the radial component of the electric field $\partial_\rho \Phi^{i(0)}$, we integrate the order $\mathcal{O}(\lambda^{-2})$ of the angular component of the Stokes' equation (3.6) to obtain

$$P^{i(-2)} = \frac{1}{2} (\partial_\rho \Phi^{i(0)})^2 \equiv \frac{1}{2} (\partial_\rho \psi)^2 \quad (3.38)$$

To calculate $U_\theta^{i(0)}$ and consequently the slip velocity, we substitute this equation into the radial component of Stokes equation of order $\mathcal{O}(\lambda^{-2})$, equation (3.5). Using the nonlinear Poisson-Boltzmann equations (3.31), equation (3.32) for the derivative of electric potential, the relation (3.38) for the pressure $P^{i(-2)}$, and the definition of ψ (3.30), we obtain

$$\partial_\rho^2 U_\theta^{i(0)} = 2 \sinh^2(\psi/2) \partial_\theta C^{o(0)}(1, \theta) - \partial_\theta \Phi^{o(0)}(1, \theta) \partial_\rho^2 \psi \quad (3.39)$$

Further integration, and using $\int_\rho^\infty \partial_\rho^2 U_\theta^{i(0)} d\rho = -\partial_\rho U_\theta^{i(0)}$, we obtain

$$\partial_\rho U_\theta^{i(0)} = -2 [\cosh(\psi/2) - 1] \frac{\partial_\theta C^{o(0)}(1, \theta)}{\sqrt{C^{o(0)}(1, \theta)}} - \partial_\theta \Phi^{o(0)}(1, \theta) \partial_\rho \psi \quad (3.40)$$

where we have used the matching condition for the order $\mathcal{O}(\lambda^{-1})$ of the radial

derivative of angular component of velocity,

$$\lim_{r \rightarrow 1} \partial_r U_\theta^{\alpha(-1)} = 0 = \lim_{\rho \rightarrow \infty} \partial_\rho U_\theta^{i(0)}. \quad (3.41)$$

Integrating equation (3.40) using the relation (3.34) and the no-slip boundary condition on the surface of the particle in the inner region, yields the angular component of the velocity to the leading order in λ in the inner region,

$$\begin{aligned} U_\theta^{i(0)} &= (\psi_0 - \psi) \partial_\theta \Phi^{\alpha(0)}(1, \theta) + 4\rho \frac{\partial_\theta C^{\alpha(0)}(1, \theta)}{\sqrt{C^{\alpha(0)}(1, \theta)}} \\ &\quad + 2\partial_\theta \ln [C^{\alpha(0)}(1, \theta)] \ln \left\{ \frac{1 - \tanh^2(\psi_0/4)}{\exp [2\rho \sqrt{C^{\alpha(0)}(1, \theta)}] - \tanh^2(\psi_0/4)} \right\} \end{aligned} \quad (3.42)$$

We can then calculate the slip velocity

$$\begin{aligned} U_{slip}^{(0)} &= \lim_{\rho \rightarrow \infty} U_\theta^{i(0)} \\ &= \psi_0 \partial_\theta \Phi^{\alpha(0)}(1, \theta) + 2 \ln \{1 - \tanh^2(\psi_0/4)\} \partial_\theta \ln [C^{\alpha(0)}(1, \theta)] \\ &= \psi_0 \partial_\theta \Phi^{\alpha(0)}(1, \theta) - 4 \ln \cosh(\psi_0/4) \partial_\theta \ln [C^{\alpha(0)}(1, \theta)]. \end{aligned} \quad (3.43)$$

This relation is equivalent to the Dukhin-Deryaguin slip formula, used as a slip boundary condition for the outer region.

Before proceeding to the physics in the outer region and calculating the velocity of the particle, we need to match the leading order radial fluxes $J_{\pm\rho}^{i(0)}$ and $J_{\pm r}^{\alpha(0)}$. From the order $\mathcal{O}(\lambda^{-1})$ of the continuity of the species equation (3.10) and the fact that $J_{\pm\rho}^{i(-1)} = 0$, we have

$$\partial_\rho J_{\pm\rho}^{i(0)} = 0 \quad (3.44)$$

So, $J_{\pm\rho}^{i(0)}$ is independent of the radial coordinate ρ in the inner region. The boundary condition on the surface of the particle leads to

$$J_{+\rho}^{i(0)}(\rho, \theta) = j_p f(\cos \theta) \quad (3.45)$$

and

$$J_{-\rho}^{i(0)}(\rho, \theta) = 0 \quad (3.46)$$

throughout the inner region. The matching condition

$$\lim_{\rho \rightarrow \infty} J_{\pm\rho}^{i(0)}(\rho, \theta) = \lim_{r \rightarrow 1} J_{\pm r}^{o(0)}(r, \theta)$$

then results in the following boundary conditions for the outer region:

$$J_{+r}^{o(0)}(r \rightarrow 1, \theta) = j_p f(\cos \theta), \quad (3.47)$$

and

$$J_{-r}^{o(0)}(r \rightarrow 1, \theta) = 0. \quad (3.48)$$

3.3 Regular Perturbation

We would like to solve the leading order equation of Stokes' flow for the nanomotor velocity. For this purpose we need to solve the leading order of the Stoke's equation in the outer region,

$$\nabla P^{o(0)} + \nabla^2 \mathbf{U}^{o(0)} + \nabla \Phi^{o(0)} \nabla^2 \Phi^{o(0)} = 0 \quad (3.16)$$

We can rewrite the leading order equations of the continuity of the species (3.20) in the form of two equations for positive and negative ions

$$-\nabla \cdot \left(\nabla C_{\pm}^{o(0)} \pm C_{\pm}^{o(0)} \nabla \Phi^{o(0)} \right) + \delta_{\pm} Pe \mathbf{U}^{o(0)} \cdot \nabla C_{\pm}^{o(0)} = 0. \quad (3.49)$$

Adding and subtracting these convection-diffusion equations for positive and negative ions, and using the fact that $C^{o(0)} \equiv C_+^{o(0)} = C_-^{o(0)}$, we obtain

$$\nabla^2 C^{o(0)} = \left(\frac{\delta_+ + \delta_-}{2} \right) Pe \mathbf{U}^{o(0)} \cdot \nabla C^{o(0)} \quad (3.50)$$

and

$$\nabla \cdot (C^{o(0)} \nabla \Phi^{o(0)}) = \left(\frac{\delta_+ - \delta_-}{2} \right) Pe \mathbf{U}^{o(0)} \cdot \nabla C^{o(0)} \quad (3.51)$$

with corresponding boundary conditions

$$\partial_r C^{o(0)} = C^{o(0)} \partial_r \Phi^{o(0)} = \delta_+ j_p \left[\frac{-1}{2} f(\cos \theta) \right] \quad r \rightarrow 1 \quad (3.52)$$

$$\partial_r C^{o(0)} = C^{o(0)} \partial_r \Phi^{o(0)} = 0 \quad r \rightarrow \infty \quad (3.53)$$

$$\mathbf{U}^{o(0)} = -\mathcal{U}^{(0)} \hat{\mathbf{z}} \quad r \rightarrow \infty \quad (3.54)$$

To proceed with the solution of the nonlinear set of equations we use a regular perturbation expansion in powers of the small parameter j_p to obtain the leading and first order equations. The expansions of the fields in powers of j_p are

$$C^{o(0)} = 1 + j_p C^{o(0,1)} + \mathcal{O}(j_p^2) \quad (3.55)$$

$$\Phi^{o(0)} = \Phi^{o(0,0)} + j_p \Phi^{o(0,1)} + \mathcal{O}(j_p^2) \quad (3.56)$$

$$\mathbf{U}^{o(0)} = j_p \mathbf{U}^{o(0,1)} + \mathcal{O}(j_p^2) \quad (3.57)$$

$$\phi^{(0)} = \phi^{(0,0)} + j_p \phi^{(0,1)} + \mathcal{O}(j_p^2) \quad (3.58)$$

$$\mathcal{U}^{(0)} = j_p \mathcal{U}^{(0,1)} + \mathcal{O}(j_p^2) \quad (3.59)$$

The leading order of the equation (3.51) with the boundary condition (3.52) on the surface of the particle and (3.53) as $r \rightarrow \infty$ leads to

$$\nabla^2 \Phi^{o(0,0)} = 0 \quad (3.60)$$

$$\partial_r \Phi^{o(0,0)} = 0 \quad r = 1 \quad (3.61)$$

$$\Phi^{o(0,0)} = 0 \quad r \rightarrow \infty \quad (3.62)$$

which has the trivial solution

$$\Phi^{o(0,0)} = 0. \quad (3.63)$$

The order $\mathcal{O}(j_p)$ of the equations (3.50) and (3.51) with boundary conditions (3.52) on the surface of the particle and (3.53) as $r \rightarrow \infty$ to first order in j_p simplify to

$$\nabla^2 C^{o(0,1)} = 0 \quad (3.64)$$

$$\partial_r C^{o(0,1)} = -\frac{1}{2} \delta_+ f(\cos \theta) \quad r = 1 \quad (3.65)$$

$$C^{o(0,1)} = 0 \quad r \rightarrow \infty \quad (3.66)$$

and

$$\nabla^2 \Phi^{o(0,1)} = 0 \quad (3.67)$$

$$\partial_r \Phi^{o(0,1)} = -\frac{1}{2} \delta_+ f(\cos \theta) \quad r = 1 \quad (3.68)$$

$$\Phi^{o(0,1)} = 0 \quad r \rightarrow \infty \quad (3.69)$$

which imply

$$C^{o(0,1)} = \Phi^{o(0,1)}. \quad (3.70)$$

Using this equality and expanding the slip velocity (3.43) in powers of j_p yields the tangential velocity at the surface of the particle

$$U_{slip}^{(0)} = j_p U_{slip}^{(0,1)} + \mathcal{O}(j_p^2) \quad (3.71)$$

where

$$U_{slip}^{(0,1)} = \left[\phi_0 - 4 \ln \cosh \left(\frac{\phi_0}{4} \right) \right] \partial_\theta \Phi^{o(0,1)}(1, \theta) \quad (3.72)$$

in which we have used the notation

$$\phi_0 \equiv \phi^{(0,0)} \quad (3.73)$$

for the electric potential at the surface of particle to the leading order in λ and j_p . Similarly, the outer region boundary condition for the radial component of the velocity at the particle surface is given by

$$U_r^{(0,1)} = 0. \quad (3.74)$$

These conditions supplement the Stokes' equation to describe the flow field around the particle to leading order in j_p .

3.4 Particle Velocity

Changing the coordinate system from the particle frame of reference to the laboratory frame of reference, the resulting equations and boundary conditions for the flow field can be written to first order in j_p as

$$-\nabla P^{o(0,1)} + \nabla^2 \mathbf{U}^{o(0,1)} = 0, \quad (3.75)$$

$$r = 1 : \quad \mathbf{U}^{(0,1)} = U_{slip}^{(0,1)} \hat{\mathbf{e}}_\theta + \mathcal{U}^{(0,1)} \hat{\mathbf{e}}_z, \quad (3.76)$$

$$r \rightarrow \infty : \quad \mathbf{U}^{o(0,1)} = 0. \quad (3.77)$$

Even though the Stokes' equation (3.75) appears to contain no explicit dependence on concentration and electric potential, the effects of these components manifest themselves through the slip boundary condition. Since velocity vanishes at infinity, we can use the Lorentz reciprocal theorem to solve for the unknown $\mathbf{U}^{o(0,1)}$. The Lorentz reciprocal theorem relates the solution of two different Stokes flow problems through

$$\int_S \hat{\mathbf{n}} \cdot \mathbb{T}^{o(0,1)} \cdot \mathbf{U}' ds = \int_S \hat{\mathbf{n}} \cdot \mathbb{T}' \cdot \mathbf{U}^{o(0,1)} ds \quad (3.78)$$

where

$$\mathbb{T}^{o(0,1)} = -p^{o(0,1)}\mathbb{I} + \nabla\mathbf{U}^{o(0,1)} + (\nabla\mathbf{U}^{o(0,1)})^T \quad (3.79)$$

is the stress tensor for the flow in our problem, whereas \mathbf{U}' and \mathbb{T}' are respectively the velocity field and its corresponding stress tensor for another Stokes flow in this geometry. In order to proceed, consider \mathbf{U}' to correspond to uniform flow over a sphere where the velocity at infinity is along the axis of symmetry and equal to $\hat{\mathbf{e}}_z$. The corresponding stress tensor in index notation (equation (A.31) from appendix A) is

$$T'_{ij} = \frac{-3}{4} \left[- \left(\delta_{i3}\partial_j\frac{1}{r} + \delta_{j3}\partial_i\frac{1}{r} \right) + \left(x_i\partial_j\partial_3\frac{1}{r} + x_j\partial_i\partial_3\frac{1}{r} \right) + \frac{2}{3}\partial_i\partial_j\partial_3\frac{1}{r} \right] \quad (3.80)$$

and the traction on the particle surface is given by

$$\hat{\mathbf{n}} \cdot \mathbb{T}' = \frac{-3}{2} \hat{\mathbf{e}}_z \quad (3.81)$$

Inserting the corresponding entities in equation (3.78), we get the form

$$\frac{-3}{2} \int_S \hat{\mathbf{e}}_z \cdot \mathbf{U}^{o(0,1)} ds = \int_S \hat{\mathbf{n}} \cdot \mathbb{T}^{o(0,1)} \cdot \hat{\mathbf{e}}_z ds \quad (3.82)$$

Since the particle is moving with constant velocity, the net force on the particle, represented by the right hand side of the above equation, must be zero. Thus, using $\hat{\mathbf{e}}_\theta \cdot \hat{\mathbf{e}}_z = -\sin\theta$ and a boundary condition for the velocity at the particle

surface (3.76), the reciprocal relation (3.82) reduces to

$$\begin{aligned} 0 &= \int_S \hat{\mathbf{e}}_z \cdot \mathbf{U}^{o(0,1)} ds = - \int_S U_{slip}^{(0,1)} \sin \theta ds + \int_S \mathcal{U}^{(0,1)} ds \\ &= -2\pi \int_0^\pi U_{slip}^{(0,1)} \sin^2 \theta d\theta + 4\pi \mathcal{U}^{(0,1)}. \end{aligned} \quad (3.83)$$

The electroviscous velocity is then found by substituting equation (3.72) into (3.83) to yield

$$\begin{aligned} \mathcal{U}^{(0,1)} &= \frac{1}{2} \int_0^\pi U_{slip}^{(0,1)} \sin^2 \theta d\theta \\ &= \frac{1}{2} \left[\phi_0 - 4 \ln \cosh \left(\frac{\phi_0}{4} \right) \right] \int_0^\pi [\partial_\theta \Phi^{o(0,1)}(1, \theta)] \sin^2 \theta d\theta \end{aligned} \quad (3.84)$$

Since the electric potential $\Phi^{o(0,1)}$ satisfies the Laplace equation (3.67), we can expand it in terms of Legendre polynomials,

$$\Phi^{o(0,1)}(r, \theta) = \sum_{n=0}^{\infty} \alpha_n \frac{P_n(\cos \theta)}{r^{n+1}}. \quad (3.85)$$

Thus, the electric potential at the surface of the particle in the outer region is

$$\Phi^{o(0,1)}(1, \theta) = \sum_{n=0}^{\infty} \alpha_n P_n(\cos \theta), \quad (3.86)$$

and for its corresponding angular derivative we have

$$\partial_\theta \Phi^{o(0,1)}(1, \theta) = \sum_{n=0}^{\infty} \alpha_n (-\sin \theta) \frac{dP_n(\cos \theta)}{d(\cos \theta)}. \quad (3.87)$$

We can evaluate the integral in (3.84) using the orthogonality of Legendre polynomials, yielding,

$$\int_0^\pi [\partial_\theta \Phi^{o(0,1)}(1, \theta)] \sin^2 \theta d\theta = -\frac{4}{3} \alpha_1 \quad (3.88)$$

which leads to the velocity

$$\mathcal{U}^{(0,1)} = \frac{-2}{3} \alpha_1 \left[\phi_0 - 4 \ln \cosh \left(\frac{\phi_0}{4} \right) \right] \quad (3.89)$$

where α_1 is given by

$$\alpha_1 = \frac{3}{8} \delta_+ \int_0^\pi P_1(\cos \theta) f(\cos \theta) \sin \theta d\theta = \frac{3}{8} \delta_+ f_1 \quad (3.90)$$

Recasting equations (3.89) and (3.90), the explicit expression for the nanomotor velocity $\mathcal{U} = j_p \mathcal{U}^{(0,1)} + \mathcal{O}(\lambda^{>0}, j_p^{>1})$ to leading order in the dimensionless Debye length λ and first order in dimensionless flux of hydrogen ions j_p becomes

$$\boxed{\mathcal{U} \simeq \frac{-1}{4} \delta_+ j_p f_1 \left[\phi_0 - 4 \ln \cosh \left(\frac{\phi_0}{4} \right) \right]} \quad (3.91)$$

where

$$\boxed{f_1 = \int_0^\pi P_1(\cos \theta) f(\cos \theta) \sin \theta d\theta = \int_{-1}^1 P_1(\eta) f(\eta) d\eta} \quad (3.92)$$

is the first coefficient of the Legendre expansion for the distribution function. In equation (3.91) the term $\ln \cosh(\phi_0/4)$ is very small compared to ϕ_0 in the range of $|\phi_0| < 2$. Thus, we can ignore this term to obtain

$$\mathcal{U} \simeq \frac{-1}{4} \delta_+ j_p f_1 \phi_0 \quad (3.93)$$

In order to show the relationship between particle velocity and the parameters of the system, the velocity equation can be written in dimensional form as

$$\begin{aligned} \underline{\mathcal{U}} &\simeq \frac{-f_1}{4} \left(\frac{\epsilon}{\mu D_+ \zeta^\infty} \right) \underline{j}_p \left[\left(\frac{RT}{zF} \right) \underline{\phi}_0 - 4 \ln \cosh \left(\frac{RT \underline{\phi}_0}{zF \cdot 4} \right) \right] \\ &\simeq \frac{-f_1}{4} \left(\frac{\epsilon RT}{zF \mu D_+ \zeta^\infty} \right) \underline{j}_p \underline{\phi}_0 \end{aligned} \quad (3.94)$$

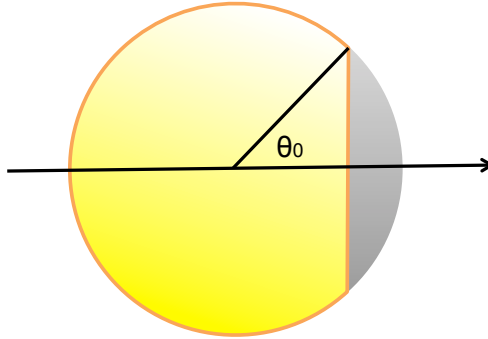


Figure 3.2. The relative areas of the source and sink can be described by θ_0 .

This equation can also be recast in terms of the Debye length λ_D as

$$\underline{\mathcal{U}} \simeq \frac{-f_1}{2} \left(\frac{\lambda_D^2 z F}{\mu D_+} \right) \underline{j}_p \underline{\phi}_0 \quad (3.95)$$

3.5 The Effect of Source-Sink Geometry

From equation (3.95) for the order $\mathcal{O}(\lambda^0, j_p^1)$ of nanomotor velocity it is evident that for fixed \underline{j}_p the only parameter determining the effect of particle geometry is f_1 . A variety of geometries can be considered by changing the relative sizes of the source and sink regions on the surface of the particle. As shown in Fig. (3.2), if the axisymmetric configuration of the particle is to be maintained, all geometries can be simply characterized by the angle θ_0 .

In the foregoing analysis, it was assumed that the flux of ions at the source and sink are uniform over each region. At steady state, there is no change in the charge of the particle with time. Consequently, the fluxes of positive ions at the source and the sink differ based on the areas of the those regions, and the following constraint applies:

$$\int_0^\pi f(\cos \theta) \sin \theta d\theta = 0 \quad (3.96)$$

At the same time, the surface integral of the absolute value of $f(\cos \theta)$ is a measure of the net amount of hydrogen peroxide that is consumed in electrocatalytic (not catalytic) reactions. To set a basis for comparison between different source/sink configurations, we consider the case where the areas of the source and the sink regions are equal ($\theta_0 = \pi/2$) to be the reference configuration for which

$f(\cos \theta) = \text{sgn}(\cos \theta)$. For this configuration,

$$\int_0^\pi |f(\theta)| \sin \theta d\theta = \int_0^{\pi/2} \sin \theta d\theta - \int_{\pi/2}^\pi \sin \theta d\theta = 2. \quad (3.97)$$

This can be considered as a constraint for other configurations to keep the electrochemically consumed amount of hydrogen peroxide fixed as a common basis for comparison. We can then examine how changing the distribution of $f(\cos \theta)$ under the above two constraints affects the velocity of the particle.

As an example, consider the flux distribution $f(\cos \theta)$ to be of the form

$$f(\cos \theta) = \begin{cases} f_+ & \text{if } \theta < \theta_0 \\ -f_- & \text{if } \theta > \theta_0 \end{cases} \quad (3.98)$$

The aforementioned constraints then lead to the requirements

$$\begin{aligned} 0 &= \int_0^\pi f(\cos \theta) \sin \theta d\theta = f_+ \int_0^{\theta_0} \sin \theta d\theta - f_- \int_{\theta_0}^\pi \sin \theta d\theta \\ &= f_+(1 - \cos \theta_0) - f_-(1 + \cos \theta_0) \end{aligned} \quad (3.99)$$

and

$$\begin{aligned} 2 &= \int_0^\pi |f(\cos \theta)| \sin \theta d\theta = f_+ \int_0^{\theta_0} \sin \theta d\theta + f_- \int_{\theta_0}^\pi \sin \theta d\theta \\ &= f_+(1 - \cos \theta_0) + f_-(1 + \cos \theta_0) \end{aligned} \quad (3.100)$$

Therefore, the uniform flux distributions must have the following dependence on the value of θ_0 :

$$f(\cos \theta) = \begin{cases} (1 - \cos \theta_0)^{-1} & \text{if } \theta < \theta_0 \\ -(1 + \cos \theta_0)^{-1} & \text{if } \theta > \theta_0 \end{cases} \quad (3.101)$$

The first Legendre coefficient f_1 is then given by

$$f_1 = \int_0^\pi P_1(\cos \theta) f(\cos \theta) \sin \theta d\theta = 1,$$

which shows that f_1 is independent of θ_0 for the model source-sink in this section.

This means that for small values of hydrogen ion flux in the limit of thin double layer, and a given amount of electrocatalytically consumed hydrogen peroxide, the nanomotor velocity is independent of source/sink geometry.

Spheroidal Nanomotor

A prolate spheroid is a body of revolution obtained by rotating an ellipse about its semi-major axis. After a problem is solved for a spherical geometry in colloid science, usually, a spheroid is the next geometry to be studied. This is because the eccentricity e of a spheroid can be changed to represent a range of geometries from a sphere ($e = 0$) to an approximate for slender bodies and rods ($0 \ll e < 1$).

In this chapter we solve the electrokinetic equation for nanomotor velocity to leading order in λ and first order in j_p , using the method of matched asymptotic expansion and van Dyke matching. We see the same scaling relationship between the parameters of the system that we observed in the case of a sphere. Also, the final result reduces to the case of a sphere in the limit of $e \rightarrow 0$.

1 Prolate Spheroidal Coordinates

An ellipse is the locus of points where the sum of their distances from two fixed points (the *foci*) in space are constant. The interfocal distance is $2c$. The line segment along the fixed points is the semi-major axis of length $2a$; the perpendicular line segment bisecting the foci is the semi-minor axis with length $2b$. A hyperbola, consisting of two disjoint curves, is the locus of points where the difference between their distances from the foci is constant. The hyperbola is orthogonal to the ellipse and these two together form a curvilinear orthogonal coordinate system in two dimensional plane.

A prolate spheroidal coordinate consists of the rotation of the aforementioned

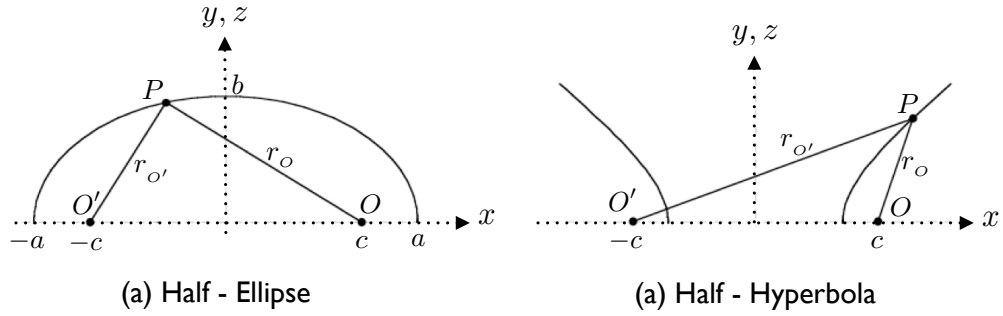


Figure 4.1. The ellipse and hyperbola in the xy -plane; in (a) $r_A + r_B$ is constant, while in (b) $|r_A - r_B|$ is constant. (with modification from [37])

coordinate system around the semi-major axis of the ellipse. The important note here to mention is that since the rotation about the symmetry axis is a 2π revolution, the rotated object is a half-ellipse rather than a fully closed ellipse. Every point in space corresponds to a tuple (ξ, η, ϕ) where ξ is the radial coordinate, η is the angular coordinate and ϕ represents the azimuthal angle. As depicted in Fig. (4.1), the radial ξ and angular η coordinates can be defined using the focal radii r_o and $r_{o'}$ in the form

$$\xi = \frac{r_o + r_{o'}}{2c} \quad (4.1)$$

and

$$\eta = \frac{|r_o - r_{o'}|}{2c}. \quad (4.2)$$

The azimuthal coordinate $\phi = \tan^{-1}\left(\frac{z}{y}\right)$ is measured from the xy -plane in an anti-clockwise fashion. The coordinates of a point in prolate spheroidal system (ξ, η, ϕ) can be transformed to the Cartesian system (x, y, z) using

$$x = c\eta\xi \quad (4.3)$$

$$y = c\sqrt{(\xi^2 - 1)(1 - \eta^2)} \cos \phi \quad (4.4)$$

$$z = c\sqrt{(\xi^2 - 1)(1 - \eta^2)} \sin \phi \quad (4.5)$$

where

$$-1 \leq \eta \leq 1, \quad (4.6)$$

$$1 \leq \xi < \infty, \quad (4.7)$$

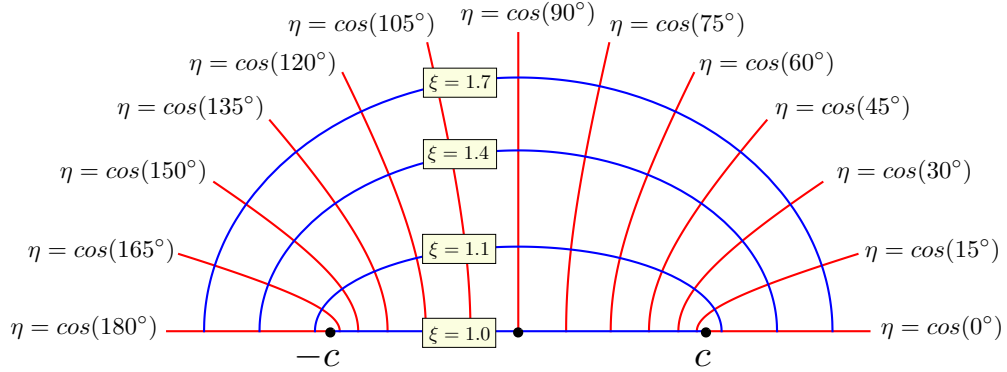


Figure 4.2. Constant coordinate curves for prolate spheroidal coordinate in a half-plane of constant ϕ .

$$0 \leq \phi < 2\pi. \quad (4.8)$$

Fig. (4.2) demonstrates the family of curves of constant radial coordinate ξ (blue curves) and the family if curves of constant angular coordinate η (red curves) in a half-plane of constant ϕ .

Using equations (4.3), (4.4), and (4.5), we can calculate the the scale factor for prolate spheroidal coordinate by taking the derivatives of the Cartesian position vector $\vec{\mathbf{r}} = x \hat{\mathbf{e}}_x + y \hat{\mathbf{e}}_y + z \hat{\mathbf{e}}_z$.

$$h_\xi = \left| \frac{\partial \vec{\mathbf{r}}}{\partial \xi} \right| = c \sqrt{\frac{\xi^2 - \eta^2}{\xi^2 - 1}} \quad (4.9)$$

$$h_\eta = \left| \frac{\partial \vec{\mathbf{r}}}{\partial \eta} \right| = c \sqrt{\frac{\xi^2 - \eta^2}{1 - \eta^2}} \quad (4.10)$$

$$h_\phi = \left| \frac{\partial \vec{\mathbf{r}}}{\partial \phi} \right| = c \sqrt{(\xi^2 - 1)(1 - \eta^2)} \quad (4.11)$$

The unit vectors are defined as

$$\hat{\mathbf{e}}_\xi = \frac{1}{h_\xi} \frac{\partial \vec{\mathbf{r}}}{\partial \xi} \quad (4.12)$$

$$\hat{\mathbf{e}}_\eta = \frac{1}{h_\eta} \frac{\partial \vec{\mathbf{r}}}{\partial \eta} \quad (4.13)$$

$$\hat{\mathbf{e}}_\phi = \frac{1}{h_\phi} \frac{\partial \vec{\mathbf{r}}}{\partial \phi} \quad (4.14)$$

and the transformation of the unit vectors from spheroidal coordinate to Cartesian coordinate is

$$\hat{\mathbf{e}}_x = \eta \sqrt{\frac{\xi^2 - 1}{\xi^2 - \eta^2}} \hat{\mathbf{e}}_\xi + \xi \sqrt{\frac{1 - \eta^2}{\xi^2 - \eta^2}} \hat{\mathbf{e}}_\eta, \quad (4.15)$$

$$\hat{\mathbf{e}}_y = \xi \sqrt{\frac{1 - \eta^2}{\xi^2 - \eta^2}} \cos \phi \hat{\mathbf{e}}_\xi - \eta \sqrt{\frac{\xi^2 - 1}{\xi^2 - \eta^2}} \cos \phi \hat{\mathbf{e}}_\eta - \sin \phi \hat{\mathbf{e}}_\phi, \quad (4.16)$$

$$\hat{\mathbf{e}}_z = \xi \sqrt{\frac{1 - \eta^2}{\xi^2 - \eta^2}} \sin \phi \hat{\mathbf{e}}_\xi - \eta \sqrt{\frac{\xi^2 - 1}{\xi^2 - \eta^2}} \sin \phi \hat{\mathbf{e}}_\eta + \cos \phi \hat{\mathbf{e}}_\phi. \quad (4.17)$$

Consequently, the vectorial differential operators in the axisymmetric prolate spheroidal system take the form

$$\begin{aligned} \vec{\nabla} f(\xi, \eta) &= \frac{\hat{\mathbf{e}}_\xi}{h_\xi} \frac{\partial}{\partial \xi} f + \frac{\hat{\mathbf{e}}_\eta}{h_\eta} \frac{\partial}{\partial \eta} f \\ &= \frac{\hat{\mathbf{e}}_\xi}{c} \sqrt{\frac{\xi^2 - 1}{\xi^2 - \eta^2}} \frac{\partial}{\partial \xi} f + \frac{\hat{\mathbf{e}}_\eta}{c} \sqrt{\frac{1 - \eta^2}{\xi^2 - \eta^2}} \frac{\partial}{\partial \eta} f \end{aligned} \quad (4.18)$$

$$\begin{aligned} \nabla^2 f(\xi, \eta) &= \frac{1}{h_\xi h_\eta h_\phi} \left[\frac{\partial}{\partial \xi} \left(\frac{h_\eta h_\phi}{h_\xi} \frac{\partial f}{\partial \xi} \right) + \frac{\partial}{\partial \eta} \left(\frac{h_\phi h_\xi}{h_\eta} \frac{\partial f}{\partial \eta} \right) \right] \\ &= \frac{1}{c^2(\xi^2 - \eta^2)} \left\{ \frac{\partial}{\partial \xi} \left[(\xi^2 - 1) \frac{\partial f}{\partial \xi} \right] + \frac{\partial}{\partial \eta} \left[(1 - \eta^2) \frac{\partial f}{\partial \eta} \right] \right\} \end{aligned} \quad (4.19)$$

$$\begin{aligned} \vec{\nabla} \cdot \vec{\mathbf{F}} &= \frac{1}{h_\xi h_\eta h_\phi} \left[\frac{\partial}{\partial \xi} (h_\eta h_\phi F_\xi) + \frac{\partial}{\partial \eta} (h_\phi h_\xi F_\eta) \right] \\ &= \frac{1}{c(\xi^2 - \eta^2)} \left\{ \frac{\partial}{\partial \xi} (\sqrt{(\xi^2 - \eta^2)(\xi^2 - 1)} F_\xi) + \frac{\partial}{\partial \eta} (\sqrt{(\xi^2 - \eta^2)(1 - \eta^2)} F_\eta) \right\} \end{aligned} \quad (4.20)$$

2 Spheroid

In the Cartesian coordinates we describe the prolate spheroid by

$$\frac{x^2}{a^2} + \frac{y^2}{b^2} + \frac{z^2}{b^2} \equiv \frac{x^2}{a^2} + \frac{r^2}{b^2} = 1 \quad (4.21)$$

where $r^2 = y^2 + z^2$ and $b \leq a$. The interfocal length $2c$ and the eccentricity e are related by

$$c = \sqrt{a^2 - b^2} = ea \quad (4.22)$$

The eccentricity is the ratio of the interfocal distance to the length of the semi-major axis, $e = c/a$ and varies as $0 \leq e \leq 1$. In the case where $e = 0$, the foci coincide and the spheroid is a sphere. The hyperbola then becomes two lines of opposite slope crossing at the origin.

In the prolate spheroidal coordinate, a prolate spheroid is represented by a surface of constant $\xi_s > 1$. For this geometry, the semi-major axis is $a = c\xi_s$ and semi-minor axis is $b = c\sqrt{\xi_s^2 - 1}$. The degenerate surface $\xi_s = 1$ corresponds to interfocal line segment. Comparing $c = ea$ and $a = c\xi_s$, we obtain

$$\xi_s = \frac{1}{e} \quad (4.23)$$

The normal \hat{n} on the surface of the spheroid in the index notation takes the form

$$\begin{aligned} n_i &= \frac{\frac{b}{a}x_1\delta_{1i} + \frac{a}{b}x_2\delta_{2i} + \frac{a}{b}x_3\delta_{3i}}{\sqrt{a^2 - e^2x_1^2}} = \frac{1}{\sqrt{R_1R_2}} \left(\frac{b}{a}x_1\delta_{1i} + \frac{a}{b}x_2\delta_{2i} + \frac{a}{b}x_3\delta_{3i} \right) \\ &= \frac{1}{\sqrt{R_1R_2}} \left(\frac{a}{b} \right) (x_i - e^2x_1\delta_{1i}) \end{aligned} \quad (4.24)$$

where the indices 1, 2 and 3 refer to x -, y - and z -axes, respectively.

3 Velocity and Pressure Field for Flow Over a Prolate Spheroid

For a free stream velocity at infinity of the form

$$\mathbf{U} = U \hat{\mathbf{e}}_x \quad (4.25)$$

where $\hat{\mathbf{e}}_x$ is the unit vector in the x direction, the velocity field and pressure field around the spheroid are given by [38]

$$\mathbf{u} = U \left\{ \hat{\mathbf{e}}_x - 2\alpha B_{1,0} \hat{\mathbf{e}}_x - \alpha \left(\frac{1}{R_2} - \frac{1}{R_1} \right) (y \hat{\mathbf{e}}_y + z \hat{\mathbf{e}}_z) + \alpha r^2 B_{3,0} \hat{\mathbf{e}}_x - 2\beta \nabla B_{1,1} \right\} \quad (4.26)$$

and

$$p = 2\mu\alpha U \left(\frac{1}{R_1} - \frac{1}{R_2} \right), \quad (4.27)$$

respectively, where

$$\alpha = \frac{2e^2}{1 - e^2} \quad \beta = \frac{e^2}{-2e + (1 + e^2)L_e}, \quad (4.28)$$

$$L_e = \ln \left(\frac{1 + e}{1 - e} \right), \quad (4.29)$$

$$R_1 = \sqrt{(x + c)^2 + r^2}, \quad (4.30)$$

$$R_2 = \sqrt{(x - c)^2 + r^2}, \quad (4.31)$$

$$B_{1,0} = \ln \left(\frac{R_2 - (x - c)}{R_1 - (x + c)} \right), \quad (4.32)$$

$$B_{1,1} = R_2 - R_1 + x B_{1,0}, \quad (4.33)$$

and

$$B_{3,0} = \frac{1}{r^2} \left(\frac{x + c}{R_1} - \frac{x - c}{R_2} \right). \quad (4.34)$$

The distribution of traction for this flow field on the surface of the sphere in the index notation is given by is

$$n_j T_{ji} = 4e\mu\alpha U \frac{1}{\sqrt{R_1 R_2}} \left(\frac{a}{b} \right) \delta_{1i} = \left(\frac{4\mu\alpha U}{ea} \right) \frac{1}{\sqrt{(\xi_s^2 - \eta^2)(\xi_s^2 - 1)}} \delta_{1i} \quad (4.35)$$

where the x -direction is represented by δ_{1i} . We will use this equation with Reynolds reciprocal theorem to calculate the nanomotor velocity. For a detailed derivation of the distribution of traction, please refer to appendix B.

4 The Model of Electrokinetic Self-Propulsion

In chapter 2, we developed a set of electrokinetic equations governing the interaction between nanomotor and surrounding fluid and ions. The length scale in this

problem is the half length of the semi-major axis, which is a . Working with the dimensionless equations, we would like to solve the Stokes' equation

$$-\nabla P + \nabla^2 \mathbf{U} + \nabla^2 \Phi \nabla \Phi = 0 \quad (2.27)$$

for the far field velocity of fluid

$$\mathbf{U}(\xi \rightarrow \infty) = -\mathcal{U} \hat{\mathbf{z}} \quad (4.36)$$

in the frame of reference attached to the particle. In the laboratory frame of reference, \mathcal{U} is the nanomotor velocity. We use the no-slip boundary condition on the surface of the particle,

$$\mathbf{U}(\xi = \xi_s) = 0. \quad (4.37)$$

The motion of ions in the electrolyte is governed by the equations of continuity of species

$$\nabla \cdot \mathbf{J}_{\pm} + Pe \mathbf{U} \cdot \nabla C_{\pm} = 0 \quad (2.26)$$

where the ion fluxes are given by

$$\mathbf{J}_{\pm} = -\delta_{\pm}^{-1} (\nabla C_{\pm} \pm C_{\pm} \nabla \Phi). \quad (2.25)$$

The particle is impermeable to negative ions

$$\hat{\mathbf{n}} \cdot \mathbf{J}_{-} \Big|_{\xi=\xi_s} = 0 \quad (2.30)$$

and the distribution of positive ions on the surface of the spheroid is given by

$$\hat{\mathbf{n}} \cdot \mathbf{J}_{+} \Big|_{\xi=\xi_s} = j_p f(\eta) \quad (2.29)$$

where the prefactor j_p is the strength of hydrogen ion flux and $f(\eta)$ is a function defined over the surface of the spheroid. Since the geometry is axisymmetric, this distribution function only depends on η . The electric potential is related to concentration of positive C_+ and negative C_- ions through the Poisson's equation,

$$2\lambda^2 \nabla^2 \Phi = -(C_+ - C_-). \quad (2.24)$$

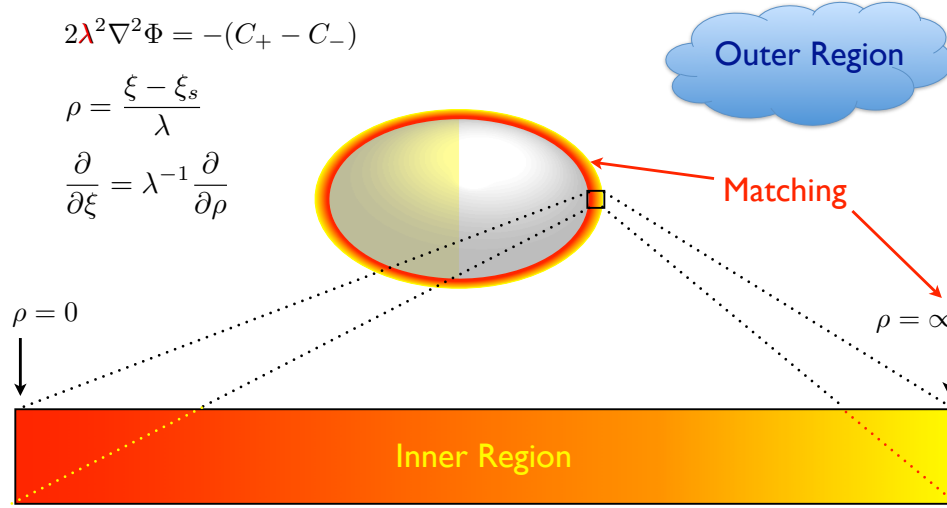


Figure 4.3. The fluid around the spheroid is divided into an inner region, where the high variation in the electric potential compensates for the smallness of λ^2 , and an outer region. By change of variable from ξ to ρ , we can expand the inner region. The surface of the spheroid is represented by $\xi = \xi_s$. We calculate the unknown coefficients of the inner and outer solutions by matching these solutions at the boundary of the two regions.

The electric potential on the surface of the conductive nanomotor is constant

$$\Phi(\xi = \xi_s) = \phi, \quad (2.31)$$

and vanishes at infinity,

$$\Phi(\xi \rightarrow \infty) = 0. \quad (2.34)$$

Far away from the particle, the electro-neutrality condition holds in the electrolyte and the concentration of ions are equal to background concentration,

$$C_{\pm}(\xi \rightarrow \infty) = 1. \quad (2.33)$$

5 Perturbation Analysis

In this chapter we solve the governing equation in the limit of small dimensionless Debye length $\lambda \ll 1$ and small dimensionless strength of hydrogen ions flux $j_p \ll 1$. We use singular perturbation analysis for the former parameter and regular perturbation analysis for the latter.

5.1 Singular Perturbation Analysis

In the Poisson equation (2.24), the small parameter λ^2 is multiplied by the highest derivative $\nabla^2\Phi$ in the equation. There is a boundary layer near the surface of the spheroid where the spatial variation of the electric potential is rapid; therefore, $\nabla^2\Phi$ can compensate for the smallness of λ^2 . That is, in this region $\lambda^2\nabla^2\Phi$ is of order one (see Fig. 4.3). We use the method of matched asymptotic expansion in which we divide the space into two region; the inner region where to the leading order in λ the term $\lambda^2\nabla^2\Phi$ is of order one and the outer region where to the leading order in the small parameter, $\lambda^2\nabla^2\Phi$ vanishes. We solve the fields in the inner and outer regions and match the corresponding orders using van Dyke matching.

To capture the rapid radial variation of electric potential in the thin boundary layer of thickness $\mathcal{O}(\lambda)$ at the surface of the particle, we stretch the domain to a stretched radial coordinate ρ that varies between zero and infinity using the transformation

$$\rho = \frac{\xi - \xi_s}{\lambda}, \quad (4.38)$$

$$\xi = \xi_s + \lambda\rho, \quad (4.39)$$

$$\partial_\xi = \lambda^{-1}\partial_\rho. \quad (4.40)$$

Then, we expand each fields G as a function of ρ in the inner region in powers of λ as

$$G^i(\rho, \theta) = \sum_{k=n_0}^{\infty} \lambda^k G^{i(k)}(\rho, \theta) \quad (4.41)$$

where the value of the integer n_0 depends on the field G and the number k in the parenthesis indicates the order of the function $G^{i(k)}$. We also expand the same field as a function of r in the outer region in powers of λ

$$G^o(r, \theta) = \sum_{k=0}^{\infty} \lambda^{2k} G^{o(2k)}(r, \theta) \quad (4.42)$$

where the outer fields of odd order are zero since the small parameter in the outer region is λ^2 . However, for the purpose of applying the van Dyke matching, we consider the outer expansion in powers of λ with terms of odd powers equal to zero, i.e. $G^{o(2k+1)} = 0$. Inserting these assumptions in the governing equations

results in different equations based on the order of the small parameter. We solve the equations for the outer and the inner regions and match the inner and the outer fields of the same order using van Dyke matching. We represent the matching condition for the field G by the notation

$$\mathbb{O}_m \mathbb{I}_n G = \mathbb{I}_n \mathbb{O}_m G \quad (4.43)$$

where $\mathbb{I}_n \mathbb{O}_m$ is the n -term inner expansion of the m -term outer solution and $\mathbb{O}_m \mathbb{I}_n$ is the m -term outer solution of the n -term inner solution. To evaluate $\mathbb{I}_n \mathbb{O}_m G$ we take the first n -terms (the terms of power λ^{n_0} to λ^{n+n_0-1}) of the following expansion in λ given ρ fixed,

$$\sum_{k=0}^{m-1} \lambda^k G^{o(k)}(1 + \lambda\rho, \theta) \quad (4.44)$$

and to evaluate $\mathbb{O}_m \mathbb{I}_n G$ we take the first m -terms (the terms of power λ^0 to λ^{m-1}) of the following expansion in λ given r -fixed,

$$\sum_{k=n_0}^{n-n_0-1} \lambda^k G^{o(k)}\left(\frac{r-1}{\lambda}, \theta\right). \quad (4.45)$$

We apply singular perturbation analysis in this section to calculate for slip velocity and lump the properties of the inner layer into a boundary condition for the fields of the outer region.

As discussed before, for the fields in the inner region, we can write an asymptotic expansion, $G^i = \sum_{n=n_0}^{\infty} \lambda^n G^{i(n)}$ where $n_0 = 0$ for C_{\pm}^i , $\Phi^{i(0)}$, $J_{\pm\theta}^i$, U_{θ}^i , ϕ and \mathcal{U} . Using equations (2.25), (2.27), and (2.28), we have $n_0 = -1$ for $J_{\pm\rho}^i$, $n_0 = 1$ for U_{ρ}^i , $n_0 = -2$ for P^i . We would like to calculate the angular component of the velocity $U_{\eta}^{i(0)}$ to the leading order in λ from which we can calculate the slip velocity

$$\mathbf{U}_{slip}^{(0)} = \hat{\mathbf{e}}_{\eta} \lim_{\rho \rightarrow \infty} U_{\eta}^{i(0)}. \quad (4.46)$$

The leading order angular component of velocity in the inner region appear in the

order $\mathcal{O}(\lambda^{-2})$ of the angular component of the the Stokes' equation,

$$\begin{aligned} & - \left(\xi_s \sqrt{\frac{1-\eta^2}{\xi_s^2-\eta^2}} \partial_\eta \right) P^{i(-2)} + \left(\xi_s \sqrt{\frac{\xi_s^2-1}{\xi_s^2-\eta^2}} \partial_\rho \right)^2 U_\eta^{i(0)} \\ & + \left(\xi_s \sqrt{\frac{1-\eta^2}{\xi_s^2-\eta^2}} \partial_\eta \right) \Phi^{i(0)} \left(\xi_s \sqrt{\frac{\xi_s^2-1}{\xi_s^2-\eta^2}} \partial_\rho \right)^2 \Phi^{i(0)} = 0 \end{aligned} \quad (4.47)$$

The velocity field on the surface of the particle should satisfy the no slip boundary condition,

$$U_\eta^{i(0)}(\rho=0) = 0. \quad (4.48)$$

To relate the pressure $P^{i(-2)}$ to electric potential $\Phi^{i(0)}$, we use the order $\mathcal{O}(\lambda^{-3})$ of the radial component of the the Stokes' equation,

$$- \left(\xi_s \sqrt{\frac{\xi_s^2-1}{\xi_s^2-\eta^2}} \partial_\rho \right) P^{i(-2)} + \frac{1}{2} \left(\xi_s \sqrt{\frac{\xi_s^2-1}{\xi_s^2-\eta^2}} \partial_\rho \right) \left[\left(\xi_s \sqrt{\frac{\xi_s^2-1}{\xi_s^2-\eta^2}} \partial_\rho \right) \Phi^{i(0)} \right]^2 = 0. \quad (4.49)$$

The Poisson's equation to the leading order in λ relates the electric potential $\Phi^{i(0)}$ to the concentration of positive $C_+^{i(0)}$ and negative $C_-^{i(0)}$ ions,

$$\left(\xi_s \sqrt{\frac{\xi_s^2-1}{\xi_s^2-\eta^2}} \partial_\rho \right)^2 \Phi^{i(0)} = - \left(C_+^{i(0)} - C_-^{i(0)} \right) / 2. \quad (4.50)$$

The potential on the surface of the conductive sphere is constant,

$$\Phi^{i(0)}(\rho=0) = \phi^{(0)}. \quad (4.51)$$

The continuity of species to the order $\mathcal{O}(\lambda^{-2})$ gives

$$\partial_\rho J_{\pm\rho}^{i(-1)} = 0 \quad (4.52)$$

with boundary conditions

$$J_{+\rho}^{i(-1)} = J_{-\rho}^{i(-1)} = 0 \quad (4.53)$$

where

$$J_{\pm\rho}^{i(-1)} = -\delta_{\pm}^{-1} \left[\left(\xi_s \sqrt{\frac{\xi_s^2 - 1}{\xi_s^2 - \eta^2}} \partial_\rho \right) C_{\pm}^{i(0)} \pm C_{\pm}^{i(0)} \left(\xi_s \sqrt{\frac{\xi_s^2 - 1}{\xi_s^2 - \eta^2}} \partial_\rho \right) \Phi^{i(0)} \right]. \quad (4.54)$$

From the equation (4.52), we find that in the inner region, the fluxes $J_{\pm\rho}^{i(-1)}$ have no radial dependence, $J_{\pm\rho}^{i(-1)} = \hat{K}_{\pm}(\eta)$. Since the order $\mathcal{O}(\lambda^{-1})$ of ion fluxes vanish (4.53) on the surface of the particle, the angular coordinate dependent functions are zero, $\hat{K}_{\pm}(\eta) = 0$, and we obtain

$$J_{\pm\rho}^{i(-1)} = 0. \quad (4.55)$$

Consequently,

$$\left(\xi_s \sqrt{\frac{\xi_s^2 - 1}{\xi_s^2 - \eta^2}} \partial_\rho \right) C_{\pm}^{i(0)} \pm C_{\pm}^{i(0)} \left(\xi_s \sqrt{\frac{\xi_s^2 - 1}{\xi_s^2 - \eta^2}} \partial_\rho \right) \Phi^{i(0)} = 0 \quad (4.56)$$

which leads to

$$C_{\pm}^{i(0)} = \hat{K}'_{\pm}(\eta) \exp(\mp \Phi^{i(0)}) = \hat{K}'_{\pm}(\eta) (\cosh \Phi^{i(0)} \mp \sinh \Phi^{i(0)}) \quad (4.57)$$

where $\hat{K}'_{\pm}(\eta)$ are angular coordinate dependent functions. Inserting these concentrations fields in to the Poisson's equation (4.50), we obtain

$$\begin{aligned} \left(\xi_s \sqrt{\frac{\xi_s^2 - 1}{\xi_s^2 - \eta^2}} \partial_\rho \right)^2 \Phi^{i(0)} &= - \left(C_+^{i(0)} - C_-^{i(0)} \right) / 2 \\ &= -\frac{1}{2} \left(\hat{K}'_+(\eta) e^{-\Phi^{i(0)}} - \hat{K}'_-(\eta) e^{\Phi^{i(0)}} \right) \\ &= -\frac{1}{2} \left[\left(\hat{K}'_+ - \hat{K}'_- \right) \cosh \Phi^{i(0)} - \left(\hat{K}'_+ + \hat{K}'_- \right) \sinh \Phi^{i(0)} \right]. \end{aligned} \quad (4.58)$$

Defining $\Theta = \left(\xi_s \sqrt{\frac{\xi_s^2 - 1}{\xi_s^2 - \eta^2}} \partial_\rho \right) \Phi^{i(0)}$, $\hat{A} = \hat{K}'_+ - \hat{K}'_-$ and $\hat{B} = \hat{K}'_+ + \hat{K}'_-$, we have

$$\left(\xi_s \sqrt{\frac{\xi_s^2 - 1}{\xi_s^2 - \eta^2}} \partial_\rho \right)^2 \Phi^{i(0)} = \Theta \partial_{\Phi^{i(0)}} \Theta = \frac{1}{2} \partial_{\Phi^{i(0)}} \Theta^2$$

$$= -\frac{1}{2} \left[\hat{A}(\eta) \cosh \Phi^{i(0)} - \hat{B}(\eta) \sinh \Phi^{i(0)} \right], \quad (4.59)$$

from which we obtain

$$\Theta^2 = -\hat{A}(\eta) \sinh \Phi^{i(0)} + \hat{B}(\eta) \cosh \Phi^{i(0)} + \hat{K}'' . \quad (4.60)$$

The electric potential in the inner layer increases with an increase in the radial coordinate, and its radial derivative is positive, $\Theta = \left(\xi_s \sqrt{\frac{\xi_s^2 - 1}{\xi_s^2 - \eta^2}} \partial_\rho \right) \Phi^{i(0)} > 0$; therefore,

$$\left(\xi_s \sqrt{\frac{\xi_s^2 - 1}{\xi_s^2 - \eta^2}} \partial_\rho \right) \Phi^{i(0)} = \left[-\hat{A}(\eta) \sinh \Phi^{i(0)} + \hat{B}(\eta) \cosh \Phi^{i(0)} + \hat{K}'' \right]^{\frac{1}{2}} . \quad (4.61)$$

For further calculations, we need to determine the coefficients \hat{A} , \hat{B} and \hat{K}'' , for which we need to match with the outer solution.

For the fields in the outer region, we can write the asymptotic expansion based on λ and there is no need for a change of variable,

$$G^o = \sum_{n=0}^{\infty} \lambda^{2n} G^{o(2n)} . \quad (4.62)$$

To the leading order in λ^2 , the Poisson's equation leads to electro-neutrality condition in the outer region

$$C_+^{o(0)} = C_-^{o(0)} \equiv C^{o(0)} . \quad (4.63)$$

We use van Dyke matching for the concentrations of positive and negative ions,

$$I_1 O_1 C_+^o(\xi, \eta) = O_1 I_1 C_+^i(\rho, \eta) \quad (4.64a)$$

$$I_1 O_1 C_-^o(\xi, \eta) = O_1 I_1 C_-^i(\rho, \eta) \quad (4.64b)$$

which along with the electroneutrality condition (4.63) results in

$$O_1 I_1 C_+^i(\rho, \eta) = O_1 I_1 C_-^i(\rho, \eta), \quad (4.65)$$

where $I_1 O_1$ is the one-term inner expansion of the one-term outer solution and $O_1 I_1$ is the one-term outer solution of the one-term inner solution, according to

standard van Dyke matching. Therefore,

$$\lim_{\substack{\lambda \rightarrow 0 \\ \xi\text{-fixed}}} \hat{K}'_+(\eta) (\cosh \Phi^{i(0)} - \sinh \Phi^{i(0)}) = \lim_{\substack{\lambda \rightarrow 0 \\ \xi\text{-fixed}}} \hat{K}'_-(\eta) (\cosh \Phi^{i(0)} + \sinh \Phi^{i(0)}) \quad (4.66)$$

or

$$\lim_{\substack{\lambda \rightarrow 0 \\ \xi\text{-fixed}}} \hat{A}(\eta) \cosh \Phi^{i(0)} = \lim_{\substack{\lambda \rightarrow 0 \\ \xi\text{-fixed}}} \hat{B}(\eta) \sinh \Phi^{i(0)}. \quad (4.67)$$

This equation gives us the relationship between \hat{A} and \hat{B} ,

$$\hat{A}(\eta) = \hat{B}(\eta) \tanh [\Phi^{i(0)}(\infty, \eta)]. \quad (4.68)$$

Inserting this relation into equation (4.61) and defining

$$\psi(\rho, \eta) = \Phi^{i(0)}(\rho, \eta) - \Phi^{i(0)}(\infty, \eta) \quad (4.69)$$

yields

$$\left(\xi_s \sqrt{\frac{\xi_s^2 - 1}{\xi_s^2 - \eta^2}} \partial_\rho \right) \Phi^{i(0)} = \left[\left(\frac{\hat{B}(\eta)}{\cosh [\Phi^{i(0)}(\infty, \eta)]} \right) \cosh(\psi) + \hat{K}'' \right]^{\frac{1}{2}}. \quad (4.70)$$

We also have

$$\hat{K}'_+ = \frac{1}{2} (\hat{A} + \hat{B}) = \left(\frac{\hat{B}(\eta)}{2 \cosh [\Phi^{i(0)}(\infty, \eta)]} \right) \exp [\Phi^{i(0)}(\infty, \eta)] \quad (4.71)$$

Therefore, we have

$$\left(\frac{\hat{B}(\eta)}{\cosh [\Phi^{i(0)}(\infty, \eta)]} \right) = 2 \hat{K}'_+ \exp [-\Phi^{i(0)}(\infty, \eta)] = 2 C_+^{i(0)}(\infty, \eta) \quad (4.72)$$

Using the fact that $C_+^{i(0)}(\infty, \eta) = C^{o(0)}(\xi_s, \eta)$, and inserting (4.72) into the radial derivative of the electric potential (4.70) yields

$$\left(\xi_s \sqrt{\frac{\xi_s^2 - 1}{\xi_s^2 - \eta^2}} \partial_\rho \right) \Phi^{i(0)} = \left[2 C^{o(0)}(\xi_s, \eta) \cosh(\psi) + \hat{K}''(\eta) \right]^{\frac{1}{2}}. \quad (4.73)$$

We further need to match the radial component of the electric field of the order $\mathcal{O}(\lambda^{-1})$ in the inner layer, that is, $E_\rho^{i(-1)} = \left(\xi_s \sqrt{\frac{\xi_s^2 - 1}{\xi_s^2 - \eta^2}} \partial_\rho \right) \Phi^{i(0)}$ with $E_\xi^{o(-1)}$ in the outer region. However, we know that the asymptotic expansion in the outer region start from the leading order in λ , and therefore, $E_\xi^{o(-1)} = 0$. Applying the van Dyke matching, we obtain

$$O_1 I_1 E_\rho^i = I_1 O_1 E_\xi^o = 0 \quad (4.74)$$

which yields

$$\lim_{\substack{\lambda \rightarrow 0 \\ \xi \text{-fixed}}} \left[2 C^{o(0)}(\xi_s, \eta) \cosh(\psi) + \hat{K}''(\eta) \right]^{\frac{1}{2}} = \left[2 C^{o(0)}(\xi_s, \eta) + \hat{K}''(\eta) \right]^{\frac{1}{2}} = 0. \quad (4.75)$$

This relation gives

$$\hat{K}''(\eta) = -2 C^{o(0)}(\xi_s, \eta) \quad (4.76)$$

and we obtain

$$\begin{aligned} \left(\xi_s \sqrt{\frac{\xi_s^2 - 1}{\xi_s^2 - \eta^2}} \partial_\rho \right) \Phi^{i(0)} &= \left[2 C^{o(0)}(\xi_s, \eta) \cosh(\psi) - 2 C^{o(0)}(\xi_s, \eta) \right]^{\frac{1}{2}} \\ &= \left[4 C^{o(0)}(\xi_s, \eta) \sinh^2 \left(\frac{\psi}{2} \right) \right]^{\frac{1}{2}}. \end{aligned} \quad (4.77)$$

Since $\partial_\rho \Phi^{i(0)} = \partial_\rho \psi$, the above equation takes the form

$$\left(\xi_s \sqrt{\frac{\xi_s^2 - 1}{\xi_s^2 - \eta^2}} \partial_\rho \right) \psi = -2 \sqrt{C^{o(0)}(\xi_s, \eta)} \sinh \left(\frac{\psi}{2} \right). \quad (4.78)$$

The minus sign is due to negative value of $\sinh \left(\frac{\psi}{2} \right)$ in the inner region. Integration of the above equation gives

$$\tanh \frac{\psi}{4} = \tanh \frac{\psi_0}{4} \exp \left[\frac{-\rho \sqrt{C^{o(0)}(\xi_s, \eta)}}{\left(\xi_s \sqrt{\frac{\xi_s^2 - 1}{\xi_s^2 - \eta^2}} \right)} \right] \quad (4.79)$$

where

$$\psi_0(\eta) = \Phi^{i(0)}(0, \eta) - \Phi^{i(0)}(\infty, \eta) \quad (4.80)$$

is the electric potential difference between the surface of the particle and the boundary of the inner region. We can recast equation (4.79) into the familiar Gouy-Chapman equation,

$$\Phi^{i(0)}(\rho, \eta) = \Phi^{i(0)}(\infty, \eta) + 4 \tanh^{-1} \left\{ \tanh \left(\frac{\psi_0}{4} \right) \exp \left[\frac{-\rho \sqrt{C^{o(0)}(\xi_s, \eta)}}{\left(\xi_s \sqrt{\frac{\xi_s^2 - 1}{\xi_s^2 - \eta^2}} \right)} \right] \right\}. \quad (4.81)$$

Also, the nonlinear Poisson's equation (4.58) takes the form

$$\partial_\rho^2 \psi = \left(\frac{1}{\xi_s} \sqrt{\frac{\xi_s^2 - \eta^2}{\xi_s^2 - 1}} \right)^2 C^{o(0)}(\xi_s, \eta) \sinh \psi \quad (4.82)$$

So far we have calculated the leading order electric potential $\Phi^{i(0)}$ in the inner layer. In order to solve the order $\mathcal{O}(\lambda^{-2})$ of the angular component of the Stokes' equation (4.47) for the leading order tangential component of the velocity $U_\eta^{i(0)}$ we need to calculate the pressure $P^{i(-2)}$ of the order $\mathcal{O}(\lambda^{-2})$. Integrating $\mathcal{O}(\lambda^{-3})$ radial component of the Stokes' equation (4.49) gives

$$P^{i(-2)} = \frac{1}{2} \left[\xi_s \left(\sqrt{\frac{\xi_s^2 - 1}{\xi_s^2 - \eta^2}} \partial_\rho \right) \Phi^{i(0)} \right]^2 + \hat{K}'''(\eta). \quad (4.83)$$

To determine $\hat{K}'''(\eta)$, we match the pressure of the order $\mathcal{O}(\lambda^{-2})$,

$$I_1 O_1 P^o = O_1 I_1 P^i. \quad (4.84)$$

Since the asymptotic expansion of fields in the outer region starts from the leading order in λ^2 , we have $P^{o(-2)} = 0$. Consequently,

$$0 = \lim_{\substack{\lambda \rightarrow 0 \\ \xi \text{-fixed}}} \frac{1}{2} \left[\xi_s \left(\sqrt{\frac{\xi_s^2 - 1}{\xi_s^2 - \eta^2}} \partial_\rho \right) \Phi^{i(0)} \right]^2 + \hat{K}'''(\eta) = \hat{K}'''(\eta), \quad (4.85)$$

where we have used the vanishing of radial component of the electric field (4.74)

of the order $\mathcal{O}(\lambda^{-1})$ at the end of the inner region. Therefore, we obtain

$$P^{i(-2)} = \frac{1}{2} \left[\xi_s \left(\sqrt{\frac{\xi_s^2 - 1}{\xi_s^2 - \eta^2}} \partial_\rho \right) \Phi^{i(0)} \right]^2 \equiv \frac{1}{2} \left[\xi_s \left(\sqrt{\frac{\xi_s^2 - 1}{\xi_s^2 - \eta^2}} \partial_\rho \right) \psi \right]^2. \quad (4.86)$$

Using the nonlinear Poisson-Boltzmann equation (4.82), equation (4.78) for the derivative of electric potential, relation (4.86) for pressure $P^{i(-2)}$, and the definition (4.69) for ψ , we would like to solve the order $\mathcal{O}(\lambda^{-2})$ of the angular component of the the Stokes' equation (4.47) for the leading order tangential component of the velocity $U_\eta^{i(0)}$,

$$\begin{aligned} \left(\xi_s \sqrt{\frac{\xi_s^2 - 1}{\xi_s^2 - \eta^2}} \partial_\rho \right)^2 U_\eta^{i(0)} &= \left(\xi_s \sqrt{\frac{1 - \eta^2}{\xi_s^2 - \eta^2}} \partial_\eta \right) P^{i(-2)} \\ &\quad - \left(\xi_s \sqrt{\frac{1 - \eta^2}{\xi_s^2 - \eta^2}} \partial_\eta \right) \Phi^{i(0)} \left(\xi_s \sqrt{\frac{\xi_s^2 - 1}{\xi_s^2 - \eta^2}} \partial_\rho \right)^2 \Phi^{i(0)}. \end{aligned}$$

The term containing pressure is

$$\begin{aligned} \left(\xi_s \sqrt{\frac{1 - \eta^2}{\xi_s^2 - \eta^2}} \partial_\eta \right) P^{i(-2)} &= \frac{1}{2} \left(\xi_s \sqrt{\frac{1 - \eta^2}{\xi_s^2 - \eta^2}} \partial_\eta \right) \left[\left(\xi_s \sqrt{\frac{\xi_s^2 - 1}{\xi_s^2 - \eta^2}} \partial_\rho \right) \psi \right]^2 \\ &= \frac{1}{2} \left(\xi_s \sqrt{\frac{1 - \eta^2}{\xi_s^2 - \eta^2}} \partial_\eta \right) \left(-2 \sqrt{C^{o(0)}(\xi_s, \eta)} \sinh(\psi/2) \right)^2 \\ &= \left(-2 \sqrt{C^{o(0)}(\xi_s, \eta)} \sinh(\psi/2) \right) \\ &\quad \times \left[\left(\xi_s \sqrt{\frac{1 - \eta^2}{\xi_s^2 - \eta^2}} \partial_\eta \right) \left(-2 \sqrt{C^{o(0)}(\xi_s, \eta)} \sinh(\psi/2) \right) \right] \\ &= \left(-2 \sqrt{C^{o(0)}(\xi_s, \eta)} \sinh(\psi/2) \right) \\ &\quad \times \left[-2 \sinh(\psi/2) \left(\xi_s \sqrt{\frac{1 - \eta^2}{\xi_s^2 - \eta^2}} \partial_\eta \right) \sqrt{C^{o(0)}(\xi_s, \eta)} \right. \\ &\quad \left. - \sqrt{C^{o(0)}(\xi_s, \eta)} \cosh(\psi/2) \left(\xi_s \sqrt{\frac{1 - \eta^2}{\xi_s^2 - \eta^2}} \partial_\eta \right) \psi \right] \end{aligned}$$

$$\begin{aligned}
&= 2 \sinh^2(\psi/2) \left(\xi_s \sqrt{\frac{1-\eta^2}{\xi_s^2 - \eta^2}} \partial_\eta \right) C^{o(0)}(\xi_s, \eta) \\
&\quad + C^{o(0)}(\xi_s, \eta) \sinh \psi \left(\xi_s \sqrt{\frac{1-\eta^2}{\xi_s^2 - \eta^2}} \partial_\eta \right) \psi
\end{aligned} \tag{4.87}$$

The electric body force takes the form

$$\begin{aligned}
&\left(\xi_s \sqrt{\frac{1-\eta^2}{\xi_s^2 - \eta^2}} \partial_\eta \right) \Phi^{i(0)} \left(\xi_s \sqrt{\frac{\xi_s^2 - 1}{\xi_s^2 - \eta^2}} \partial_\rho \right)^2 \Phi^{i(0)} \\
&= \left(\xi_s \sqrt{\frac{1-\eta^2}{\xi_s^2 - \eta^2}} \partial_\eta \right) (\psi + \Phi^{i(0)}(\infty, \eta)) \left(\xi_s \sqrt{\frac{\xi_s^2 - 1}{\xi_s^2 - \eta^2}} \partial_\rho \right)^2 \psi \\
&= \left(\xi_s \sqrt{\frac{1-\eta^2}{\xi_s^2 - \eta^2}} \partial_\eta \right) \psi \left(\xi_s \sqrt{\frac{\xi_s^2 - 1}{\xi_s^2 - \eta^2}} \partial_\rho \right)^2 \psi \\
&\quad + \left(\xi_s \sqrt{\frac{1-\eta^2}{\xi_s^2 - \eta^2}} \partial_\eta \right) \Phi^{i(0)}(\infty, \eta) \left(\xi_s \sqrt{\frac{\xi_s^2 - 1}{\xi_s^2 - \eta^2}} \partial_\rho \right)^2 \psi \\
&= C^{o(0)}(\xi_s, \eta) \sinh \psi \left(\xi_s \sqrt{\frac{1-\eta^2}{\xi_s^2 - \eta^2}} \partial_\eta \right) \psi \\
&\quad + \left(\xi_s \sqrt{\frac{1-\eta^2}{\xi_s^2 - \eta^2}} \partial_\eta \right) \Phi^{i(0)}(\infty, \eta) \left(\xi_s \sqrt{\frac{\xi_s^2 - 1}{\xi_s^2 - \eta^2}} \partial_\rho \right)^2 \psi
\end{aligned} \tag{4.88}$$

Therefore, the angular component of the velocity to the leading order in λ becomes

$$\begin{aligned}
\left(\xi_s \sqrt{\frac{\xi_s^2 - 1}{\xi_s^2 - \eta^2}} \partial_\rho \right)^2 U_\eta^{i(0)} &= 2 \sinh^2(\psi/2) \left(\xi_s \sqrt{\frac{1-\eta^2}{\xi_s^2 - \eta^2}} \partial_\eta \right) C^{o(0)}(\xi_s, \eta) \\
&\quad - \left(\xi_s \sqrt{\frac{1-\eta^2}{\xi_s^2 - \eta^2}} \partial_\eta \right) \Phi^{i(0)}(\infty, \eta) \left(\xi_s \sqrt{\frac{\xi_s^2 - 1}{\xi_s^2 - \eta^2}} \partial_\rho \right)^2 \psi
\end{aligned} \tag{4.89}$$

Integrating the above equation gives us

$$\begin{aligned}
& \int_{\rho}^{\infty} \left(\xi_s \sqrt{\frac{\xi_s^2 - 1}{\xi_s^2 - \eta^2}} \partial_{\rho} \right)^2 U_{\eta}^{i(0)} d\rho = \left(\xi_s \sqrt{\frac{\xi_s^2 - 1}{\xi_s^2 - \eta^2}} \right)^2 \int_{\rho}^{\infty} \partial_{\rho} U_{\eta}^{i(0)} d\rho \\
& = 2 \left(\xi_s \sqrt{\frac{1 - \eta^2}{\xi_s^2 - \eta^2}} \partial_{\eta} \right) C^{o(0)}(\xi_s, \eta) \int_{\rho}^{\infty} \sinh^2(\psi/2) d\rho \\
& \quad - \left(\xi_s \sqrt{\frac{1 - \eta^2}{\xi_s^2 - \eta^2}} \partial_{\eta} \right) \Phi^{i(0)}(\infty, \eta) \left(\xi_s \sqrt{\frac{\xi_s^2 - 1}{\xi_s^2 - \eta^2}} \right)^2 \int_{\rho}^{\infty} \partial_{\rho}^2 \psi d\rho \\
& = 2 \left(\xi_s \sqrt{\frac{1 - \eta^2}{\xi_s^2 - \eta^2}} \partial_{\eta} \right) C^{o(0)}(\xi_s, \eta) \int_{\psi}^0 \sinh^2(\psi/2) \left(\frac{\partial \rho}{\partial \psi} \right) d\psi \\
& \quad - \left(\xi_s \sqrt{\frac{1 - \eta^2}{\xi_s^2 - \eta^2}} \partial_{\eta} \right) \Phi^{i(0)}(\infty, \eta) \left(\xi_s \sqrt{\frac{\xi_s^2 - 1}{\xi_s^2 - \eta^2}} \right)^2 \left[\partial_{\rho} \psi \right]_{\rho}^{\infty} \\
& = 2 \left(\xi_s \sqrt{\frac{1 - \eta^2}{\xi_s^2 - \eta^2}} \partial_{\eta} \right) C^{o(0)}(\xi_s, \eta) \\
& \quad \times \int_{\psi}^0 \frac{\sinh^2(\psi/2)}{-2 \left(\frac{1}{\xi_s} \sqrt{\frac{\xi_s^2 - \eta^2}{\xi_s^2 - 1}} \right) \sqrt{C^{o(0)}(\xi_s, \eta)} \sinh(\psi/2)} d\psi \\
& \quad + \left(\xi_s \sqrt{\frac{1 - \eta^2}{\xi_s^2 - \eta^2}} \partial_{\eta} \right) \Phi^{i(0)}(\infty, \eta) \left(\xi_s \sqrt{\frac{\xi_s^2 - 1}{\xi_s^2 - \eta^2}} \right)^2 \partial_{\rho} \psi \\
& = - \frac{\left(\xi_s \sqrt{\frac{1 - \eta^2}{\xi_s^2 - \eta^2}} \partial_{\eta} \right) C^{o(0)}(\xi_s, \eta)}{\sqrt{C^{o(0)}(\xi_s, \eta)}} \left(\xi_s \sqrt{\frac{\xi_s^2 - 1}{\xi_s^2 - \eta^2}} \right) \int_{\psi}^0 \sinh(\psi/2) d\psi \\
& \quad + \left(\xi_s \sqrt{\frac{1 - \eta^2}{\xi_s^2 - \eta^2}} \partial_{\eta} \right) \Phi^{i(0)}(\infty, \eta) \left(\xi_s \sqrt{\frac{\xi_s^2 - 1}{\xi_s^2 - \eta^2}} \right)^2 \partial_{\rho} \psi \\
& = 2 \frac{\left(\xi_s \sqrt{\frac{1 - \eta^2}{\xi_s^2 - \eta^2}} \partial_{\eta} \right) C^{o(0)}(\xi_s, \eta)}{\sqrt{C^{o(0)}(\xi_s, \eta)}} \left(\xi_s \sqrt{\frac{\xi_s^2 - 1}{\xi_s^2 - \eta^2}} \right) [\cosh(\psi/2) - 1] \\
& \quad + \left(\xi_s \sqrt{\frac{1 - \eta^2}{\xi_s^2 - \eta^2}} \partial_{\eta} \right) \Phi^{i(0)}(\infty, \eta) \left(\xi_s \sqrt{\frac{\xi_s^2 - 1}{\xi_s^2 - \eta^2}} \right)^2 \partial_{\rho} \psi \quad (4.90)
\end{aligned}$$

Using the relation $\int_{\rho}^{\infty} \partial_{\rho}^2 U_{\eta}^{i(0)} d\rho = -\partial_{\rho} U_{\eta}^{i(0)}$ we obtain

$$\begin{aligned}
& - \left(\xi_s \sqrt{\frac{\xi_s^2 - 1}{\xi_s^2 - \eta^2}} \right)^2 \partial_{\rho} U_{\eta}^{i(0)} \\
& = 2 \frac{\left(\xi_s \sqrt{\frac{1-\eta^2}{\xi_s^2 - \eta^2}} \partial_{\eta} \right) C^{o(0)}(\xi_s, \eta)}{\sqrt{C^{o(0)}(\xi_s, \eta)}} \left(\xi_s \sqrt{\frac{\xi_s^2 - 1}{\xi_s^2 - \eta^2}} \right) [\cosh(\psi/2) - 1] \\
& \quad + \left(\xi_s \sqrt{\frac{1-\eta^2}{\xi_s^2 - \eta^2}} \partial_{\eta} \right) \Phi^{i(0)}(\infty, \eta) \left(\xi_s \sqrt{\frac{\xi_s^2 - 1}{\xi_s^2 - \eta^2}} \right)^2 \partial_{\rho} \psi \quad (4.91)
\end{aligned}$$

Factoring out $\left(\xi_s \sqrt{\frac{\xi_s^2 - 1}{\xi_s^2 - \eta^2}} \right)$ from the both sides of the equation yields

$$\begin{aligned}
\left(\xi_s \sqrt{\frac{\xi_s^2 - 1}{\xi_s^2 - \eta^2}} \partial_{\rho} \right) U_{\eta}^{i(0)} & = -2 [\cosh(\psi/2) - 1] \frac{\left(\xi_s \sqrt{\frac{1-\eta^2}{\xi_s^2 - \eta^2}} \partial_{\eta} \right) C^{o(0)}(\xi_s, \eta)}{\sqrt{C^{o(0)}(\xi_s, \eta)}} \\
& \quad - \left(\xi_s \sqrt{\frac{1-\eta^2}{\xi_s^2 - \eta^2}} \partial_{\eta} \right) \Phi^{i(0)}(\infty, \eta) \left(\xi_s \sqrt{\frac{\xi_s^2 - 1}{\xi_s^2 - \eta^2}} \partial_{\rho} \right) \psi \quad (4.92)
\end{aligned}$$

Further integration of this equation using the relation (4.79) and the no-slip boundary condition gives us the inner tangential velocity to the leading order in λ ,

$$\begin{aligned}
U_{\eta}^{i(0)} & = (\psi_0 - \psi) \left(\xi_s \sqrt{\frac{1-\eta^2}{\xi_s^2 - \eta^2}} \partial_{\eta} \right) \Phi^{i(0)}(\infty, \eta) \\
& \quad + 4 \frac{\rho}{\xi_s \sqrt{\frac{\xi_s^2 - 1}{\xi_s^2 - \eta^2}}} \frac{\left(\xi_s \sqrt{\frac{1-\eta^2}{\xi_s^2 - \eta^2}} \partial_{\eta} \right) C^{o(0)}(\xi_s, \eta)}{\sqrt{C^{o(0)}(\xi_s, \eta)}} \\
& \quad + 2 \left(\xi_s \sqrt{\frac{1-\eta^2}{\xi_s^2 - \eta^2}} \partial_{\eta} \right) \ln C^{o(0)}(\xi_s, \eta) \ln \left\{ \frac{1 - \tanh^2(\psi_0/4)}{\exp \left[\frac{2\rho \sqrt{C^{o(0)}(\xi_s, \eta)}}{\xi_s \sqrt{\frac{\xi_s^2 - 1}{\xi_s^2 - \eta^2}}} \right] - \tanh^2(\psi_0/4)} \right\} \quad (4.93)
\end{aligned}$$

Considering $\Phi^{i(0)}(\infty, \eta) = \Phi^{o(0)}(\xi_s, \eta)$, the slip velocity takes the form

$$\begin{aligned} U_{slip}^{(0)} &= \lim_{\rho \rightarrow \infty} U_{\eta}^{i(0)} \\ &= \psi_0 \left(\xi_s \sqrt{\frac{1 - \eta^2}{\xi_s^2 - \eta^2}} \partial_{\eta} \right) \Phi^{o(0)}(\xi_s, \eta) \\ &\quad + 2 \ln \{1 - \tanh^2(\psi_0/4)\} \left(\xi_s \sqrt{\frac{1 - \eta^2}{\xi_s^2 - \eta^2}} \partial_{\eta} \right) \ln C^{o(0)}(\xi_s, \eta) \end{aligned} \quad (4.94)$$

$$\begin{aligned} &= \psi_0 \left(\xi_s \sqrt{\frac{1 - \eta^2}{\xi_s^2 - \eta^2}} \partial_{\eta} \right) \Phi^{o(0)}(\xi_s, \eta) \\ &\quad - 4 \ln \cosh(\psi_0/4) \left(\xi_s \sqrt{\frac{1 - \eta^2}{\xi_s^2 - \eta^2}} \partial_{\eta} \right) \ln C^{o(0)}(\xi_s, \eta) \end{aligned} \quad (4.95)$$

This relation is the equivalent form of the Dukhin-Deryaguin slip formula that is used as a slip boundary condition for the outer region.

So far we have calculated the slip velocity as a boundary condition for Stokes flow in the outer region. We need to have the leading order fluxes of ions as boundary condition for the continuity of species in the outer region too. For this purpose, we use the order $\mathcal{O}(\lambda^{-1})$ of the equation of continuity of species (2.26) in the inner region,

$$\partial_{\rho} J_{\pm\rho}^{i(0)} + \frac{\xi_s^2(2\xi_s^2 - 1 - \eta^2)}{(\xi_s^2 - \eta^2) \sqrt{(\xi_s^2 - \eta^2)(\xi_s^2 - 1)}} J_{\pm\rho}^{i(-1)} = 0. \quad (4.96)$$

From equation (4.55) we know that $J_{\pm\rho}^{i(-1)} = 0$, and therefore we have

$$\partial_{\rho} J_{\pm\rho}^{i(0)} = 0 \quad (4.97)$$

which means

$$J_{\pm\rho}^{i(0)}(\rho, \eta) = \hat{K}_{\pm}^{i(0)}(\eta) \quad (4.98)$$

This equation is valid in the inner region and should satisfy the boundary condition on the surface of the particle with boundary conditions

$$J_{+\rho}^{i(0)} \Big|_{\rho=0} = j_p f(\eta), \quad (4.99)$$

$$J_{-\rho}^{i(0)} \Big|_{\rho=0} = 0. \quad (4.100)$$

We obtain $\hat{K}_+^{''''}(\eta) = j_p f(\eta)$ and $\hat{K}_-^{''''}(\eta) = 0$. So, for the leading order of ion fluxes in the inner region we have

$$J_{+\rho}^{i(0)}(\rho, \eta) = j_p f(\eta), \quad (4.101)$$

$$J_{-\rho}^{i(0)}(\rho, \eta) = 0. \quad (4.102)$$

These boundary conditions, along with the matching conditions $J_{\pm\rho}^{i(0)}(\rho \rightarrow \infty, \eta) = J_{\pm\xi}^{o(0)}(\xi \rightarrow \xi_s, \eta)$, give the boundary condition of the leading order ion fluxes for the outer region,

$$J_{+\xi}^{o(0)}(\xi_s, \eta) = j_p f(\eta), \quad (4.103)$$

$$J_{-\xi}^{o(0)}(\xi_s, \eta) = 0. \quad (4.104)$$

5.2 Regular Perturbation Analysis

Having lumped the properties of the inner layer into boundary conditions for the outer region, we would like to solve the leading order far field velocity of fluid in the frame of reference of the particle,

$$\mathbf{U}^{o(0)} = -\mathcal{U}^{(0)} \hat{\mathbf{e}}_x, \quad (4.105)$$

where $\mathcal{U}^{(0)}$ is the nanomotor velocity in the laboratory frame of reference to the leading order in λ . To do this, we use the leading order of Stoke's equation,

$$-\nabla P^{o(0)} + \nabla^2 \mathbf{U}^{o(0)} + \nabla \Phi^{o(0)} \nabla^2 \Phi^{o(0)} = 0 \quad (4.106)$$

with the slip velocity (4.95) boundary condition

$$\mathbf{U}^{o(0)}(\xi_s, \eta) = U_{slip}^{(0)} \hat{\mathbf{e}}_\eta. \quad (4.107)$$

Using the electro-neutrality condition $C^{o(0)} = C_+^{o(0)} = C_-^{o(0)}$, the equations of continuity of species to the leading order in λ takes the form

$$\nabla \cdot \mathbf{J}_{\pm}^{o(0)} + Pe \mathbf{U}^{o(0)} \cdot \nabla C^{o(0)} = 0 \quad (4.108)$$

where

$$J_{\pm\xi}^{o(0)} = -\delta_{\pm}^{-1} \left[\left(\xi_s \sqrt{\frac{1-\eta^2}{\xi_s^2 - \eta^2}} \partial_{\eta} \right) C^{o(0)} \pm C^{o(0)} \left(\xi_s \sqrt{\frac{1-\eta^2}{\xi_s^2 - \eta^2}} \partial_{\eta} \right) \Phi^{o(0)} \right] \quad (4.109)$$

and boundary conditions

$$J_{+\xi}^{o(0)}(\xi_s, \eta) = j_p f(\eta), \quad (4.103)$$

$$J_{-\xi}^{o(0)}(\xi_s, \eta) = 0, \quad (4.104)$$

in the beginning of the inner region and the far field ($\xi \rightarrow \infty$) boundary conditions

$$\nabla \Phi^o = 0, \quad (4.110)$$

$$C_{\pm}^o = 1, \quad (4.111)$$

$$\mathbf{J}_{\pm}^o = 0. \quad (4.112)$$

We can rewrite the equation (4.108) in the form

$$-\nabla \cdot (\nabla C^{o(0)} \pm C^{o(0)} \nabla \Phi^{o(0)}) + \delta_{\pm} Pe \mathbf{U}^{o(0)} \cdot \nabla C^{o(0)} = 0. \quad (4.113)$$

Adding and subtracting the above equations for positive and negative ions, we obtain

$$\nabla^2 C^{o(0)} = \left(\frac{\delta_+ + \delta_-}{2} \right) Pe \mathbf{U}^{o(0)} \cdot \nabla C^{o(0)} \quad (4.114)$$

$$\nabla \cdot (C^{o(0)} \nabla \Phi^{o(0)}) = \left(\frac{\delta_+ - \delta_-}{2} \right) Pe \mathbf{U}^{o(0)} \cdot \nabla C^{o(0)} \quad (4.115)$$

with corresponding boundary conditions in the beginning of the outer region ($\xi \rightarrow \xi_s$)

$$\left(\xi_s \sqrt{\frac{\xi_s^2 - 1}{\xi_s^2 - \eta^2}} \partial_{\xi} \right) C^{o(0)} = C^{o(0)} \left(\xi_s \sqrt{\frac{\xi_s^2 - 1}{\xi_s^2 - \eta^2}} \partial_{\xi} \right) \Phi^{o(0)} = \delta_+ j_p \left[\frac{-1}{2} f(\eta) \right], \quad (4.116)$$

and the far field ($\xi \rightarrow \infty$) boundary condition

$$\left(\xi_s \sqrt{\frac{\xi_s^2 - 1}{\xi_s^2 - \eta^2}} \partial_\xi \right) C^{o(0)} = C^{o(0)} \left(\xi_s \sqrt{\frac{\xi_s^2 - 1}{\xi_s^2 - \eta^2}} \partial_\xi \right) \Phi^{o(0)} = 0. \quad (4.117)$$

These equations are still nonlinear and thus making them difficult to solve. We linearize the equations by solving them in the limit of small j_p . Expansions of the fields in powers of j_p are of the forms

$$C^{o(0)} = 1 + j_p C^{o(0,1)} + \mathcal{O}(j_p^2), \quad (4.118)$$

$$\Phi^{o(0)} = \Phi^{o(0,0)} + j_p \Phi^{o(0,1)} + \mathcal{O}(j_p^2), \quad (4.119)$$

$$\phi^{(0)} = \phi_0 + \mathcal{O}(j_p), \quad (4.120)$$

$$\mathbf{U}^{o(0)} = j_p \mathbf{U}^{o(0,1)} + \mathcal{O}(j_p^2), \quad (4.121)$$

$$\mathcal{U}^{(0)} = j_p \mathcal{U}^{(0,1)} + \mathcal{O}(j_p^2), \quad (4.122)$$

$$P^{o(0)} = j_p P^{o(0,1)} + \mathcal{O}(j_p^2). \quad (4.123)$$

in which we have used the notation

$$\phi_0 \equiv \phi^{(0,0)} \quad (4.124)$$

for the electric potential at the surface of particle to the leading order in λ and j_p . To leading order in j_p equation (4.115) with boundary conditions (4.116) on the surface of the particle and (4.117) as ξ goes to infinity result in

$$\nabla^2 \Phi^{o(0,0)} = 0 \quad (4.125)$$

$$\left(\xi_s \sqrt{\frac{\xi_s^2 - 1}{\xi_s^2 - \eta^2}} \partial_\xi \right) \Phi^{o(0,0)} = 0 \quad \xi = \xi_s \quad (4.126)$$

$$\Phi^{o(0,0)} = 0 \quad \xi \rightarrow \infty \quad (4.127)$$

Therefore, $\Phi^{o(0,0)} = 0$, and consequently, on the surface,

$$\Phi^{o(0,0)}(\xi_s, \eta) = 0 \quad (4.128)$$

To first order in j_p equations (4.114) and (4.115) with boundary conditions (4.116)

on the surface of the particle and (4.117) as $\xi \rightarrow \infty$ result in

$$\nabla^2 C^{o(0,1)} = 0 \quad (4.129)$$

$$\left(\xi_s \sqrt{\frac{\xi_s^2 - 1}{\xi_s^2 - \eta^2}} \partial_\xi \right) C^{o(0,1)} = -\frac{1}{2} \delta_+ f(\eta) \quad \xi = \xi_s \quad (4.130)$$

$$C^{o(0,1)} = 0 \quad \xi \rightarrow \infty \quad (4.131)$$

and

$$\nabla^2 \Phi^{o(0,1)} = 0 \quad (4.132)$$

$$\left(\xi_s \sqrt{\frac{\xi_s^2 - 1}{\xi_s^2 - \eta^2}} \partial_\xi \right) \Phi^{o(0,1)} = -\frac{1}{2} \delta_+ f(\eta) \quad \xi = \xi_s \quad (4.133)$$

$$\Phi^{o(0,1)} = 0 \quad \xi \rightarrow \infty \quad (4.134)$$

which yields

$$C^{o(0,1)} = \Phi^{o(0,1)}. \quad (4.135)$$

The Stokes' equation to the leading order in j_p takes the form

$$-\nabla P^{o(0,1)} + \nabla^2 \mathbf{U}^{o(0,1)} = 0 \quad (4.136)$$

This equation apparently doesn't contain any dependence on concentration and electric potential as the differential equation has no electric body force term. However, the effect of electric potential appears in the slip velocity boundary condition. To leading order in j_p on the surface of the particle (beginning of the outer region) we have

$$U_\xi^{(0,1)} = 0 \quad (4.137)$$

For the tangential velocity, we use the Taylor expansion $\ln \cosh x = \frac{x^2}{2} - \frac{x^4}{12} + \dots$ and equation (4.135), to expand the slip velocity (4.95) in powers of j_p ,

$$U_{slip}^{(0)} = j_p U_{slip}^{(0,1)} + \mathcal{O}(j_p^2), \quad (4.138)$$

where

$$U_{slip}^{(0,1)} = \left[\phi_0 - 4 \ln \cosh \left(\frac{\phi_0}{4} \right) \right] \left(\xi_s \sqrt{\frac{1 - \eta^2}{\xi_s^2 - \eta^2}} \partial_\eta \right) \Phi^{o(0,1)}(\xi_s, \eta). \quad (4.139)$$

Changing the coordinates from particle frame of reference to laboratory frame of reference, we can solve the velocity using

$$-\nabla P^{o(0,1)} + \nabla^2 \mathbf{U}^{o(0,1)} = 0 \quad (4.140)$$

$$\xi = \xi_s : \quad \mathbf{U}^{(0,1)} = U_{slip}^{(0,1)} \hat{\mathbf{e}}_\eta + \mathcal{U}^{(0,1)} \hat{\mathbf{e}}_x \quad (4.141)$$

$$\xi \rightarrow \infty : \quad \mathbf{U}^{o(0,1)} = 0 \quad (4.142)$$

The particle is moving with constant velocity; therefore, according to Newton's first law, the particle is force-free, $\mathbf{F}^{o(0,1)} = 0$. Since velocity vanishes at infinity, we can exploit the Lorentz reciprocal theorem to solve for the unknown $\mathcal{U}^{(0,1)}$. The Lorentz reciprocal theorem relates the solution of two different Stokes flows through

$$\int_S ds \hat{\mathbf{n}} \cdot \mathbb{T}^{o(0,1)} \cdot \mathbf{U}' = \int_S ds \hat{\mathbf{n}} \cdot \mathbb{T}' \cdot \mathbf{U}^{o(0,1)} \quad (4.143)$$

where

$$\mathbb{T}^{o(0,1)} = -p^{o(0,1)} \mathbb{I} + \nabla \mathbf{U}^{o(0,1)} + (\nabla \mathbf{U}^{o(0,1)})^T \quad (4.144)$$

is the stress tensor for the flow in our problem, whereas \mathbf{U}' and \mathbb{T}' are respectively the known velocity field and the stress tensor of another Stokes flow for this geometry. In order to proceed, let's assume that \mathbf{U}' corresponds to a flow caused by a spheroid with velocity $\hat{\mathbf{e}}_x$. The corresponding traction on the surface, according to appendix **B**, is

$$\hat{\mathbf{n}} \cdot \mathbb{T}' = \frac{-4\alpha}{e\sqrt{(\xi_s^2 - \eta^2)(\xi_s^2 - 1)}} \hat{\mathbf{e}}_x \quad (4.145)$$

Inserting the corresponding entities in equation (4.143) yields

$$\int_S ds \hat{\mathbf{n}} \cdot \mathbb{T}' \cdot \mathbf{U}^{o(0,1)} = \int_S ds \hat{\mathbf{n}} \cdot \mathbb{T}^{o(0,1)} \cdot \hat{\mathbf{e}}_x \quad (4.146)$$

The force-free condition leads to $\int_S ds \hat{\mathbf{n}} \cdot \mathbb{T}^{o(0,1)} \cdot \hat{\mathbf{e}}_x = \mathbf{F}_x^{o(0,1)} = 0$, and using the integral relation, $\int_S ds \hat{\mathbf{n}} \cdot \mathbb{T}' \cdot \mathbf{U}^{o(0,1)} = -4\alpha \int_S ds \frac{1}{e\sqrt{(\xi_s^2 - \eta^2)(\xi_s^2 - 1)}} \hat{\mathbf{e}}_x \cdot \mathbf{U}^{o(0,1)}$, we

obtain

$$\int_S ds \frac{1}{e\sqrt{(\xi_s^2 - \eta^2)(\xi_s^2 - 1)}} \hat{\mathbf{e}}_x \cdot \mathbf{U}^{o(0,1)} = 0 \quad (4.147)$$

The surface element on the surface of the spheroid ($\xi = \xi_s$) is

$$ds = h_\eta d\eta h_\phi d\phi = e \sqrt{\frac{\xi_s^2 - \eta^2}{1 - \eta^2}} e \sqrt{(\xi_s^2 - 1)(1 - \eta^2)} d\eta d\phi \quad (4.148)$$

and we have

$$\begin{aligned} \frac{ds}{e\sqrt{(\xi_s^2 - \eta^2)(\xi_s^2 - 1)}} &= \frac{d\eta d\phi}{e\sqrt{(\xi_s^2 - \eta^2)(\xi_s^2 - 1)}} e \sqrt{\frac{\xi_s^2 - \eta^2}{1 - \eta^2}} e \sqrt{(\xi_s^2 - 1)(1 - \eta^2)} \\ &= e d\eta d\phi. \end{aligned} \quad (4.149)$$

Using

$$\hat{\mathbf{e}}_x \cdot \hat{\mathbf{e}}_\eta = \xi_s \sqrt{\frac{1 - \eta^2}{\xi_s^2 - \eta^2}}, \quad (4.150)$$

the integral equation (4.147) takes the form

$$\begin{aligned} 0 &= \int_S ds \frac{1}{e\sqrt{(\xi_s^2 - \eta^2)(\xi_s^2 - 1)}} \hat{\mathbf{e}}_x \cdot \mathbf{U}^{o(0,1)} \\ &= \int_S e d\eta d\phi \left\{ \left(\xi_s \sqrt{\frac{1 - \eta^2}{\xi_s^2 - \eta^2}} \right) \left[\phi_0 - 4 \ln \cosh \left(\frac{\phi_0}{4} \right) \right] \right. \\ &\quad \left. \times \left(\xi_s \sqrt{\frac{1 - \eta^2}{\xi_s^2 - \eta^2}} \partial_\eta \right) \Phi^{o(0,1)}(\xi_s, \eta) + \mathcal{U}^{(0,1)} \right\} \end{aligned} \quad (4.151)$$

Therefore,

$$\mathcal{U}^{(0,1)} = -\frac{1}{2} \left[\phi_0 - 4 \ln \cosh \left(\frac{\phi_0}{4} \right) \right] \xi_s \int_S d\eta \left(\xi_s \sqrt{\frac{1 - \eta^2}{\xi_s^2 - \eta^2}} \right)^2 \partial_\eta \Phi^{o(0,1)}(\xi_s, \eta) \quad (4.152)$$

To take the integral, we need to solve for $\Phi^{m(0,1)}$ that satisfies the Laplace equation.

The general form solution for this geometry is

$$\Phi^{m(0,1)} = \sum_{n=0}^{\infty} A_n Q_n(\xi) P_n(\eta) \quad (4.153)$$

where P_n and Q_n are the Legendre functions of first and second kind, respectively. The function $Q_n(\xi)$ can be written either in the form [39]

$$Q_n(\xi) = P_n(\xi)Q_0(\xi) - \sum_{k=0}^{n-1} \frac{(2k+1)[1 - (-1)^{n+k}]}{(n+k+1)(n-k)} P_k(\xi) \quad (4.154)$$

where

$$Q_0(\xi) = \frac{1}{2} \ln \frac{\xi+1}{\xi-1} \quad (4.155)$$

or in the form [40]

$$Q_n(\xi) = \frac{\sqrt{\pi} \Gamma(n+1)}{\Gamma(n+\frac{3}{2}) (2\xi)^{n+1}} F\left(\frac{1}{2}n+1, \frac{1}{2}n+\frac{1}{2}; n+\frac{3}{2}; \xi^{-2}\right) \quad n \geq 0 \quad (4.156)$$

where the gamma function is

$$\Gamma(n) = \int_0^\infty t^{n-1} e^{-t} dt \quad (4.157)$$

and the hypergeometric function is

$$F(a, b; c; z) = \sum_{k=0}^{\infty} \frac{(a)_k (b)_k}{(c)_k k!} z^k \quad |z| < 1. \quad (4.158)$$

with

$$(a)_0 = 1, \quad (a)_k = \Gamma(a+k)/\Gamma(a) \quad k \geq 0. \quad (4.159)$$

We calculate the coefficients A_n using

$$\left(\xi_s \sqrt{\frac{\xi_s^2 - 1}{\xi_s^2 - \eta^2}} \partial_\xi \right) \Phi^{o(0,1)} = -\frac{1}{2} \delta_+ f(\eta) \quad \xi = \xi_s \quad (4.160)$$

that is,

$$\partial_\xi \Phi^{o(0,1)} \Big|_{\xi=\xi_s} = -\frac{\delta_+}{2\xi_s} \sqrt{\frac{\xi_s^2 - \eta^2}{\xi_s^2 - 1}} f(\eta) \quad (4.161)$$

Therefore,

$$\sum_{n=0}^{\infty} A_n \partial_\xi Q_n(\xi) \Big|_{\xi=\xi_s} P_n(\eta) = -\frac{\delta_+}{2\xi_s} \sqrt{\frac{\xi_s^2 - \eta^2}{\xi_s^2 - 1}} f(\eta) \quad (4.162)$$

Using the orthogonality relation

$$\int_{-1}^1 d\eta P_n(\eta) P_m(\eta) = \frac{2}{2n+1} \delta_{mn} \quad (4.163)$$

we obtain

$$A_n = - \left(\frac{2n+1}{4} \right) \left(\frac{1}{\partial_\xi Q_n(\xi) \Big|_{\xi=\xi_s}} \right) \delta_+ \int_{-1}^1 d\eta \frac{1}{\xi_s} \sqrt{\frac{\xi_s^2 - \eta^2}{\xi_s^2 - 1}} P_n(\eta) f(\eta) \quad (4.164)$$

and therefore,

$$\mathcal{U}^{(0,1)} = -\frac{1}{2} \left[\phi_0 - 4 \ln \cosh \left(\frac{\phi_0}{4} \right) \right] \xi_s \sum_{n=0}^{\infty} A_n Q_n(\xi_s) \int_{-1}^1 d\eta \left(\sqrt{\frac{1-\eta^2}{\xi_s^2 - \eta^2}} \right)^2 \partial_\eta P_n(\eta) \quad (4.165)$$

We can write the final results as

$$\boxed{\mathcal{U} \simeq \frac{-1}{4} \delta_+ \mathcal{F} j_p \left[\phi_0 - 4 \ln \cosh \left(\frac{\phi_0}{4} \right) \right]} \quad (4.166)$$

where the geometric factor is

$$\begin{aligned} \mathcal{F} &= -\xi_s \sum_{n=0}^{\infty} Q_n(\xi_s) \left(\frac{2n+1}{2\partial_\xi Q_n(\xi) \Big|_{\xi=\xi_s}} \right) \left[\int_{-1}^1 d\eta \sqrt{\frac{\xi_s^2 - \eta^2}{\xi_s^2 - 1}} P_n(\eta) f(\eta) \right] \\ &\times \left[\int_{-1}^1 d\eta \left(\sqrt{\frac{1-\eta^2}{\xi_s^2 - \eta^2}} \right)^2 \partial_\eta P_n(\eta) \right]. \end{aligned} \quad (4.167)$$

In the limit $e \rightarrow 0$, \mathcal{F} reduces to

$$\mathcal{F} = \int_{-1}^1 d\eta P_1(\eta) f(\eta) \equiv f_1 \quad (4.168)$$

which is the same as in case of the sphere, that is, equation (3.92).

Design Principles

1 Introduction

In the preceding chapters, we studied the physics of electrokinetic self-propulsion, and formulated a mathematical model to describe it (chapter 2). Using the method of matched asymptotic expansions, we solved the model problem for spherical (chapter 3) and spheroidal particles (chapter 4) through rigorous mathematical calculations. While we solved the nonlinear equations to the leading order in dimensionless Debye length and first order in dimensionless strength of hydrogen ion flux, we can, in principle, solve the equations to higher orders of the small parameter(s) and obtain for precise solutions. The possibility to solve the equations with controllable approximation to our desired precision is an important advantage of perturbation analysis. In addition, it yields an analytical result that demonstrates the interplay between the parameters of the physical system under study.

Another approach for establishing a relationship between the parameters of the physical system is to perform a scaling analysis. Such an analysis is based on certain assumptions, and there is no control over the precision of the approximation. Moreover, the results are in the form of a proportionality relationship rather than an equality. This type of analysis has been frequently used in the nanomotor studies for its simplicity. In this chapter, we will apply scaling analysis to find a relationship between the velocity of the nanomotor and the parameters of the system. We will discuss the validity of the results and show how scaling analysis can be misleading in understanding the dependence of velocity on Debye length

and its related quantities.

We will study the limits of accuracy of the perturbation analysis, and also use numerical calculations to find the maximum possible velocity that can be achieved by nanomotors. Using the aforementioned studies, we will discuss the design principles that lead us to develop nanomotors with desired properties.

2 Scaling Analysis

Using scaling analysis, Moran *et al.* [26] have proposed the electroviscous velocity

$$\underline{U}_{ev} \propto \frac{\underline{h}\lambda_D F}{\mu D_+} \underline{\phi}_0 \underline{j}^p \quad (5.1)$$

for a nanorod of length \underline{h} and interfacial potential $\underline{\phi}_0$. The difference between this formula and our equation (3.95) for the nanomotor velocity is the appearance of the nanomotor length h instead of Debye length λ_D in the numerator of equation (5.1). Moran *et al.* have not provided a fully detailed explanation of these assumptions in order to derive their result. In this section, we will derive the same relationship for cylindrical and spherical nanomotors, including a detailed explanation of the assumptions involved to determine the possible source for the difference.

Assumption (1): The current of ions is limited to a region of thickness λ_D around the particle's surface. The current of ions pass through a region in space with average cross sectional area $\underline{A}_{current}$. These ions are produced from a surface area \underline{A}_{flux} . The current of ions in the Debye layer is equal to production current

$$\underline{I} \propto zF \underline{A}_{flux} \underline{j}^p. \quad (5.2)$$

Assumption (2): The electric field in the Debye layer that pulls the ion from source to sink is constant. The current of ions is related to electric field E_0 in the Debye layer through

$$\underline{I} \propto \underline{\sigma} \underline{A}_{current} \underline{E}_0 \quad (5.3)$$

where $\underline{\sigma}$ is the conductivity of the electrolyte.

Assumption (3): The charge density in the Debye layer is equal to the background charge density. This assumption implies

$$\varrho = \frac{z^2 F^2 \zeta^\infty D_+}{RT} = \frac{\epsilon D_+}{\lambda_D^2}. \quad (5.4)$$

Therefore,

$$\underline{E}_0 \propto \frac{\underline{A}_{flux}}{\underline{A}_{current}} \frac{zF \tilde{j}^p}{\varrho} = \frac{\underline{A}_{flux}}{\underline{A}_{current}} \frac{zF \tilde{j}^p \lambda_D^2}{\epsilon D_+} \quad (5.5)$$

Assumption (4): The double layer is very thin compared to particle size, $\lambda_D \ll \underline{R}$ (\underline{R} is the radius of either the rod or the sphere). In the case of a sphere, $\underline{A}_{flux} = \frac{1}{2}(4\pi \underline{R}^2)$ and $\underline{A}_{current} = 2\pi \underline{R}^2 \lambda_D / \pi \underline{R}$, leading to the uniform electric field

$$\underline{E}_0^{sph} \propto \frac{\underline{R}}{\lambda_D} \frac{zF \tilde{j}^p \lambda_D^2}{\epsilon D_+} = \frac{zF \tilde{j}^p \underline{R} \lambda_D}{\epsilon D_+}. \quad (5.6)$$

For a cylinder of length \underline{L} and radius \underline{R} , we have $\frac{\underline{A}_{flux}}{\underline{A}_{current}} = \frac{\pi \underline{R}^2 + \frac{1}{2}(2\pi \underline{R} \underline{L})}{2\pi \underline{R} \lambda_D} = \frac{\underline{R} + \underline{L}}{2\lambda_D}$. When the aspect ratio of the cylinder $\underline{L}/2\underline{R}$ is either very large or of order one, $\frac{\underline{A}_{flux}}{\underline{A}_{current}} \propto \frac{\underline{L}}{\lambda_D}$. In that case, the electric field for the cylinder is

$$\underline{E}_0^{cyl} \propto \frac{\underline{L}}{\lambda_D} \frac{zF \tilde{j}^p \lambda_D^2}{\epsilon D_+} = \frac{zF \tilde{j}^p \underline{L} \lambda_D}{\epsilon D_+}. \quad (5.7)$$

Defining \underline{h} to be the particle's length, where $\underline{h} = 2\underline{R}$ for a sphere and $\underline{h} = \underline{L}$ for a cylinder, equations (5.6) and (5.7) can be written in the unified form

$$\underline{E}_0 \propto \frac{zF \tilde{j}^p \underline{h} \lambda_D}{\epsilon D_+}. \quad (5.8)$$

From the Poisson-Boltzmann equation, $\epsilon \nabla^2 \phi = -\rho_e$, we can define a characteristic charge density ρ_{e_0} within the Debye layer as

$$\rho_{e_0} \propto \frac{\epsilon \phi_0}{\lambda_D^2}. \quad (5.9)$$

The electroviscous velocity can then be obtained from the Stokes equation as

$$\underline{u}_{ev} \propto \frac{\rho_{e_0} \underline{E}_0}{\mu / \underline{d}^2} \propto \left(\frac{\underline{d}}{\lambda_D} \right)^2 \frac{\epsilon \phi_0 \underline{E}_0}{\mu}, \quad (5.10)$$

where d is the viscous length scale.

Assumption (5): The viscous length d is equal to Debye length λ_D since the body force $\rho_e \mathbf{E}$ deriving the flow is primarily in the Debye layer. Based on this assumption, the electric field in equation (5.8) can be substituted into expression (5.10) for the particle velocity to yield

$$\underline{u}_{ev} \propto \frac{z \hbar \lambda_D F}{\mu D_+} \phi_0 \underline{j}_p^p \quad (5.11)$$

For $z = 1$, this expression reduces to equation (5.1) proposed in [26]. Equation (5.11) has two evident flaws. First, by increasing the length of the nanomotor, the velocity of the nanomotor increases without bound. This contradicts experimental observations. Also, since the Debye length is inversely proportional to ion charge z , the velocity will be independent of ion charge while in practice z is a parameter of the problem that can affect the dynamics of the nanomotor. The major reason behind the failure of the scaling analysis is that assuming a uniform electric field inside the double layer (assumption 2) is in violation of the requirement that the nanomotor surface be an equipotential surface. Therefore, the simplifying assumptions underlying the scaling analysis can be misleading in determining the relationship between nanomotor velocity and the parameters of the system, underscoring the need for a more detailed and rigorous analysis such as perturbation analysis.

3 The limits

We used the method of matched asymptotic expansions to solve the model for nanomotor velocity in the limit of very thin double layer ($\lambda_D/a \ll 1$) using singular perturbation analysis and weak hydrogen ion flux ($j_p \ll 1$). To the leading order in dimensionless Debye length λ and first order in strength of hydrogen ion flux

j_p , the nanomotor velocity is found to be

$$\underline{u}^{(0,1)} \simeq -\frac{\mathcal{F}}{4} \left(\frac{\epsilon}{\mu D_+ \mathcal{C}^\infty} \right) \underline{j}_p \left[\left(\frac{RT}{zF} \right) \underline{\phi}_0 - 4 \ln \cosh \left(\frac{RT}{zF} \frac{\underline{\phi}_0}{4} \right) \right] \quad (5.12)$$

where the geometric factor \mathcal{F} depends on particle geometry and the surface distribution of hydrogen ion flux. In the regime that these motors work, $10 \text{ mV} < \underline{\phi}_0 < 60 \text{ mV}$, the velocity of nanomotor exhibits negligible non-linearity in $\underline{\phi}_0$. That is, $\left(\frac{RT}{zF} \right) \underline{\phi}_0 \gg 4 \ln \cosh \left(\frac{RT}{4zF} \underline{\phi}_0 \right)$, and the velocity can be written as

$$\underline{u}^{(0,1)} \simeq -\frac{\mathcal{F}}{4} \left(\frac{\epsilon RT}{zF \mu D_+ \mathcal{C}^\infty} \right) \underline{j}_p \underline{\phi}_0^{(0,0)} \simeq -\frac{\mathcal{F}}{2} \left(\frac{\lambda_D^2 zF}{\mu D_+} \right) \underline{j}_p \underline{\phi}_0^{(0,0)} \quad (5.13)$$

In the domain of small parameters the velocity is independent of Peclet number because diffusive transport of ions is much faster than their convective transport. Although the size of the particle does not explicitly appear in these equations, its effect is to determine the range of validity of the perturbation analysis. The dimensionless flux strength is related to the particle size through $j_p = \underline{j}_p / \mathcal{J}^* = (\underline{j}_p / D_s \mathcal{C}^\infty) a$. Since the results of the perturbation analysis are expected to be valid for small j_p , increasing the particle size leads to a smaller range of validity in terms of the dimensional flux strength \underline{j}_p , and equation (5.13) will be valid for a smaller range of particle velocities. The conditions for small parameters

$$j_p = a \frac{\underline{j}_p}{D_s \mathcal{C}^\infty} \ll 1 \implies a \ll \frac{D_s \mathcal{C}^\infty}{\underline{j}_p} \quad (5.14)$$

and

$$\lambda = \frac{\lambda_D}{a} \ll 1 \implies a \gg \lambda_D \quad (5.15)$$

yields the expression

$$\underline{j}_p \ll \frac{D_s \mathcal{C}^\infty}{\lambda_D} \quad (5.16)$$

which implies that with decreasing pH (increasing \mathcal{C}^∞), the range of values of hydrogen ion flux for which we can use the results of the perturbation analysis increases.

The perturbation analysis is valid only for small values of hydrogen ion flux. To determine the maximum possible velocities and hydrogen ion fluxes within the model, we numerically solved the equations and boundary conditions using COMSOL Multiphysics 4.1a. In our calculations, we used the COMSOL modules Stokes flow and mathematical equations, with the zero Peclet approximation. We studied the dynamics of a spherical nanomotor of radius $1\ \mu\text{m}$ at different background concentrations corresponding to pH values of 5.2, 5.6, 6.0, 6.5 and 7.0. In the actual experiments, when the solution is exposed to air, carbon dioxide is dissolved in water and reduces the pH of the liquid. Therefore, we studied the dynamics of the nanomotor at smaller values of pH to examine the effect of changes in the background concentrations.

The maximum limit of velocity is reached when the hydrogen ion concentration becomes zero at the sink. Any further increase in the intensity \underline{j}_p at that point results in non-physical negative hydrogen ion concentrations at the sink. We determined the maximum velocity and maximum flux intensity for each pH and interfacial potential in our parameter space. The interfacial potentials considered in these computations are 5, 10, 15, \dots , 45, 50 mV.

Fig. 5.1a shows the maximum velocity of the nanomotor as a function of interfacial potential ϕ_0 for different values of pH. For a given value of ϕ_0 , the maximum nanomotor velocity increases with decreasing pH. While the maximum nanomotor velocities for all values of pH are about the same at lower values of ϕ_0 , their differences become more pronounced with increasing values of interfacial potential.

The effect of background concentration on the limiting hydrogen ion flux is depicted in Fig. 5.1b. For fixed ϕ_0 , the maximum flux decreases with increasing pH. The limiting state is determined by the concentration of hydrogen ions around the sink. At higher values of pH, the background concentration of hydrogen ions around the sink is low; therefore, a smaller strength of hydrogen ion flux is required to bring the concentration of hydrogen ions to zero at the sink. At lower values of pH, even for low values of ϕ_0 , the limiting flux has high values. With increasing interfacial potential, the concentration of hydrogen ions around the particle increases, and higher value of limiting flux is required to consume all of the hydrogen ions around the sink.

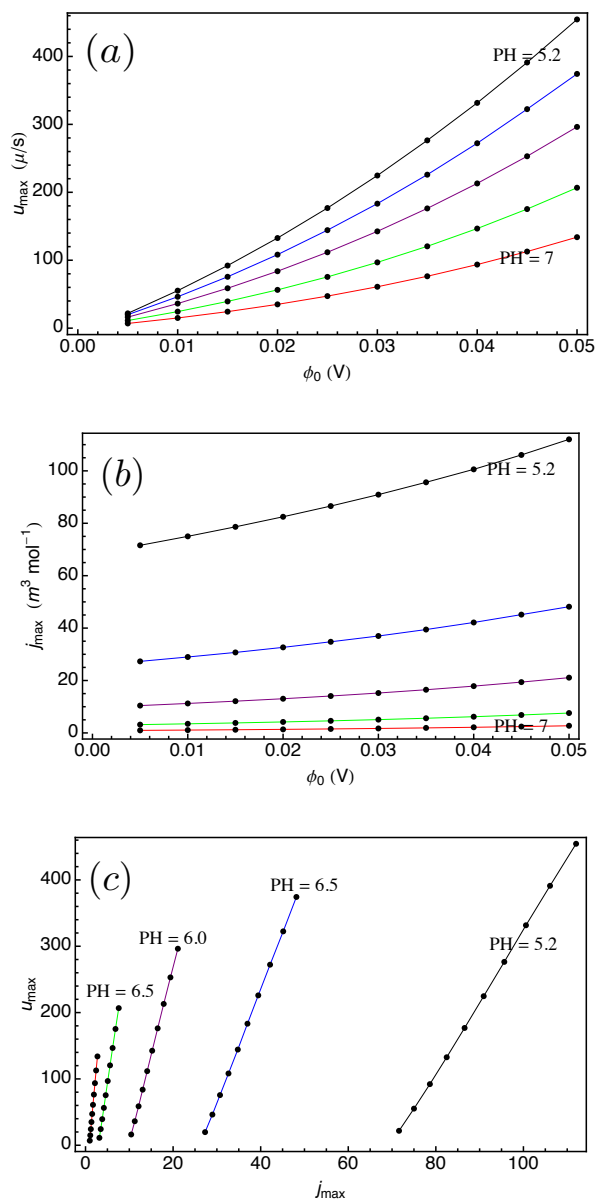


Figure 5.1. (a) Maximum velocity versus interfacial potential at different pH's. (b) maximum hydrogen ion flux versus interfacial potential at different pH's. (c) maximum velocity versus maximum interfacial potential at different pH's.

Fig. 5.1c demonstrates the relationship between the limiting velocity and limiting flux for different values of pH. It is clear from the figure that a given velocity can be achieved at lower flux as the pH increases. However, the highest achievable velocity decreases with decreasing pH.

4 Discussion

The dependence of nanomotor velocity on physical parameters such as viscosity, temperature, diffusivity, pH and charge of ions can be inferred by

$$\underline{u}^{(0,1)} \propto \left(\frac{\epsilon RT}{zF \mu D_+ C_\infty} \right) \underline{j}_p \underline{\phi}_0 \propto \left(\frac{\lambda_D^2 z F}{\mu D_+} \right) \underline{j}_p \underline{\phi}_0 \quad (5.17)$$

In addition to providing a better understanding of the experimental data, this equation furnishes us with a prediction tool for designing better nanomotors.

Increasing the viscosity leads to a reduction in nanomotor velocity. At low Reynolds number, inertial effects are negligible and viscous effects dominate flow behavior. An increase in viscosity results in a larger drag force, and consequently, a slower motion of the nanomotor. The effect of temperature is complicated by its effect on other parameters, such as viscosity or diffusivity. Nanomotor velocity has a nearly linear dependence on interfacial potential.

Increasing the diffusivity results in less asymmetry in the cloud of ions, leading to a smaller driving force on fluid elements, and a smaller particle velocity. The background concentration plays an interesting role. At high pH (near 7), where the concentration of hydrogen ions is low at a given flux, the ions should move from the source toward the sink so that the motor can function. However, at lower pH values, for the same amount of flux, there are more hydrogen ions available near the sink. Therefore, there is a smaller driving force for the produced ions from the source to move toward the sink, resulting in less force on fluid elements, and consequently, less velocity.

The velocity equation (5.17) shows that increasing the interfacial potentials leads to a higher speed for the nanomotor. Experimentally, we may be able to add some functional groups to the surface of the particle to make it more negatively charged. However, this manipulation has a counter effect by reducing the active sites on the particle needed for electrocatalytic decomposition of hydrogen peroxide. There can be an optimum point between these counter effects which can be tested experimentally.

Dynamics of Nanorotors

1 Introduction

All nanorotors must break inversion symmetry to induce rotation; beyond this simple geometrical fact, some particular mechanisms have been proposed for the origin of the resultant torques: bubble-derived [30], or electrokinetic [31] forces directed perpendicular to the motor axis and centered either towards one end of the rotor [30] or roughly through the rotor's geometrical center [31], as depicted in Figure 6.1. Tadpole-shaped hybrid Pt/TiO₂ nanorotors [41, 42] provide a third class of such devices.

Axisymmetric *linear* nanomotors are characterized by a deterministic linear speed v and a stochastic orientational diffusion coefficient D_o (plus a trivial contribution from translational diffusion D_t which does not couple directly to the powered motion). Therefore, a linear motor has two characteristic times: the time for powered motion to overcome translational diffusion, D_t/v^2 , and the time over which the motor orientation is forgotten, $\tau_o = D_o^{-1}$. Since linear nanomotors are axisymmetric, the motor's symmetry axis is always aligned with the instantaneous velocity. In contrast, rotary motors introduce a new timescale $\tau_\omega = 2\pi\omega^{-1}$ set by the angular velocity and nanorotor orientation has a more complex relationship with the instantaneous direction of the trajectory, a relationship which can be analyzed to extract information about the spatial distribution of driving forces along the surface of the rotor.

Most nanorotors developed to date are based on an underlying cylindrical

nanomotor geometry, with an added asymmetry-breaking part as a compositional variation. Hence, they retain a well-defined structural axis which is easily visible in optical microscopy. The asymmetric force distribution on the nanorotor generates not only a net torque, but also net forces along and perpendicular to this axis. The main axis of a nanorod is not necessarily tangent to the trajectory, in contrast to the case for translationally linear nanomotors.

In order to specify the orientation of the nanorotor with respect to its trajectory, we define ϕ (see Fig. 6.2(c)) to be the angle between the symmetry axis of the nanorod $\hat{\mathbf{n}}$ and the direction of translational velocity. Namely, $\phi = \cos^{-1}(\hat{\mathbf{n}} \cdot \vec{v}/v)$ or

$$\tan \phi = \frac{v_p}{v_n}, \quad (6.1)$$

where $\phi = \frac{\pi}{2}$ and $\phi = 0$ represent the motion of the nanorod perpendicular ($v_n = 0$, Fig. 6.2(d)) and tangent ($v_p = 0$) to its trajectory, respectively. The angle ϕ is easily extracted from experimental motor trajectories. (see Fig 6.2)

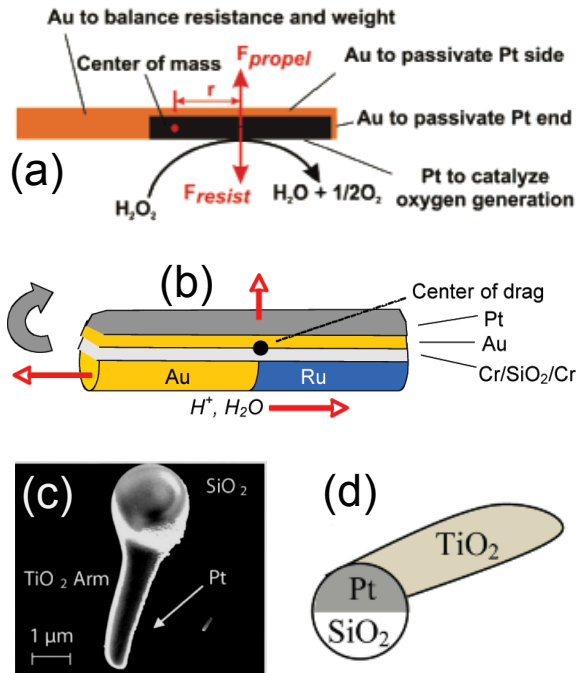


Figure 6.1. Nanorotors must break axial symmetry in some manner. Experimental implementations include (a) Au rods with asymmetric Pt patches [30], (b) Rh/Au rods with SiO₂/Au/Pt layers applied to one side [31], and (c) [41] and (d) [42] tadpole-like SiO₂/Pt/TiO₂ structures.

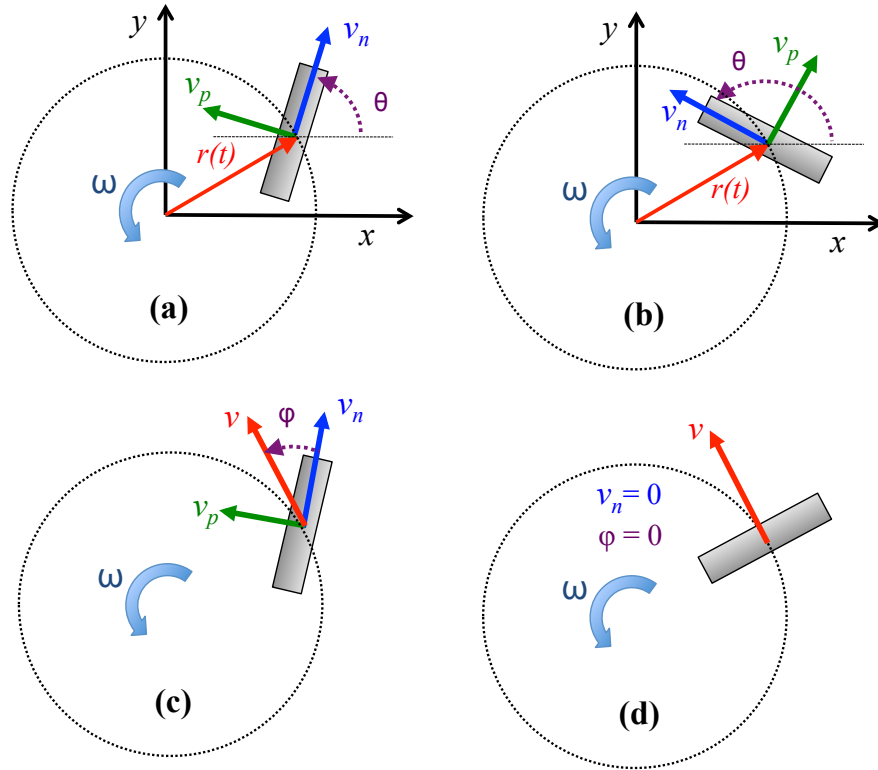


Figure 6.2. The deterministic motion of a nanorotor along a circular path with nanorotor head pointing (a) outside and (b) inside of the circle. (c) The angle ϕ is between the axis of the nanorod of direction $\hat{\mathbf{n}}$ and the direction of velocity. (d) If there is no force acting along the axis of the nanorod, its axis is perpendicular to its trajectory.

The instantaneous state of deterministic motion decomposes into solid rotation with angular velocity ω around some point \mathcal{O} fixed in the body frame and translation of point \mathcal{O} with velocity \vec{v} in the plane. The angular velocity ω is independent of \mathcal{O} . On symmetry grounds, the ideal (i.e. purely deterministic) trajectory of a nanorotor must be circular, and the instantaneous translational velocity can be decomposed into components along (v_n) and perpendicular (v_p) to the structural axis of the rotor. The radius of the trajectory is then:

$$R = \frac{\sqrt{v_n^2 + v_p^2}}{\omega} \equiv \frac{v}{\omega}. \quad (6.2)$$

The “observable” orientation, velocity, and angular velocity of the rotor can be related directly to the “unobservable” net force and net torque in order to gain insight into the motor mechanism. Since Stokes flow is linear, we can write the

net force \vec{F} and net torque \vec{L} on the motor as a linear superposition of \vec{v} and ω :

$$\vec{F} = \mathbb{A} \cdot \vec{v} + \mathbb{B}^T \cdot \vec{\omega}, \quad (6.3a)$$

$$\vec{L} = \mathbb{B} \cdot \vec{v} + \mathbb{D} \cdot \vec{\omega}, \quad (6.3b)$$

where \mathbb{A} and \mathbb{D} are true tensors and \mathbb{B} is a pseudo-tensor. These tensorial coefficients in principle depend on the geometry and electrokinetic characteristics of the system, but in the regime of dynamics of nanorotors, we can approximate these coefficients to be sole functions of geometry.

Assume that an operating nanomotor can be held immobile by an external force $-\vec{F}$ and torque $-\vec{L}$, i.e. that the action of the motor produces force and torque \vec{F} and \vec{L} . Compare this to a passive particle of the same dimensions on which external force and torque (\vec{F}, \vec{L}) are applied. At low Reynolds number, the steady motion of such a particle is linearly related to the applied (\vec{F}, \vec{L}) in a manner similar to (6.3). Since the Stokes equations are linear, we may add the two flows just discussed to obtain a flow corresponding to the sum of the forces, which is zero. The motor mechanism also produces body forces on the fluid; these are unchanged by the introduction of the second flow if the transport processes involved in the mechanism are fast enough. For an electrokinetic motor, the relevant transport is ionic diffusion over distances comparable to the motor size, corresponding to a speed $D_{\text{ion}}/\ell \sim 10^3 \mu\text{m/s}$ for $\ell \sim 1\mu\text{m}$. The assumption of unchanged forces is good to the extent that this exceeds the motor speed. Thus, the velocity and angular velocity of the motor are directly related to its Stokes drag coefficient even though the flow pattern driven directly by the motor mechanism may be very different from that around a body simply dragged through the fluid.

To proceed with applying the linear relations (6.3) to our problem and identifying the geometry-dependent tensorial coefficients, we approximate the rotary nanorod as an axisymmetric particle with fore-and-aft symmetry and a mirror symmetry plane containing the rotation axis passing through \mathcal{O} . Consider the situation reflected through the symmetry plane and the reversibility of Stokes flow: For a nanorod with non-translational motion ($v = 0$), according to equation (6.3a), reversing ω should reverse the direction of force while, due to the symmetry of the particle, \vec{F} should be indifferent to the direction of rotation. This leads to

$\mathbb{B}^T \cdot \omega = 0$. For a particle with solely translational dynamics ($\omega = 0$) along or perpendicular to the symmetry plane, there would be no torque acting on the particle in the z -direction (perpendicular to the plane of motion) and $\mathbb{B} \cdot \vec{v}$ has zero component in the z -direction. Moreover, the corresponding components of velocity and force along and perpendicular to the symmetry plane are proportional: $F_n \propto v_n$ and $F_p \propto v_p$, where F_n and F_p are the components of the net force along $\hat{\mathbf{n}}$ and $\hat{\mathbf{p}}$, respectively. Therefore the linearity relations (6.3) can be simplified to

$$\vec{v} = \mathbb{A}^{-1} \cdot \vec{F} = A_n^{-1} F_n \hat{\mathbf{n}} + A_p^{-1} F_p \hat{\mathbf{p}}, \quad (6.4a)$$

$$\omega = (\mathbb{D}^{-1} \cdot \mathbf{L})_z = D_z^{-1} L_z, \quad (6.4b)$$

where L_z is the net torque in the z -direction. The parameters A_n , A_p and D_z depend on the shape of the nanorotor (and its surroundings). For example, a sphere of radius a (with \mathcal{O} at its center) in an unbounded fluid of viscosity η has $A_n = A_p = 6\pi\eta a$ and $D_z = 8\pi\eta a^3$. The prolate spheroid (defined by $a^{-2}x^2 + b^{-2}(y^2 + z^2) = 1$ where $a \geq b$) provides a better approximation to the shape of actual nanorotors: by changing the eccentricity $e = \sqrt{1 - (b/a)^2}$, it can be smoothly transitioned from a sphere to a long thin needle. In an unbounded Stokes flow, the prolate spheroid has shape parameters [43]:

$$A_n = (6\pi\eta a) \frac{8}{3} e^3 \left[-2e + (e^2 + 1) \ln \left(\frac{1+e}{1-e} \right) \right]^{-1} \quad (6.5a)$$

$$A_p = (6\pi\eta a) \frac{16}{3} e^3 \left[2e + (3e^2 - 1) \ln \left(\frac{1+e}{1-e} \right) \right]^{-1} \quad (6.5b)$$

$$D_z = (8\pi\eta a^3) \frac{\frac{4}{3} e^3 (2 - e^2)}{\left[-2e + (e^2 + 1) \ln \left(\frac{1+e}{1-e} \right) \right]}. \quad (6.5c)$$

A video of the dynamics of a nanorotor provides us with the dimensions, translational velocity v and angular velocity ω of the nanorod in addition to the angle ϕ . Approximating the nanorod by a spheroid, eccentricity e can be assigned based on the dimensions of the particle. Using the geometrical factor D_z given by (6.5c) for the motion of particle in an unbounded domain as a first approximation and taking advantage of the linearity in equation (6.4b) with ω , we can calculate the net torque $L_z = D_z \omega$ on the particle in the z direction. Also, using the velocity

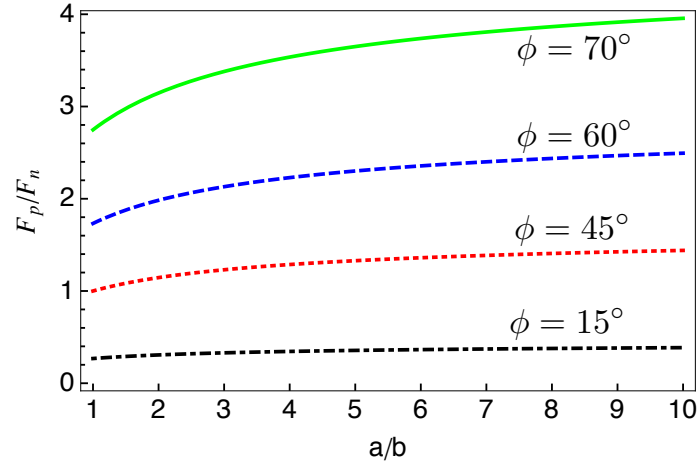


Figure 6.3. With an increase in the aspect ratio of the spheroid or an increase in the angle ϕ the ratio of the force perpendicular to the symmetry axis and the force parallel to symmetry axis increases.

v , the angle ϕ and the eccentricity, the force can be calculated as

$$F = \sqrt{F_n^2 + F_p^2} = v \sqrt{A_n^2 \cos^2 \phi + A_p^2 \sin^2 \phi}. \quad (6.6)$$

From a design perspective, we would like to apply the force and torque on a particle of given dimension so that we obtain the desired translational, angular velocity and nanorod's orientation with respect to its trajectory. Recasting the equation (6.1) using the geometrical coefficients yields

$$\frac{F_p}{F_n} = \frac{A_p}{A_n} \tan \phi, \quad (6.7)$$

which shows that for a given geometry, ϕ is a measure of the relative strength of the net force perpendicular to and along the nanorod axis. Fig. 6.3 shows this relation for different values of ϕ as a function of the aspect ratio $a/b = \sqrt{1 - e^2}$ (the ratio of the semi-major axis to the semi-minor axis). For a given angle ϕ , the magnitude of the perpendicular force to the tangential force (with respect to the axis of the nanorotor) increases with an increase in the relative length of the nanorotor. Fig. 6.4 shows that, for a fixed a , increasing the aspect ratio (making the rotor smaller) requires less force to achieve a desired velocity.

The analysis so far has been based on approximating a nanorotor by a prolate

spheroid. However, linearity of Stokes flow can be exploited for designing other kinds of geometries. In order to have fast in-place rotors, we need to minimize the net force and maximize the net torque on the particle. Our analysis provides us with insight into designing more efficient rotors. The tadpole structure in Fig. (6.5), for example, would be one way of making a rotor that minimizes the net force acting on the particle while maximizing the net torque around the center of mass. This structure can be fabricated using the methods explained in Ref [41] and [44].

The nanomotor in our example consists of a bead and an arm. The bead is a spherical SiO_2 particle in which the bottom hemisphere is coated with Pt. The arm is a TiO_2 backbone whose top is partly covered by Pt. There are two major forces acting on this particle when we place it in a hydrogen peroxide solution. The force exerted on the arm, \vec{F}_{arm} , and the force acting on the lower part of the bead, \vec{F}_{bead} , due to a reaction on Pt surfaces. The angle α corresponds to the angle between the top of the arm and the plane separating Pt and SiO_2 on the bead. The net force acting on the particle is given by

$$F_{net} = (F_{arm}^2 + F_{bead}^2 - 2F_{arm}F_{bead} \cos \alpha)^{\frac{1}{2}}. \quad (6.8)$$

As θ becomes smaller and the forces on the arm and the bead become aligned with

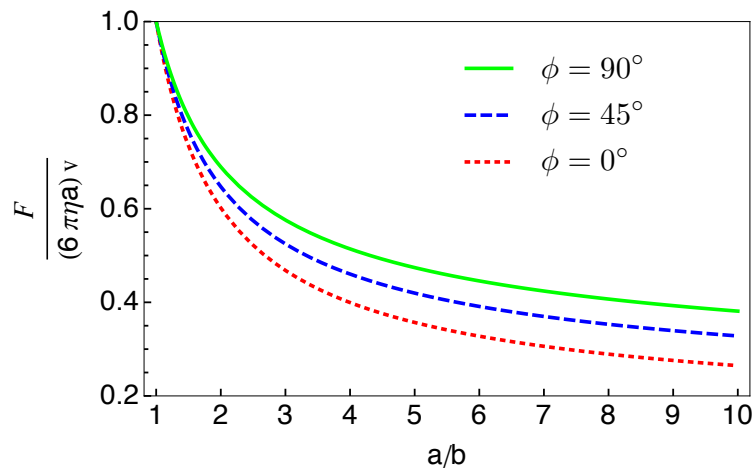


Figure 6.4. For a given particle geometry and magnitude of driving force, the particle whose angle ϕ is smaller will achieve a higher velocity. The highest velocity occurs at $\phi = 0$ when the the symmetric axis of spheroid is tangent to the trajectory.

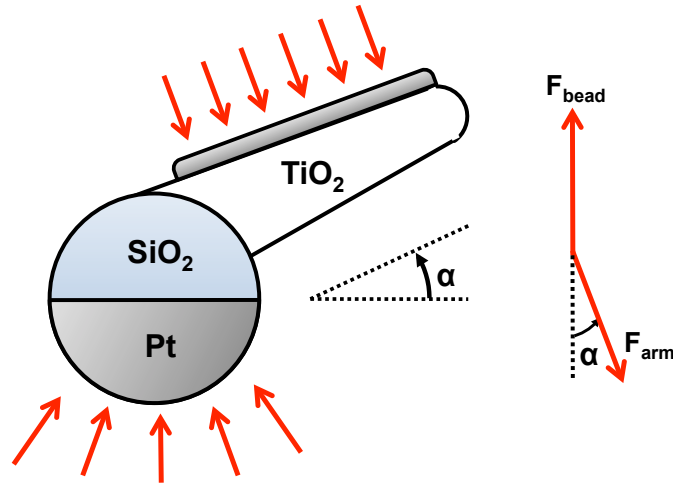


Figure 6.5. The final structure has a minimized net force and a maximized net torque. The angle between the arm and the substrate during the fabrication can adjust the force and torque. The lower the angle, the lower the net force in the direction of the axis of the arm.

each other, the value of F_{net} becomes smaller and the nano-tadpole has a higher tendency to rotate in place.

We can also exploit the analysis to examine the possible mechanisms of nanomotor dynamics. Previous work on nanorotors at Penn State [31] resulted in ultrafast nanorotors that could rotate in-place (Fig. (6.1b)). These nanorods had a Pt/Au cap and it was conjectured that this cap would pull the nanomotor toward the center of the circular orbit, making it appear as if the rod rotated in place. However,

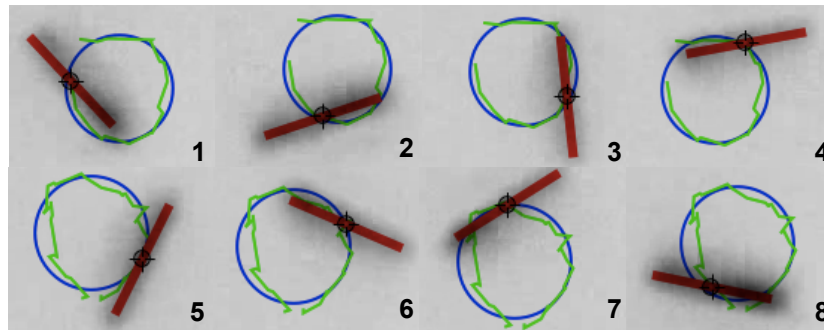


Figure 6.6. Trajectory of one counter-clockwise rotation of the slow nanorotor in Ref [30] . (Green) Actual path of the center of mass of the nanorod; which shows stochastic fluctuations of the center of mass position. (Blue) The fitted equivalent circle to the actual trajectory. The rod is almost pointing toward the inside of the circle or tangent to the circle. (The frames are not equidistance in time)

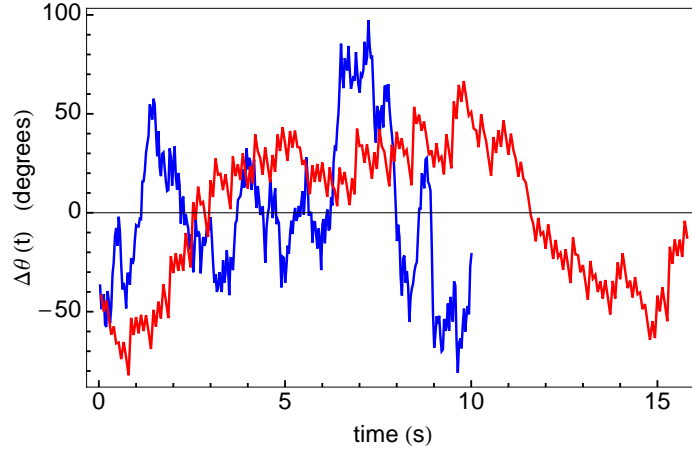


Figure 6.7. Angular fluctuation $\Delta\theta(t)$ for nanorotors in (red) Ref [30] and (blue) Ref [31]. The deviation of the orientation of the nanomotor from the deterministic orientation can be significant (up to 90°).

equation (6.2) for the radius of curvature indicates that the addition of the lateral force increases the net force, and consequently, increases the radius of the trajectory, contradicting the initial argument. That leaves us with an open question of what is really the mechanism behind the fast in-place rotation of these particles.

The nanorotor made by Qin et al [30] (Fig. (6.1a)) is believed to move due to the force exerted perpendicular to the axis of the nanorod by bubble propulsion. In their proposed mechanism, the force along the axis of the rod is zero. For such a system, the direction angle (6.7) is zero and the direction of the axis of the nanorod is perpendicular to its trajectory of motion (Fig. 6.2(d)). However, the nanorotor in [30] exhibits an angle far from $\phi = 0$. In Fig. (6.6), we have analyzed the quasi-circular path provided in the supporting information of Ref [30]. The rod is closer to being tangent to the trajectory than perpendicular. Again, that leaves us with an open question of what is the real mechanism behind the motion of these nanorotors.

2 Stochastic Brownian Contribution

So far, we have discussed the deterministic aspect of nanomotor motion leading to a circular trajectory. However, the coupling between the deterministic rotational motion and the stochastic orientational dynamics leads to the experimentally ob-

served quasi-circular trajectories. In designing a nanorotor we would like to know how the parameters of the nanorotor affect the trajectory of the nanorotor, or how to design a nanorotor to have more control over its trajectory.

As we discussed in the beginning of this chapter, nanorotors have two natural time scales: the characteristic orientational time, $\tau_o = D_o^{-1}$, and the deterministic rotation period, $\tau_\omega = 2\pi\omega^{-1}$. The deviation of the trajectory from a perfect circular path depends on these time scales. In the case where $\tau_\omega \ll \tau_o$ during one rotation, the influence of the stochastic component is small, and the nanorotor's path is close to circular. However, in the limit $\tau_\omega \gg \tau_o$, the direction of the nanorotor changes many times, before the nanorotor completes a deterministic rotation, and therefore, the observer may not even recognize the circular trajectory. The translationally-linear nanomotors, fabricated experimentally, are, in fact, in this category. These particles are meant to be fabricated as perfect axisymmetric objects. However, due to defects, the nanomotor is not perfectly axisymmetric. This leads to a net torque on the particle while moving, and the particle has the tendency to rotate. Since the asymmetry in structure is also very small, however, the resulting torque and angular velocity are very small, and consequently, the characteristic rotation time, τ_ω , is very large. Therefore, the observed dynamics of these particles appears to be linear, with an occasional change of direction of the nanomotors, instead of quasi-circular paths.

We analyzed the deterministic rotational and the stochastic orientational dynamics of the slow [30] and fast [31] nanorotors from the videos in the supporting information of their corresponding papers. The measured average angular velocities are $\omega_{slow} = 22.3$ rpm and $\omega_{fast} = 279.8$ rpm for the slow and fast nanorotors, respectively. The corresponding characteristic rotation times (period) are $\tau_{\omega,slow} = 2.7$ s and $\tau_{\omega,fast} = 0.2$ s.

During the time period that the particle performs a full rotation around its center of mass, it completes a cycle around its trajectory. While the particle is rotating around its center of mass with average angular velocity ω , it simultaneously receives stochastic kicks from the fluid elements, causing deviations in the direction of the nanorotor velocity, and turning its circular path into quasi-circular trajectories. At each instance, the difference between the actual orientation of the nanorod and its expected deterministic orientation can be described by the

temporal angle fluctuation

$$\Delta\theta(t) = \theta(t) - \omega t, \quad (6.9)$$

where θ characterizes the orientation of the nanomotor, as depicted in Fig. (6.2). Fig. (6.7) shows the angular fluctuations for the nanorotors of Refs [30, 31]. It is clear from the figure that the angular deviation can be significant, showing the effect of the stochastic component on the direction of nanomotor velocity.

In order to calculate the orientational diffusion coefficients from the videos, we calculated the temporal angle fluctuation

$$\delta\theta(t; \Delta t) = \Delta\theta(t + \Delta t) - \Delta\theta(t) \quad (6.10)$$

during the time interval Δt . If the change in the direction of the nanorotor is due to Brownian kicks, the distribution of temporal angular deviation for time difference Δt should follow the normal distribution

$$N(\delta\theta; \langle\delta\theta\rangle, \sigma) = \frac{1}{\sqrt{2\pi}\sigma} \exp\left(-\frac{(\delta\theta - \langle\delta\theta\rangle)^2}{2\sigma^2}\right), \quad (6.11)$$

where, for one-dimensional diffusion in θ coordinate the average temporal angular deviation is zero $\langle\delta\theta\rangle = 0$, and the width of the distribution is related to the orientational diffusion coefficient D_o through

$$\sigma = \sqrt{2D_o\Delta t}. \quad (6.12)$$

Figures (6.8) and (6.9) show that the distributions of temporal angular deviation fit the normal distribution, with the center of the distribution nearly at zero. This suggests that the temporal angular deviation can be represented by a one-dimensional random walker.

The diffusion coefficients of the slow and fast nanorotors were found to be $D_{o,slow} = 0.102 \text{ rad}^2\text{s}^{-1}$ and $D_{o,fast} = 0.462 \text{ rad}^2\text{s}^{-1}$, respectively (see Fig. (6.10)). The corresponding characteristic times of orientational diffusion are $\tau_{o,slow} = 50 \text{ s}$ and $\tau_{o,fast} = 2.165 \text{ s}$. Since $\tau_{o,slow} \gg \tau_{\omega,slow}$, the slow nanorotor follows a path close to a circular trajectory (see Fig. 6.6). For the fast rotor, $\tau_{o,fast}$ is one order of magnitude larger than $\tau_{\omega,slow}$, and therefore, we expect to see a trajectory close to a

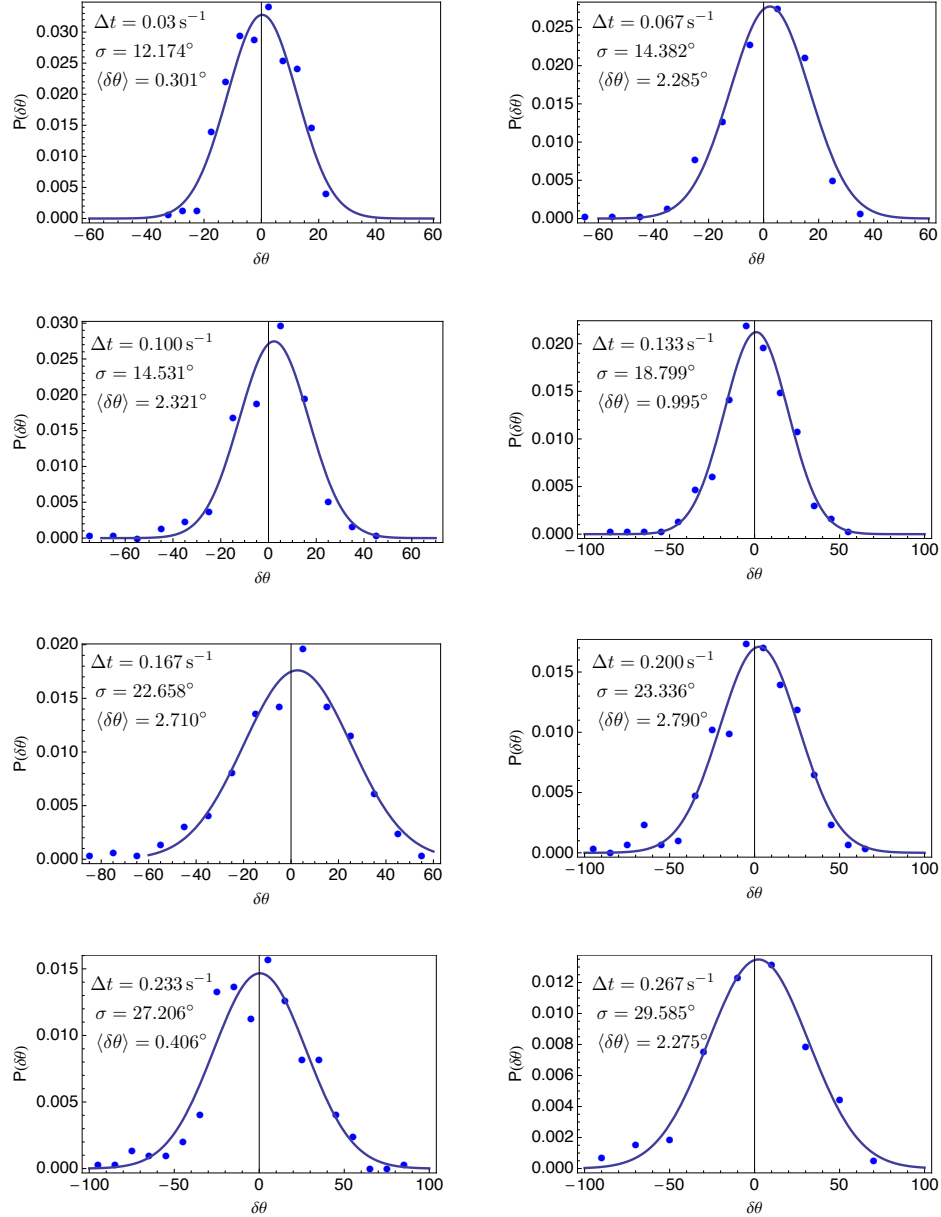


Figure 6.8. The fit distributions of the temporal angular deviation $\delta\theta$ for the nanorotor of Ref [31] to normal distribution for different time intervals Δt .

circular path. For a spheroidal nanorotor in unbounded domain, the characteristic time of orientation is given by $\tau_o = D_z/kT$, where D_z is the geometrical coefficient (6.5c), k is the Boltzmann factor, and T is the absolute temperature. For a nanorotor of given geometry with known torque L_z , we can calculate the period τ_ω using the linearity relation (6.4b), and compare it with τ_o to determine the

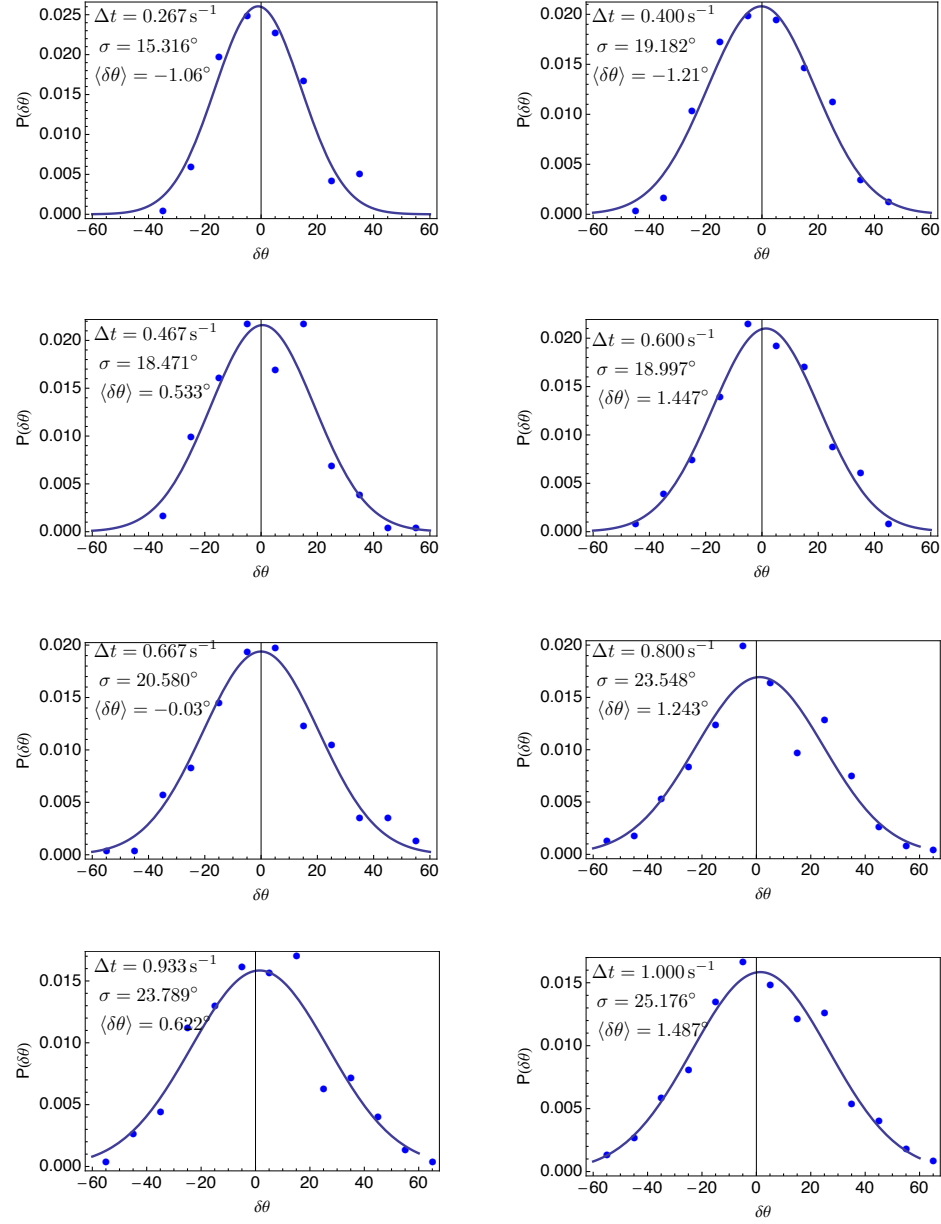


Figure 6.9. The fit distributions of the temporal angular deviation $\delta\theta$ for nanorotor of Ref [30] to normal distribution for different time intervals Δt .

trajectory of the nanorotor.

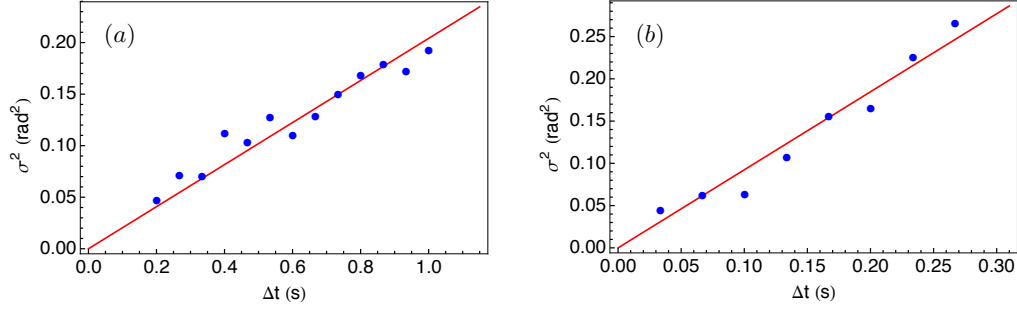


Figure 6.10. Orientational Diffusion Coefficient $D_{ort} = \frac{\sigma^2}{2\Delta t}$ for (a) Ref [30]: $D_o = 0.102 \text{ rad}^2 \text{ s}^{-1}$ and (b) Ref [31]: $D_o = 0.462 \text{ rad}^2 \text{ s}^{-1}$.

3 Discussion

In this chapter, the steady state deterministic trajectory of a nanorotor, with a center of mass translational velocity \vec{v} and an angular velocity ω around the center of mass, was shown to be a circular path of radius $R = v/\omega$. In order to decrease the radius of the trajectory and make an in-place rotor, the net torque on the particle must be maximized while minimizing the net force on the nanorotor. A structure that could demonstrate the application of our proposed design principle was also suggested. The validity of the various mechanisms proposed for the motion of nanorotors can be investigated by simply looking at their trajectories and the orientations of particles with respect to their trajectories. The deviation from a circular path to a quasi-circular one can be attributed to rotational Brownian dynamics, from which the rotational diffusion coefficient of the rods was calculated. The rotational diffusion coefficient must be minimized to yield a nanorotor that has the smallest deviation from the circular trajectory.

Coupling of Deterministic and Stochastic Dynamics in Powered Random Walkers

1 Introduction

Orientational and translational diffusion are considered to be independent physical processes of a particle. Nanorotors represent a system of powered random walkers in which these two processes are tightly coupled. The deterministic circular motion, by itself, is a steady state motion which doesn't change the center of the circular trajectory (the guiding center) with time. The stochastic orientational dynamics for an unpowered nanorotor can also lead to a change of the direction of the nanorotor without any translational motion. However, in a powered nanorotor the deterministic dynamics and the stochastic rotational dynamics are coupled to each other, leading to displacement, and an effective translational diffusion of the nanorotor over time. In this chapter, we study this coupling and the relation between the rotational diffusion of the nanorotor to its powered translational diffusion.

While in ordinary unpowered colloidal nanorods, even for translational motion under an external driving force, the Brownian translational and orientational diffusion are independent, for nanomotors the direction of the deterministic powered

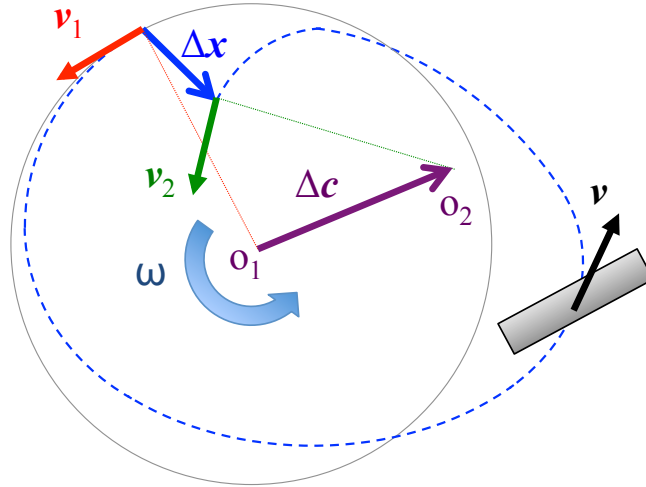


Figure 7.1. The particle rotates due to the net torque and its velocity has an angle with respect to the axis of the rod due to the asymmetric distribution of force on the particle. The Brownian orientational diffusion deviates the particle's path from a circular (solid) to a quasi-circular (dashed). This process results in change in the direction of velocity $\mathbf{v}_1 \neq \mathbf{v}_2$, the displacement in the position of center of mass $\Delta \mathbf{x}$, and the displacement $\Delta \mathbf{c}$ in position of the guiding center after one rotation. o_1 and o_2 are the guiding centers in the beginning and end of one rotation, respectively.

motion is influenced by the stochastic orientational component.

Many theoretical models have been proposed solely to explain the mechanism of deterministic motion for different nanomotors. An interesting feature of motion at this length scale is the contribution of both deterministic and stochastic dynamics to the motion of the nanorod. The deterministic dynamics happens in the form of linear or rotational motion. The Brownian orientational and translational diffusion of nanorotors are characterized by the diffusion coefficients D_{ort} and D_{trs} , respectively. Understanding the full dynamics of nanomotors and the possible emergent phenomena, therefore, requires an understanding of how the deterministic and stochastic dynamics interact.

Nanorotors are a class of nanomotors whose deterministic motion is well characterized by translational v and angular ω velocities on a circular path of radius $R = v/\omega$ as described in chapter 6. The rotational dynamics is a result of the asymmetric distribution of force on the surface of the nanorotor leading to a net torque on the particle and also (for nanorotors that happen to be in the shape of a rod) the net forces both along and perpendicular to the axis of the nanorod.

Consequently, the velocity would not be along the axis of the nanorod and the particle acquires an angle with respect to its trajectory (see Fig. 7.1). Depending on the direction of ω , the nanorotor may rotate clockwise or counter-clockwise. This chirality results in a constraint on the dynamics of nanorotor, which is the major distinction between linear motors and nanorotors.

In this chapter, we study the effect of coupling between deterministic translational and stochastic orientational dynamics of a powered random walker; focusing on the motion of nanorotors. Separately, neither a powered orientationally non-diffuser, nor an unpowered orientational diffuser, will exhibit center of mass (CoM) diffusion. When these two act together in the form of a powered orientational diffuser, the stochastic orientational dynamics causes the nanoparticle to deviate from its deterministic circular path into a quasi-circular path (see Fig 7.1). This leads to a displacement of the CoM and the guiding center of rotation after one period T_1 of deterministic rotation. We will refer to a “period” in a shorthand fashion but it signifies one “period of deterministic motion”.

2 Modeling

In this section we will correlate the deterministic and stochastic properties of a nanorotor to its long run translational behavior. We work in units of v for velocity, $\omega^{-1} \equiv T_1/2\pi$ for time and $R = v/\omega$ for length. Within these units, $v = \omega = R = 1$ and $T_1 = 2\pi$. We divide the time into very short spans $[t, t + dt)$. As demonstrated in Fig. 7.2a, at time t stochastic rotational diffusion changes the orientation of the particles velocity by $d\theta_{\text{RND}}$ and simultaneously makes a displacement $d\mathbf{c}$ (“c” stands for the center of rotation) for the guiding center. During $(t, t + dt)$, the nanorotor rotates deterministically around its new guiding center leading to displacement $d\mathbf{x}$ in the CoM (Fig. 7.2b).

If we draw the position vectors \mathbf{r}_1 , \mathbf{r}_2 and \mathbf{r}_3 from the same origin (Fig. 7.2c), the total motion in the reference frame of the guiding center is a displacement $d\mathbf{p}$ (“p” stands for perimeter) of a random walker that moves on a circle with a deterministic velocity superimposed by a stochastic motion. We call this circular path in the reference frame of the guiding center the “c-frame circle”. It is important to note that although the nanomotor moves on quasi-circular trajectories in the laboratory

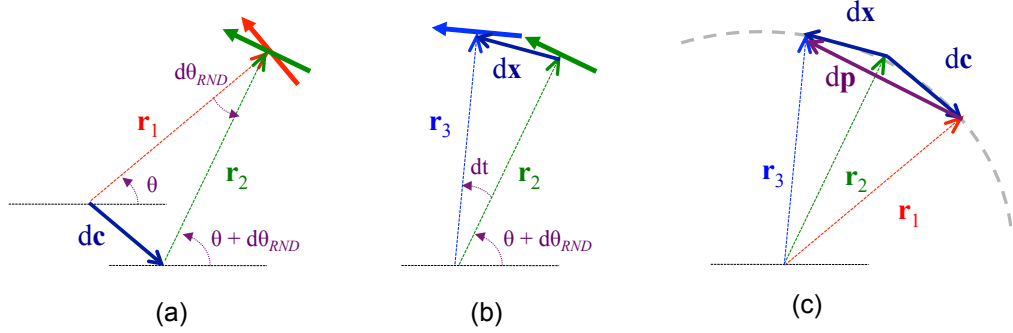


Figure 7.2. Dynamics of nanorotor in the time span $[t, t + dt)$ (a) At time t the particle exhibits an stochastic orientational change of size $d\theta_{RND}$. A displacement of $d\mathbf{c} = \mathbf{r}_1 - \mathbf{r}_2$ is resulted in the instantaneous center of rotation. (b) During the time period $(t, t + dt)$, the particle does deterministic translational motion, leading to displacement of the center of mass by $d\mathbf{x} = \mathbf{r}_3 - \mathbf{r}_2$. (c) In the frame of reference of the guiding center, the nanorotor performs a deterministic displacement $d\mathbf{x}$ superimposed by stochastic displacement $d\mathbf{c}$ leading to a displacement $d\mathbf{p} = d\mathbf{x} - d\mathbf{c}$ on a circular path.

frame of reference, it follows a perfect circular path in the reference frame of the guiding center.

The stochastic orientational contribution $d\theta_{RND}$ has a one-dimensional Gaussian distribution with properties $\langle d\theta_{RND} \rangle = 0$ and $\langle d\theta_{RND}^2 \rangle = \sigma^2 dt$ where

$$\sigma^2 = \frac{2D_{\text{ort}}}{\omega} \quad (7.1)$$

is the dimensionless variance of Brownian orientational change at time $t = 1$. Using the normalized variable $dW_t = d\theta_{RND}/\sigma$, for which

$$\langle dW_t \rangle = 0, \quad \langle dW_t^2 \rangle = dt, \quad (7.2)$$

and hence,

$$\langle e^{i\sigma dW_t} \rangle = e^{-\sigma^2 dt/2}. \quad (7.3)$$

The total change in the direction of motion during the time interval $[t, t + dt)$ becomes

$$d\theta = dt + \sigma dW_t \quad (7.4)$$

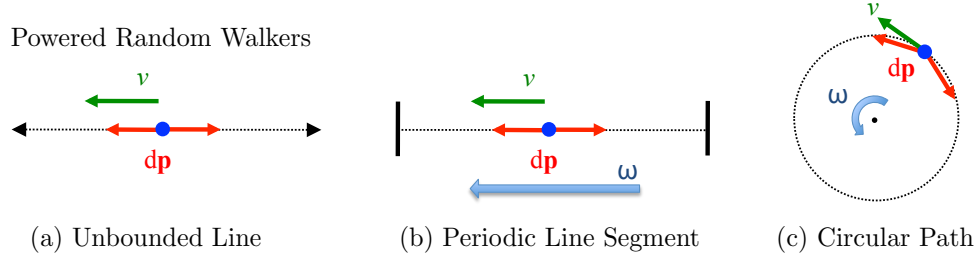


Figure 7.3. One dimensional powered random walkers (a) on an unbounded line, since the deterministic displacement scales with t while the stochastic part scales with $t^{\frac{1}{2}}$, on long run as $t \rightarrow \infty$, the deterministic dynamics dominates the total dynamic of the random walker. (b) Constraining the dynamics from unbounded line to the motion on a line segment with periodic boundary condition changes physics of the problem and introduce a natural time scale $2\pi\omega^{-1}$ depending on the length of the segment and velocity of the particle. This dynamic can be well represented by a powered random walker on a circular path with translational velocity v and angular velocity ω .

and the orientation θ_t of the particle at time t is

$$\theta_t = t + \sum_{0 \leq s < t} \sigma dW_s \quad (7.5)$$

in which without the lose of generality we have set $\theta_0 = 0$.

Representing the position vectors of Fig. 7.2 in the complex plane by $\mathbf{r}_1 = e^{i\theta_t}$, $\mathbf{r}_2 = e^{i(\theta_t + \sigma dW)}$, and $\mathbf{r}_3 = e^{i(\theta_t + \sigma dW + dt)}$, we obtain the displacements

$$d\mathbf{x}_t = \mathbf{r}_3 - \mathbf{r}_2 = e^{i(\theta_t + \sigma dW_t)} (e^{idt} - 1), \quad (7.6)$$

$$d\mathbf{c}_t = \mathbf{r}_1 - \mathbf{r}_2 = e^{i\theta_t} (1 - e^{\sigma dW_t}), \quad (7.7)$$

$$d\mathbf{p}_t = d\mathbf{x}_t - d\mathbf{c}_t = \mathbf{r}_3 - \mathbf{r}_1 = e^{i\theta_t} [e^{i(dt + \sigma dW_t)} - 1]. \quad (7.8)$$

The core of our analysis is to calculate the change in these three types of displacement after n periods T_n , that is, $\Delta\mathbf{r}(T_n)$ where $\mathbf{r} = \mathbf{x}, \mathbf{c}$ or \mathbf{p} . As we discussed previously, the rotational deterministic motion of the particle imposes a chirality constraint, depending on clockwise or counterclockwise rotation, on the dynamics of the particle moving along a circular path. The orientational stochastic dynamics changes the direction of motion, and correspondingly changes the location of the guiding center (displacement of the instantaneous center of rotation). For an unpowered nanorotor, we don't have a guiding center, but a

point at distance R from a nanorotor has a stochastic motion on a circle with the origin at the position of the CoM of the particle. Powering the particle would superimpose a deterministic motion onto the particle dynamics. Therefore, in the frame of reference of the guiding center, the particle moves on a circular path, and the displacement on this c-frame circle is a combination of stochastic and deterministic displacement.

The constraints on movement along the c-frame circle has principal importance in understanding the dynamics of the nanorotor and the interaction between the deterministic and stochastic dynamics. Consider a one dimensional powered random walker on an unbounded line (see Fig 7.3a); the deterministic displacement scales with t while the stochastic part scales with $t^{\frac{1}{2}}$; in the long run $t \rightarrow \infty$, the deterministic dynamics dominates. However, constraining the dynamics to a line segment with periodic boundary conditions (see Fig 7.3b) changes the physics of the problem, and introduces a natural time scale $2\pi\omega^{-1}$ which depends on the length of the segment and velocity of the particle. If we look at the displacement only at discrete multiples of $2\pi\omega^{-1}$, we don't see the effect of deterministic motion and it looks like the particle only moves due to Brownian dynamics. This is the consequence of the periodic boundary conditions and the natural time scale of the system.

The dynamics of a powered random walker with translational velocity v and angular velocity ω along a circular path (see Fig 7.3c) is similar to the motion of a powered random walker on a line segment with periodic boundary conditions. The difference between the two is that the displacement vector over time on the line segment is one dimensional while in case of the circular path the displacement is a two dimensional vector. In the one dimensional problem, the displacements are not correlated, that is, $\langle \Delta \mathbf{p}(T_1) \cdot \Delta \mathbf{p}(T_2) \rangle = 0$, however, in the circular motion $\langle \Delta \mathbf{p}(T_1) \cdot \Delta \mathbf{p}(T_2) \rangle < 0$, since if the displacement returns on itself on the second turn, the dot product is more negative than the case where the particle doesn't return on itself.

Before moving into the detailed calculation, we study two limiting cases, $\sigma \gg 1$ and $\sigma \ll 1$, using scaling analysis to predict the long-time behavior of the powered random walker. At long times the mean square displacement over time for the CoM and the guiding center will be equal, $\lim_{T_n \rightarrow \infty} \frac{\langle |\Delta \mathbf{x}|^2 \rangle}{T_n} = \lim_{T_n \rightarrow \infty} \frac{\langle |\Delta \mathbf{c}|^2 \rangle}{T_n}$. In

the limit of large $\sigma = \frac{2D_{\text{ort}}}{\omega}$, the characteristic time of the deterministic motion is much larger than the characteristic time of the orientational diffusion. We can subdivide the trajectory of a particle to a set of blobs analogous to a conformation of a polymer chain. The sequential displacements of the particle after one period inside a blob are correlated, but the end to end distance of a trajectories inside blobs are weakly correlated or uncorrelated. The time scale for the rotor to go through a blob is the time that the particle can forget most of its correlations in successive displacements, that is, the characteristic time of orientational diffusion, $\tau = \frac{1}{D_{\text{ort}}}$. During this time period, the particle moves a distance $l \propto v\tau$ where v is the linear velocity of the particle. We can define an effective translational diffusion for the nanorotor as

$$D_{\text{eff}} \propto \frac{l^2}{\tau} \propto \frac{v^2}{D_{\text{ort}}} \quad \text{for } \sigma \gg 1. \quad (7.9)$$

In the limit $\sigma \ll 1$ during one rotation, the center of mass has small displacement equal to $l \propto R \Delta\theta$ where R is the radius of the c-frame circle and $\Delta\theta = \sqrt{D_{\text{ort}} \tau}$ is the total angular deviation in the direction of the velocity over one period $\tau \propto \omega^{-1}$. Therefore, the effective translational diffusion would be

$$D_{\text{eff}} \propto \frac{(R \Delta\theta)^2}{\tau} \propto \frac{v^2}{\omega^2} D_{\text{ort}} \quad \text{for } \sigma \ll 1. \quad (7.10)$$

So far, we formulated the problem and studied the limiting cases. In the next section, we calculate the mean square displacement of the three different types of displacements and the correlation functions that explain their behavior.

3 Mathematical Derivations

In our analysis, we represent the two dimensional vectors in a complex plane. We will use frequently the inner product between the vectors for calculating the correlation functions. Since we are in the complex plane instead of Cartesian coordinates, we work out the dot product in the complex plane. We represent the Cartesian vector $\vec{A} = A(\cos \phi_A \hat{e}_x + \sin \phi_A \hat{e}_y)$ in the complex plane by a corresponding complex number $\mathbf{A} = Ae^{i\phi_A}$. The dot product of two vectors \vec{A} and \vec{B} in the Cartesian

plane is $\vec{A} \cdot \vec{B} = AB \cos(\phi_A - \phi_B)$. The product of their corresponding complex numbers (one is conjugated) is $\mathbf{A}\bar{\mathbf{B}} = AB e^{i(\phi_A - \phi_B)}$. Therefore, the correspondence to the dot product in the complex plane is

$$\vec{A} \cdot \vec{B} = \Re \{ \mathbf{A}\bar{\mathbf{B}} \} = \Re \{ \bar{\mathbf{A}}\mathbf{B} \} \quad (7.11)$$

where \Re is the real-part operator. In our derivations we work with the product of complex numbers as the dot product and at the end, we will use the real part of the complex number.

3.1 Velocity Correlation Function

The coupling of stochastic orientational dynamics to the deterministic dynamics of the nanorotor not only deviates the trajectory from circular to quasi-circular, but also changes the direction of the particle velocity after each rotation. We would like to determine the number of periods of deterministic oscillations before the particle forgets its initial direction of velocity.

The direction of the nanomotor velocity at each instant is described by the angle $\phi_t = \theta_t + \frac{\pi}{2}$. We define the velocity correlation function after k rotation to be the inner product between the initial velocity and the velocity at time T_k ,

$$C_v(k) = \Re \{ \langle e^{-i\phi_0} e^{i\phi_{T_k}} \rangle \} \equiv \Re \{ \langle e^{i\theta_{T_k}} \rangle \} \quad (7.12)$$

where $T_k = kT_1$ is the time of k deterministic oscillation, and $T_1 = 2\pi$ is the period of one oscillation. Using the identity (7.3), we calculate

$$\begin{aligned} \langle e^{i\theta_{T_k}} \rangle &= \left\langle \exp \left(iT_k + i \sum_{0 \leq s < T_k} \sigma dW_s \right) \right\rangle = \prod_{0 \leq s < T_k} \langle e^{i\sigma dW_s} \rangle \\ &= \prod_{0 \leq s < T_k} e^{-\sigma^2 ds/2} = e^{-\sigma^2 T_k/2} \end{aligned} \quad (7.13)$$

We obtain,

$$\boxed{C_v(k) = e^{-k/k_c}} \quad (7.14)$$

where the characteristic rotation k_c is

$$\boxed{k_c = (\pi\sigma^2)^{-1}}. \quad (7.15)$$

3.2 Diffusion on the C-Frame Circle

We begin our analysis of the three types of displacement (i.e., $d\mathbf{p}$, $d\mathbf{x}$, $d\mathbf{c}$) with the displacement $d\mathbf{p}$ of the moving object on a circle in the frame of reference of the guiding center. The particle is constrained to move in a circle via deterministic and stochastic displacements. The displacement during the time span $[t, t + dt]$ is

$$d\mathbf{p}_t = e^{i\theta_t} [e^{i(dt+\sigma dW_t)} - 1] \quad (7.16)$$

and we would like to calculate the root-mean-square displacement $\langle |\mathbf{p}(T_n)|^2 \rangle$ after n deterministic rotations,

$$\langle |\mathbf{p}(T_n)|^2 \rangle = \left\langle \left| \sum_{0 \leq u < T_n} d\mathbf{p}_u \right|^2 \right\rangle = \sum_u \langle d\mathbf{p}_u^2 \rangle + \sum_{u > s} \langle d\bar{\mathbf{p}}_s d\mathbf{p}_u \rangle + \sum_{u < s} \langle d\bar{\mathbf{p}}_s d\mathbf{p}_u \rangle. \quad (7.17)$$

where u and s represent time in these summations. Depending on the magnitude of u and s with respect to each other ($u = s$, $u > s$ or $u < s$), we have three different summations of $\langle d\bar{\mathbf{p}}_s d\mathbf{p}_u \rangle$ on the right hand side of the above equation.

In case where $u = s \equiv t$, we have

$$\begin{aligned} d\bar{\mathbf{p}}_t d\mathbf{p}_t &= e^{-i\theta_t} [e^{-i(dt+\sigma dW_t)} - 1] e^{i\theta_t} [e^{i(dt+\sigma dW_t)} - 1] \\ &= [e^{-i(dt+\sigma dW_t)} - 1] [e^{i(dt+\sigma dW_t)} - 1] \\ &= 2[1 - \cos(dt + \sigma dW_t)] \end{aligned} \quad (7.18)$$

We need the expansion of this equation to the first order in dt .

$$\langle d\bar{\mathbf{p}}_t d\mathbf{p}_t \rangle = 2 \langle 1 - \cos(dt + \sigma dW_t) \rangle = \sigma^2 dt + \mathcal{O}(dt^2) \quad (7.19)$$

For $u > s$, we have

$$d\bar{\mathbf{p}}_s d\mathbf{p}_u = e^{-i\theta_s} [e^{-i(dt_s+\sigma dW_s)} - 1] e^{i\theta_u} [e^{i(dt_u+\sigma dW_u)} - 1]$$

$$\begin{aligned}
&= e^{i(\theta_u - \theta_s)} [e^{-i(dt_s + \sigma dW_s)} - 1] [e^{i(dt_u + \sigma dW_u)} - 1] \\
&= e^{i(u-s)} e^{i\sigma dW_s} \exp\left(i\sigma \sum_{s < t' < u} dW_{t'}\right) [e^{-i(dt_s + \sigma dW_s)} - 1] [e^{i(dt_u + \sigma dW_u)} - 1] \\
&= e^{i(u-s)} \exp\left(i\sigma \sum_{s < t' < u} dW_{t'}\right) e^{-idt_s} [1 - e^{i(dt_s + \sigma dW_s)}] [e^{i(dt_u + \sigma dW_u)} - 1]
\end{aligned} \tag{7.20}$$

where we have arranged the terms so that they are independent of each other and therefore, the average of the whole term will be the product of average of the individual terms. Taking the average of $d\bar{\mathbf{p}}_s d\mathbf{p}_u$ and keeping the terms to the second order in dt gives us

$$\begin{aligned}
\langle d\bar{\mathbf{p}}_s d\mathbf{p}_u \rangle &= e^{i(u-s)} \left(\prod_{s < t' < u} \langle e^{i\sigma dW_{t'}} \rangle \right) e^{-idt_s} [1 - e^{idt_s} \langle e^{i\sigma dW_s} \rangle] [e^{idt_u} \langle e^{i\sigma dW_u} \rangle - 1] \\
&= e^{i(u-s)} \left(\prod_{s < t' < u} e^{-\sigma^2 dt_{t'}/2} \right) e^{-idt_s} [1 - e^{idt_s} e^{-\sigma^2 dt_s/2}] [e^{idt_u} e^{-\sigma^2 dt_u/2} - 1] \\
&= e^{i(u-s)} e^{-\sigma^2(u-s)/2} e^{-idt_s} \left[1 - e^{(i - \frac{\sigma^2}{2})dt_s} \right] \left[e^{(i - \frac{\sigma^2}{2})dt_u} - 1 \right] \\
&= e^{i(u-s)} e^{-\sigma^2(u-s)/2} \left(1 - idt_s + \mathcal{O}(dt_s^2) \right) \left[- \left(i - \frac{\sigma^2}{2} \right) dt_s + \mathcal{O}(dt_s^2) \right] \\
&\quad \times \left[\left(i - \frac{\sigma^2}{2} \right) dt_u + \mathcal{O}(dt_u^2) \right] \\
&= - \left(i - \frac{\sigma^2}{2} \right)^2 dt_s dt_u e^{i(u-s)} e^{-\sigma^2|u-s|/2} + \mathcal{O}(dt^3)
\end{aligned} \tag{7.21}$$

Similarly, for $u < s$ we can write

$$\begin{aligned}
d\bar{\mathbf{p}}_s d\mathbf{p}_u &= e^{-i\theta_s} [e^{-i(dt_s + \sigma dW_s)} - 1] e^{i\theta_u} [e^{i(dt_u + \sigma dW_u)} - 1] \\
&= e^{-i(\theta_s - \theta_u)} [e^{-i(dt_s + \sigma dW_s)} - 1] [e^{i(dt_u + \sigma dW_u)} - 1] \\
&= e^{-i(s-u)} e^{-i\sigma dW_u} \exp\left(-i\sigma \sum_{u < t' < s} dW_{t'}\right) [e^{-i(dt_s + \sigma dW_s)} - 1] [e^{i(dt_u + \sigma dW_u)} - 1] \\
&= e^{i(u-s)} \exp\left(-i\sigma \sum_{u < t' < s} dW_{t'}\right) e^{idt_u} [e^{-i(dt_s + \sigma dW_s)} - 1] [1 - e^{-i(dt_u + \sigma dW_u)}]
\end{aligned} \tag{7.22}$$

By taking the average and expanding to the second order in dt we obtain

$$\begin{aligned}
\langle d\bar{\mathbf{p}}_s d\mathbf{p}_u \rangle &= e^{i(u-s)} \left(\prod_{u < t' < s} \langle e^{-i\sigma dW_{t'}} \rangle \right) e^{idt_u} [e^{-idt_s} \langle e^{-i\sigma dW_s} \rangle - 1] [1 - e^{-idt_u} \langle e^{-i\sigma dW_u} \rangle] \\
&= e^{i(u-s)} \left(\prod_{u < t' < s} e^{-\sigma^2 dt_{t'}/2} \right) e^{idt_u} [e^{-idt_s} e^{-\sigma^2 dt_s/2} - 1] [1 - e^{-idt_u} e^{-\sigma^2 dt_u/2}] \\
&= e^{i(u-s)} e^{-\sigma^2(s-u)/2} e^{idt_u} \left[e^{-(i+\frac{\sigma^2}{2})dt_s} - 1 \right] \left[1 - e^{-(i+\frac{\sigma^2}{2})dt_u} \right] \\
&= e^{i(u-s)} e^{-\sigma^2|u-s|/2} \left(1 + idt_u + \mathcal{O}(dt_u^2) \right) \left[- \left(i + \frac{\sigma^2}{2} \right) dt_s + \mathcal{O}(dt_s^2) \right] \\
&\quad \times \left[\left(i + \frac{\sigma^2}{2} \right) dt_u + \mathcal{O}(dt_u^2) \right] \\
&= - \left(i + \frac{\sigma^2}{2} \right)^2 dt_s dt_u e^{i(u-s)} e^{-\sigma^2|u-s|/2} + \mathcal{O}(dt^3) \tag{7.23}
\end{aligned}$$

Therefore, we have

$$u > s : \quad \langle d\bar{\mathbf{p}}_s d\mathbf{p}_u \rangle = \left[\left(1 - \frac{\sigma^4}{4} \right) + i\sigma^2 \right] dt_s dt_u e^{i(u-s)} e^{-\sigma^2|u-s|/2} + \mathcal{O}(dt^3) \tag{7.24}$$

$$s > u : \quad \langle d\bar{\mathbf{p}}_s d\mathbf{p}_u \rangle = \left[\left(1 - \frac{\sigma^4}{4} \right) - i\sigma^2 \right] dt_s dt_u e^{i(u-s)} e^{-\sigma^2|u-s|/2} + \mathcal{O}(dt^3) \tag{7.25}$$

If $u < s$, the only difference is that $u - s$ becomes $s - u$; writing $|u - s|$ covers both cases. We can now calculate the root-mean-square of displacement on the circular trajectory in the frame of reference of guiding center after time T .

$$\begin{aligned}
\langle |\mathbf{p}(T)|^2 \rangle &= \left\langle \left| \sum_{0 \leq u < T} d\mathbf{p}_u \right|^2 \right\rangle = \sum_u \langle d\mathbf{p}_u^2 \rangle + \sum_{u > s} \langle d\bar{\mathbf{p}}_s d\mathbf{p}_u \rangle + \sum_{u < s} \langle d\bar{\mathbf{p}}_s d\mathbf{p}_u \rangle \\
&\simeq \sigma^2 T + \left(1 - \frac{\sigma^4}{4} \right) \int_0^T \int_0^T e^{i(u-s) - \sigma^2|u-s|/2} du ds \\
&\quad + i\sigma^2 \int_0^T \int_0^u e^{i(u-s) - \sigma^2|u-s|/2} du ds - i\sigma^2 \int_0^T \int_0^s e^{i(u-s) - \sigma^2|u-s|/2} ds du \tag{7.26}
\end{aligned}$$

In the following, we see that the last two terms in the right side of the equation are complex conjugates,

$$\begin{aligned}
& i\sigma^2 \int_0^T \int_0^u e^{i(u-s)-\sigma^2|u-s|/2} du ds - i\sigma^2 \int_0^T \int_0^s e^{i(u-s)-\sigma^2|u-s|/2} ds du \\
= & i\sigma^2 \int_0^T \int_0^u e^{i(u-s)-\sigma^2(u-s)/2} du ds - i\sigma^2 \int_0^T \int_0^s e^{-i(s-u)-\sigma^2(s-u)/2} ds du \\
= & i\sigma^2 \int_0^T \int_0^u e^{(i-\sigma^2/2)(u-s)} du ds + (-i\sigma^2) \int_0^T \int_0^s e^{(-i-\sigma^2/2)(s-u)} ds du \\
= & i\sigma^2 \int_0^T \int_0^u e^{(i-\sigma^2/2)(u-s)} du ds + (-i\sigma^2) \int_0^T \int_0^u e^{(-i-\sigma^2/2)(u-s)} du ds \\
= & 2\Re \left\{ i\sigma^2 \int_0^T \int_0^u e^{(i-\sigma^2/2)(u-s)} du ds \right\} \tag{7.27}
\end{aligned}$$

We first calculate the argument, and then select its real part.

$$\begin{aligned}
i\sigma^2 \int_0^T \int_0^u e^{(i-\sigma^2/2)(u-s)} du ds &= i\sigma^2 \int_0^T du e^{(i-\sigma^2/2)u} \int_0^u e^{-(i-\sigma^2/2)s} ds \\
&= i\sigma^2 \int_0^T du e^{(i-\sigma^2/2)u} \left[\frac{e^{-(i-\sigma^2/2)s}}{-(i-\frac{\sigma^2}{2})} \right]_0^u \\
&= \frac{i\sigma^2}{-(i-\frac{\sigma^2}{2})} \int_0^T du e^{(i-\sigma^2/2)u} \left[e^{-(i-\sigma^2/2)s} - 1 \right] \\
&= \frac{i\sigma^2}{-(i-\frac{\sigma^2}{2})} \int_0^T du \left[1 - e^{(i-\sigma^2/2)u} \right] \\
&= \frac{i\sigma^2}{-(i-\frac{\sigma^2}{2})} \left[u - \frac{e^{(i-\sigma^2/2)u}}{(i-\frac{\sigma^2}{2})} \right]_0^T \\
&= \frac{i\sigma^2}{-(i-\frac{\sigma^2}{2})} \left[T - \frac{e^{(i-\sigma^2/2)T} - 1}{(i-\frac{\sigma^2}{2})} \right] \\
&= \frac{i\sigma^2}{i(1+i\frac{\sigma^2}{2})} \left[\frac{e^{(i-\sigma^2/2)T} - 1}{(i-\frac{\sigma^2}{2})} - T \right] \tag{7.28}
\end{aligned}$$

If $T = T_n = 2\pi n$ is the time for n deterministic oscillations, $e^{iT_n} = 1$, and we have

$$2\Re \left\{ i\sigma \int_0^{T_n} \int_0^u e^{(i-\sigma^2/2)(u-s)} du ds \right\}$$

$$\begin{aligned}
&= 2\Re \left\{ \frac{\sigma^2}{(1 + i\frac{\sigma^2}{2})} \left[\frac{e^{(-\sigma^2/2)T_n} - 1}{(i - \frac{\sigma^2}{2})} - T_n \right] \right\} \\
&= 2\Re \left\{ \frac{\sigma^2 \left[e^{(-\sigma^2/2)T_n} - 1 \right]}{(i - \frac{\sigma^2}{2})(1 + i\frac{\sigma^2}{2})} - \frac{\sigma^2 T_n}{(1 + i\frac{\sigma^2}{2})} \right\} \\
&= 2\sigma^2 \left[e^{(-\sigma^2/2)T_n} - 1 \right] \Re \left\{ \frac{1}{-\sigma^2 + i(1 - \frac{\sigma^4}{4})} \right\} - 2\sigma^2 T_n \Re \left\{ \frac{1}{(1 + i\frac{\sigma^2}{2})} \right\} \\
&= 2\sigma^2 \left[e^{(-\sigma^2/2)T_n} - 1 \right] \left\{ \frac{-\sigma^2}{\sigma^4 + (1 - \frac{\sigma^4}{4})^2} \right\} - 2\sigma^2 T_n \left\{ \frac{1}{(1 + \frac{\sigma^4}{4})} \right\} \\
&= -2 \left\{ \frac{\sigma^4}{\sigma^4 + (1 - \frac{\sigma^4}{4})^2} \right\} \left[e^{(-\sigma^2/2)T_n} - 1 \right] - \left\{ \frac{2\sigma^2}{(1 + \frac{\sigma^4}{4})} \right\} T_n \quad (7.29)
\end{aligned}$$

which gives us the result of last two terms in equation (7.26). We also need to calculate the double integral, $\int_0^T \int_0^T e^{i(u-s) - \sigma^2|u-s|/2} du ds$, in equation (7.26). To do so, we use the change of variables

$$\alpha = u - s, \quad \beta = u + s \quad (7.30)$$

The variable α can vary between $-T$ ($u = 0, s = T$) and T ($u = T, s = 0$), and the variable β can change between $2T - |\alpha|$ and $|\alpha|$. The Jacobian of the transformation is $1/2$, that is $du ds = \frac{1}{2} d\alpha d\beta$. Therefore,

$$\begin{aligned}
\int_0^T \int_0^T e^{i(u-s) - \sigma^2|u-s|/2} du ds &= \frac{1}{2} \int_{-T}^T d\alpha e^{i\alpha - \frac{\sigma^2}{2}|\alpha|} \int_{|\alpha|}^{2T-|\alpha|} d\beta \\
&= \int_{-T}^T d\alpha e^{i\alpha - \frac{\sigma^2}{2}|\alpha|} (T - |\alpha|) \\
&= 2\Re \left\{ \int_0^T d\alpha e^{i\alpha - \frac{\sigma^2}{2}\alpha} (T - \alpha) \right\} \quad (7.31)
\end{aligned}$$

Defining $\mathbf{z} = \frac{\sigma^2}{2} - i$, we have

$$\begin{aligned}
\int_0^T d\alpha e^{-\mathbf{z}\alpha} (T - \alpha) &= T \int_0^T d\alpha e^{-\mathbf{z}\alpha} - \int_0^T d\alpha \alpha e^{-\mathbf{z}\alpha} \\
&= \frac{T}{\mathbf{z}} (1 - e^{-\mathbf{z}T}) + \frac{T}{\mathbf{z}} e^{-\mathbf{z}T} - \frac{1}{\mathbf{z}^2} (1 - e^{-\mathbf{z}T}) \quad (7.32)
\end{aligned}$$

$$= \frac{T}{\mathbf{z}} - \frac{1}{\mathbf{z}^2} (1 - e^{-\mathbf{z}T}) \quad (7.33)$$

We are interested in the displacement after n deterministic oscillations, where $T_n = 2\pi n$. This gives $e^{-\mathbf{z}T_n} = e^{-\frac{\sigma^2}{2}T_n}$ and

$$\begin{aligned} \Re \left\{ \frac{T_n}{\mathbf{z}} - \frac{1}{\mathbf{z}^2} (1 - e^{-\frac{\sigma^2}{2}T_n}) \right\} &= \frac{T_n \Re\{\mathbf{z}\}}{|\mathbf{z}|^2} - \frac{\Re\{\mathbf{z}^2\}}{|\mathbf{z}^2|^2} (1 - e^{-\frac{\sigma^2}{2}T_n}) \\ &= T_n \left(\frac{\frac{\sigma^2}{2}}{\frac{\sigma^4}{4} + 1} \right) - \frac{\left(\frac{\sigma^4}{4} - 1\right)}{\left(\frac{\sigma^4}{4} - 1\right)^2 + \sigma^4} (1 - e^{-\frac{\sigma^2}{2}T_n}) \end{aligned} \quad (7.34)$$

Therefore, we obtain

$$\boxed{\int_0^{T_n} \int_0^{T_n} e^{i(u-s) - \sigma^2|u-s|/2} du ds = 2T_n \left(\frac{\frac{\sigma^2}{2}}{\frac{\sigma^4}{4} + 1} \right) - 2 \frac{\left(\frac{\sigma^4}{4} - 1\right)}{\left(\frac{\sigma^4}{4} - 1\right)^2 + \sigma^4} (1 - e^{-\frac{\sigma^2}{2}T_n})} \quad (7.35)$$

We will use this equation later when we discuss the displacement of the center of mass and the guiding center. The root-mean-square displacement of the circle in the reference frame of guiding center is

$$\begin{aligned} \langle |\mathbf{p}(T_n)|^2 \rangle &= \left\langle \left(\sum_{0 \leq u < T_n} d\mathbf{p}_u \right)^2 \right\rangle = \sum_u \langle d\mathbf{p}_u^2 \rangle + \sum_{u>s} \langle d\bar{\mathbf{p}}_s d\mathbf{p}_u \rangle + \sum_{u<s} \langle d\bar{\mathbf{p}}_s d\mathbf{p}_u \rangle \\ &\simeq \sigma^2 T_n + \left(1 - \frac{\sigma^4}{4}\right) \int_0^{T_n} \int_0^{T_n} e^{i(u-s) - \sigma^2|u-s|/2} du ds \\ &\quad + 2\Re \left\{ i\sigma \int_0^{T_n} \int_0^u e^{(i-\sigma^2/2)(u-s)} du ds \right\} \\ &= \sigma^2 T_n + \left(1 - \frac{\sigma^4}{4}\right) \left\{ \left(\frac{\sigma^2}{\frac{\sigma^4}{4} + 1} \right) T_n - \frac{(\sigma^4 - 4)/2}{\left(\frac{\sigma^4}{4} - 1\right)^2 + \sigma^4} (1 - e^{-\frac{\sigma^2}{2}T_n}) \right\} \\ &\quad - 2 \left\{ \frac{\sigma^4}{\sigma^4 + \left(1 - \frac{\sigma^4}{4}\right)^2} \right\} \left[e^{(-\sigma^2/2)T_n} - 1 \right] - \left\{ \frac{2\sigma^2}{\left(1 + \frac{\sigma^4}{4}\right)} \right\} T_n \\ &= \left[e^{(-\sigma^2/2)T_n} - 1 \right] \left\{ \left(1 - \frac{\sigma^4}{4}\right) \frac{(\sigma^4 - 4)/2}{\left(\frac{\sigma^4}{4} - 1\right)^2 + \sigma^4} - \frac{2\sigma^4}{\sigma^4 + \left(1 - \frac{\sigma^4}{4}\right)^2} \right\} \end{aligned}$$

$$+T_n \left\{ \sigma^2 + \left(1 - \frac{\sigma^4}{4}\right) \left(\frac{\sigma^2}{\frac{\sigma^4}{4} + 1}\right) - \frac{2\sigma^2}{1 + \frac{\sigma^4}{4}} \right\} \quad (7.36)$$

Calculate the terms in the curly brackets

$$\begin{aligned} & \left(1 - \frac{\sigma^4}{4}\right) \frac{(\sigma^4 - 4)/2}{\left(\frac{\sigma^4}{4} - 1\right)^2 + \sigma^4} - \frac{2\sigma^4}{\sigma^4 + \left(1 - \frac{\sigma^4}{4}\right)^2} \\ &= \left(1 - \frac{\sigma^4}{4}\right) \frac{-2\left(1 - \frac{\sigma^4}{4}\right)}{\left(\frac{\sigma^4}{4} - 1\right)^2 + \sigma^4} - \frac{2\sigma^4}{\sigma^4 + \left(1 - \frac{\sigma^4}{4}\right)^2} \\ &= \frac{-2\left(1 - \frac{\sigma^4}{4}\right)^2 - 2\sigma^4}{\left(\frac{\sigma^4}{4} - 1\right)^2 + \sigma^4} = -2 \end{aligned} \quad (7.37)$$

and

$$\begin{aligned} \sigma^2 + \left(1 - \frac{\sigma^4}{4}\right) \left(\frac{\sigma^2}{\frac{\sigma^4}{4} + 1}\right) - \frac{2\sigma^2}{1 + \frac{\sigma^4}{4}} &= \sigma^2 + \left(1 - \frac{\sigma^4}{4} - 2\right) \left(\frac{\sigma^2}{\frac{\sigma^4}{4} + 1}\right) \\ &= \sigma^2 - \sigma^2 = 0 \end{aligned} \quad (7.38)$$

gives us

$$\boxed{\frac{\langle |\mathbf{p}(T_n)|^2 \rangle}{T_n} = \frac{2\left(1 - e^{-\frac{\sigma^2}{2}T_n}\right)}{T_n} = \frac{1 - e^{-n\pi\sigma^2}}{n\pi}} \quad (7.39)$$

In the limit of long time

$$\boxed{\lim_{T_n \rightarrow \infty} \frac{\langle |\mathbf{p}(T_n)|^2 \rangle}{T_n} = 0} \quad (7.40)$$

3.3 Displacement of the Center of Mass

The displacement of the center of mass during the time interval $[t, t + dt)$ is

$$d\mathbf{x}_t = e^{i(\theta_t + \sigma dW_t)} (e^{idt} - 1) \quad (7.41)$$

and we would like to calculate the root-mean-square of displacement of the center of mass after n periods,

$$\langle |\mathbf{x}(T)|^2 \rangle = \left\langle \left| \sum_{0 \leq u < T} d\mathbf{x}_u \right|^2 \right\rangle = \sum_u \langle d\mathbf{x}_u^2 \rangle + \sum_{u \neq s} \langle d\bar{\mathbf{x}}_u d\mathbf{x}_s \rangle \quad (7.42)$$

We calculate $\langle d\bar{\mathbf{x}}_s d\mathbf{x}_u \rangle$ for cases $u = s \equiv t$, $u > s$ and $u < s$. For the first case

$$\begin{aligned} d\bar{\mathbf{x}}_t d\mathbf{x}_t &= [e^{-i(\theta_t + \sigma dW_t)} (e^{-idt} - 1)] [e^{i(\theta_t + \sigma dW_t)} (e^{idt} - 1)] \\ &= (e^{-idt} - 1) (e^{idt} - 1) = 2[1 - \cos(dt)] \end{aligned} \quad (7.43)$$

and

$$\langle d\bar{\mathbf{x}}_t d\mathbf{x}_t \rangle = 2 \langle 1 - \cos(dt) \rangle = dt^2 + \mathcal{O}(dt^4) \quad (7.44)$$

On the other hand, for $u > s$,

$$\begin{aligned} d\bar{\mathbf{x}}_s d\mathbf{x}_u &= [e^{-i(\theta_s + \sigma dW_s)} (e^{-idt_s} - 1)] [e^{i(\theta_u + \sigma dW_u)} (e^{idt_u} - 1)] \\ &= [e^{-idt_s} - 1] \exp \left(i(u-s) + i\sigma \sum_{s < t' \leq u} dW_{t'} \right) [e^{idt_u} - 1] \\ &= e^{i(u-s)} [e^{-idt_s} - 1] [e^{idt_u} - 1] e^{i\sigma dW_u} \exp \left(i\sigma \sum_{s < t' < u} dW_{t'} \right) \end{aligned} \quad (7.45)$$

The terms are independent, and we can take the average,

$$\begin{aligned} \langle d\bar{\mathbf{x}}_s d\mathbf{x}_u \rangle &= e^{i(u-s)} [e^{-idt_s} - 1] [e^{idt_u} - 1] \langle e^{i\sigma dW_u} \rangle \prod_{s < t' < u} \langle e^{i\sigma dW_{t'}} \rangle \\ &= e^{i(u-s)} [e^{-idt_s} - 1] [e^{idt_u} - 1] e^{-\sigma^2 dt_u / 2} \prod_{s < t' < u} e^{-\sigma^2 dt' / 2} \\ &= e^{i(u-s)} \left(-idt_s + \mathcal{O}(dt_s^2) \right) \left(idt_u + \mathcal{O}(dt_u^2) \right) \left(1 - \sigma^2 dt_u / 2 + \mathcal{O}(dt_u^2) \right) e^{-\sigma^2(u-s)/2} \\ &= dt_s dt_u e^{i(u-s)} e^{-\sigma^2(u-s)/2} + \mathcal{O}(dt^3) \end{aligned} \quad (7.46)$$

If $u < s$, the only difference is that $u - s$ becomes $s - u$; writing $|u - s|$ covers both cases. Then, for the root-mean-square-displacement of the center of mass we have

$$\begin{aligned}
\langle |\mathbf{x}(T)|^2 \rangle &= \left\langle \left(\sum_{0 \leq u < T} d\mathbf{x}_u \right)^2 \right\rangle = \sum_u \langle d\mathbf{x}_u^2 \rangle + \sum_{u \neq s} \langle d\bar{\mathbf{x}}_u d\mathbf{x}_s \rangle \\
&\simeq \left(\frac{T}{dt} \right) dt^2 + \int_0^T \int_0^T e^{i(u-s) - \sigma^2|u-s|/2} du ds \\
&\simeq \int_0^T \int_0^T e^{i(u-s) - \sigma^2|u-s|/2} du ds \tag{7.47}
\end{aligned}$$

$$T \int_{-\infty}^{\infty} e^{is - \sigma^2|s|/2} ds = T \left(\frac{-1}{i - \sigma^2/2} + \frac{1}{i + \sigma^2/2} \right) = T \frac{\sigma^2}{\sigma^4/4 + 1} = \frac{4\sigma^2}{\sigma^4 + 4} T \tag{7.48}$$

Using the identity (7.35) we obtain

$$\boxed{\frac{\langle |\mathbf{x}(T_n)|^2 \rangle}{T_n} \simeq \left(\frac{\sigma^2}{\frac{\sigma^4}{4} + 1} \right) - \frac{(\sigma^4 - 4)/2}{\left(\frac{\sigma^4}{4} - 1 \right)^2 + \sigma^4} \left(\frac{1 - e^{-\frac{\sigma^2}{2} T_n}}{T_n} \right)} \tag{7.49}$$

Depending on the choice of displacement per number of rotations, $\frac{\langle |\mathbf{x}(T_n)|^2 \rangle}{T_n}$ varies. In the limit of long time, $n \rightarrow \infty$, this equation reduces to

$$\boxed{4D_\infty = \lim_{T_n \rightarrow \infty} \frac{\langle |\mathbf{x}(T_n)|^2 \rangle}{T_n} \simeq \left(\frac{\sigma^2}{\frac{\sigma^4}{4} + 1} \right)} \tag{7.50}$$

3.4 Displacement of the Guiding Center

In this section, we employ the same methodology that we have used in the previous two sections. The displacement of the guiding center during the time span $[t, t + dt]$ is

$$d\mathbf{c}_t = (-e^{i\theta t}) [e^{i\sigma dW_t} - 1] \tag{7.51}$$

In order to calculate

$$\langle |\mathbf{c}(T)|^2 \rangle = \left\langle \left| \sum_{0 \leq u < T} d\mathbf{c}_u \right|^2 \right\rangle = \sum_u \langle d\mathbf{c}_u^2 \rangle + \sum_{u \neq s} \langle d\bar{\mathbf{c}}_u d\mathbf{c}_s \rangle \tag{7.52}$$

we calculate $\langle d\bar{\mathbf{c}}_s d\mathbf{c}_u \rangle$ for $u = s \equiv t$, $u > s$ and $u < s$. In the first case,

$$d\bar{\mathbf{c}}_t d\mathbf{c}_t = [e^{-i\sigma dW_s} - 1] [e^{i\sigma dW_t} - 1] = 2(1 - \cos(\sigma dW_t)) \quad (7.53)$$

and to the first order in dt we have

$$\langle d\bar{\mathbf{c}}_t d\mathbf{c}_t \rangle = 2 \langle 1 - \cos(\sigma dW_t) \rangle = \sigma^2 dt + \mathcal{O}(dt^2). \quad (7.54)$$

For $u > s$,

$$\begin{aligned} d\bar{\mathbf{c}}_s d\mathbf{c}_u &= [e^{-i\sigma dW_s} - 1] \exp\left(i(u-s) + i\sigma \sum_{s \leq t' < u} dW_{t'}\right) [e^{i\sigma dW_u} - 1] \\ &= e^{i(t-s)} [1 - e^{i\sigma dW_s}] \exp\left(i\sigma \sum_{s < t' < u} dW_{t'}\right) [e^{i\sigma dW_u} - 1] \end{aligned} \quad (7.55)$$

and averaging gives us

$$\begin{aligned} \langle d\bar{\mathbf{c}}_s d\mathbf{c}_u \rangle &= e^{i(u-s)} \langle 1 - e^{i\sigma dW_s} \rangle \prod_{s < t' < u} \langle e^{i\sigma dW_{t'}} \rangle \langle e^{i\sigma dW_u} - 1 \rangle \\ &= e^{i(t-s)} \left(-\sigma^2 dt_s / 2 + \mathcal{O}(dt^2) \right) e^{-\sigma^2(u-s)/2} \left(\sigma^2 dt_u / 2 + \mathcal{O}(dt^2) \right) \end{aligned} \quad (7.56)$$

If $u < s$, the only difference is that $u - s$ becomes $s - u$; writing $|u - s|$ covers both cases. The root mean square displacement of the guiding center after time T_n is calculated by

$$\begin{aligned} \langle |\mathbf{c}(T_n)|^2 \rangle &= \left\langle \left| \sum_{0 \leq u < T_n} d\mathbf{c}_u \right|^2 \right\rangle = \sum_u \langle d\mathbf{c}_u^2 \rangle + \sum_{u \neq s} \langle d\bar{\mathbf{c}}_u d\mathbf{c}_s \rangle \\ &\simeq \sigma^2 T_n - \frac{\sigma^4}{4} \int_0^{T_n} \int_0^{T_n} e^{i(u-s) - \sigma^2 |u-s|/2} du ds \end{aligned} \quad (7.57)$$

Therefore, using identity (7.35), we obtain

$$\boxed{\frac{\langle |\mathbf{c}(T_n)|^2 \rangle}{T_n} \simeq \left(\frac{\sigma^2}{\frac{\sigma^4}{4} + 1} \right) + \left(\frac{\sigma^4}{4} \right) \frac{(\sigma^4 - 4)/2}{(\frac{\sigma^4}{4} - 1)^2 + \sigma^4} \left(\frac{1 - e^{-\frac{\sigma^2}{2} T_n}}{T_n} \right)} \quad (7.58)$$

Depending on the choice of displacement per number of rotations, $\frac{\langle |\mathbf{x}(T_n)|^2 \rangle}{T_n}$ varies. In the limit of long time $n \rightarrow \infty$, this equation reduces to

$$4D_\infty = \lim_{T_n \rightarrow \infty} \frac{\langle |\mathbf{c}(T_n)|^2 \rangle}{T_n} \simeq \left(\frac{\sigma^2}{\frac{\sigma^4}{4} + 1} \right) \quad (7.59)$$

In the limit, $T_N \rightarrow \infty$, the root-mean-square of displacement of center of mass and displacement of the guiding center are equal,

$$4D_\infty = \lim_{T_n \rightarrow \infty} \frac{\langle |\mathbf{x}(T_n)|^2 \rangle}{T_n} = \lim_{T_n \rightarrow \infty} \frac{\langle |\mathbf{c}(T_n)|^2 \rangle}{T_n} \quad (7.60)$$

So far, we calculated the displacement after time T_n for three different types of displacement. In the next three sections, we calculate the correlation functions of these displacements.

3.5 Displacement Correlation Function on the C-Frame Circle

Let's define the displacement of the circle during the k th rotation by

$$\Delta \mathbf{p}(k) = \mathbf{p}(T_k) - \mathbf{p}(T_{k-1}) \quad (7.61)$$

where $T_k = 2\pi k$ and $\mathbf{p}(T_k)$ is the position of the rotor on the circle at time T_k . Then, we have

$$\Delta \mathbf{p}(k) = \sum_{T_{k-1} \leq u < T_k} d\mathbf{p}_u \quad (7.62)$$

The displacement correlation function of on the circle is then defined as

$$C_{\Delta \mathbf{p}}(k) = \Re \left\{ \langle \overline{\Delta \mathbf{p}}(1) \Delta \mathbf{p}(k) \rangle \right\} \quad (7.63)$$

We first calculate the argument, and then take the real part.

$$\langle \overline{\Delta \mathbf{p}}(1) \Delta \mathbf{p}(k) \rangle = \left\langle \sum_{0 \leq s < T_1} \sum_{T_{k-1} \leq u < T_k} d\overline{\mathbf{p}}_s d\mathbf{p}_u \right\rangle$$

$$\begin{aligned}
&= - \left(i - \frac{\sigma^2}{2} \right)^2 \int_0^{T_1} \int_{T_{k-1}}^{T_k} e^{i(u-s) - \sigma^2(u-s)/2} du ds \\
&= \left(-\frac{\sigma^4}{4} \right) \int_0^{T_1} e^{-\left(i - \frac{\sigma^2}{2}\right)s} ds \int_{T_{k-1}}^{T_k} e^{\left(i - \frac{\sigma^2}{2}\right)u} du \\
&= - \left(i - \frac{\sigma^2}{2} \right)^2 \left(\frac{-1}{\left(i - \frac{\sigma^2}{2}\right)} e^{-\left(i - \frac{\sigma^2}{2}\right)s} \Big|_0^{T_1} \right) \left(\frac{1}{\left(i - \frac{\sigma^2}{2}\right)} e^{\left(i - \frac{\sigma^2}{2}\right)u} \Big|_{T_{k-1}}^{T_k} \right) \\
&= - \left(i - \frac{\sigma^2}{2} \right)^2 \frac{-1}{\left(i - \frac{\sigma^2}{2}\right)^2} \left(e^{\pi\sigma^2} - 1 \right) \left(e^{-k\pi\sigma^2} - e^{-(k-1)\pi\sigma^2} \right) \\
&= - \left(1 - e^{\pi\sigma^2} \right)^2 e^{-k\pi\sigma^2} \tag{7.64}
\end{aligned}$$

Then,

$$\boxed{C_{\Delta\mathbf{p}}(k) = - \left(1 - e^{\pi\sigma^2} \right)^2 e^{-k\pi\sigma^2}} \tag{7.65}$$

3.6 Displacement Correlation Function for the Center of Mass

Similar to previous section, we define the displacement during the k th rotation by

$$\Delta\mathbf{x}(k) = \mathbf{x}(T_k) - \mathbf{x}(T_{k-1}) \tag{7.66}$$

where $T_k = 2\pi k$ and $\mathbf{x}(T_k)$ is the position of the center of mass of the powered random walker at time T_k . Then, we have

$$\Delta\mathbf{x}(k) = \sum_{T_{k-1} \leq u < T_k} d\mathbf{x}_u \tag{7.67}$$

The displacement correlation function is then defined as

$$C_{\Delta\mathbf{x}}(k) = \Re \left\{ \langle \overline{\Delta\mathbf{x}}(1) \Delta\mathbf{x}(k) \rangle \right\} \tag{7.68}$$

We have

$$\langle \overline{\Delta\mathbf{x}}(1) \Delta\mathbf{x}(k) \rangle = \left\langle \sum_{0 \leq s < T_1} \sum_{T_{k-1} \leq u < T_k} d\overline{\mathbf{x}}_s d\mathbf{x}_u \right\rangle$$

$$\begin{aligned}
&= \int_0^{T_1} \int_{T_{k-1}}^{T_k} e^{i(u-s)-\sigma^2(u-s)/2} du ds \\
&= \int_0^{T_1} e^{-(i-\frac{\sigma^2}{2})s} ds \int_{T_{k-1}}^{T_k} e^{(i-\frac{\sigma^2}{2})u} du \\
&= \left(\frac{-1}{(i-\frac{\sigma^2}{2})} e^{-(i-\frac{\sigma^2}{2})s} \Big|_0^{T_1} \right) \left(\frac{1}{(i-\frac{\sigma^2}{2})} e^{(i-\frac{\sigma^2}{2})u} \Big|_{T_{k-1}}^{T_k} \right) \\
&= \frac{-1}{(i-\frac{\sigma^2}{2})^2} \left(e^{\pi\sigma^2} - 1 \right) \left(e^{-k\pi\sigma^2} - e^{-(k-1)\pi\sigma^2} \right) \\
&= \frac{1}{(i-\frac{\sigma^2}{2})^2} \left(1 - e^{\pi\sigma^2} \right)^2 e^{-k\pi\sigma^2} \tag{7.69}
\end{aligned}$$

By taking the real part of this equation, we obtain

$$\boxed{C_{\Delta\mathbf{x}}(k) = \frac{\left(\frac{\sigma^4}{4} - 1\right)}{\left(\frac{\sigma^4}{4} - 1\right)^2 + \sigma^4} \left(1 - e^{\pi\sigma^2}\right)^2 e^{-k\pi\sigma^2}} \tag{7.70}$$

3.7 Displacement Correlation Function for the Guiding Center

Let's define the displacement of the instantaneous center of rotation during the k th rotation by

$$\Delta\mathbf{c}(k) = \mathbf{c}(T_k) - \mathbf{c}(T_{k-1}) \tag{7.71}$$

where $T_k = 2\pi k$ and $\mathbf{c}(T_k)$ is the position of the instantaneous center of rotation of the powered random walker at time T_k . Then, we have

$$\Delta\mathbf{c}(k) = \sum_{T_{k-1} \leq u < T_k} d\mathbf{c}_u \tag{7.72}$$

The displacement correlation function of the instantaneous center of rotation is then defined as

$$C_{\Delta\mathbf{c}}(k) = \Re \left\{ \langle \overline{\Delta\mathbf{c}}(1) \Delta\mathbf{c}(k) \rangle \right\} \tag{7.73}$$

We have

$$\begin{aligned}
\langle \overline{\Delta \mathbf{c}}(1) \Delta \mathbf{c}(k) \rangle &= \left\langle \sum_{0 \leq s < T_1} \sum_{T_{k-1} \leq u < T_k} d\overline{\mathbf{c}}_s d\mathbf{c}_u \right\rangle \\
&= \left(-\frac{\sigma^4}{4} \right) \int_0^{T_1} \int_{T_{k-1}}^{T_k} e^{i(u-s) - \sigma^2(u-s)/2} du ds \\
&= \left(-\frac{\sigma^4}{4} \right) \int_0^{T_1} e^{-(i - \frac{\sigma^2}{2})s} ds \int_{T_{k-1}}^{T_k} e^{(i - \frac{\sigma^2}{2})u} du \\
&= \left(-\frac{\sigma^4}{4} \right) \left(\frac{-1}{(i - \frac{\sigma^2}{2})} e^{-(i - \frac{\sigma^2}{2})s} \Big|_0^{T_1} \right) \left(\frac{1}{(i - \frac{\sigma^2}{2})} e^{(i - \frac{\sigma^2}{2})u} \Big|_{T_{k-1}}^{T_k} \right) \\
&= \left(-\frac{\sigma^4}{4} \right) \frac{-1}{(i - \frac{\sigma^2}{2})^2} (e^{\pi\sigma^2} - 1) (e^{-k\pi\sigma^2} - e^{-(k-1)\pi\sigma^2}) \\
&= \left(-\frac{\sigma^4}{4} \right) \frac{1}{(i - \frac{\sigma^2}{2})^2} (1 - e^{\pi\sigma^2})^2 e^{-k\pi\sigma^2} \tag{7.74}
\end{aligned}$$

Then,

$$\boxed{C_{\Delta \mathbf{c}}(k) = \frac{\left(-\frac{\sigma^4}{4}\right) \left(\frac{\sigma^4}{4} - 1\right)}{\left(\frac{\sigma^4}{4} - 1\right)^2 + \sigma^4} (1 - e^{\pi\sigma^2})^2 e^{-k\pi\sigma^2}} \tag{7.75}$$

By comparison we see

$$\boxed{C_{\Delta \mathbf{c}}(k) = \left(-\frac{\sigma^4}{4}\right) C_{\Delta \mathbf{x}}(k)} \tag{7.76}$$

4 Results and Discussion

The stochastic orientational dynamics changes the direction of motion of the nanorotor after each rotation. At low σ^2 , it is expected to have less deviation from the circular path, and therefore, less deviation in the direction of velocity after one rotation (see Fig. 7.4). In this domain the deterministic rotational constraint is stronger than the orientational stochastic dynamics. We calculated the velocity correlation function

$$C_{\mathbf{v}}(k) = e^{-k/k_c} \tag{7.14}$$

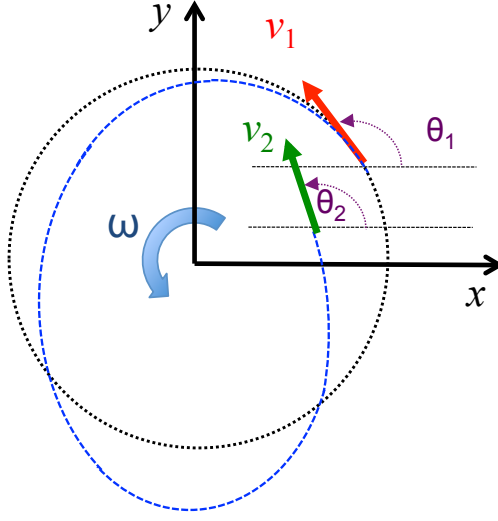


Figure 7.4. Stochastic rotational dynamics of the nanorotor deviates its path from circular to quasi-circular. Simultaneously, after one rotation, the direction of velocity v_2 of the particle changes with respect to its initial direction v_1 .

where the characteristic rotation number

$$k_c = (\pi\sigma^2)^{-1} \quad (7.15)$$

is a measure of number of rotations that a nanorotor requires to forget the orientation of its initial velocity. Variances around $\sigma^2 = \pi^{-1} \simeq 0.32$ represent a domain where the particle starts to forget its velocity after each rotation.

The dynamics of the nanorotor on the c-frame circle is the result of the motion of a powered random walker constrained to move on a circular path. We calculated the mean-square displacement of the particle over time on the c-frame circle,

$$\frac{\langle |\mathbf{p}(T_n)|^2 \rangle}{T_n} = \frac{2 \left(1 - e^{-\frac{\sigma^2}{2} T_n} \right)}{T_n} = \frac{1 - e^{-n\pi\sigma^2}}{n\pi} \quad (7.39)$$

With an increase in the time span of measurement, the mean-square displacement over time decreases (see Fig. 7.5) and over long time goes to zero.

$$\lim_{T_n \rightarrow \infty} \frac{\langle |\mathbf{p}(T_n)|^2 \rangle}{T_n} = 0 \quad (7.40)$$

This is one of the consequences of being constrained to move on a circular path.

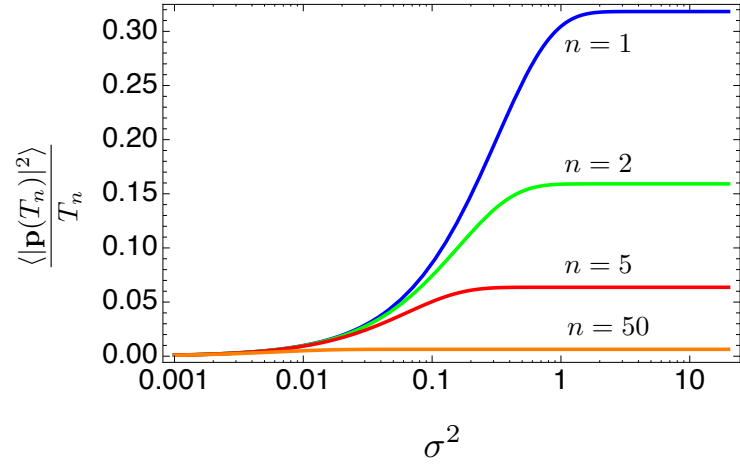


Figure 7.5. The diffusion $\frac{\langle |\mathbf{p}(T_n)|^2 \rangle}{T_n}$ of powered random walker on a circle whose center is the guiding center. Increase in the time span, $T_n = 2\pi n$, over which the random walker moves, the diffusion on the circle reduces, approaching zero.

Over long time, the particle moves a distance more than half the perimeter of the circle; however, the current position of the particle on the c-frame circle could be achieved at earlier times if the particle would choose the reverse direction.

We also observed that the mean-square displacement of center of mass and the guiding center over long time are equal and linear in time.

$$4D_\infty = \lim_{T_n \rightarrow \infty} \frac{\langle |\mathbf{x}(T_n)|^2 \rangle}{T_n} = \lim_{T_n \rightarrow \infty} \frac{\langle |\mathbf{c}(T_n)|^2 \rangle}{T_n} \simeq \left(\frac{\sigma^2}{\frac{\sigma^4}{4} + 1} \right) \quad (7.60)$$

This means that the powered random walker over long time behaves as an unpowered random walker with an effective translational diffusion coefficient

$$D_\infty = \left(\frac{\frac{\sigma^2}{4}}{\frac{\sigma^4}{4} + 1} \right) \quad (7.77)$$

In the limit of small $\sigma \ll 1$ we obtain

$$D_\infty \propto \sigma^2 \Rightarrow \frac{\omega}{v^2} D_{\text{eff}} \propto \frac{D_{\text{ort}}}{\omega} \Rightarrow D_{\text{eff}} \propto \frac{v^2}{\omega^2} D_{\text{ort}} \quad (7.78)$$

which is the same as the result of scaling analysis (7.10). In the limit of $\sigma \gg 1$ we

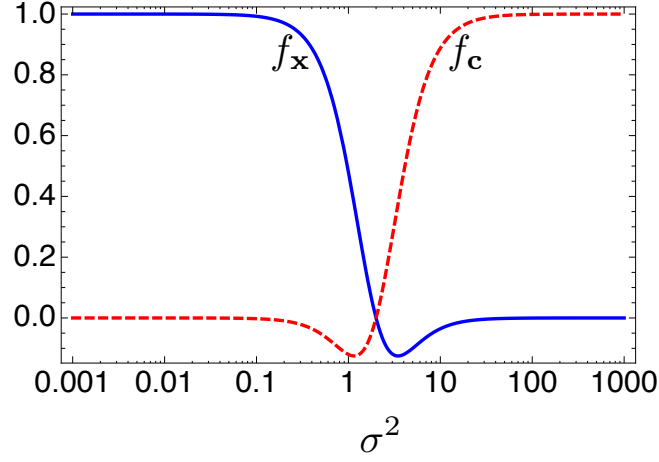


Figure 7.6. The functions, f_x (solid blue curve), and f_c (dashed red curve), multiplied by $\frac{\langle |\mathbf{p}(T_n)|^2 \rangle}{T_n}$ show the deviation of $\frac{\langle |\mathbf{x}(T_n)|^2 \rangle}{T_n}$ and $\frac{\langle |\mathbf{c}(T_n)|^2 \rangle}{T_n}$ from the limiting value $4D_\infty$.

obtain

$$D_\infty \propto \sigma^{-2} \Rightarrow \frac{\omega}{v^2} D_{\text{eff}} \propto \frac{\omega}{D_{\text{ort}}} \Rightarrow D_{\text{eff}} \propto \frac{v^2}{D_{\text{ort}}} \quad (7.79)$$

which is consistent with the scaling analysis (7.9).

For short mean-square displacement over time after n period we have

$$\frac{\langle |\mathbf{x}(T_n)|^2 \rangle}{T_n} = 4D_\infty + f_x(\sigma) \frac{\langle |\mathbf{p}(T_n)|^2 \rangle}{T_n} \quad (7.80)$$

and

$$\frac{\langle |\mathbf{c}(T_n)|^2 \rangle}{T_n} = 4D_\infty + f_c(\sigma) \frac{\langle |\mathbf{p}(T_n)|^2 \rangle}{T_n} \quad (7.81)$$

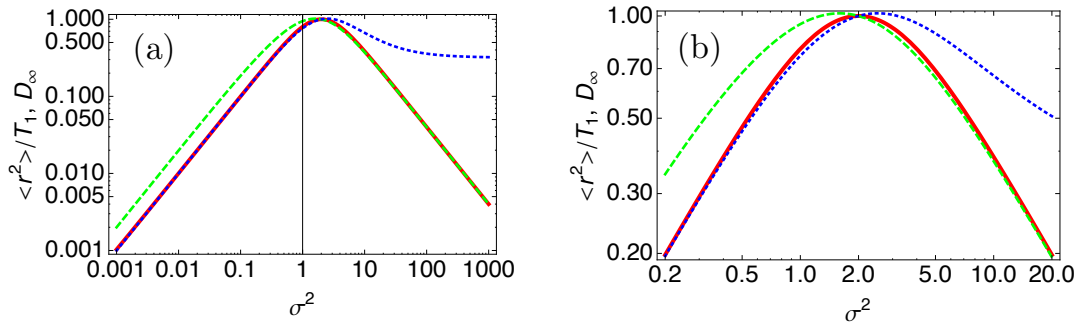


Figure 7.7. (a) The curves of $\langle |\mathbf{x}(T_1)| \rangle / T_1$ (dashed green), $\langle |\mathbf{c}(T_1)| \rangle / T_1$ (dotted blue), and $4D_\infty$ (red). (b) the same curve in more details near the peak. The maximum of $4D_\infty$ occurs at $\sigma^2 = 2$.

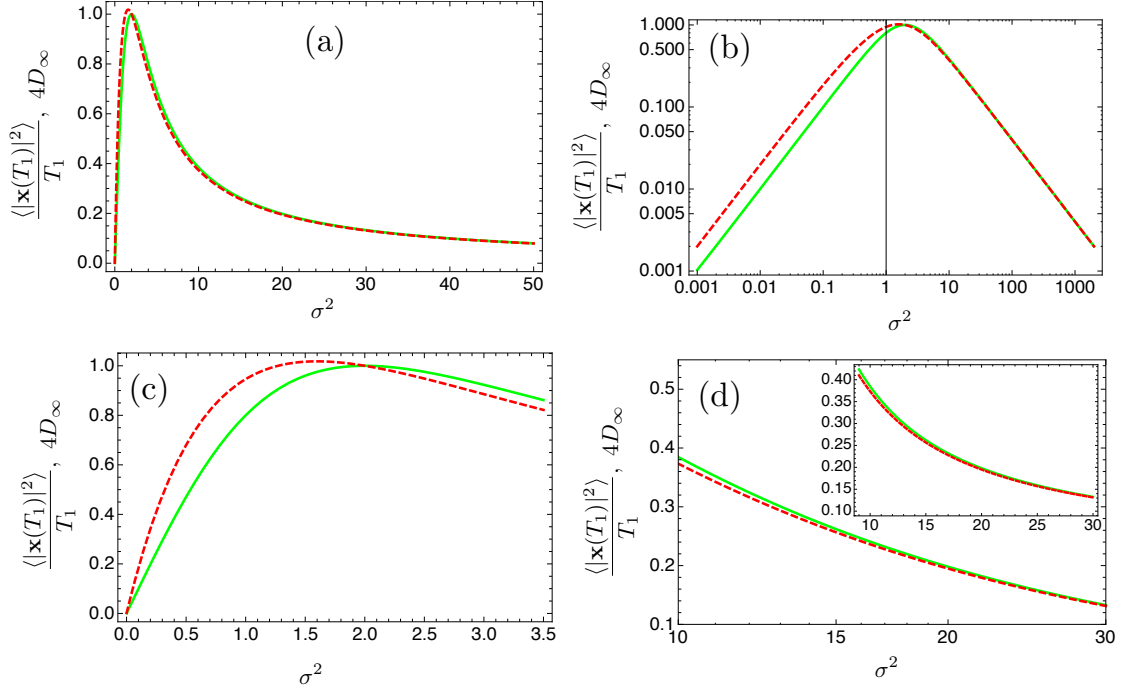


Figure 7.8. The curves of $\frac{\langle |\mathbf{x}(T_1)|^2 \rangle}{T_1}$ (dashed red) and $4D_\infty$ (solid green) vs σ^2 . In the linear-linear plot (a) it seems as both curves almost fall over each other even for small values of σ^2 , however the log-linear plot (b) shows that for small values of σ^2 the two curves are distinct and after the peak for large values of σ^2 they coincide. (c) is the peak in more details and (d) is the region where the curves begin to coincide. (Inset: the linear-linear plot of the main log-linear plot.)

where

$$f_{\mathbf{x}}(\sigma) = \frac{-\left(\frac{\sigma^4}{4} - 1\right)}{\left(\frac{\sigma^4}{4} - 1\right)^2 + \sigma^4} \quad (7.82)$$

and

$$f_{\mathbf{c}}(\sigma) = \frac{\left(\frac{\sigma^4}{4}\right) \left(\frac{\sigma^4}{4} - 1\right)}{\left(\frac{\sigma^4}{4} - 1\right)^2 + \sigma^4} \quad (7.83)$$

are functions of σ^2 (see Fig. 7.6). The root-mean-square of displacement after one rotation, that is, $\frac{\langle |\mathbf{x}(T_1)|^2 \rangle}{T_1}$ and $\frac{\langle |\mathbf{c}(T_1)|^2 \rangle}{T_1}$ along with the limiting behavior $4D_\infty$ are demonstrated in Fig. (7.7)

For dynamics of the center of mass at small values of σ^2 we see that $\frac{\langle |\mathbf{x}(T_1)|^2 \rangle}{T_1}$ and $4D_\infty$ behave as two distinct curves, (see Fig 7.8) while at higher values of σ^2 , in a region where $f_{\mathbf{x}} \simeq 0$ these two curves begin to coincide. With increasing the

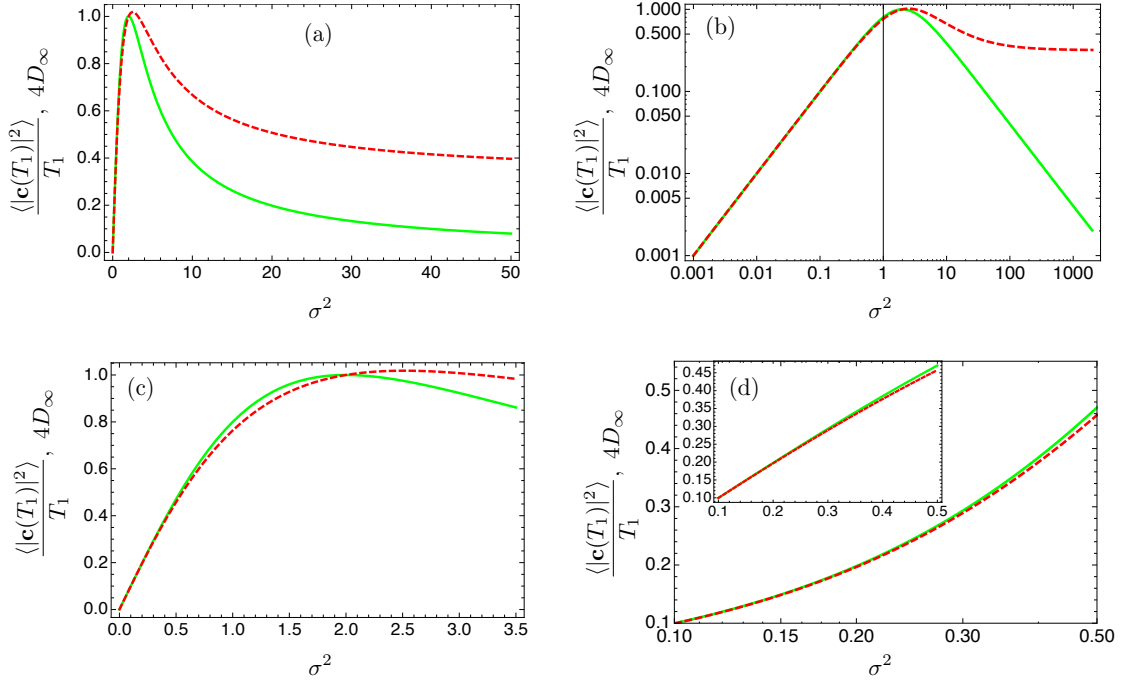


Figure 7.9. The curves of $\frac{\langle |\mathbf{c}(T_1)|^2 \rangle}{T_1}$ (dashed red) and $4D_\infty$ (solid green) vs σ^2 . The linear-linear (a) and log-linear (b) plots show that for small values the two curves coincide and near the peak dissociate. (c) is the peak in more details and (d) is the region where the curves take parts. (Inset: the linear-linear plot of the main log-linear plot.)

observation time T_n , the curves σ^2 , $\frac{\langle |\mathbf{x}(T_n)|^2 \rangle}{T_n}$ and $4D_\infty$ coincide at smaller values of σ^2 .

In the case of the displacement of the guiding center over time, at small values of σ^2 , $\frac{\langle |\mathbf{c}(T_1)|^2 \rangle}{T_1}$ and $4D_\infty$ coincide with each other (see Fig 7.8). These two curves begin to separate in a region where $f_c \simeq 0$. This is the domain where the velocity of the nanorotor loses most of its memory (due to the circular path constraint in the reference frame of the guiding center) after one deterministic period of oscillation. With increase in the observation time T_n , the curves σ^2 , $\frac{\langle |\mathbf{c}(T_n)|^2 \rangle}{T_n}$ and $4D_\infty$ begin to separate at higher values of σ^2 .

The most important outcome of this study is the diffusive behavior of the nanorotors at long times. To see this more clearly, let's work in dimensional units and insert $\sigma^2 = \frac{2D_{\text{out}}}{\omega}$ and $(\frac{\omega}{v^2}) D_{\text{eff}} = D_\infty$ into the effective translational diffusion

coefficient (7.77) to obtain

$$D_{\text{eff}} = \frac{1}{2} \frac{v^2}{\omega} \frac{\frac{D_{\text{ort}}}{\omega}}{\left(\frac{D_{\text{ort}}}{\omega}\right)^2 + 1} \quad (7.84)$$

This equation demonstrates that the coupling of the deterministic components of the motion (v and ω) and stochastic orientational diffusion D_{ort} at long times produces an effective translational diffusion D_{eff} .

The total translational diffusion coefficient $D_{\text{trs}}^{\text{tot}}$ of the nanorotor is the sum of its translational diffusion coefficient D_{trs} and the effective translational diffusion D_{eff} . So, it is important to know the relative contribution of D_{trs} and D_{eff} to $D_{\text{trs}}^{\text{tot}}$. It shows the importance of the coupling on the general dynamics of the nanorotor.

The measured translational diffusion coefficient for a 2 μm long nanorod in water is $D_{\text{trs}} = 0.4 \mu\text{m}^2 \text{s}^{-1}$ [18]. In chapter 6 we calculated the orientational diffusion coefficient of nanorotors from the videos in the supporting informations of [30] and [31]. For the former we have $\omega = 22.29 \text{ rpm} = 2.334 \text{ rad/s}^{-1}$, $D_{\text{ort}} = 0.102 \text{ rad}^2\text{s}^{-1}$, and approximately, $v \sim 10 \mu\text{m/s}$ which gives us $\sigma^2 = 0.087 \text{ rad}^2$ and $D_{\text{eff}} = 0.934 \mu\text{m}^2 \text{s}^{-1}$. The effective translational diffusion is more than two times the nanrod's translational diffusion. This shows that even for small values of $\sigma^2 \ll 1$, the effective translational diffusion has important effect. For the nanorotor in [31] we have $\omega = 279.79 \text{ rpm} = 29.3 \text{ rad s}^{-1}$, $D_{\text{ort}} = 0.462 \text{ rad}^2\text{s}^{-1}$, and approximately, $v \sim 30 \mu\text{m s}^{-1}$ [24] which gives us $\sigma^2 = 0.032 \text{ rad}^2$ and $D_{\text{eff}} = 0.242 \mu\text{m}^2 \text{s}^{-1}$. Therefore, in the fast nanorotor, the effective translational diffusion is approximately half the translational diffusion of the unpowered nanorod.

In addition to the effective translational diffusive dynamics of the nanorotors, we also calculated the correlation between the displacements after different periods. The displacement correlation function is defined as the correlation between the displacements during the first and k th rotation for variable \mathbf{r} ($= \mathbf{x}, \mathbf{c}$ or \mathbf{p}) to be

$$C_{\Delta\mathbf{r}}(k) = \Re \{ \langle \overline{\Delta\mathbf{r}}(1) \Delta\mathbf{r}(k) \rangle \}. \quad (7.85)$$

For the powered random walker on the c-frame circle we have

$$C_{\Delta\mathbf{p}}(k) = - \left(1 - e^{\pi\sigma^2} \right)^2 e^{-k\pi\sigma^2}. \quad (7.86)$$

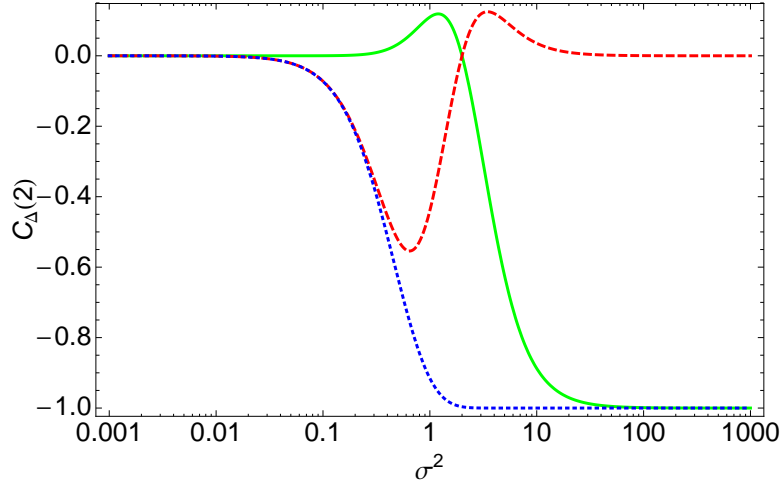


Figure 7.10. (Dotted blue) $C_{\Delta p}(2)$ (Dashed red) $C_{\Delta x}(2)$ (Solid Green) $C_{\Delta c}(2)$. Both $C_{\Delta p}(2)$ and $C_{\Delta c}(2)$ go to -1 at large values of σ .

As we predicted while discussing the difference between moving on a segment with periodic boundary conditions and on a circle, the correlation function is negative for displacements on a circle, while it is zero for displacements on the segment with periodic boundary conditions. This is due to the restriction that the particle has to move on a circular path. Similarly, we calculated the correlation function for the displacements of CoM

$$C_{\Delta x}(k) = f_x(\sigma) C_{\Delta p}(k) \quad (7.87)$$

and for the displacement of the guiding center,

$$C_{\Delta c}(k) = f_c(\sigma) C_{\Delta p}(k). \quad (7.88)$$

It is clear from Fig. 7.10 that both $C_{\Delta p}(2)$ and $C_{\Delta c}(2)$ go to -1 at large values of σ . This behavior is the direct consequence of chirality and the restriction of the powered random walker to move on the c-frame circle.

Fig. 7.11 demonstrates the effect of the restriction of motion on the c-frame circle at large values of $\sigma \gg 1$. We can write the displacement correlation function

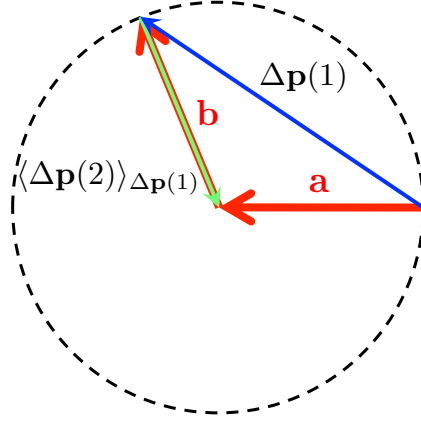


Figure 7.11. $\Delta \mathbf{p}(1)$ can be written as the sum of two vectors $\Delta \mathbf{p}(1) = \mathbf{a} + \mathbf{b}$ where \mathbf{a} is a constant vector, and \mathbf{b} varies depending on the amount of the stochastic component of dynamics over one period. For large values of $\sigma \gg 1$ \mathbf{b} can achieve all the possible orientations. The average of $\Delta \mathbf{p}(2)$ given $\Delta \mathbf{p}(1)$ fixed, in this domain of σ is a vector that begins at the end of $\Delta \mathbf{p}(1)$ and ends at the center of the circle. Therefore, we have $\langle \Delta \mathbf{p}(2) \rangle_{\Delta \mathbf{p}(1)} = -\mathbf{b}$.

in the form of

$$C_{\Delta \mathbf{p}}(2) = \Re \{ \langle \overline{\Delta \mathbf{p}}(1) \Delta \mathbf{p}(2) \rangle \} = \Re \{ \langle \overline{\Delta \mathbf{p}}(1) (\langle \Delta \mathbf{p}(2) \rangle_{\Delta \mathbf{p}(1)}) \rangle \}. \quad (7.89)$$

In the right hand side $\langle \Delta \mathbf{p}(2) \rangle_{\Delta \mathbf{p}(1)}$ means the average of $\Delta \mathbf{p}(2)$ given $\Delta \mathbf{p}(1)$ is fixed. During the first period, the powered random walker undergoes the displacement $\Delta \mathbf{p}(1)$. Since in the regime of large σ the vector $\Delta \mathbf{p}(1)$ can obtain all the possible displacement on the circle, the average $\langle \Delta \mathbf{p}(2) \rangle_{\Delta \mathbf{p}(1)}$ is a vector from the end of $\Delta \mathbf{p}(1)$ to the center of the circle. At the same time we can write the vector $\Delta \mathbf{p}(1)$ in the form of a sum of two other vectors $\Delta \mathbf{p}(1) = \mathbf{a} + \mathbf{b}$ where \mathbf{a} is a constant and as shown in Fig. 7.11 we have $\mathbf{b} = -\langle \Delta \mathbf{p}(2) \rangle_{\Delta \mathbf{p}(1)}$. Therefore, for the correlation function we obtain

$$C_{\Delta \mathbf{p}}(2) = \Re \{ \langle \overline{\Delta \mathbf{p}}(1) (\langle \Delta \mathbf{p}(2) \rangle_{\Delta \mathbf{p}(1)}) \rangle \} = -\overline{\mathbf{b}\mathbf{b}} + \overline{\mathbf{b}}\langle \mathbf{a} \rangle. \quad (7.90)$$

Since on a circle of radius 1 we have $\overline{\mathbf{b}\mathbf{b}} = 1$ and in this domain of σ the average $\langle \mathbf{a} \rangle = 0$ vanishes, we obtain

$$C_{\Delta \mathbf{p}}(2) = -1 \quad \text{for} \quad \sigma \gg 1 \quad (7.91)$$

which is the behavior we observed in Fig. 7.10.

We can use the same argument for the correlation function of guiding center reaching -1 at large values of σ . In general we can write

$$\Delta \mathbf{x} = \Delta \mathbf{c} + \Delta \mathbf{p} \quad (7.92)$$

for the relationship between the three types of displacement. At large values of σ the characteristic time of deterministic rotation ω^{-1} is much bigger than the characteristic time of orientational diffusion D_{ort}^{-1} . In this domain the displacement of the center of mass $\Delta \mathbf{x}$ is negligible compared to the two other types of displacements. Therefore, we can write $\Delta \mathbf{c} \simeq -\Delta \mathbf{p}$ and for the displacement correlation function of the guiding center we have

$$C_{\Delta \mathbf{c}}(2) = \Re \{ \langle \overline{\Delta \mathbf{c}}(1) \Delta \mathbf{c}(2) \rangle \} = \Re \{ \langle [-\overline{\Delta \mathbf{p}}(1)] [-\Delta \mathbf{p}(2)] \rangle \} = C_{\Delta \mathbf{p}}(2) \quad (7.93)$$

as we observe in Fig. 7.10.

Future Research

In this thesis, we discussed the deterministic dynamics of electrocatalytic nanomotors, moving by electrokinetic self-propulsion. A mathematical model is proposed and solved in the limit of thin double layer and small intensity of hydrogen ion flux for spherical and spheroidal geometries. The models lumps all the kinetic properties of the chemical reactions on the surface of the particle into a surface distribution of hydrogen ion flux. Also, the physical properties of the solution, such as viscosity and diffusivity of ions, are assumed to be constant. For future work, we suggest considering an appropriate kinetic model for the chemical reaction and revisit the model under the new condition.

In the proposed model, we concentrated on the deterministic dynamics of a single nanomotor in the unbounded domain. We did not consider the motor-motor interaction and the motor-substrate interaction. The interaction of a nanomotor with other nanomotors, or the substrate, can be the subject of further studies.

We analyzed the deterministic and the orientational stochastic component of nanomotor dynamics. We observed that the deterministic motion of a nanomotor is along a circular path. The coupling of these deterministic dynamics with stochastic orientational dynamics deviates the nanomotor's trajectory from a circular to a quasi-circular path. From analyzing the experimental data, we observed that the stochastic orientational dynamics of nanomotors follows the statistics of a one dimensional random walker. We suggest studying the effect of particle geometry on its orientational diffusion and consequently the deviation from the circular path.

We studied the effect of coupling of deterministic dynamics of nanomotors and

the stochastic orientational dynamics. This coupling leads to an effective translational diffusion, which is of the same order of magnitude as the translational diffusion of unpowered nanorods for the experimentally analyzed nanorotors. We suggest running experiments to calculate the effective translational diffusion and compare the data with our theoretical predictions.

Appendix A

Stokes' Flow Past a Sphere

A sphere of radius $r = a$ moves with velocity $\mathbf{U} = U \hat{\mathbf{U}}$ in a Newtonian fluid of viscosity μ . Working in units of $\mathbf{x}^* \sim a$ and $\mathbf{U}^* \sim U$, dimensionless quantities are used to describe the flow by the dimensionless Stokes equation

$$\nabla \cdot \mathbb{T} = -\nabla p + \nabla^2 \mathbf{u} = 0 \quad (\text{A.1})$$

and boundary conditions

$$\mathbf{u} = \hat{\mathbf{U}} \quad \text{at} \quad r = 1, \quad (\text{A.2})$$

$$\mathbf{u} = 0 \quad \text{at} \quad r \rightarrow \infty. \quad (\text{A.3})$$

Taking the divergence of the Stokes equation and using the continuity equation for incompressible fluid $\nabla \cdot \mathbf{u} = 0$, we obtain the Laplace's equation for the pressure field,

$$\nabla^2 p = 0. \quad (\text{A.4})$$

The fundamental solution of Laplace equation for a given quantity Φ ,

$$\nabla^2 \Phi = 0 \quad (\text{A.5})$$

is

$$\Phi^{(0)}(\mathbf{x}) = \frac{1}{|\mathbf{x}|} \equiv \frac{1}{r} \quad (\text{A.6})$$

from which we can construct the other solutions of the Laplace equation as decaying harmonic tensors of rank n as

$$\Phi^{(-n)}(\mathbf{x}) = (-1)^n \overbrace{\nabla \nabla \cdots \nabla}^n \frac{1}{r}, \quad (\text{A.7})$$

and the growing harmonic tensor of rank n as

$$\Phi^{(n)}(\mathbf{x}) = r^{2n+1} \Phi^{(-n)}(\mathbf{x}). \quad (\text{A.8})$$

Correspondingly, the first three decaying harmonic tensors, used extensively in our analysis, in the vectorial and index notation take the forms

$$\Phi^{(-1)}(\mathbf{x}) = -\nabla \frac{1}{r} = \frac{\mathbf{x}}{r^3}, \quad (\text{A.9})$$

$$\Phi_i^{(-1)}(\mathbf{x}) = \frac{x_i}{r^3}, \quad (\text{A.10})$$

$$\Phi^{(-2)}(\mathbf{x}) = \nabla \nabla \frac{1}{r} = \frac{3\mathbf{x}\mathbf{x}}{r^5} - \frac{\mathbb{I}}{r^3}, \quad (\text{A.11})$$

$$\Phi_{ij}^{(-2)}(\mathbf{x}) = \frac{3x_i x_j}{r^5} - \frac{\delta_{ij}}{r^3}, \quad (\text{A.12})$$

$$\Phi^{(-3)}(\mathbf{x}) = -\nabla \nabla \nabla \frac{1}{r}, \quad (\text{A.13})$$

$$\Phi_{ijk}^{(-3)}(\mathbf{x}) = 3 \left[\frac{5x_i x_j x_k}{r^7} - \left(\frac{\delta_{ij} x_k}{r^5} + \frac{\delta_{ik} x_j}{r^5} + \frac{\delta_{jk} x_i}{r^5} \right) \right]. \quad (\text{A.14})$$

Therefore, we can write the solution for Laplace equation (A.4) of the pressure field p as a linear combination of decaying harmonics whose coefficients are linear in $\hat{\mathbf{U}}$,

$$p = A_i^{(0)} \hat{\mathbf{U}}_i \Phi^{(0)} + A_{ij}^{(-1)} \hat{\mathbf{U}}_i \Phi_j^{(-1)} + A_{ijk}^{(-2)} \hat{\mathbf{U}}_i \Phi_{jk}^{(-2)} + A_{ijkl}^{(-3)} \hat{\mathbf{U}}_i \Phi_{jkl}^{(-3)} + \cdots \quad (\text{A.15})$$

where “ A ” tensorial coefficients solely depend on geometry. We cannot use growing harmonics since they diverge at the far field where the pressure goes to zero. A sphere is an isotropic object, and these coefficients should be isotropic tensors. Therefore, $A_i^{(0)} = 0$, $A_{ij}^{(-1)} = \lambda_1 \delta_{ij}$, $A_{ijk}^{(-2)} = \lambda_2 \epsilon_{ijk}$, $A_{ijkl}^{(-3)} = \lambda_3 \delta_{ij} \delta_{kl} + \lambda_4 \delta_{ik} \delta_{jl} + \lambda_5 \delta_{il} \delta_{jk}$, and \cdots . Because of parity, $\lambda_2 = 0$ and because of the Laplace equation, the product $A_{ijkl}^{(-3)} \Phi_{jkl}^{(-3)}$ vanishes. The rest of the terms vanish either due to parity

or Laplace equation. The pressure solution takes the form

$$p = A_{ij}^{(-1)} \hat{\mathbf{U}}_i \Phi_j^{(-1)} = \lambda_1 \delta_{ij} \hat{\mathbf{U}}_i \Phi_j^{(-1)} = \lambda_1 \hat{\mathbf{U}}_j \Phi_j^{(-1)} \equiv \lambda_1 \hat{\mathbf{U}}_j \frac{x_j}{r^3} \quad (\text{A.16})$$

The velocity field can be divided into two parts, $\mathbf{u} = \mathbf{u}^h + \mathbf{u}^p$; the homogeneous part \mathbf{u}^h that only satisfies $\nabla^2 \mathbf{u}^h = 0$ and the inhomogeneous (particular) solution \mathbf{u}^p that satisfies the equation $\nabla^2 \mathbf{u}^p - \nabla p = 0$. We have

$$\mathbf{u}^p = \frac{1}{2} p \mathbf{x} \quad (\text{A.17})$$

where, in tensor notation, takes the form

$$u_i^p = \frac{1}{2} p x_i = \frac{\lambda_1}{2} \hat{\mathbf{U}}_j \Phi_j^{(-1)} x_i \equiv \frac{\lambda_1}{2} \hat{\mathbf{U}}_j \frac{x_j x_i}{r^3} \quad (\text{A.18})$$

The next step is to find the homogeneous solution of the velocity field. In doing so, we write the solution as a combination of decaying harmonic terms whose coefficients are linear in $\hat{\mathbf{U}}$.

$$u_i^h = C_{ij}^{(0)} \hat{\mathbf{U}}_j \Phi^{(0)} + C_{ijk}^{(-1)} \hat{\mathbf{U}}_j \Phi_k^{(-1)} + C_{ijkl}^{(-2)} \hat{\mathbf{U}}_j \Phi_{kl}^{(-2)} + C_{ijklm}^{(-3)} \hat{\mathbf{U}}_j \Phi_{klm}^{(-3)} + \dots \quad (\text{A.19})$$

Again, ‘‘C’’ tensorial coefficients must be isotropic due to the isotropy of the sphere. Hence, $C_{ij}^{(0)} = \lambda'_0 \delta_{ij}$, $C_{ijk}^{(-1)} = \lambda'_1 \epsilon_{ijk}$, $C_{ijkl}^{(-2)} = \lambda'_2 \delta_{ij} \delta_{kl} + \lambda'_3 \delta_{ik} \delta_{jl} + \lambda'_4 \delta_{il} \delta_{jk}$ and \dots $\lambda'_1 = 0$ and $C_{ijklm}^{(-3)} = 0$ because of parity. We have $C_{ijkl}^{(-2)} \Phi_{kl}^{(-2)} = (\lambda'_3 + \lambda'_4) \Phi_{ij}^{(-2)}$ as a result of the Laplace equation ($\Phi_{kk}^{(-2)} = 0$) and symmetry of $\Phi_{ij}^{(-2)}$. Using the notation $\lambda'' \equiv \lambda'_3 + \lambda'_4$, the homogeneous solution takes the form

$$u_i^h = \lambda'_0 \delta_{ij} \hat{\mathbf{U}}_j \Phi^{(0)} + \lambda'' \hat{\mathbf{U}}_j \Phi_{ij}^{(-2)} \quad (\text{A.20})$$

So, we can write the velocity field as

$$\begin{aligned} u_i &= u_i^h + u_i^p = \lambda'_0 \delta_{ij} \hat{\mathbf{U}}_j \Phi^{(0)} + \frac{\lambda_1}{2} \hat{\mathbf{U}}_j \Phi_j^{(-1)} x_i + \lambda'' \hat{\mathbf{U}}_j \Phi_{ij}^{(-2)} \\ &= \hat{\mathbf{U}}_j \left[\lambda'_0 \delta_{ij} \Phi^{(0)} + \frac{\lambda_1}{2} \Phi_j^{(-1)} x_i + \lambda'' \Phi_{ij}^{(-2)} \right] \end{aligned} \quad (\text{A.21})$$

We then apply the boundary condition $u_i(r = 1) = \hat{\mathbf{U}}_i$ at the surface of the sphere

$$\begin{aligned}\hat{\mathbf{U}}_i &= \hat{\mathbf{U}}_j \left[\lambda'_0 \delta_{ij} + \frac{\lambda_1}{2} x_j x_i + \lambda'' (3x_i x_j - \delta_{ij}) \right] \\ &= \hat{\mathbf{U}}_j \left[(\lambda'_0 - \lambda'') \delta_{ij} + \left(\frac{\lambda_1}{2} + 3\lambda'' \right) x_i x_j \right] \\ &= (\lambda'_0 - \lambda'') \hat{\mathbf{U}}_i + \left(\frac{\lambda_1}{2} + 3\lambda'' \right) x_i x_j \hat{\mathbf{U}}_j\end{aligned}\quad (\text{A.22})$$

to obtain

$$\lambda'' = \lambda'_0 - 1 = -\frac{\lambda_1}{6}.\quad (\text{A.23})$$

Applying the continuity equation to this flow field

$$\begin{aligned}\nabla \cdot \mathbf{u} = \partial_i u_i &= \hat{\mathbf{U}}_j \left[\lambda'_0 \delta_{ij} \partial_i \Phi^{(0)} + \frac{\lambda_1}{2} \partial_i \Phi_j^{(-1)} x_i + \frac{\lambda_1}{2} \Phi_j^{(-1)} \partial_i x_i + \lambda'' \partial_i \Phi_{ij}^{(-2)} \right] \\ &= \hat{\mathbf{U}}_j \left[-\lambda'_0 \delta_{ij} \Phi_i^{(-1)} - \frac{\lambda_1}{2} \Phi_{ij}^{(-2)} x_i + \frac{\lambda_1}{2} \Phi_j^{(-1)} \delta_{ii} - \lambda'' \Phi_{ij}^{(-3)} \right] \\ &= \hat{\mathbf{U}}_j \left[-\lambda'_0 \delta_{ij} \frac{x_i}{r^3} - \frac{\lambda_1}{2} \left(\frac{3x_i x_j}{r^5} - \frac{\delta_{ij}}{r^3} \right) x_i + 3 \frac{\lambda_1}{2} \frac{x_j}{r^3} \right]\end{aligned}\quad (\text{A.24})$$

$$= \left(-\lambda'_0 + \frac{\lambda_1}{2} \right) \hat{\mathbf{U}}_j \frac{x_j}{r^3} = 0,\quad (\text{A.25})$$

gives us

$$\lambda'_0 = \frac{\lambda_1}{2}\quad (\text{A.26})$$

which yields the following values for the coefficients

$$\lambda'_0 = \frac{3}{4}, \quad \lambda_1 = \frac{3}{2}, \quad \lambda'' = -\frac{1}{4}\quad (\text{A.27})$$

Combining these results gives the pressure field and velocity field caused by a moving sphere in a fluid as

$$p = \frac{3}{2} \hat{\mathbf{U}}_j \Phi_j^{(-1)} \equiv \frac{3}{2} \hat{\mathbf{U}}_j \frac{x_j}{r^3}\quad (\text{A.28})$$

$$u_i = \frac{3}{4} \hat{\mathbf{U}}_j \left[\delta_{ij} \Phi^{(0)} + \Phi_j^{(-1)} x_i - \frac{1}{3} \Phi_{ij}^{(-2)} \right]\quad (\text{A.29})$$

The next step is to calculate the stress tensor in the fluid and the force applied by the sphere on the fluid. For this purpose, we use the constitutive equation

$$T_{ij} = -p\delta_{ij} + 2E_{ij} \quad (\text{A.30})$$

For the strain deformation tensor we write

$$\begin{aligned} 2E_{ij} &= \partial_i u_j + \partial_j u_i \\ &= \frac{3}{4} \hat{\mathbf{U}}_k \left[\delta_{jk} \partial_i \Phi^{(0)} + \partial_i \Phi_k^{(-1)} x_j + \Phi_k^{(-1)} \partial_i x_j - \frac{1}{3} \partial_i \Phi_{jk}^{(-2)} \right] \\ &+ \frac{3}{4} \hat{\mathbf{U}}_k \left[\delta_{ik} \partial_j \Phi^{(0)} + \partial_j \Phi_k^{(-1)} x_i + \Phi_k^{(-1)} \partial_j x_i - \frac{1}{3} \partial_j \Phi_{ik}^{(-2)} \right] \\ &= \frac{3}{4} \hat{\mathbf{U}}_k \left[-\delta_{jk} \Phi_i^{(-1)} - \Phi_{ik}^{(-2)} x_j + \Phi_k^{(-1)} \delta_{ij} + \frac{1}{3} \Phi_{ijk}^{(-3)} \right] \\ &+ \frac{3}{4} \hat{\mathbf{U}}_k \left[-\delta_{ik} \Phi_j^{(-1)} - \Phi_{jk}^{(-2)} x_i + \Phi_k^{(-1)} \delta_{ji} + \frac{1}{3} \Phi_{jik}^{(-3)} \right] \\ &= \frac{3}{4} \hat{\mathbf{U}}_k \left[\left(2\delta_{ij} \Phi_k^{(-1)} - \delta_{ik} \Phi_j^{(-1)} - \delta_{jk} \Phi_i^{(-1)} \right) - \left(\Phi_{jk}^{(-2)} x_i + \Phi_{ik}^{(-2)} x_j \right) + \frac{2}{3} \Phi_{ijk}^{(-3)} \right] \end{aligned}$$

from which we obtain the following relation for the stress tensor

$$T_{ij} = \frac{-3}{4} \hat{\mathbf{U}}_k \left[\left(\delta_{ik} \Phi_j^{(-1)} + \delta_{jk} \Phi_i^{(-1)} \right) + \left(\Phi_{jk}^{(-2)} x_i + \Phi_{ik}^{(-2)} x_j \right) - \frac{2}{3} \Phi_{ijk}^{(-3)} \right] \quad (\text{A.31})$$

In order to calculate the drag force applied by a fluid on the sphere we first calculate traction $\hat{f}_i = n_j T_{ij}$. Working with dimensionless quantities, the normal of the sphere surface equals the position vector, that is, $n_i = x_i$. So, we have (on the surface of sphere $r = 1$)

$$\begin{aligned} \hat{f}_i = x_j T_{ij} &= \frac{-3}{4} \hat{\mathbf{U}}_k \left[\left(\delta_{ik} x_j x_j + \delta_{jk} x_j x_i \right) + \left((3x_j x_k - \delta_{jk}) x_i x_j + (3x_i x_k - \delta_{ik}) x_j x_j \right) \right. \\ &\quad \left. - \frac{2}{3} \times 3 \left(5x_i x_j x_k x_j - (\delta_{ij} x_k x_j + \delta_{ik} x_j x_j + \delta_{jk} x_i x_j) \right) \right] \\ &= \frac{-3}{4} \hat{\mathbf{U}}_k \left[\left(\delta_{ik} + x_k x_i \right) + \left((2x_i x_k) + (3x_i x_k - \delta_{ik}) \right) \right. \\ &\quad \left. \times -2 \left(5x_i x_k - (x_k x_i + \delta_{ik} + x_i x_k) \right) \right] \\ &= \frac{-3}{4} \hat{\mathbf{U}}_k \times 2\delta_{ik} = \frac{-3}{2} \hat{\mathbf{U}}_i \quad (\text{A.32}) \end{aligned}$$

We can now calculate the drag force

$$\hat{F}_i^{drag} = \int_S \hat{f}_i dA = 4\pi \times \left(\frac{-3}{2} \hat{\mathbf{U}}_i \right) = -6\pi \hat{\mathbf{U}}_i \quad (\text{A.33})$$

The sphere is force free, so the force \hat{F} applied by the sphere to the fluid is equal in magnitude to drag force but opposite in direction.

$$\hat{F}_i = -\hat{F}_i^{drag} = 6\pi \hat{\mathbf{U}}_i \quad (\text{A.34})$$

We can substitute $\hat{\mathbf{U}}_i = \frac{1}{6\pi} \hat{F}_i$ and rewrite the pressure field, velocity field and stress tensor field in terms of applied force.

$$p = \frac{1}{4\pi} \hat{F}_j \Phi_j^{(-1)} \quad (\text{A.35})$$

$$u_i = \frac{1}{8\pi} \hat{F}_j \left[\delta_{ij} \Phi^{(0)} + \Phi_j^{(-1)} x_i - \frac{1}{3} \Phi_{ij}^{(-2)} \right] \quad (\text{A.36})$$

$$T_{ij} = \frac{-1}{8\pi} \hat{F}_k \left[\left(\delta_{ik} \Phi_j^{(-1)} + \delta_{jk} \Phi_i^{(-1)} \right) + \left(\Phi_{jk}^{(-2)} x_i + \Phi_{ik}^{(-2)} x_j \right) - \frac{2}{3} \Phi_{ijk}^{(-3)} \right] \quad (\text{A.37})$$

Working with dimensional quantities $\underline{\mathbf{x}} = a\mathbf{x}$, $\underline{\mathbf{u}} = U\mathbf{u}$, $\underline{p} = \frac{\mu U}{a} p$, $\underline{\mathbb{T}} = \frac{\mu U}{a} \mathbb{T}$, $\underline{\mathbf{F}} = \mu U a \hat{\mathbf{F}}$, $\underline{\Phi}_i^{(0)} = a^{-1} \Phi_i^{(0)}$, $\underline{\Phi}_i^{(-1)} = a^{-2} \Phi_i^{(-1)}$, $\underline{\Phi}_i^{(-2)} = a^{-3} \Phi_i^{(-2)}$, $\underline{\Phi}_i^{(-3)} = a^{-4} \Phi_i^{(-3)}$, these equations take the dimensional form

$$\underline{p} = \frac{1}{4\pi} \underline{F}_j \underline{\Phi}_j^{(-1)} \quad (\text{A.38})$$

$$\underline{u}_i = \frac{1}{8\pi\mu} \underline{F}_j \left[\delta_{ij} \underline{\Phi}^{(0)} + \underline{\Phi}_j^{(-1)} \underline{x}_i - \frac{1}{3} a^2 \underline{\Phi}_{ij}^{(-2)} \right] \quad (\text{A.39})$$

$$\underline{T}_{ij} = \frac{-1}{8\pi} \underline{F}_k \left[\left(\delta_{ik} \underline{\Phi}_j^{(-1)} + \delta_{jk} \underline{\Phi}_i^{(-1)} \right) + \left(\underline{\Phi}_{jk}^{(-2)} \underline{x}_i + \underline{\Phi}_{ik}^{(-2)} \underline{x}_j \right) - \frac{2}{3} a^2 \underline{\Phi}_{ijk}^{(-3)} \right] \quad (\text{A.40})$$

The moving sphere in fluid in the limit of $a \rightarrow 0$ acts like a point force of strength $\underline{\mathbf{F}}$. Therefore, the contribution of the moving object to the flow field can be summarized in a terms of $\underline{\mathbf{F}}\delta(\mathbf{x} - \mathbf{x}_0)$ in the Stokes equation

$$\underline{\nabla} \underline{p} + \mu \underline{\nabla}^2 \underline{\mathbf{u}} + \underline{\mathbf{F}}\delta(\mathbf{x} - \mathbf{x}_0) = 0 \quad (\text{A.41})$$

The solution to Stokes equation with a point-force is given by

$$\underline{p}(\underline{\mathbf{x}}) = \frac{1}{8\pi} \underline{\mathcal{P}}_j(\underline{\mathbf{x}}, \underline{\mathbf{x}}_0) \underline{F}_j \quad (\text{A.42})$$

$$\underline{u}_i(\underline{\mathbf{x}}) = \frac{1}{8\pi\mu} \underline{\mathcal{G}}_{ij}(\underline{\mathbf{x}}, \underline{\mathbf{x}}_0) \underline{F}_j \quad (\text{A.43})$$

$$\underline{\mathcal{T}}_{ij}(\underline{\mathbf{x}}) = \frac{1}{8\pi} \underline{\mathcal{T}}_{ijk}(\underline{\mathbf{x}}, \underline{\mathbf{x}}_0) \underline{F}_k \quad (\text{A.44})$$

where using the notation $\underline{\xi} = \underline{\mathbf{x}} - \underline{\mathbf{x}}_0$, these Green functions are

$$\begin{aligned} \underline{\mathcal{P}}_j(\underline{\xi}) &= 2\underline{\Phi}_j^{(-1)}(\underline{\xi}) \\ &= 2\frac{\underline{\xi}_j}{\underline{\xi}^3} \end{aligned} \quad (\text{A.45})$$

$$\begin{aligned} \underline{\mathcal{G}}_{ij}(\underline{\xi}) &= \delta_{ij}\underline{\Phi}^{(0)} + \underline{\xi}_i\underline{\Phi}_j^{(-1)}(\underline{\xi}) \\ &= \frac{\delta_{ij}}{\underline{\xi}} + \frac{\underline{\xi}_i\underline{\xi}_j}{\underline{\xi}^3} \end{aligned} \quad (\text{A.46})$$

$$\begin{aligned} \underline{\mathcal{T}}_{ijk}(\underline{\xi}) &= -\left[\left(\delta_{ik}\underline{\Phi}_j^{(-1)}(\underline{\xi}) + \delta_{jk}\underline{\Phi}_i^{(-1)}(\underline{\xi}) \right) + \left(\underline{\xi}_i\underline{\Phi}_{jk}^{(-2)}(\underline{\xi}) + \underline{\xi}_j\underline{\Phi}_{ik}^{(-2)}(\underline{\xi}) \right) \right] \\ &= -6\frac{\underline{\xi}_i\underline{\xi}_j\underline{\xi}_k}{\underline{\xi}^5} \end{aligned} \quad (\text{A.47})$$

Stokes' Flow Past a Spheroid

1 Spheroid

An spheroid in the Cartesian coordinates is defined by

$$\frac{x^2}{a^2} + \frac{y^2}{b^2} + \frac{z^2}{b^2} \equiv \frac{x^2}{a^2} + \frac{r^2}{b^2} = 1, \quad (\text{B.1})$$

where $r^2 = y^2 + z^2$ and $b \leq a$. The focal length $2c$ and the eccentricity e ($0 \leq e < 1$) are related by

$$c = \sqrt{a^2 - b^2} = ea \quad (\text{B.2})$$

and the eccentricity is related to a and b by

$$(1 - e^2) = \frac{b^2}{a^2} \quad (\text{B.3})$$

or

$$b^2 = a^2(1 - e^2). \quad (\text{B.4})$$

2 Velocity and Pressure Field

For a free stream velocity at infinity of the form

$$\mathbf{U} = U \hat{\mathbf{e}}_x \quad (\text{B.5})$$

where $\hat{\mathbf{e}}_x$ is the unit vector in the x direction, the velocity and pressure fields around the spheroid are given by [38]

$$\mathbf{u} = U \left\{ \hat{\mathbf{e}}_x - 2\alpha B_{1,0} \hat{\mathbf{e}}_x - \alpha \left(\frac{1}{R_2} - \frac{1}{R_1} \right) (y \hat{\mathbf{e}}_y + z \hat{\mathbf{e}}_z) + \alpha r^2 B_{3,0} \hat{\mathbf{e}}_x - 2\beta \nabla B_{1,1} \right\} \quad (\text{B.6})$$

and

$$p = 2\mu\alpha U \left(\frac{1}{R_1} - \frac{1}{R_2} \right), \quad (\text{B.7})$$

respectively, where

$$\alpha = \frac{2e^2}{1-e^2} \quad \beta = \frac{e^2}{-2e + (1+e^2)L_e}, \quad (\text{B.8})$$

$$L_e = \ln \left(\frac{1+e}{1-e} \right), \quad (\text{B.9})$$

$$R_1 = \sqrt{(x+c)^2 + r^2}, \quad (\text{B.10})$$

$$R_2 = \sqrt{(x-c)^2 + r^2}, \quad (\text{B.11})$$

$$B_{1,0} = \ln \left(\frac{R_2 - (x-c)}{R_1 - (x+c)} \right), \quad (\text{B.12})$$

$$B_{1,1} = R_2 - R_1 + x B_{1,0}, \quad (\text{B.13})$$

and

$$B_{3,0} = \frac{1}{r^2} \left(\frac{x+c}{R_1} - \frac{x-c}{R_2} \right). \quad (\text{B.14})$$

We would like to calculate the stress tensor on the surface of the particle. To do so we will use the following identities;

$$\partial_j R_1 = \frac{1}{R_1} (x_j + c \delta_{1j}). \quad (\text{B.15})$$

$$\partial_j R_2 = \frac{1}{R_2} (x_j - c \delta_{1j}). \quad (\text{B.16})$$

$$\partial_j B_{1,0} = \frac{x_j - (R_2 + c) \delta_{1j}}{R_2 [R_2 - (x_1 - c)]} - \frac{x_j - (R_1 - c) \delta_{1j}}{R_1 [R_1 - (x_1 + c)]} \quad (\text{B.17})$$

$$\frac{\partial}{\partial x_i} \left[\frac{1}{R_2} (x_j - c \delta_{1j}) \right] = \frac{\delta_{ij}}{R_2} - \frac{x_i x_j - c(x_i \delta_{1j} + x_j \delta_{1i}) + c^2 \delta_{1i} \delta_{1j}}{R_2^3} \quad (\text{B.18})$$

$$\frac{\partial}{\partial x_i} \left[\frac{1}{R_1} (x_j + c \delta_{1j}) \right] = \frac{\delta_{ij}}{R_1} - \frac{x_i x_j + c(x_i \delta_{1j} + x_j \delta_{1i}) + c^2 \delta_{1i} \delta_{1j}}{R_1^3} \quad (\text{B.19})$$

$$\begin{aligned} \frac{\partial}{\partial x_i} \left[\frac{x_j - (R_2 + c) \delta_{1j}}{R_2 [R_2 - (x_1 - c)]} \right] &= \frac{R_2 \delta_{ij} - (x_i - c \delta_{1i}) \delta_{1j}}{R_2^2 [R_2 - (x_1 - c)]} - [x_j - (R_2 + c) \delta_{1j}] \\ &\quad \times \frac{2R_2(x_i - c \delta_{1i}) - (x_1 - c)(x_i - c \delta_{1i}) - R_2^2 \delta_{1i}}{R_2^3 [R_2 - (x_1 - c)]^2} \end{aligned} \quad (\text{B.20})$$

and,

$$\begin{aligned} \frac{\partial}{\partial x_i} \left[\frac{x_j - (R_1 - c) \delta_{1j}}{R_1 [R_1 - (x_1 + c)]} \right] &= \frac{R_1 \delta_{ij} - (x_i + c \delta_{1i}) \delta_{1j}}{R_1^2 [R_1 - (x_1 + c)]} - [x_j - (R_1 - c) \delta_{1j}] \\ &\quad \times \frac{2R_1(x_i + c \delta_{1i}) - (x_1 + c)(x_i + c \delta_{1i}) - R_1^2 \delta_{1i}}{R_1^3 [R_1 - (x_1 + c)]^2} \end{aligned} \quad (\text{B.21})$$

The normal $\hat{\mathbf{n}}$ on the surface of the spheroid is

$$n_i = \frac{\frac{b}{a} x_1 \delta_{1i} + \frac{a}{b} x_2 \delta_{2i} + \frac{a}{b} x_3 \delta_{3i}}{\sqrt{a^2 - e^2 x_1^2}} = \frac{1}{\sqrt{R_1 R_2}} \left(\frac{a}{b} \right) (x_i - e^2 x_1 \delta_{1i}) \quad (\text{B.22})$$

For convenience in the calculations we define the vector

$$n'_i = x_i - e^2 x_1 \delta_{1i} \quad (\text{B.23})$$

which is related to the normal by $n_j = \frac{1}{\sqrt{R_1 R_2}} \left(\frac{a}{b} \right) n'_j$. The following identities hold on the surface of the spheroid.

$$r^2 = (1 - e^2)(a^2 - x_1^2) \quad (\text{B.24})$$

$$R_1 = a + e x_1 \quad (\text{B.25})$$

$$R_2 = a - e x_1 \quad (\text{B.26})$$

$$B_{1,0} = \ln \left(\frac{1+e}{1-e} \right) = L_e \quad (\text{B.27})$$

$$B_{3,0} = \frac{2e}{(1 - e^2)(a^2 - e^2 x_1^2)} = \frac{1}{R_1 R_2} \frac{2e}{(1 - e^2)} \quad (\text{B.28})$$

$$a^2 - (R_1 - c)x_1 = (a - x_1)R_1 \quad (\text{B.29})$$

$$a^2 - (R_2 + c)x_1 = (a - x_1)R_2 \quad (\text{B.30})$$

$$a^2 + cx_1 = aR_1 \quad (\text{B.31})$$

$$a^2 - cx_1 = aR_2 \quad (\text{B.32})$$

$$R_1 - (x_1 + c) = (1 - e)(x - a) \quad (\text{B.33})$$

$$R_2 - (x_1 - c) = (1 + e)(x - a) \quad (\text{B.34})$$

$$\frac{1}{R_2} + \frac{1}{R_1} = \frac{2a}{R_1 R_2} \quad (\text{B.35})$$

$$\frac{1}{R_2} - \frac{1}{R_1} = \frac{2ex_1}{R_1 R_2} \quad (\text{B.36})$$

$$n'_j(x_j \delta_{1i} + x_i \delta_{1j}) = (1 - e^2)(x_1 x_i + a^2 \delta_{1i}) \quad (\text{B.37})$$

$$n'_j \delta_{1j} \delta_{1i} = x_1(1 - e^2) \delta_{1i} \quad (\text{B.38})$$

$$n'_j(x_j + c \delta_{1j}) = b^2 + cx_1(1 - e^2) = R_1 a(1 - e^2) \quad (\text{B.39})$$

$$x_i - (R_1 - c) \delta_{1i} = (x_i - x_1 \delta_{1i}) - [R_1 - (x_1 + c)] \delta_{1i} \quad (\text{B.40})$$

$$x_i - (R_2 + c) \delta_{1i} = (x_i - x_1 \delta_{1i}) - [R_2 - (x_1 - c)] \delta_{1i} \quad (\text{B.41})$$

$$x_j x_j - e^2 x_1 x_1 = b^2 \quad (\text{B.42})$$

$$x_2 x_2 + x_3 x_3 = (1 - e^2)(a^2 - x_1 x_1). \quad (\text{B.43})$$

$$\begin{aligned} \frac{1}{R_2[R_2 - (x_1 - c)]} - \frac{1}{R_1[R_1 - (x_1 + c)]} &= \frac{1}{R_2(a - x_1)(1 + e)} - \frac{1}{R_1(a - x_1)(1 - e)} \\ &= \frac{R_1(1 - e) - R_2(1 + e)}{R_1 R_2(a - x_1)(1 - e^2)} \\ &= \frac{(R_1 - R_2) - e(R_1 + R_2)}{R_1 R_2(a - x_1)(1 - e^2)} \\ &= \frac{(2ex_1) - e(2a)}{R_1 R_2(a - x_1)(1 - e^2)} \end{aligned}$$

$$\begin{aligned}
&= \frac{-2e(a-x_1)}{R_1 R_2 (a-x_1)(1-e^2)} \\
&= \frac{-2e}{R_1 R_2 (1-e^2)} \tag{B.44}
\end{aligned}$$

$$\begin{aligned}
\frac{1}{R_2[R_2-(x_1-c)]} + \frac{1}{R_1[R_1-(x_1+c)]} &= \frac{1}{R_2(a-x_1)(1+e)} + \frac{1}{R_1(a-x_1)(1-e)} \\
&= \frac{R_1(1-e) + R_2(1+e)}{R_1 R_2 (a-x_1)(1-e^2)} \\
&= \frac{(R_1 + R_2) + e(-R_1 + R_2)}{R_1 R_2 (a-x_1)(1-e^2)} \\
&= \frac{(2a) + e(-2ex_1)}{R_1 R_2 (a-x_1)(1-e^2)} \\
&= \frac{2(a-e^2x_1)}{R_1 R_2 (a-x_1)(1-e^2)} \tag{B.45}
\end{aligned}$$

$$\begin{aligned}
\frac{1}{R_2-(x_1-c)} - \frac{1}{R_1-(x_1+c)} &= \frac{1}{(1+e)(a-x_1)} - \frac{1}{(1-e)(a-x_1)} \\
&= \frac{(1-e) - (1+e)}{(1-e^2)(a-x_1)} \\
&= \frac{-2e}{(1-e^2)(a-x_1)} \tag{B.46}
\end{aligned}$$

$$= \frac{-2e(a^2 - e^2x_1^2)}{R_1 R_2 (1-e^2)(a-x_1)} \tag{B.47}$$

2.1 Simplified Velocity Field

To proceed further with deriving the stress tensor, we rewrite the velocity equation in index notation,

$$u_i/U = (1 - 2\alpha B_{1,0} + \alpha r^2 B_{3,0})\delta_{1i} - \alpha \left(\frac{1}{R_2} - \frac{1}{R_1} \right) (x_2\delta_{2i} + x_3\delta_{3i}) - 2\beta \frac{\partial}{\partial x_i} B_{1,1} \tag{B.48}$$

We first simplify the above equation.

$$r^2 B_{3,0} \delta_{1i} = \left(\frac{x_1 + c}{R_1} - \frac{x_1 - c}{R_2} \right) \delta_{1i} = -x_1 \left(\frac{1}{R_2} - \frac{1}{R_1} \right) \delta_{1i} + c \left(\frac{1}{R_2} + \frac{1}{R_1} \right) \delta_{1i} \quad (\text{B.49})$$

$$\begin{aligned} \left(\frac{1}{R_2} - \frac{1}{R_1} \right) (x_2 \delta_{2i} + x_3 \delta_{3i}) &= \left(\frac{1}{R_2} - \frac{1}{R_1} \right) (x_i - x_1 \delta_{1i}) \\ &= \left(\frac{1}{R_2} - \frac{1}{R_1} \right) x_i - x_1 \left(\frac{1}{R_2} - \frac{1}{R_1} \right) \delta_{1i} \end{aligned} \quad (\text{B.50})$$

$$\begin{aligned} \frac{\partial}{\partial x_i} B_{1,1} &= \partial_i R_2 - \partial_i R_1 + \delta_{1i} B_{1,0} + x_1 \partial_i B_{1,0} \\ &= \frac{1}{R_2} (x_i - c \delta_{1i}) - \frac{1}{R_1} (x_i + c \delta_{1i}) + \delta_{1i} B_{1,0} + x_1 \partial_i B_{1,0} \\ &= x_i \left(\frac{1}{R_2} - \frac{1}{R_1} \right) - c \delta_{1i} \left(\frac{1}{R_2} + \frac{1}{R_1} \right) + \delta_{1i} B_{1,0} + x_1 \partial_i B_{1,0} \end{aligned} \quad (\text{B.51})$$

$$\begin{aligned} u_i/U &= \delta_{1i} - 2\alpha B_{1,0} \delta_{1i} + \alpha r^2 B_{3,0} \delta_{1i} - \alpha \left(\frac{1}{R_2} - \frac{1}{R_1} \right) (x_i - x_1 \delta_{1i}) \\ &\quad - \alpha \left(\frac{1 - e^2}{e^2} \right) \frac{\partial}{\partial x_i} B_{1,1} \\ &= \delta_{1i} - 2\alpha B_{1,0} \delta_{1i} - \alpha x_1 \left(\frac{1}{R_2} - \frac{1}{R_1} \right) \delta_{1i} + \alpha c \left(\frac{1}{R_2} + \frac{1}{R_1} \right) \delta_{1i} \\ &\quad - \alpha \left(\frac{1}{R_2} - \frac{1}{R_1} \right) x_i + \alpha x_1 \left(\frac{1}{R_2} - \frac{1}{R_1} \right) \delta_{1i} \\ &\quad - \alpha \left(\frac{1 - e^2}{e^2} \right) x_i \left(\frac{1}{R_2} - \frac{1}{R_1} \right) + \alpha \left(\frac{1 - e^2}{e^2} \right) c \delta_{1i} \left(\frac{1}{R_2} + \frac{1}{R_1} \right) \\ &\quad - \alpha \left(\frac{1 - e^2}{e^2} \right) \delta_{1i} B_{1,0} - \alpha \left(\frac{1 - e^2}{e^2} \right) x_1 \partial_i B_{1,0} \\ &= \delta_{1i} - 2\alpha B_{1,0} \delta_{1i} - \alpha \left(\frac{1 - e^2}{e^2} \right) \delta_{1i} B_{1,0} - \alpha \left(\frac{1 - e^2}{e^2} \right) x_1 \partial_i B_{1,0} \\ &\quad + \alpha c \left(\frac{1}{R_2} + \frac{1}{R_1} \right) \delta_{1i} + \alpha \left(\frac{1 - e^2}{e^2} \right) c \delta_{1i} \left(\frac{1}{R_2} + \frac{1}{R_1} \right) \\ &\quad - \alpha \left(\frac{1}{R_2} - \frac{1}{R_1} \right) x_i - \alpha \left(\frac{1 - e^2}{e^2} \right) x_i \left(\frac{1}{R_2} - \frac{1}{R_1} \right) \end{aligned}$$

$$\begin{aligned}
&= \delta_{1i} - \alpha \left(\frac{1+e^2}{e^2} \right) \delta_{1i} B_{1,0} - \alpha \left(\frac{1-e^2}{e^2} \right) x_1 \partial_i B_{1,0} \\
&\quad + \frac{\alpha c}{e^2} \left(\frac{1}{R_2} + \frac{1}{R_1} \right) \delta_{1i} - \frac{\alpha}{e^2} \left(\frac{1}{R_2} - \frac{1}{R_1} \right) x_i
\end{aligned} \tag{B.52}$$

Let's define

$$u_i^{(1)} = \delta_{1i} B_{1,0} \tag{B.53}$$

$$u_i^{(2)} = \left(\frac{1}{R_2} + \frac{1}{R_1} \right) c \delta_{1i} - \left(\frac{1}{R_2} - \frac{1}{R_1} \right) x_i \tag{B.54}$$

$$u_i^{(3)} = \partial_i B_{1,0} \tag{B.55}$$

The velocity formula then takes the form

$$u_i = \delta_{1i} - \alpha \left(\frac{1+e^2}{e^2} \right) u_i^{(1)} + \left(\frac{\alpha}{e^2} \right) u_i^{(2)} - \alpha \left(\frac{1-e^2}{e^2} \right) x_1 u_i^{(3)} \tag{B.56}$$

We further define

$$\boxed{\alpha' = \frac{\alpha U}{e^2}} \tag{B.57}$$

to obtain

$$\boxed{u_i = U \delta_{1i} - \alpha' (1+e^2) u_i^{(1)} + \alpha' u_i^{(2)} - \alpha' (1-e^2) x_1 u_i^{(3)}} \tag{B.58}$$

3 The Distribution of Traction on the Surface of the Spheroid

3.1 Introduction to Strain Tensor E_{ji}

For the gradient of velocity field, we have

$$\begin{aligned}
\partial_j u_i &= -\alpha' (1+e^2) \partial_j u_i^{(1)} + \alpha' \partial_j u_i^{(2)} - \alpha' (1-e^2) \partial_j (x_1 u_i^{(3)}) \\
&= -\alpha' (1+e^2) \partial_j u_i^{(1)} + \alpha' \partial_j u_i^{(2)} - \alpha' (1-e^2) \delta_{1j} u_i^{(3)} - \alpha' (1-e^2) x_1 \partial_j u_i^{(3)}
\end{aligned} \tag{B.59}$$

We form the strain tensor, $E_{ji} = \partial_i u_j + \partial_j u_i$, from the velocity field

$$\begin{aligned} E_{ji} = & -\alpha'(1+e^2) \left[\partial_j u_i^{(1)} + \partial_i u_j^{(1)} \right] + \alpha' \left[\partial_j u_i^{(2)} + \partial_i u_j^{(2)} \right] \\ & -\alpha'(1-e^2) \left[\delta_{1j} u_i^{(3)} + \delta_{1i} u_j^{(3)} \right] - \alpha'(1-e^2) x_1 \left[\partial_j u_i^{(3)} + \partial_i u_j^{(3)} \right] \end{aligned} \quad (\text{B.60})$$

where

$$\delta_{1j} u_i^{(3)} = \delta_{1j} \partial_i B_{1,0} = \partial_i (\delta_{1j} B_{1,0}) = \partial_i u_j^{(1)}, \quad (\text{B.61})$$

and

$$\delta_{1j} u_i^{(3)} + \delta_{1i} u_j^{(3)} = \partial_i u_j^{(1)} + \partial_j u_i^{(1)} \quad (\text{B.62})$$

Therefore, the strain tensor takes the form

$$E_{ji} = -2\alpha' \left[\partial_j u_i^{(1)} + \partial_i u_j^{(1)} \right] + \alpha' \left[\partial_j u_i^{(2)} + \partial_i u_j^{(2)} \right] - \alpha'(1-e^2) x_1 \left[\partial_j u_i^{(3)} + \partial_i u_j^{(3)} \right] \quad (\text{B.63})$$

Defining

$$\boxed{E_{ji}^{(k)} = \partial_i u_j^{(k)} + \partial_j u_i^{(k)} \quad k = 1, 2, 3} \quad (\text{B.64})$$

we can write the strain tensor in the form

$$\boxed{E_{ji} = -2\alpha' E_{ji}^{(1)} + \alpha' E_{ji}^{(2)} - \alpha'(1-e^2) x_1 E_{ji}^{(3)}} \quad (\text{B.65})$$

In order to calculate the distribution of traction on the surface of the spheroid we need to calculate $n_j E_{ji}$. To do so, we first calculate the terms $n'_j E_{ji}^{(k)}$ for each k and later form the final equation for the distribution of traction. We will decompose the elements into two perpendicular directions δ_{1i} and $x_i - x_1 \delta_{1i}$. The first one δ_{1i} represents the direction of the symmetric axis and the second one $x_i - x_1 \delta_{1i}$ represent the vectors in a plane perpendicular to the axis of symmetry.

3.2 Term $n'_j E_{ji}^{(1)}$

We use the identity

$$\partial_j B_{1,0} = \frac{x_j - (R_2 + c) \delta_{1j}}{R_2 [R_2 - (x_1 - c)]} - \frac{x_j - (R_1 - c) \delta_{1j}}{R_1 [R_1 - (x_1 + c)]} \quad (\text{B.66})$$

to calculate

$$E_{ij}^{(1)} = E_{ji}^{(1)} = \partial_j(B_{1,0}\delta_{1i}) + \partial_i(B_{1,0}\delta_{1j}) = \frac{(x_j\delta_{1i} + x_i\delta_{1j}) - 2(R_2 + c)\delta_{1j}\delta_{1i}}{R_2[R_2 - (x_1 - c)]} - \frac{(x_j\delta_{1i} + x_i\delta_{1j}) - 2(R_1 - c)\delta_{1j}\delta_{1i}}{R_1[R_1 - (x_1 + c)]} \quad (\text{B.67})$$

Using the identities

$$n'_j(x_j\delta_{1i} + x_i\delta_{1j}) = (1 - e^2)(a^2\delta_{1i} + x_1x_i) \quad (\text{B.68})$$

and

$$n'_j\delta_{1j}\delta_{1i} = (1 - e^2)x_1\delta_{1i} \quad (\text{B.69})$$

we obtain

$$n'_jE_{ji}^{(1)} = (1 - e^2) \left\{ \frac{(a^2\delta_{1i} + x_1x_i) - 2(R_2 + c)x_1\delta_{1i}}{R_2[R_2 - (x_1 - c)]} - \frac{(a^2\delta_{1i} + x_1x_i) - 2(R_1 - c)x_1\delta_{1i}}{R_1[R_1 - (x_1 + c)]} \right\} \quad (\text{B.70})$$

To simplify the equation further, we separate the terms and use the appropriate identities.

$$\begin{aligned} n'_jE_{ji}^{(1)} &= (1 - e^2) \left\{ (a^2\delta_{1i} + x_1x_i) \left(\frac{1}{R_2[R_2 - (x_1 - c)]} - \frac{1}{R_1[R_1 - (x_1 + c)]} \right) \right. \\ &\quad - 2x_1\delta_{1i} \left(\frac{R_2}{R_2[R_2 - (x_1 - c)]} - \frac{R_1}{R_1[R_1 - (x_1 + c)]} \right) \\ &\quad \left. - 2cx_1\delta_{1i} \left(\frac{1}{R_2[R_2 - (x_1 - c)]} + \frac{1}{R_1[R_1 - (x_1 + c)]} \right) \right\} \\ &= (1 - e^2) \left\{ (a^2\delta_{1i} + x_1x_i) \left(\frac{1}{R_2[R_2 - (x_1 - c)]} - \frac{1}{R_1[R_1 - (x_1 + c)]} \right) \right. \\ &\quad - 2x_1\delta_{1i} \left(\frac{1}{R_2 - (x_1 - c)} - \frac{1}{R_1 - (x_1 + c)} \right) \\ &\quad \left. - 2eax_1\delta_{1i} \left(\frac{1}{R_2[R_2 - (x_1 - c)]} + \frac{1}{R_1[R_1 - (x_1 + c)]} \right) \right\} \\ &= (1 - e^2) \left\{ (a^2\delta_{1i} + x_1x_i) \frac{1}{R_1R_2} \left(\frac{-2e}{1 - e^2} \right) \right\} \end{aligned}$$

$$\begin{aligned}
& -2x_1\delta_{1i} \left(\frac{-2e(a^2 - e^2x_1^2)}{R_1R_2(1 - e^2)(a - x_1)} \right) \\
& -2eax_1\delta_{1i} \left(\frac{2(a - e^2x_1)}{R_1R_2(a - x_1)(1 - e^2)} \right) \Big\} \\
= & \frac{-2e}{R_1R_2} \left\{ (a^2\delta_{1i} + x_1x_i) - 2x_1\delta_{1i} \left(\frac{a^2 - e^2x_1^2}{a - x_1} \right) + 2ax_1\delta_{1i} \left(\frac{a - e^2x_1}{a - x_1} \right) \right\}
\end{aligned} \tag{B.71}$$

$$\begin{aligned}
& -2x_1\delta_{1i} \left(\frac{a^2 - e^2x_1^2}{a - x_1} \right) + 2ax_1\delta_{1i} \left(\frac{a - e^2x_1}{a - x_1} \right) \\
& = -2x_1\delta_{1i} \left(\frac{a^2 - e^2x_1^2}{a - x_1} - \frac{a^2 - e^2ax_1}{a - x_1} \right) \\
& = -2x_1\delta_{1i} \left(\frac{e^2x_1(a - x_1)}{a - x_1} \right) = -2e^2x_1^2\delta_{1i}
\end{aligned} \tag{B.72}$$

Then we have

$$n'_j E_{ji}^{(1)} = \frac{-2e}{R_1R_2} \left\{ (a^2\delta_{1i} + x_1x_i) - 2e^2x_1^2\delta_{1i} \right\} \tag{B.73}$$

We decompose this equation into the two perpendicular directions δ_{1i} and $x_i - x_1\delta_{1i}$.

$$\begin{aligned}
(a^2\delta_{1i} + x_1x_i) - 2e^2x_1^2\delta_{1i} & = (a^2\delta_{1i} + x_1x_i - x_1x_1\delta_{1i} + x_1x_1\delta_{1i}) - 2e^2x_1^2\delta_{1i} \\
& = a^2\delta_{1i} + x_1(x_i - x_1\delta_{1i}) + x_1x_1\delta_{1i} - 2e^2x_1^2\delta_{1i} \\
& = x_1(x_i - x_1\delta_{1i}) + (a^2 + x_1^2 - 2e^2x_1^2)\delta_{1i}
\end{aligned} \tag{B.74}$$

Therefore, the first term of the strain tensor becomes

$$\boxed{n'_j E_{ji}^{(1)} = \frac{-2ex_1}{R_1R_2}(x_i - x_1\delta_{1i}) + \frac{-2e(a^2 + x_1^2 - 2e^2x_1^2)}{R_1R_2}\delta_{1i}} \tag{B.75}$$

3.3 Term $n'_j E_{ji}^{(2)}$

For $R_1 = \sqrt{(x_1 + c)^2 + x_2^2 + x_3^2}$ the derivative with respect to x_j gives

$$\partial_j R_1 = \frac{1}{2R_1} \partial_j [(x_1 + c)^2 + x_2^2 + x_3^2] = \frac{1}{R_1} (x_j + c \delta_{1j}). \tag{B.76}$$

Similarly, for $R_2 = \sqrt{(x_1 - c)^2 + x_2^2 + x_3^2}$ we have

$$\partial_j R_2 = \frac{1}{2R_2} \partial_j [(x_1 - c)^2 + x_2^2 + x_3^2] = \frac{1}{R_2} (x_j - c \delta_{1j}). \quad (\text{B.77})$$

$$u_i^{(2)} = \left(\frac{1}{R_2} + \frac{1}{R_1} \right) c \delta_{1i} - \left(\frac{1}{R_2} - \frac{1}{R_1} \right) x_i \quad (\text{B.78})$$

$$\begin{aligned} \partial_j \left(\frac{1}{R_2} + \frac{1}{R_1} \right) c \delta_{1i} &= - \left[\frac{(x_j - c \delta_{1j})}{R_2^3} + \frac{(x_j + c \delta_{1j})}{R_1^3} \right] c \delta_{1i} \\ &= \left(\frac{1}{R_2^3} + \frac{1}{R_1^3} \right) (-c x_j \delta_{1i}) + \left(\frac{1}{R_2^3} - \frac{1}{R_1^3} \right) c^2 \delta_{1i} \delta_{1j} \end{aligned} \quad (\text{B.79})$$

$$\begin{aligned} \partial_j \left[-x_i \left(\frac{1}{R_2} - \frac{1}{R_1} \right) \right] &= -\delta_{ij} \left(\frac{1}{R_2} - \frac{1}{R_1} \right) + x_i \left[\frac{(x_j - c \delta_{1j})}{R_2^3} - \frac{(x_j + c \delta_{1j})}{R_1^3} \right] \\ &= -\delta_{ij} \left(\frac{1}{R_2} - \frac{1}{R_1} \right) + x_i x_j \left(\frac{1}{R_2^3} - \frac{1}{R_1^3} \right) \\ &\quad - c x_i \delta_{1j} \left(\frac{1}{R_2^3} + \frac{1}{R_1^3} \right) \end{aligned} \quad (\text{B.80})$$

Therefore,

$$\begin{aligned} \partial_j u_i^{(2)} &= -\delta_{ij} \left(\frac{1}{R_2} - \frac{1}{R_1} \right) + (x_i x_j + c^2 \delta_{1i} \delta_{1j}) \left(\frac{1}{R_2^3} - \frac{1}{R_1^3} \right) \\ &\quad - c (x_i \delta_{1j} + x_j \delta_{1i}) \left(\frac{1}{R_2^3} + \frac{1}{R_1^3} \right) \end{aligned} \quad (\text{B.81})$$

and consequently,

$$\begin{aligned} E_{ji}^{(2)} &= -2\delta_{ij} \left(\frac{1}{R_2} - \frac{1}{R_1} \right) + 2(x_i x_j + c^2 \delta_{1i} \delta_{1j}) \left(\frac{1}{R_2^3} - \frac{1}{R_1^3} \right) \\ &\quad - 2c (x_i \delta_{1j} + x_j \delta_{1i}) \left(\frac{1}{R_2^3} + \frac{1}{R_1^3} \right) \end{aligned} \quad (\text{B.82})$$

Using the identities

$$n'_j \delta_{ji} = n'_i = x_i - e^2 x_1 \delta_{1i} \quad (\text{B.83})$$

$$n'_j(x_i x_j + e^2 \delta_{1i} \delta_{1j}) = a^2(1 - e^2)(x_i + e^2 x_1 \delta_{1i}) \quad (\text{B.84})$$

$$n'_j(x_i \delta_{1j} + x_j \delta_{1i}) = (1 - e^2)(x_1 x_i + a^2 \delta_{1i}) \quad (\text{B.85})$$

we obtain

$$\begin{aligned} n'_j E_{ji}^{(2)} &= -2(x_i - e^2 x_1 \delta_{1i}) \left(\frac{1}{R_2} - \frac{1}{R_1} \right) + 2a^2(1 - e^2)(x_i + e^2 x_1 \delta_{1i}) \left(\frac{1}{R_2^3} - \frac{1}{R_1^3} \right) \\ &\quad - 2c(1 - e^2)(x_1 x_i + a^2 \delta_{1i}) \left(\frac{1}{R_2^3} + \frac{1}{R_1^3} \right) \end{aligned} \quad (\text{B.86})$$

We need to simplify this equation further. First we decompose the terms into the two perpendicular directions δ_{1i} and $x_i - x_1 \delta_{1i}$.

$$x_i - e^2 x_1 \delta_{1i} = x_i - x_1 \delta_{1i} + x_1 \delta_{1i} - e^2 x_1 \delta_{1i} = (x_i - x_1 \delta_{1i}) + (1 - e^2)x_1 \delta_{1i} \quad (\text{B.87})$$

$$x_i + e^2 x_1 \delta_{1i} = x_i - x_1 \delta_{1i} + x_1 \delta_{1i} + e^2 x_1 \delta_{1i} = (x_i - x_1 \delta_{1i}) + (1 + e^2)x_1 \delta_{1i} \quad (\text{B.88})$$

$$x_1 x_i + a^2 \delta_{1i} = x_1 x_i - x_1 x_1 \delta_{1i} + x_1 x_1 \delta_{1i} + a^2 \delta_{1i} = x_1(x_i - x_1 \delta_{1i}) + (x_1^2 + a^2) \delta_{1i} \quad (\text{B.89})$$

$$\frac{1}{R_2} - \frac{1}{R_1} = \frac{R_1 - R_2}{R_1 R_2} = \frac{(a + ex) - (a - ex)}{R_1 R_2} = \frac{2ex_1}{R_1 R_2} \quad (\text{B.90})$$

$$a \left(\frac{1}{R_2^3} - \frac{1}{R_1^3} \right) - ex_1 \left(\frac{1}{R_2^3} + \frac{1}{R_1^3} \right) = \frac{1}{R_2^3}(a - ex_1) - \frac{1}{R_1^3}(a + ex_1) = \frac{1}{R_2^2} - \frac{1}{R_1^2} \quad (\text{B.91})$$

and

$$\begin{aligned} &(1 + e^2)ax_1 \left(\frac{1}{R_2^3} - \frac{1}{R_1^3} \right) - e(x_1^2 + a^2) \left(\frac{1}{R_2^3} + \frac{1}{R_1^3} \right) \\ &= \frac{1}{R_2^3}(ax_1 + e^2 ax_1 - ex_1^2 - ea^2) - \frac{1}{R_1^3}(ax_1 + e^2 ax_1 + ex_1^2 + ea^2) \\ &= \frac{1}{R_2^3}(a - ex_1)(x_1 - ea) - \frac{1}{R_1^3}(a + ex_1)(x_1 + ea) \\ &= \frac{(x_1 - ea)}{R_2^2} - \frac{(x_1 + ea)}{R_1^2} \end{aligned} \quad (\text{B.92})$$

which gives

$$\begin{aligned}
& 2a^2(1-e^2)(x_i + e^2x_1\delta_{1i}) \left(\frac{1}{R_2^3} - \frac{1}{R_1^3} \right) - 2c(1-e^2)(x_1x_i + a^2\delta_{1i}) \left(\frac{1}{R_2^3} + \frac{1}{R_1^3} \right) \\
&= 2a(1-e^2) \left\{ a(x_i + e^2x_1\delta_{1i}) \left(\frac{1}{R_2^3} - \frac{1}{R_1^3} \right) - e(x_1x_i + a^2\delta_{1i}) \left(\frac{1}{R_2^3} + \frac{1}{R_1^3} \right) \right\} \\
&= 2a(1-e^2) \left\{ a[(x_i - x_1\delta_{1i}) + (1+e^2)x_1\delta_{1i}] \left(\frac{1}{R_2^3} - \frac{1}{R_1^3} \right) \right. \\
&\quad \left. - e[x_1(x_i - x_1\delta_{1i}) + (x_1^2 + a^2)\delta_{1i}] \left(\frac{1}{R_2^3} + \frac{1}{R_1^3} \right) \right\} \\
&= 2a(1-e^2) \left\{ (x_i - x_1\delta_{1i}) \left[a \left(\frac{1}{R_2^3} - \frac{1}{R_1^3} \right) - ex_1 \left(\frac{1}{R_2^3} + \frac{1}{R_1^3} \right) \right] \right. \\
&\quad \left. + \delta_{1i} \left[(1+e^2)ax_1 \left(\frac{1}{R_2^3} - \frac{1}{R_1^3} \right) - e(x_1^2 + a^2) \left(\frac{1}{R_2^3} + \frac{1}{R_1^3} \right) \right] \right\} \\
&= 2a(1-e^2) \left\{ (x_i - x_1\delta_{1i}) \left(\frac{1}{R_2^2} - \frac{1}{R_1^2} \right) + \delta_{1i} \left[\frac{(x_1 - ea)}{R_2^2} - \frac{(x_1 + ea)}{R_1^2} \right] \right\}
\end{aligned} \tag{B.93}$$

Therefore,

$$\begin{aligned}
n'_j E_{ji}^{(2)} &= -\frac{4ex_1}{R_1R_2} [(x_i - x_1\delta_{1i}) + (1-e^2)x_1\delta_{1i}] \\
&\quad + 2a(1-e^2) \left\{ (x_i - x_1\delta_{1i}) \left(\frac{1}{R_2^2} - \frac{1}{R_1^2} \right) + \delta_{1i} \left[\frac{(x_1 - ea)}{R_2^2} - \frac{(x_1 + ea)}{R_1^2} \right] \right\}
\end{aligned} \tag{B.94}$$

Recasting the above equation, we get

$$\begin{aligned}
n'_j E_{ji}^{(2)} &= \frac{-4ex_1}{R_1R_2} (x_i - x_1\delta_{1i}) + 2a(1-e^2) \left(\frac{1}{R_2^2} - \frac{1}{R_1^2} \right) (x_i - x_1\delta_{1i}) \\
&\quad + \frac{-4ex_1^2}{R_1R_2} (1-e^2)\delta_{1i} + 2a(1-e^2) \left[\frac{(x_1 - ea)}{R_2^2} - \frac{(x_1 + ea)}{R_1^2} \right] \delta_{1i}
\end{aligned} \tag{B.95}$$

Using

$$\frac{(x_1 - ea)}{R_2^2} - \frac{(x_1 + ea)}{R_1^2} = x_1 \left(\frac{1}{R_2^2} - \frac{1}{R_1^2} \right) - ea \left(\frac{1}{R_2^2} + \frac{1}{R_1^2} \right) \tag{B.96}$$

the final form at this stage becomes

$$\begin{aligned}
n'_j E_{ji}^{(2)} &= \frac{-4ex_1}{R_1 R_2} (x_i - x_1 \delta_{1i}) + 2a(1 - e^2) \left(\frac{1}{R_2^2} - \frac{1}{R_1^2} \right) (x_i - x_1 \delta_{1i}) \\
&\quad + \frac{-4ex_1^2}{R_1 R_2} (1 - e^2) \delta_{1i} + 2ax_1(1 - e^2) \left(\frac{1}{R_2^2} - \frac{1}{R_1^2} \right) \delta_{1i} \\
&\quad - 2ea^2(1 - e^2) \left(\frac{1}{R_2^2} + \frac{1}{R_1^2} \right) \delta_{1i}
\end{aligned} \tag{B.97}$$

3.4 Term $n'_j E_{ji}^{(3)}$

Finally, we would like to calculate

$$E_{ji}^{(3)} = \partial_i u_j^{(3)} + \partial_j u_i^{(3)} = \partial_i \partial_j B_{1,0} + \partial_j \partial_i B_{1,0} \tag{B.98}$$

We have

$$\partial_j B_{1,0} = \frac{x_j - (R_2 + c) \delta_{1j}}{R_2 [R_2 - (x_1 - c)]} - \frac{x_j - (R_1 - c) \delta_{1j}}{R_1 [R_1 - (x_1 + c)]} \tag{B.99}$$

and from that

$$\begin{aligned}
\frac{\partial}{\partial x_i} \left(\frac{x_j - (R_2 + c) \delta_{1j}}{R_2 [R_2 - (x_1 - c)]} \right) &= \frac{\delta_{ij} - \frac{1}{R_2} (x_i - c \delta_{1i}) \delta_{1j}}{R_2 [R_2 - (x_1 - c)]} - [x_j - (R_2 + c) \delta_{1j}] \\
&\quad \times \frac{[R_2 - (x_1 - c)] \partial_i R_2 + R_2 [\partial_i R_2 - \partial_i x_1]}{R_2^2 [R_2 - (x_1 - c)]^2} \\
&= \frac{R_2 \delta_{ij} - (x_i - c \delta_{1i}) \delta_{1j}}{R_2^2 [R_2 - (x_1 - c)]} - [x_j - (R_2 + c) \delta_{1j}] \\
&\quad \times \frac{2(x_i - c \delta_{1i}) - \frac{1}{R_2} (x_1 - c)(x_i - c \delta_{1i}) - R_2 \delta_{1i}}{R_2^2 [R_2 - (x_1 - c)]^2} \\
&= \frac{R_2 \delta_{ij} - (x_i - c \delta_{1i}) \delta_{1j}}{R_2^2 [R_2 - (x_1 - c)]} - [x_j - (R_2 + c) \delta_{1j}] \\
&\quad \times \left(\frac{2R_2(x_i - c \delta_{1i}) - (x_1 - c)(x_i - c \delta_{1i}) - R_2^2 \delta_{1i}}{R_2^3 [R_2 - (x_1 - c)]^2} \right)
\end{aligned} \tag{B.100}$$

and similarly,

$$\frac{\partial}{\partial x_i} \left(\frac{x_j - (R_1 - c) \delta_{1j}}{R_1 [R_1 - (x_1 + c)]} \right) = \frac{R_1 \delta_{ij} - (x_i + c \delta_{1i}) \delta_{1j}}{R_1^2 [R_1 - (x_1 + c)]} - [x_j - (R_1 - c) \delta_{1j}]$$

$$\times \frac{2R_1(x_i + c \delta_{1i}) - (x_1 + c)(x_i + c \delta_{1i}) - R_1^2 \delta_{1i}}{R_1^3 [R_1 - (x_1 + c)]^2} \quad (\text{B.101})$$

So, we can write

$$\begin{aligned} \partial_i \partial_j B_{1,0} = & \left(\frac{R_2 \delta_{ij} - (x_i - c \delta_{1i}) \delta_{1j}}{R_2^2 [R_2 - (x_1 - c)]} \right) \\ & - [x_j - (R_2 + c) \delta_{1j}] \left(\frac{2R_2(x_i - c \delta_{1i}) - (x_1 - c)(x_i - c \delta_{1i}) - R_2^2 \delta_{1i}}{R_2^3 [R_2 - (x_1 - c)]^2} \right) \\ & - \left(\frac{R_1 \delta_{ij} - (x_i + c \delta_{1i}) \delta_{1j}}{R_1^2 [R_1 - (x_1 + c)]} \right) \\ & + [x_j - (R_1 - c) \delta_{1j}] \left(\frac{2R_1(x_i + c \delta_{1i}) - (x_1 + c)(x_i + c \delta_{1i}) - R_1^2 \delta_{1i}}{R_1^3 [R_1 - (x_1 + c)]^2} \right) \end{aligned} \quad (\text{B.102})$$

and therefore,

$$\begin{aligned} E_{ij}^{(3)} = & \left(\frac{2R_2 \delta_{ij} - (x_i \delta_{1j} + x_j \delta_{1i}) + 2c \delta_{1i} \delta_{1j}}{R_2^2 [R_2 - (x_1 - c)]} \right) \\ & - [x_j - (R_2 + c) \delta_{1j}] \left(\frac{2R_2(x_i - c \delta_{1i}) - (x_1 - c)(x_i - c \delta_{1i}) - R_2^2 \delta_{1i}}{R_2^3 [R_2 - (x_1 - c)]^2} \right) \\ & - [x_i - (R_2 + c) \delta_{1i}] \left(\frac{2R_2(x_j - c \delta_{1j}) - (x_1 - c)(x_j - c \delta_{1j}) - R_2^2 \delta_{1j}}{R_2^3 [R_2 - (x_1 - c)]^2} \right) \\ & - \left(\frac{2R_1 \delta_{ij} - (x_i \delta_{1j} + x_j \delta_{1i}) - 2c \delta_{1i} \delta_{1j}}{R_1^2 [R_1 - (x_1 + c)]} \right) \\ & + [x_j - (R_1 - c) \delta_{1j}] \left(\frac{2R_1(x_i + c \delta_{1i}) - (x_1 + c)(x_i + c \delta_{1i}) - R_1^2 \delta_{1i}}{R_1^3 [R_1 - (x_1 + c)]^2} \right) \\ & + [x_i - (R_1 - c) \delta_{1i}] \left(\frac{2R_1(x_j + c \delta_{1j}) - (x_1 + c)(x_j + c \delta_{1j}) - R_1^2 \delta_{1j}}{R_1^3 [R_1 - (x_1 + c)]^2} \right) \end{aligned} \quad (\text{B.103})$$

Using this relation, we can write down the last term of strain tensor as

$$\begin{aligned} n'_j E_{ji}^{(3)} = & \left(\frac{2R_2(x_i - e^2 x_1 \delta_{1i}) - (1 - e^2)(x_1 x_i + a^2 \delta_{1i}) + 2c x_1 (1 - e^2) \delta_{1i}}{R_2^2 [R_2 - (x_1 - c)]} \right) \\ & - (1 - e^2)(a - x_1) R_2 \left(\frac{[2R_2 - (x_1 - c)](x_i - c \delta_{1i}) - R_2^2 \delta_{1i}}{R_2^3 [R_2 - (x_1 - c)]^2} \right) \end{aligned}$$

$$\begin{aligned}
& -[x_i - (R_2 + c) \delta_{1i}] \left(\frac{[2R_2 - (x_1 - c)]aR_2(1 - e^2) - R_2^2 (1 - e^2)x_1}{R_2^3 [R_2 - (x_1 - c)]^2} \right) \\
& - \left(\frac{2R_1(x_i - e^2x_1\delta_{1i}) - (1 - e^2)(x_1x_i + a^2\delta_{1i}) - 2c x_1(1 - e^2)\delta_{1i}}{R_1^2 [R_1 - (x_1 + c)]} \right) \\
& + (1 - e^2)(a - x_1)R_1 \left(\frac{[2R_1 - (x_1 + c)](x_i + c \delta_{1i}) - R_1^2 \delta_{1i}}{R_1^3 [R_1 - (x_1 + c)]^2} \right) \\
& + [x_i - (R_1 - c) \delta_{1i}] \left(\frac{[2R_1 - (x_1 + c)]aR_1(1 - e^2) - R_1^2 (1 - e^2)x_1}{R_1^3 [R_1 - (x_1 + c)]^2} \right)
\end{aligned} \tag{B.104}$$

Using $c = ea$, $R_1 = a + ex_1$ and $R_2 = a - ex_1$ we have the identities

$$x_1x_i + a^2\delta_{1i} - 2cx_1\delta_{1i} = x_1(x_i - c\delta_{1i}) + a\delta_{1i}(a - ex_1) = x_1(x_i - c\delta_{1i}) + a\delta_{1i}R_2 \tag{B.105}$$

$$x_1x_i + a^2\delta_{1i} + 2cx_1\delta_{1i} = x_1(x_i + c\delta_{1i}) + a\delta_{1i}R_1 \tag{B.106}$$

$$x_i - (R_1 - c) \delta_{1i} = (x_i - x_1\delta_{1i}) - [R_1 - (x_1 + c)]\delta_{1i} \tag{B.107}$$

$$x_i - (R_2 + c) \delta_{1i} = (x_i - x_1\delta_{1i}) - [R_2 - (x_1 - c)]\delta_{1i} \tag{B.108}$$

For the ease of dealing with simplifying these equations, we define

$$A_1 = [R_1 - (x_1 + c)] = (1 - e)(a - x_1) \tag{B.109}$$

and

$$A_2 = [R_2 - (x_1 - c)] = (1 + e)(a - x_1) \tag{B.110}$$

to achieve

$$\begin{aligned}
n'_j E_{ji}^{(3)} & = \left(\frac{2R_2(x_i - e^2x_1\delta_{1i}) - (1 - e^2)[x_1(x_i - c\delta_{1i}) + aR_2\delta_{1i}]}{R_2^2 A_2} \right) \\
& - (1 - e^2)(a - x_1) \left(\frac{(R_2 + A_2)(x_i - c \delta_{1i}) - R_2^2 \delta_{1i}}{R_2^2 A_2^2} \right) \\
& - (1 - e^2)[(x_i - x_1\delta_{1i}) - A_2\delta_{1i}] \left(\frac{aA_2 + (a - x_1)R_2}{R_2^2 A_2^2} \right) \\
& - \left(\frac{2R_1(x_i - e^2x_1\delta_{1i}) - (1 - e^2)[x_1(x_i + c\delta_{1i}) + aR_1\delta_{1i}]}{R_1^2 A_1} \right) \\
& + (1 - e^2)(a - x_1) \left(\frac{(R_1 + A_1)(x_i + c \delta_{1i}) - R_1^2 \delta_{1i}}{R_1^2 A_1^2} \right)
\end{aligned}$$

$$+(1 - e^2)[(x_i - x_1\delta_{1i}) - A_1\delta_{1i}] \left(\frac{aA_1 + (a - x_1)R_1}{R_1^2 A_1^2} \right) \quad (\text{B.111})$$

and then simplifying

$$\begin{aligned} n'_j E_{ji}^{(3)} = & \left(\frac{2R_2(x_i - e^2 x_1 \delta_{1i}) - (1 - e^2)[x_1(x_i - c\delta_{1i}) + aR_2\delta_{1i}]}{R_2^2 A_2} \right) \\ & - (1 - e) \left(\frac{A_2(x_i - c\delta_{1i}) + R_2[x_i - (R_2 + c)\delta_{1i}]}{R_2^2 A_2} \right) \\ & - [(x_i - x_1\delta_{1i}) - A_2\delta_{1i}] \left(\frac{a(1 - e^2) + (1 - e)R_2}{R_2^2 A_2} \right) \\ & - \left(\frac{2R_1(x_i - e^2 x_1 \delta_{1i}) - (1 - e^2)[x_1(x_i + c\delta_{1i}) + aR_1\delta_{1i}]}{R_1^2 A_1} \right) \\ & + (1 + e) \left(\frac{A_1(x_i + c\delta_{1i}) + R_1[x_i - (R_1 - c)\delta_{1i}]}{R_1^2 A_1} \right) \\ & + [(x_i - x_1\delta_{1i}) - A_1\delta_{1i}] \left(\frac{a(1 - e^2) + (1 + e)R_1}{R_1^2 A_1} \right) \quad (\text{B.112}) \end{aligned}$$

We can further write it in the form

$$\begin{aligned} n'_j E_{ji}^{(3)} = & \left(\frac{2R_2(x_i - e^2 x_1 \delta_{1i}) - (1 - e^2)[x_1(x_i - c\delta_{1i}) + aR_2\delta_{1i}]}{R_2^2 A_2} \right) \\ & - \left(\frac{(1 - e)A_2(x_i - c\delta_{1i}) + (1 - e)R_2[(x_i - x_1\delta_{1i}) - A_2\delta_{1i}]}{R_2^2 A_2} \right) \\ & - [(x_i - x_1\delta_{1i}) - A_2\delta_{1i}] \left(\frac{a(1 - e^2) + (1 - e)R_2}{R_2^2 A_2} \right) \\ & - \left(\frac{2R_1(x_i - e^2 x_1 \delta_{1i}) - (1 - e^2)[x_1(x_i + c\delta_{1i}) + aR_1\delta_{1i}]}{R_1^2 A_1} \right) \\ & + \left(\frac{(1 + e)A_1(x_i + c\delta_{1i}) + (1 + e)R_1[(x_i - x_1\delta_{1i}) - A_1\delta_{1i}]}{R_1^2 A_1} \right) \\ & + [(x_i - x_1\delta_{1i}) - A_1\delta_{1i}] \left(\frac{a(1 - e^2) + (1 + e)R_1}{R_1^2 A_1} \right) \quad (\text{B.113}) \end{aligned}$$

to

$$n'_j E_{ji}^{(3)} = \left(\frac{2R_2(x_i - e^2 x_1 \delta_{1i}) - (1 - e^2)[x_1(x_i - c\delta_{1i}) + aR_2\delta_{1i}]}{R_2^2 A_2} \right)$$

$$\begin{aligned}
& - \left(\frac{(1-e)(x_i - c \delta_{1i})}{R_2^2} \right) \\
& - [(x_i - x_1 \delta_{1i}) - A_2 \delta_{1i}] \left(\frac{a(1-e^2) + 2(1-e)R_2}{R_2^2 A_2} \right) \\
& - \left(\frac{2R_1(x_i - e^2 x_1 \delta_{1i}) - (1-e^2)[x_1(x_i + c \delta_{1i}) + aR_1 \delta_{1i}]}{R_1^2 A_1} \right) \\
& + \left(\frac{(1+e)(x_i + c \delta_{1i})}{R_1^2} \right) \\
& + [(x_i - x_1 \delta_{1i}) - A_1 \delta_{1i}] \left(\frac{a(1-e^2) + 2(1+e)R_1}{R_1^2 A_1} \right) \quad (\text{B.114})
\end{aligned}$$

Dissociating the terms yields

$$\begin{aligned}
n'_j E_{ji}^{(3)} & = \left(\frac{2(x_i - e^2 x_1 \delta_{1i})}{R_2 A_2} - \frac{(1-e^2)x_1(x_i - c \delta_{1i})}{R_2^2 A_2} - \frac{(1-e^2)a \delta_{1i}}{R_2 A_2} \right) \\
& - \left(\frac{(1-e)(x_i - c \delta_{1i})}{R_2^2} \right) \\
& - [(x_i - x_1 \delta_{1i}) - A_2 \delta_{1i}] \left(\frac{a(1-e^2)}{R_2^2 A_2} + \frac{2(1-e)}{R_2 A_2} \right) \\
& - \left(\frac{2(x_i - e^2 x_1 \delta_{1i})}{R_1 A_1} - \frac{(1-e^2)x_1(x_i + c \delta_{1i})}{R_1^2 A_1} - \frac{(1-e^2)a \delta_{1i}}{R_1 A_1} \right) \\
& + \left(\frac{(1+e)(x_i + c \delta_{1i})}{R_1^2} \right) \\
& + [(x_i - x_1 \delta_{1i}) - A_1 \delta_{1i}] \left(\frac{a(1-e^2)}{R_1^2 A_1} + \frac{2(1+e)}{R_1 A_1} \right) \quad (\text{B.115})
\end{aligned}$$

Using the identities

$$\frac{(1-e^2)x_1(x_i - c \delta_{1i})}{R_2^2 A_2} + \frac{(1-e)(x_i - c \delta_{1i})}{R_2^2} = \frac{(1-e^2)a(x_i - c \delta_{1i})}{R_2^2 A_2} \quad (\text{B.116})$$

$$\frac{(1-e^2)x_1(x_i + c \delta_{1i})}{R_1^2 A_1} + \frac{(1+e)(x_i + c \delta_{1i})}{R_1^2} = \frac{(1-e^2)a(x_i + c \delta_{1i})}{R_1^2 A_1} \quad (\text{B.117})$$

we get

$$\begin{aligned}
n'_j E_{ji}^{(3)} & = \left(\frac{2(x_i - e^2 x_1 \delta_{1i})}{R_2 A_2} - \frac{(1-e^2)a(x_i - c \delta_{1i})}{R_2^2 A_2} - \frac{(1-e^2)a \delta_{1i}}{R_2 A_2} \right) \\
& - [(x_i - x_1 \delta_{1i}) - A_2 \delta_{1i}] \left(\frac{a(1-e^2)}{R_2^2 A_2} + \frac{2(1-e)}{R_2 A_2} \right)
\end{aligned}$$

$$\begin{aligned}
& - \left(\frac{2(x_i - e^2 x_1 \delta_{1i})}{R_1 A_1} - \frac{(1 - e^2)a(x_i + c\delta_{1i})}{R_1^2 A_1} - \frac{(1 - e^2)a\delta_{1i}}{R_1 A_1} \right) \\
& + [(x_i - x_1 \delta_{1i}) - A_1 \delta_{1i}] \left(\frac{a(1 - e^2)}{R_1^2 A_1} + \frac{2(1 + e)}{R_1 A_1} \right) \quad (\text{B.118})
\end{aligned}$$

We further use the identities

$$x_i + c\delta_{1i} = (x_i - x_1 \delta_{1i}) - A_1 \delta_{1i} + R_1 \delta_{1i} \quad (\text{B.119})$$

$$x_i - c\delta_{1i} = (x_i - x_1 \delta_{1i}) - A_2 \delta_{1i} + R_2 \delta_{1i} \quad (\text{B.120})$$

to obtain

$$\begin{aligned}
n'_j E_{ji}^{(3)} & = \left(\frac{2(x_i - e^2 x_1 \delta_{1i})}{R_2 A_2} - \frac{2(1 - e^2)a\delta_{1i}}{R_2 A_2} \right) \\
& - [(x_i - x_1 \delta_{1i}) - A_2 \delta_{1i}] \left(\frac{2a(1 - e^2)}{R_2^2 A_2} + \frac{2(1 - e)}{R_2 A_2} \right) \\
& - \left(\frac{2(x_i - e^2 x_1 \delta_{1i})}{R_1 A_1} - \frac{2(1 - e^2)a\delta_{1i}}{R_1 A_1} \right) \\
& + [(x_i - x_1 \delta_{1i}) - A_1 \delta_{1i}] \left(\frac{2a(1 - e^2)}{R_1^2 A_1} + \frac{2(1 + e)}{R_1 A_1} \right) \quad (\text{B.121})
\end{aligned}$$

recasting the equation we get

$$\begin{aligned}
n'_j E_{ji}^{(3)} & = -[(x_i - x_1 \delta_{1i}) - A_2 \delta_{1i}] \left[\frac{2a(1 - e^2)}{R_2^2 A_2} \right] \\
& + \left(\frac{2}{R_2 A_2} \right) [(x_i - e^2 x_1 \delta_{1i}) - (1 - e^2)a\delta_{1i} - [(x_i - x_1 \delta_{1i}) - A_2 \delta_{1i}](1 - e)] \\
& + [(x_i - x_1 \delta_{1i}) - A_1 \delta_{1i}] \left[\frac{2a(1 - e^2)}{R_1^2 A_1} \right] \\
& - \left(\frac{2}{R_1 A_1} \right) [(x_i - e^2 x_1 \delta_{1i}) - (1 - e^2)a\delta_{1i} - [(x_i - x_1 \delta_{1i}) - A_1 \delta_{1i}](1 + e)] \quad (\text{B.122})
\end{aligned}$$

Thus gives

$$\begin{aligned}
& (x_i - e^2 x_1 \delta_{1i}) - (1 - e^2)a\delta_{1i} - [(x_i - x_1 \delta_{1i}) - A_2 \delta_{1i}](1 - e) \\
& = (x_i - e^2 x_1 \delta_{1i}) - (1 - e^2)a\delta_{1i} - (1 - e)(x_i - x_1 \delta_{1i}) + (a - x_1)(1 - e^2)\delta_{1i}
\end{aligned}$$

$$\begin{aligned}
&= (x_i - e^2 x_1 \delta_{1i}) - (x_i - x_1 \delta_{1i} - e x_i + e x_1 \delta_{1i}) - (1 - e^2) x_1 \delta_{1i} \\
&= (1 - e^2) x_1 \delta_{1i} + e(x_i - x_1 \delta_{1i}) - (1 - e^2) x_1 \delta_{1i} \\
&= e(x_i - x_1 \delta_{1i})
\end{aligned} \tag{B.123}$$

Similarly, we have

$$\begin{aligned}
&(x_i - e^2 x_1 \delta_{1i}) - (1 - e^2) a \delta_{1i} - [(x_i - x_1 \delta_{1i}) - A_1 \delta_{1i}](1 + e) \\
&= (x_i - e^2 x_1 \delta_{1i}) - (1 - e^2) a \delta_{1i} - (1 + e)(x_i - x_1 \delta_{1i}) + (a - x_1)(1 - e^2) \delta_{1i} \\
&= (x_i - e^2 x_1 \delta_{1i}) - (x_i - x_1 \delta_{1i} + e x_i - e x_1 \delta_{1i}) - (1 - e^2) x_1 \delta_{1i} \\
&= (1 - e^2) x_1 \delta_{1i} - e(x_i - x_1 \delta_{1i}) - (1 - e^2) x_1 \delta_{1i} \\
&= -e(x_i - x_1 \delta_{1i})
\end{aligned} \tag{B.124}$$

$$\begin{aligned}
n'_j E_{ji}^{(3)} &= -2a(1 - e^2)(x_i - x_1 \delta_{1i}) \left(\frac{1}{R_2^2 A_2} - \frac{1}{R_1^2 A_1} \right) \\
&\quad + 2a(1 - e^2) \delta_{1i} \left(\frac{1}{R_2^2} - \frac{1}{R_1^2} \right) \\
&\quad + 2e(x_i - x_1 \delta_{1i}) \left(\frac{1}{R_2 A_2} + \frac{1}{R_1 A_1} \right) \\
&= 2a(1 - e^2) \delta_{1i} \left(\frac{1}{R_2^2} - \frac{1}{R_1^2} \right) \\
&\quad + 2(x_i - x_1 \delta_{1i}) \left\{ e \left(\frac{1}{R_2 A_2} + \frac{1}{R_1 A_1} \right) - a(1 - e^2) \left(\frac{1}{R_2^2 A_2} - \frac{1}{R_1^2 A_1} \right) \right\}
\end{aligned} \tag{B.125}$$

$$\begin{aligned}
\frac{1}{R_2 A_2} + \frac{1}{R_1 A_1} &= \frac{1}{R_2(1 + e)(a - x_1)} + \frac{1}{R_1(1 - e)(a - x_1)} \\
&= \left(\frac{1}{R_1 R_2 (1 - e^2)(a - x_1)} \right) [R_1(1 - e) + R_2(1 + e)] \\
&= \left(\frac{1}{R_1 R_2 (1 - e^2)(a - x_1)} \right) [(a + e x_1)(1 - e) + (a - e x_1)(1 + e)] \\
&= \left(\frac{1}{R_1 R_2 (1 - e^2)(a - x_1)} \right) \\
&\quad \times \{ a[(1 - e) + (1 + e)] + e x_1[(1 - e) - (1 + e)] \}
\end{aligned}$$

$$\begin{aligned}
&= \frac{2(a - e^2x_1)}{R_1R_2(1 - e^2)(a - x_1)} = \frac{2(a^2 - e^2x_1^2)(a - e^2x_1)}{R_1^2R_2^2(1 - e^2)(a - x_1)} \\
&= \frac{2(a^3 - e^2a^2x_1 - e^2ax_1^2 + e^4x_1^3)}{R_1^2R_2^2(1 - e^2)(a - x_1)} \tag{B.126}
\end{aligned}$$

$$\begin{aligned}
\frac{1}{R_2^2A_2} - \frac{1}{R_1^2A_1} &= \frac{1}{R_2^2(1 + e)(a - x_1)} - \frac{1}{R_1^2(1 - e)(a - x_1)} \\
&= \left(\frac{1}{R_1^2R_2^2(1 - e^2)(a - x_1)} \right) [R_1^2(1 - e) - R_2^2(1 + e)] \\
&= \left(\frac{1}{R_1^2R_2^2(1 - e^2)(a - x_1)} \right) [(a + ex_1)^2(1 - e) - (a - ex_1)^2(1 + e)] \\
&= \left(\frac{1}{R_1^2R_2^2(1 - e^2)(a - x_1)} \right) \\
&\quad \times \{[(a + ex_1)^2 - (a - ex_1)^2] - e[(a + ex_1)^2 + (a - ex_1)^2]\} \\
&= \left(\frac{1}{R_1^2R_2^2(1 - e^2)(a - x_1)} \right) [4eax_1 - 2e(a^2 + e^2x_1^2)] \tag{B.127}
\end{aligned}$$

$$\begin{aligned}
&(a^3 - e^2a^2x_1 - e^2ax_1^2 + e^4x_1^3) - a(1 - e^2)[2ax_1 - (a^2 + e^2x_1^2)] \\
&= (a^3 - e^2a^2x_1 - e^2ax_1^2 + e^4x_1^3) \\
&\quad - (2a^2x_1 - a^3 - e^2ax_1^2 - 2e^2a^2x_1 + e^2a^3 + e^4ax_1^2) \\
&= 2a^3 + e^2a^2x_1 + e^4x_1^3 - (2a^2x_1 + e^2a^3 + e^4ax_1^2) \\
&= 2a^2(a - x_1) - e^2a^2(a - x_1) - e^4x_1^2(a - x_1) \\
&= (2a^2 - e^2a^2 - e^4x_1^2)(a - x_1) \tag{B.128}
\end{aligned}$$

$$\begin{aligned}
&e \left(\frac{1}{R_2A_2} + \frac{1}{R_1A_1} \right) - a(1 - e^2) \left(\frac{1}{R_2^2A_2} - \frac{1}{R_1^2A_1} \right) \\
&= \left(\frac{2e(a^3 - e^2a^2x_1 - e^2ax_1^2 + e^4x_1^3)}{R_1^2R_2^2(1 - e^2)(a - x_1)} \right) - a(1 - e^2) \left(\frac{2e[2ax_1 - (a^2 + e^2x_1^2)]}{R_1^2R_2^2(1 - e^2)(a - x_1)} \right) \\
&= \left(\frac{2e}{R_1^2R_2^2(1 - e^2)(a - x_1)} \right) \\
&\quad \times \{ (a^3 - e^2a^2x_1 - e^2ax_1^2 + e^4x_1^3) - a(1 - e^2)[2ax_1 - (a^2 + e^2x_1^2)] \} \\
&= \left(\frac{2e}{R_1^2R_2^2(1 - e^2)(a - x_1)} \right) \{ (2a^2 - e^2a^2 - e^4x_1^2)(a - x_1) \}
\end{aligned}$$

$$= \frac{2e(2a^2 - e^2a^2 - e^4x_1^2)}{R_1^2R_2^2(1 - e^2)} \quad (\text{B.129})$$

$$\boxed{n'_j E_{ji}^{(3)} = 2a(1 - e^2) \left(\frac{1}{R_2^2} - \frac{1}{R_1^2} \right) \delta_{1i} + \left(\frac{4e(2a^2 - e^2a^2 - e^4x_1^2)}{R_1^2R_2^2(1 - e^2)} \right) (x_i - x_1\delta_{1i})} \quad (\text{B.130})$$

3.5 Strain Tensor

Let's summarize what we have

$$\boxed{E_{ji} = -2\alpha' E_{ji}^{(1)} + \alpha' E_{ji}^{(2)} - \alpha'(1 - e^2)x_1 E_{ji}^{(3)}} \quad (\text{B.131})$$

$$\boxed{n'_j E_{ji}^{(1)} = \frac{-2ex_1}{R_1R_2} (x_i - x_1\delta_{1i}) + \frac{-2e(a^2 + x_1^2 - 2e^2x_1^2)}{R_1R_2} \delta_{1i}} \quad (\text{B.132})$$

$$\begin{aligned} n'_j E_{ji}^{(2)} &= \frac{-4ex_1}{R_1R_2} (x_i - x_1\delta_{1i}) + 2a(1 - e^2) \left(\frac{1}{R_2^2} - \frac{1}{R_1^2} \right) (x_i - x_1\delta_{1i}) \\ &\quad + \frac{-4ex_1^2}{R_1R_2} (1 - e^2)\delta_{1i} + 2ax_1(1 - e^2) \left(\frac{1}{R_2^2} - \frac{1}{R_1^2} \right) \delta_{1i} \\ &\quad - 2ea^2(1 - e^2) \left(\frac{1}{R_2^2} + \frac{1}{R_1^2} \right) \delta_{1i} \end{aligned} \quad (\text{B.133})$$

$$\boxed{n'_j E_{ji}^{(3)} = 2a(1 - e^2) \left(\frac{1}{R_2^2} - \frac{1}{R_1^2} \right) \delta_{1i} + \left(\frac{4e(2a^2 - e^2a^2 - e^4x_1^2)}{R_1^2R_2^2(1 - e^2)} \right) (x_i - x_1\delta_{1i})} \quad (\text{B.134})$$

We now calculate $n'_j E_{ji}$

$$\begin{aligned} \alpha'^{-1} n'_j E_{ji} &= -2E_{ji}^{(1)} + E_{ji}^{(2)} - (1 - e^2)x_1 E_{ji}^{(3)} \\ &= \frac{4ex_1}{R_1R_2} (x_i - x_1\delta_{1i}) + \frac{4e(a^2 + x_1^2 - 2e^2x_1^2)}{R_1R_2} \delta_{1i} \\ &\quad + \frac{-4ex_1}{R_1R_2} (x_i - x_1\delta_{1i}) + 2a(1 - e^2) \left(\frac{1}{R_2^2} - \frac{1}{R_1^2} \right) (x_i - x_1\delta_{1i}) \\ &\quad + \frac{-4ex_1^2}{R_1R_2} (1 - e^2)\delta_{1i} + 2ax_1(1 - e^2) \left(\frac{1}{R_2^2} - \frac{1}{R_1^2} \right) \delta_{1i} \end{aligned}$$

$$\begin{aligned}
& -2ea^2(1-e^2) \left(\frac{1}{R_2^2} + \frac{1}{R_1^2} \right) \delta_{1i} \\
& -2ax_1(1-e^2) \left(\frac{1}{R_2^2} - \frac{1}{R_1^2} \right) \delta_{1i} + 2ae^2x_1(1-e^2) \left(\frac{1}{R_2^2} - \frac{1}{R_1^2} \right) \delta_{1i} \\
& -x_1 \left(\frac{4e(2a^2 - e^2a^2 - e^4x_1^2)}{R_1^2R_2^2} \right) (x_i - x_1\delta_{1i}) \tag{B.135}
\end{aligned}$$

Recasting the equation we obtain

$$\begin{aligned}
\alpha'^{-1}n'_jE_{ji} &= \frac{4e\delta_{1i}}{R_1R_2} [(a^2 + x_1^2 - 2e^2x_1^2) - x_1^2(1-e^2)] \\
&+ 2ea(1-e^2)\delta_{1i} \left[ex_1 \left(\frac{1}{R_2^2} - \frac{1}{R_1^2} \right) - a \left(\frac{1}{R_2^2} + \frac{1}{R_1^2} \right) \right] \\
&+ 4e(x_i - x_1\delta_{1i}) \left[a(1-e^2) \left(\frac{1}{2e} \right) \left(\frac{1}{R_2^2} - \frac{1}{R_1^2} \right) - x_1 \left(\frac{2a^2 - e^2a^2 - e^4x_1^2}{R_1^2R_2^2} \right) \right] \tag{B.136}
\end{aligned}$$

In order to simplify the equation, we work on the terms individually

$$(a^2 + x_1^2 - 2e^2x_1^2) - x_1^2(1-e^2) = a^2 - e^2x_1^2 \tag{B.137}$$

$$ex_1 \left(\frac{1}{R_2^2} - \frac{1}{R_1^2} \right) - a \left(\frac{1}{R_2^2} + \frac{1}{R_1^2} \right) = -\frac{1}{R_2}(a-ex_1) - \frac{1}{R_1}(a+ex_1) = -\left(\frac{1}{R_2} + \frac{1}{R_1} \right) \tag{B.138}$$

$$\begin{aligned}
& a(1-e^2) \left(\frac{1}{2e} \right) \left(\frac{1}{R_2^2} - \frac{1}{R_1^2} \right) - x_1 \left(\frac{2a^2 - e^2a^2 - e^4x_1^2}{R_1^2R_2^2} \right) \\
&= a(1-e^2) \left(\frac{1}{2e} \right) \left(\frac{4eax_1}{R_1^2R_2^2} \right) - x_1 \left(\frac{2a^2 - e^2a^2 - e^4x_1^2}{R_1^2R_2^2} \right) \\
&= \left(\frac{2a^2x_1 - 2e^2a^2x_1}{R_1^2R_2^2} \right) - \left(\frac{2a^2x_1 - e^2a^2x_1 - e^4x_1^3}{R_1^2R_2^2} \right) \\
&= \frac{e^4x_1^3 - e^2a^2x_1}{R_1^2R_2^2} = \frac{-e^2x_1(a^2 - e^2x_1^2)}{R_1^2R_2^2} = \frac{-e^2x_1(a-ex_1)(a+ex_1)}{R_1^2R_2^2} \\
&= \frac{-e^2x_1}{R_1R_2} \tag{B.139}
\end{aligned}$$

Inserting these terms, we obtain,

$$\alpha'^{-1}n'_jE_{ji} = \frac{4e\delta_{1i}}{R_1R_2} (a^2 - e^2x_1^2) - 2ea(1-e^2)\delta_{1i} \left(\frac{1}{R_2} + \frac{1}{R_1} \right) - \frac{4e^3x_1}{R_1R_2} (x_i - x_1\delta_{1i})$$

$$\begin{aligned}
&= \frac{4e\delta_{1i}}{R_1R_2}(a^2 - e^2x_1^2) - 2ea(1 - e^2)\delta_{1i} \left(\frac{2a}{R_1R_2} \right) - \frac{4e^3x_1}{R_1R_2}(x_i - x_1\delta_{1i}) \\
&= \frac{4e\delta_{1i}}{R_1R_2} [(a^2 - e^2x_1^2) - (1 - e^2)a^2] - \frac{4e^3x_1}{R_1R_2}(x_i - x_1\delta_{1i}) \\
&= \frac{4e\delta_{1i}}{R_1R_2}(e^2a^2 - e^2x_1^2) - \frac{4e^3x_1}{R_1R_2}(x_i - x_1\delta_{1i}) \tag{B.140}
\end{aligned}$$

Therefore, we have

$$\alpha'^{-1}n'_jE_{ji} = \frac{4e^3(a^2 - x_1^2)}{R_1R_2}\delta_{1i} - \frac{4e^3x_1}{R_1R_2}(x_i - x_1\delta_{1i}) \tag{B.141}$$

Using the definition $\alpha' = \alpha U/e^2$ we obtain,

$$\boxed{n'_jE_{ji} = \alpha U \left(\frac{4e(a^2 - x_1^2)}{R_1R_2} \right) \delta_{1i} - \alpha U \left(\frac{4ex_1}{R_1R_2} \right) (x_i - x_1\delta_{1i})} \tag{B.142}$$

3.6 Stress Tensor and Distribution of Traction

The stress tensor is defined as

$$T_{ji} = -p\delta_{ji} + \mu E_{ji} \tag{B.143}$$

and the distribution of traction is calculated through

$$n'_jT_{ji} = -pn'_j\delta_{ji} + \mu n'_jE_{ji} = -pn'_i + \mu n'_jE_{ji} \tag{B.144}$$

For the pressure term we have

$$\begin{aligned}
-pn'_i &= -2\mu\alpha U \left(\frac{1}{R_1} - \frac{1}{R_2} \right) (x_i - e^2x_1\delta_{1i}) \\
&= -2\mu\alpha U \left(\frac{-2ex_1}{R_1R_2} \right) [(x_i - x_1\delta_{1i}) + (1 - e^2)x_1\delta_{1i}] \\
&= \mu\alpha U \left(\frac{4ex_1}{R_1R_2} \right) (x_i - x_1\delta_{1i}) + \mu\alpha U \left(\frac{4ex_1^2(1 - e^2)}{R_1R_2} \right) \delta_{1i} \tag{B.145}
\end{aligned}$$

Inserting this into the traction equation, we obtain

$$n'_jT_{ji} = -pn'_i + \mu n'_jE_{ji}$$

$$\begin{aligned}
&= \mu\alpha U \left(\frac{4ex_1}{R_1R_2} \right) (x_i - x_1\delta_{1i}) + \mu\alpha U \left(\frac{4ex_1^2(1-e^2)}{R_1R_2} \right) \delta_{1i} \\
&\quad + \mu\alpha U \left(\frac{4e(a^2-x_1^2)}{R_1R_2} \right) \delta_{1i} - \mu\alpha U \left(\frac{4ex_1}{R_1R_2} \right) (x_i - x_1\delta_{1i}) \\
&= \mu\alpha U \left(\frac{4e\delta_{1i}}{R_1R_2} \right) [(a^2-x_1^2) + x_1^2(1-e^2)] \\
&= \mu\alpha U \left(\frac{4e\delta_{1i}}{R_1R_2} \right) (a^2 - e^2x_1^2) \\
&= \mu\alpha U \left(\frac{4e\delta_{1i}}{R_1R_2} \right) R_1R_2
\end{aligned}$$

Therefore

$$n'_j T_{ji} = 4e\mu\alpha U \delta_{1i} \quad (\text{B.146})$$

Using $n_j = \frac{1}{\sqrt{R_1R_2}} \left(\frac{a}{b} \right) n'_j$ the distribution of traction on the surface of the spheroid is

$$\boxed{n_j T_{ji} = 4e\mu\alpha \frac{1}{\sqrt{R_1R_2}} \left(\frac{a}{b} \right) \delta_{1i}} \quad (\text{B.147})$$

We have

$$\lim_{e \rightarrow 0} e\alpha = \frac{3}{8} \quad (\text{B.148})$$

and

$$\lim_{e \rightarrow 0} R_1R_2 = a^2 \quad (\text{B.149})$$

Therefore, in the limit $e \rightarrow 0$ we obtain

$$\lim_{e \rightarrow 0} n_j T_{ji} = \frac{3}{2} \frac{\mu U}{a} \delta_{1i} \quad (\text{B.150})$$

which is the distribution of traction on the surface of a sphere of radius a . This can be a confirmation of the accuracy of our final results.

In the prolate spheroidal coordinates (ξ, η, ϕ) , we have $x_1 = c\eta\xi$ and on the surface of the particle $\xi_s = e^{-1}$. This results in

$$\begin{aligned}
R_1R_2 &= (a + ex_1)(a - ex_1) = a^2 - e^2x_1^2 = a^2 - e^2(ae\xi_s\eta)^2 \\
&= a^2(1 - e^2\eta^2) = a^2e^2(\xi_s^2 - \eta^2)
\end{aligned} \quad (\text{B.151})$$

$$\begin{aligned}
n_j T_{ji} &= 4e\mu\alpha U \frac{1}{\sqrt{a^2 e^2 (\xi_s^2 - \eta^2)}} \left(\frac{a}{b}\right) \delta_{1i} \\
&= 4\mu\alpha U \frac{1}{\sqrt{\xi_s^2 - \eta^2}} \left(\frac{1}{b}\right) \delta_{1i}
\end{aligned} \tag{B.152}$$

We also have

$$\frac{1}{b} = \frac{1}{a\sqrt{(1-e^2)}} = \frac{1}{ea\sqrt{(e^{-2}-1)}} = \frac{1}{ea\sqrt{\xi_s^2-1}} \tag{B.153}$$

Therefore,

$$\boxed{n_j T_{ji} = \left(\frac{4\mu\alpha U}{ea}\right) \frac{1}{\sqrt{(\xi_s^2 - \eta^2)(\xi_s^2 - 1)}} \delta_{1i}} \tag{B.154}$$

Bibliography

- [1] PURCELL, E. (1977) "LIFE AT LOW REYNOLDS-NUMBER," *Am. J. Phys.*, **45**(1), pp. 3–11.
- [2] COLINVAUX, P. (1979) "LIFE AT LOW REYNOLDS-NUMBER," *Nature*, **277**(5695), pp. 353–354.
- [3] M. G. L. VAN DEN HEUVEL, C. D. (2000) "Motor Proteins at Work for Nanotechnology," *Science*, **317**, pp. 333–336.
- [4] M. SCHLIWA, G. W. (2003) "Molecular Motors," *Nature*, **422**, pp. 759–765.
- [5] C. MAVROIDIS, M. L. Y., A. DUBEY (2004) "Molecular Machines," *Ann. Rev. Biomed. Eng.*, **6**, pp. 363–395.
- [6] MIRKOVIC, T., N. S. ZACHARIA, G. D. SCHOLES, and G. A. OZIN (2010) "Nanolocation-Catalytic Nanomotors and Nanorotors," *Small*, **6**(2), pp. 159–167.
- [7] EBBENS, S. J. and J. R. HOWSE (2010) "In pursuit of propulsion at the nanoscale," *Soft Matter*, **6**(4), p. 726.
- [8] WANG, J. and K. M. MANESH (2010) "Motion Control at the Nanoscale," *Small*, **6**(3), pp. 338–345.
- [9] MIRKOVIC, T., N. S. ZACHARIA, G. D. SCHOLES, and G. A. OZIN (2010) "Fuel for Thought: Chemically Powered Nanomotors Out-Swim Nature's Flagellated Bacteria," *Acs Nano*, **4**(4), pp. 1782–1789.
- [10] SEN, A., M. IBELE, Y. HONG, and D. VELEGOL (2009) "Chemo and phototactic nano/microbots," *Faraday Discuss.*, **143**, p. 15.
- [11] WANG, J. (2009) "Can Man-Made Nanomachines Compete with Nature Biomotors?" *Acs Nano*, **3**(1), pp. 4–9.

- [12] PAXTON, W. F., S. SUNDARARAJAN, T. E. MALLOUK, and A. SEN (2006) “Chemical locomotion,” *Angew Chem Int Edit*, **45**(33), pp. 5420–5429.
- [13] KUNG, H. H. and M. C. KUNG (2006) “Catalytic nanomotors - promising leads for new catalytic applications,” *Appl Catal A-Gen*, **309**(2), pp. 159–161.
- [14] DREYFUS, R., J. BAUDRY, M. L. ROPER, M. FERMIGIER, H. A. STONE, and J. BIBETTE (2005) “Microscopic artificial swimmers,” *Nature*, **437**(7060), p. 862.
- [15] PAXTON, W., A. SEN, and T. MALLOUK (2005) “Motility of catalytic nanoparticles through self-generated forces,” *Chem-Eur J*, **11**(22), pp. 6462–6470.
- [16] OZIN, G., I. MANNERS, S. FOURNIER-BIDOZ, and A. ARSENAULT (2005) “Dream nanomachines,” *Adv. Mater.*, **17**(24), pp. 3011–3018.
- [17] ISMAGILOV, R., A. SCHWARTZ, N. BOWDEN, and G. WHITESIDES (2002) “Autonomous movement and self-assembly,” *Angew Chem Int Edit*, **41**(4), p. 652.
- [18] PAXTON, W., K. KISTLER, C. OLMEDA, A. SEN, S. S. ANGELO, Y. CAO, T. MALLOUK, P. LAMMERT, and V. CRESPI (2004) “Catalytic nanomotors: Autonomous movement of striped nanorods,” *J Am Chem Soc*, **126**(41), pp. 13424–13431.
- [19] LAMMERT, P., J. PROST, and R. BRUINSMA (1996) “Ion drive for vesicles and cells,” *J Theor Biol*, **178**(4), pp. 387–391.
- [20] GOLESTANIAN, R., T. LIVERPOOL, and A. AJDARI (2005) “Propulsion of a Molecular Machine by Asymmetric Distribution of Reaction Products,” *Phys. Rev. Lett.*, **94**(22), p. 220801.
- [21] SAIDULU, N. B. and K. L. SEBASTIAN (2008) “Interfacial tension model for catalytically driven nanorods,” *J. Chem. Phys.*, **128**(7), p. 074708.
- [22] GOLESTANIAN, R. (2009) “Anomalous Diffusion of Symmetric and Asymmetric Active Colloids,” *Phys. Rev. Lett.*, **102**(18), p. 188305.
- [23] YARIV, E. (2011) “Electrokinetic self-propulsion by inhomogeneous surface kinetics,” *Proceedings of the Royal Society A: Mathematical, Physical and Engineering Sciences*, **467**(2130), pp. 1645–1664.
- [24] WANG, Y., R. M. HERNANDEZ, D. J. BARTLETT, J. M. BINGHAM, T. R. KLINE, A. SEN, and T. E. MALLOUK (2006) “Bipolar electrochemical mechanism for the propulsion of catalytic nanomotors in hydrogen peroxide solutions,” *Langmuir*, **22**(25), pp. 10451–10456.

- [25] PAXTON, W. F., P. T. BAKER, T. R. KLINE, Y. WANG, T. E. MALLOUK, and A. SEN (2006) “Catalytically induced electrokinetics for motors and micropumps,” *J Am Chem Soc*, **128**(46), pp. 14881–14888.
- [26] MORAN, J., P. WHEAT, and J. POSNER (2010) “Locomotion of electrocatalytic nanomotors due to reaction induced charge autoelectrophoresis,” *Phys. Rev. E*, **81**(6), p. 065302.
- [27] LYKLEMA, J. (1995) *Fundamentals of Interface and Colloid Science, vol.2*, Elsevier.
- [28] WHEAT, P. M., N. A. MARINE, J. L. MORAN, and J. D. POSNER (2010) “Rapid Fabrication of Bimetallic Spherical Motors,” *Langmuir*, **26**(16), pp. 13052–13055.
- [29] FOURNIER-BIDOZ, S., A. C. ARSENAULT, I. MANNERS, and G. A. OZIN (2005) “Synthetic self-propelled nanorotors,” *Chem. Commun.*, (4), p. 441.
- [30] QIN, L., M. J. BANHOLZER, X. XU, L. HUANG, and C. A. MIRKIN (2007) “Rational design and synthesis of catalytically driven nanorotors,” *J Am Chem Soc*, **129**(48), pp. 14870–+.
- [31] WANG, Y., S. TO FEI, Y.-M. BYUN, P. E. LAMMERT, V. H. CRESPI, A. SEN, and T. E. MALLOUK (2009) “Dynamic Interactions between Fast Microscale Rotors,” *J Am Chem Soc*, **131**(29), pp. 9926–+.
- [32] LAOCHAROENSUK, R., J. BURDICK, and J. WANG (2008) “Carbon-nanotube-induced acceleration of catalytic nanomotors,” *Acs Nano*, **2**(5), pp. 1069–1075.
- [33] DEMIROK, U. K., R. LAOCHAROENSUK, K. M. MANESH, and J. WANG (2008) “Ultrafast Catalytic Alloy Nanomotors,” *Angew Chem Int Edit*, **47**(48), pp. 9349–9351.
- [34] ZACHARIA, N. S., Z. S. SADEQ, and G. A. OZIN (2009) “Enhanced speed of bimetallic nanorod motors by surface roughening,” *Chem. Commun.*, (39), p. 5856.
- [35] BRUUS, H. (2008) *Theoretical Microfluidics*, Oxford University Press.
- [36] HINCH, E. J. (1991) *Perturbation Methods*, Cambridge University Press, Cambridge.
- [37] FALLOON, P. E. “Theory and Computation of Spheroidal Harmonics with General Arguments,” M.Sc. thesis (2001).

- [38] CHWANG, A. T. and T. Y.-T. WU (1975) “Hydromechanics of low-Reynolds-number flow. Part 2. Singularity method for Stokes flows,” *J. Fluid Mech.*, **67**(1), pp. 787–815.
- [39] ZWILLINGER, D. (2003) *CRC Standard Mathematical Tables and Formulae*, 31st ed., JChapman & Hall/CRC, New York.
- [40] TEMME, N. M. (1996) *Special Functions and an Introduction to the Classical Functions of Mathematical Physics*, John Wiley & Sons, Inc., New York.
- [41] GIBBS, J. G. and Y.-P. ZHAO (2009) “Design and Characterization of Rotational Multicomponent Catalytic Nanomotors,” *Small*, **5**(20), pp. 2304–2308.
- [42] GIBBS, J. G., S. KOTHARI, D. SAINTILLAN, and Y. P. ZHAO (2011) “Geometrically Designing the Kinematic Behavior of Catalytic Nanomotors,” *Nano Lett.*, **11**(6), pp. 2543–2550.
- [43] KIM, S. and S. J. KARRILA (2005) *Microhydrodynamics: Principles and Selected Applications*, Dover Publications.
- [44] YE, S. and R. L. CARROLL (2010) “Design and Fabrication of Bimetallic Colloidal “Janus” Particles,” *ACS Appl. Mater. Interfaces*, **2**(3), pp. 616–620.

Vita

Amir Nourhani

nourhani@gmail.com

Education

- 2012 Ph.D. in Chemical Engineering, The Pennsylvania State University
- 2007 M.Sc. in Theoretical Physics, Sharif University of Technology
- 2007 B.Sc. in Solid State Physics, Amirkabir University of Technology
- 2003 B.Sc. in Polymer Engineering, Amirkabir University of Technology

Awards

- Personal Excellence Award for Best Candidacy Exam (thesis proposal), Chemical Engineering Department, Penn State University, 2009.
- Larry Duda Personal Excellence Award for Outstanding Graduate Student Performance, Chemical Engineering Department, Penn State University, 2009.

Presentations and Talks

- A. Nourhani, P.E. Lammert, A. Borhan, V.H. Crespi, “*Dimensional transitions for coupled rotational/translational diffusion in powered nanorotors*”, APS March Meeting, 2012.
- A. Nourhani, P.E. Lammert, A. Borhan, V.H. Crespi, “*Electrokinetic self-Propulsion of a Catalytic Nanomotor; a Perturbation Analysis*”, 64th APS DFD Meeting, 2011.

Publications

Four papers will be the outcome of this dissertation.